

## **DISSERTATION**

# **Synthesis and Characterization of Transition Metal Oxo Clusters and their Use as Co-Monomers in the Preparation of Hybrid Polymers**

ausgeführt zum Zwecke der Erlangung des akademischen Grades eines  
Doktors der Naturwissenschaften unter der Leitung von

**Univ.-Prof. Dr. Ulrich Schubert**

Institut für Materialchemie

E165

eingereicht an der Technischen Universität Wien  
Fakultät für Technische Chemie

von

**Mag. Franz René Kogler**

Matr. Nr. 9601830

Zeileborgasse 14-16/12, 1120 Wien

Wien, am 16.12.2005

## Acknowledgements

I would like to express my gratitude to my supervisor *Prof. Ulrich Schubert* for giving me the opportunity to undertake my thesis in his research group. His supportive and considerate guidance throughout the last years, providing me with lots of scientific space, allowed me to grow as both a person and a chemist.

Special thanks go to *Wolfgang Binder* and *Prof. Gerhard Zifferer* for valuable discussions about polymer chemistry, *Denise Dragan* for her supportive work in terms of hybrid materials (ultimately making her the most experienced 'Zr<sub>4</sub>-chemist') and for supplying the entire 7<sup>th</sup> floor with coffee, *Guido Kickelbick* for his introduction to 'single crystal X-ray diffraction for dummies' and for continuous support in terms of crystallography and bureaucracy, *Herwig Peterlik* for performing SAXS measurements and for comprehensive inter-disciplinary discussions, *Michael Puchberger* for pushing spectroscopic characterizations forward and for innumerable measurements and discussions, *Prof. Sabine Seidler* for providing me access to materials characterization and *Thomas Koch* for his sedulous engagement in characterizing my materials (most commonly during the weekends).

My thanks go to all my (former) colleagues and co-workers

*Akira, Artem, Bea, Christian, Christina F., Christina R., Christoph, Claudia F., Claudia V., Didi, Dini, Dieter H., Dieter R.* (causing an exciting time by working in the same fume hood), *Doris B., Doris E., Fatmir, Grace* (the kindest Chinese I have ever met), *Harald, Helmut, Horst* (for teaching me how to prepare pigs and much more), *Isabella, Jim, Kornél, Maia, Melitta, Mirka, Nico, Patrycja, Philipp, Ralf, Rupert* (for being the real technician in our group), *Sandra, Sorin, Susan, Thomas Ga., Thomas Gi., Uli, Urska, Viki* and *Wolfgang*

for a pleasant and/or scientific working atmosphere.

My final and greatest debt is to my parents for their perpetual support and love, to my grandmother (who will of course join the celebrations - again) and to Martin for spending much of the non-chemist life with me (ranging from underground places to high mountain areas).

## Kurzfassung

In anorganisch-organischen Hybridmaterialien sind die Bausteine auf molekularer Ebene verknüpft. Die Vielzahl der potentiellen Anwendungsmöglichkeiten stellt eine der größten Herausforderungen an die Materialwissenschaften und an die Materialchemie dar. Eine wichtige Unterklasse der Hybridmaterialien sind Polymere, die durch nanometergroße, oberflächenmodifizierte Übergangsmetall-Oxo-Cluster verstärkt sind.

Im ersten Teil der Arbeit wird die Herstellung von oberflächenmodifizierten Übergangsmetall-Oxo-Clustern durch kontrollierte Hydrolyse- und Kondensationsreaktionen von Übergangsmetall-alkoxiden in der Gegenwart von Carbonsäuren mit polymerisierbaren und nicht-polymerisierbaren Gruppen beschrieben. Durch die Reaktion von Zirkoniumbutoxid mit Carbonsäuren wurden zwei verschiedene Clustergeometrien erhalten. Die Reaktionen von Zirkoniumbutoxid mit Isobuttersäure, 5-Norbornen-2-carbonsäure oder einer Mischung aus Isobuttersäure und Methacrylsäure, führten zur Bildung von kristallinen Clustern der allgemeinen Zusammensetzung  $\text{Zr}_6\text{O}_4(\text{OH})_4(\text{carboxylat})_{12}$ . Vynlessigsäure oder eine Mischung aus Essigsäure und Methacrylsäure hingegen formten Cluster vom Typ  $\text{Zr}_{12}\text{O}_8(\text{OH})_8(\text{carboxylat})_{24}$ . Weiters wurden Isobuttersäure und 5-Norbornen-2-carbonsäure erfolgreich zur Herstellung von Titanium-Oxo-Clustern eingesetzt. NMR spektroskopische Untersuchungen gaben Aufschluss über das Verhalten der Cluster in Lösung. Die Carboxylatliganden zeigten raschen Austausch bei Raumtemperatur, die Cluster-Struktur jedoch blieb erhalten.

Im zweiten Teil der Arbeit wird die Verwendung von Zirkonium-Oxo-Clustern als Co-Monomere in freien radikalischen Polymerisationen beschrieben. In den Systemen bestehend aus dem Cluster  $\text{Zr}_4\text{O}_2(\text{methacrylat})_{12}$  und Methylmethacrylat oder Styrol wurden die optimalen Polymerisationsbedingungen durch Variation der Polymerisationsparameter und durch die Anwendung einer stufenweisen Polymerisation ausgearbeitet. Die thermischen Eigenschaften der quervernetzten Hybridmaterialien wurden untersucht. Die Molekulargewichte konnten bestimmt werden, nachdem die Clustereinheiten mit Acetylaceton zerstört wurden.

Durch stufenweise Co-Polymerisation von Styrol mit unterschiedlichen Mengen des Clusters  $\text{Zr}_6\text{O}_4(\text{OH})_4(\text{methacrylat})_{12}$  wurden quervernetzte polymere Materialien erhalten. Diese wurden thermisch, thermomechanisch und mechanisch vollständig charakterisiert. Röntgenkleinwinkelstreuexperimente wiesen auf eine Aggregation der Cluster in den Hybridpolymeren hin, was durch TEM-Aufnahmen bestätigt wurde. In Quellversuchen wurde nachgewiesen, dass die Quervernetzung mit der Konzentration des quervernetzenden Clusters zusammenhängt.

Die Co-Polymerisation von Styrol mit Clustern mit wenig- oder nichtreaktiven Liganden resultierte in Hybridmaterialien mit verbesserten thermischen Eigenschaften, allerdings waren diese löslich in Ethylacetat, das heißt eine Quervernetzung fand nicht statt.

## Abstract

The combination of inorganic and organic components at the molecular level is a challenging task in materials science and chemistry, offering a wide variety of possible applications. An important sub-class of inorganic-organic hybrid materials are polymers reinforced by structurally well-defined nanosized transition metal oxo clusters with polymerizable surface ligands.

In the first part of the work, organically modified transition metal oxo clusters were prepared both with polymerizable and non-polymerizable ligands. Zirconium oxo clusters were prepared by controlled hydrolysis and condensation reactions of zirconium butoxide in the presence of various carboxylic acids. Depending on the type of carboxylic acid applied in the syntheses, two kinds of zirconium oxo clusters were obtained: The reaction of zirconium butoxide with either isobutyric acid, 5-norbornene-2-carboxylic acid, or a mixture of isobutyric acid and methacrylic acid, resulted in the formation of clusters of the general composition  $\text{Zr}_6\text{O}_4(\text{OH})_4(\text{carboxylate})_{12}$ . When vinylacetic acid or a mixture of acetic acid and methacrylic acid were used, clusters of the general composition  $\text{Zr}_{12}\text{O}_8(\text{OH})_8(\text{carboxylate})_{24}$  were obtained. Furthermore, isobutyric acid and 5-norbornene-2-carboxylic acid were used in the preparation of titanium oxo clusters. To learn more about the behaviour of zirconium oxo clusters in solution, a detailed NMR spectroscopic investigation was carried out. The carboxylate bonded surface ligands showed fast exchange with each other but the cluster structure was preserved in solution.

In the second part of the work, zirconium oxo clusters were applied as co-monomers in free radical polymerizations. Optimum conditions for the co-polymerizations of  $\text{Zr}_4\text{O}_2(\text{methacrylate})_{12}$  with methyl methacrylate or styrene were established by varying the polymerization conditions and by applying a step-wise polymerization. The thermal properties of the cross-linked hybrid materials were investigated, and the molecular weight of the polymer was determined after destroying the cluster units with acetyl acetone.

A step-wise co-polymerization of  $\text{Zr}_6\text{O}_4(\text{OH})_4(\text{methacrylate})_{12}$  in various concentrations with styrene resulted in cross-linked hybrid polymers. The thermal properties, such as onset temperatures of thermal decomposition and glass transition temperatures, were improved. The materials were further characterized by thermomechanical and mechanical measurements. Small angle X-ray scattering measurements showed that the clusters were aggregated in the hybrid polymers. This was confirmed with TEM and STEM images. Swelling experiments clearly proved that cross-linking was related to the proportion of the cross-linking cluster in the material.

When styrene was co-polymerized with clusters carrying less- or non-reactive surface ligands, hybrid materials were obtained which showed improved thermal properties but were soluble in organic solvents such as ethyl acetate, i.e. cross-linking did not take place.

Parts of this work have been published

Improvement of the thermal stability of cluster-crosslinked polystyrene and poly(methyl methacrylate) by optimization of the polymerization conditions. Y. Gao, F.R. Kogler and U. Schubert, *Journal of Polymer Science, Part A: Polymer Chemistry*, **2005**, 43, 6586

Surface modified zirconium oxide clusters and their use as components for inorganic-organic hybrid materials. Y. Gao, D.S. Dragan, M. Jupa, F.R. Kogler, M. Puchberger and U. Schubert, *Materials Research Society Symposia Proceedings*, **2005**, 847, 539

Control of the ratio of functional and non-functional ligands in clusters of the type  $\text{Zr}_6\text{O}_4(\text{OH})_4(\text{carboxylate})_{12}$  for their use as building blocks for inorganic-organic hybrid polymers. F.R. Kogler, M. Jupa, M. Puchberger and U. Schubert, *Journal of Materials Chemistry*, **2004**, 14, 3133

Structural chemistry of titanium alkoxides substituted by the chelating bidentate ligands isoeugenolate or 2-aminoethanolate. H. Fric, F.R. Kogler, M. Puchberger and U. Schubert, *Zeitschrift für Naturforschung B: Journal of Chemical Sciences*, **2004**, 59, 1241

## Index of Abbreviations

|  |   |
|--|---|
| acac                                       | Acetylacetonate   |
| ATR  | Attenuated Total Reflection   |
| BPO  | Benzoyl peroxide  |
| Bu, <sup>n</sup> Bu                        | Butyl   |
| COSY                                       | Correlated Spectroscopy   |
| Cp   | Cyclopentadiene   |
| DMF  | Dimethyl formamide  |
| DMA  | Dynamic Mechanical Analysis   |
| DSC  | Differential Scanning Calorimetry                                     |
| d <sub>sw</sub>                            | Degree of Swelling  |
| Et   | Ethyl   |
| EXAFS                                      | Extended X-Ray Absorption Fine Structure                              |
| EXSY                                       | Exchange Spectroscopy   |
| FTIR                                       | Fourier Transform Infrared Spectroscopy                               |
| HMBC                                       | Heteronuclear Multiple Bond Correlation                               |
| HSQC                                       | Heteronuclear Single Quantum Coherence                                |
| HOAc                                       | Acetic acid   |
| HOIsob                                     | Isobutyric acid   |
| HOMc                                       | Methacrylic acid  |
| HONor <sub>b</sub> <sup>endo/exo/mix</sup> | endo / exo / (mixture of endo and exo) 5-Norbornene-2-carboxylic acid |
| HOProp                                     | Propionic acid  |
| HOVinac                                    | Vinylacetic acid  |
| ICP-OES                                    | Inductively Coupled Plasma Optical Emission Spectroscopy              |
| <sup>i</sup> Pr                            | Isopropyl   |
| IR   | Infrared Spectroscopy   |
| LPO  | Lauroyl peroxide  |
| MDSC                                       | Modulated Differential Scanning Calorimetry                           |
| MMA  | Methyl methacrylate   |
| M <sub>n</sub>                             | Number average molecular weight                                       |

|                               |   |
|-------------------------------|---|
| NBB                           | Nanosized Building Block  |
| NMR                           | Nuclear Magnetic Resonance  |
| OAc                           | Acetate   |
| OIsob                         | Isobutyrate   |
| OMc                           | Methacrylate  |
| ONorb <sub>endo/exo/mix</sub> | endo / exo / (mixture of endo and exo)-5-Norbornene-2-carboxylate |
| OProp                         | Propionate  |
| OVinac                        | Vinylacetate  |
| P <sub>d</sub>                | Polydispersity  |
| pK                            | Negative logarithm of the dissociation constant                   |
| POSS                          | Polyhedral Oligomeric Silsesquioxanes                             |
| PMMA                          | Poly(methyl methacrylate)   |
| Pr, <sup>n</sup> Pr           | Propyl  |
| PS                            | Polystyrene   |
| PTFE                          | Polytetrafluoroethylene   |
| ROMP                          | Ring Opening Metathesis Polymerization                            |
| SAXS                          | Small Angle X-Ray Scattering                                      |
| SEC                           | Size Exclusion Chromatography                                     |
| STEM                          | Scanning Transmission Electron Microscopy                         |
| t <sub>g</sub>                | Gelation time   |
| T <sub>g</sub>                | Glass transition temperature                                      |
| TEM                           | Transmission Electron Microscopy                                  |
| TGA                           | Thermogravimetric Analysis  |
| THF                           | Tetrahydrofuran   |
| TMA                           | Thermal Mechanical Analysis                                       |
| TOCSY                         | Total Correlated Spectroscopy                                     |
| wt                            | weight  |
| XRD                           | X-Ray Diffraction   |

### NMR Abbreviations

|          |                |
|----------|----------------|
| $\delta$ | Chemical Shift |
| s        | Singlet        |
| d        | Doublet        |
| t        | Triplet        |
| q        | Quartet        |
| m        | Multiplet      |
| br       | broad          |

### Infrared Abbreviations

|    |             |
|----|-------------|
| vs | very strong |
| s  | strong      |
| m  | medium      |
| w  | weak        |
| vw | very weak   |
| sh | shoulder    |
| br | broad       |

### Cluster Abbreviations

|                          |   |
|--------------------------|---|
| Ti6-Norb <sub>mix</sub>  | $\text{Ti}_6\text{O}_4(\text{OPr})_8(\text{ONorb}_{\text{mix}})_8$  |
| Zr12                     | $\text{Zr}_{12}\text{O}_8(\text{OH})_8(\text{OProp})_{24}$  |
| Zr12-Ac                  | $\text{Zr}_{12}\text{O}_8(\text{OH})_8(\text{OAc})_{24}$  |
| Zr12-AcMc                | $\text{Zr}_{12}\text{O}_8(\text{OH})_8(\text{OAc})_{16}(\text{OMc})_8 \cdot 6\text{HOAc}$                           |
| Zr12-Vinac               | $\text{Zr}_{12}\text{O}_8(\text{OH})_8(\text{OVinac})_{24} \cdot 6\text{HOVinac}$                                   |
| Zr4                      | $\text{Zr}_4\text{O}_2(\text{OMc})_{12}$  |
| Zr6                      | $\text{Zr}_6\text{O}_4(\text{OH})_4(\text{OMc})_{12}$   |
| Zr6-Isob                 | $\text{Zr}_6\text{O}_4(\text{OH})_4(\text{OIsob})_{12}(\text{H}_2\text{O}) \cdot 3\text{HOIsob}$                    |
| Zr6-McIsob               | $\text{Zr}_6\text{O}_4(\text{OH})_4(\text{OMc})_8(\text{OIsob})_4(\text{BuOH}) \cdot 4\text{HOOCR}$                 |
| Zr6-Norb <sub>endo</sub> | $\text{Zr}_6\text{O}_4(\text{OH})_4(\text{ONorb}_{\text{endo}})_{12} \cdot 3\text{HONorb}_{\text{endo}}$            |
| Zr6-Norb <sub>exo</sub>  | $\text{Zr}_6\text{O}_4(\text{OH})_4(\text{ONorb}_{\text{exo}})_{12}(\text{BuOH}) \cdot 3\text{HONorb}_{\text{exo}}$ |
| Zr6-Norb <sub>mix</sub>  | $\text{Zr}_6\text{O}_4(\text{OH})_4(\text{ONorb}_{\text{mix}})_{12} \cdot 3\text{HONorb}_{\text{mix}}$              |



# Table of Contents

|       |   |    |
|-------|---|----|
| 1     | Introduction .....  | 1  |
| 1.1   | Inorganic-Organic Hybrid Materials .....  | 1  |
| 1.2   | Design Strategies for Inorganic-Organic Hybrid Materials .....  | 2  |
| 1.3   | Sol-Gel Process .....   | 5  |
| 1.3.1 | Hydrolytic Sol-Gel Process .....  | 5  |
| 1.3.2 | Non-Hydrolytic Sol-Gel Processes .....  | 7  |
| 1.3.3 | Carboxylic Acid Sol-Gel Process .....   | 8  |
| 2     | Research Goals .....  | 10 |
| 3     | Zirconium Oxo Clusters .....  | 11 |
| 3.1   | Preparation of Zirconium Oxo Clusters .....   | 14 |
| 3.1.1 | $\text{Zr}_6\text{O}_4(\text{OH})_4(\text{OIsob})_{12}(\text{H}_2\text{O}) \cdot 3\text{HOIsob}$ .....    | 15 |
| 3.1.2 | $\text{Zr}_6\text{O}_4(\text{OH})_4(\text{OMc})_8(\text{OIsob})_4(\text{BuOH}) \cdot 4\text{HOOCR}$ ..... | 20 |
| 3.1.3 | $\text{Zr}_6\text{O}_4(\text{OH})_4(5\text{-Norbornene-2-carboxylate})_{12}$ .....                        | 24 |
| 3.1.4 | $\text{Zr}_{12}\text{O}_8(\text{OH})_8(\text{OVinac})_{24} \cdot 6\text{HOVinac}$ .....                   | 36 |
| 3.1.5 | $\text{Zr}_{12}\text{O}_8(\text{OH})_8(\text{OAc})_{16}(\text{OMc})_8 \cdot 6\text{HOAc}$ .....           | 40 |
| 3.2   | Zirconium Oxo Clusters in Solution .....  | 44 |
| 3.2.1 | $\text{Zr}_4\text{O}_2(\text{OMc})_{12}$ .....  | 44 |
| 3.2.2 | $\text{Zr}_6\text{O}_4(\text{OH})_4(\text{OMc})_{12}$ .....   | 50 |
| 3.2.3 | $\text{Zr}_{12}\text{O}_8(\text{OH})_8(\text{OProp})_{24}$ .....  | 52 |
| 3.2.4 | Conclusion.....   | 55 |
| 3.3   | Considerations about Cluster Formation .....  | 56 |
| 3.3.1 | Type of Zirconium Alkoxide.....   | 56 |
| 3.3.2 | Type of Carboxylic Acid .....   | 57 |
| 3.3.3 | Stoichiometric Ratio of Alkoxide and Carboxylic Acid .....  | 60 |
| 3.3.4 | Conclusion.....   | 61 |
| 4     | Titanium Oxo Clusters .....   | 62 |
| 4.1   | $\text{Ti}_6\text{O}_4(\text{OPr})_8(\text{ONorb}_{\text{mix}})_8$ .....                                  | 62 |

|        |   |     |
|--------|---|-----|
| 4.2    | $\text{Ti}_6\text{O}_4(\text{OEt})_8(\text{Olsob})_8$ and $\text{Ti}_6\text{O}_4(\text{OPr})_8(\text{Olsob})_8$ .....   | 64  |
| 4.3    | $\text{Ti}_6\text{O}_6(\text{O}^i\text{Pr})_6(\text{Olsob})_6$ .....  | 66  |
| 4.4    | $\text{Ti}_2(\text{OPr})_6(\text{isoeugenolate})_2$ .....   | 67  |
| 5      | Hybrid Polymers .....   | 69  |
| 5.1    | $\text{Zr}_4\text{O}_2(\text{OMc})_{12}$ Modified Polymers .....  | 69  |
| 5.1.1  | $\text{Zr}_4\text{O}_2(\text{OMc})_{12}$ Modified Poly(methyl methacrylate) .....   | 69  |
| 5.1.2  | $\text{Zr}_4\text{O}_2(\text{OMc})_{12}$ Modified Polystyrene .....   | 80  |
| 5.1.3  | Determination of Residual Zr in the Cleaved Polymers .....  | 87  |
| 5.1.4  | Optimization of the Polymerization Conditions .....   | 90  |
| 5.1.5  | Conclusion .....  | 102 |
| 5.2    | $\text{Zr}_6\text{O}_4(\text{OH})_4(\text{OMc})_{12}$ Modified Polystyrene .....  | 103 |
| 5.2.1  | Optimization of the Polymerization Conditions .....   | 103 |
| 5.2.2  | Preparation of $\text{Zr}_6\text{O}_4(\text{OH})_4(\text{OMc})_{12}$ Doped Bulk Polymers .....  | 106 |
| 5.2.3  | Thermal Properties .....  | 107 |
| 5.2.4  | Infrared Spectroscopy .....   | 115 |
| 5.2.5  | Swelling Behaviour .....  | 116 |
| 5.2.6  | Specific Gravity .....  | 117 |
| 5.2.7  | Thermal Mechanical Analysis .....   | 118 |
| 5.2.8  | Dynamic Mechanical Properties .....   | 120 |
| 5.2.9  | Mechanical Properties .....   | 133 |
| 5.2.10 | Microhardness .....   | 141 |
| 5.2.11 | Small Angle X-Ray Scattering .....  | 145 |
| 5.2.12 | Transmission Electron Microscopy .....  | 149 |
| 5.2.13 | Conclusions .....   | 152 |
| 5.3    | Polystyrene Modified with Clusters Carrying Less- or Non-reactive Ligands .....   | 154 |
| 5.3.1  | Polystyrene Modified with $\text{Zr}_{12}\text{O}_8(\text{OH})_8(\text{OAc})_{24}$ or $\text{Zr}_{12}\text{O}_8(\text{OH})_8(\text{OProp})_{24}$ .....              | 154 |
| 5.3.2  | Polystyrene Modified with $\text{Zr}_{12}\text{O}_8(\text{OH})_8(\text{OVinac})_{24}$ or $\text{Zr}_6\text{O}_4(\text{OH})_4(\text{ONorb}_{\text{mix}})_{12}$ ..... | 157 |
| 5.3.3  | Polystyrene Modified with $\text{Zr}_{12}\text{O}_8(\text{OH})_8(\text{OAc})_{16}(\text{OMc})_8$ .....  | 159 |
| 5.3.4  | Conclusion .....  | 161 |

|        |  |     |
|--------|--|-----|
| 6      | Experimental .....   | 162 |
| 6.1    | General Techniques and Used Materials .....  | 162 |
| 6.2    | Analytical Techniques .....  | 163 |
| 6.2.1  | Single Crystal X-Ray Diffraction.....  | 163 |
| 6.2.2  | Nuclear Magnetic Resonance Spectroscopy.....   | 163 |
| 6.2.3  | Thermogravimetric Analysis.....  | 164 |
| 6.2.4  | Differential Scanning Calorimetry .....  | 165 |
| 6.2.5  | Elemental Analysis.....  | 166 |
| 6.2.6  | Fourier Transform Infrared Spectroscopy.....   | 166 |
| 6.2.7  | Size Exclusion Chromatography.....   | 166 |
| 6.2.8  | Modulated Differential Scanning Calorimetry .....  | 167 |
| 6.2.9  | Inductively Coupled Plasma Optical Emission Spectroscopy .....   | 168 |
| 6.2.10 | Specific Gravity .....   | 169 |
| 6.2.11 | Thermal Mechanical Analysis .....  | 169 |
| 6.2.12 | Dynamic Mechanical Analysis .....  | 170 |
| 6.2.13 | Tension Tests.....   | 172 |
| 6.2.14 | Compression Tests .....  | 173 |
| 6.2.15 | Microhardness.....   | 174 |
| 6.2.16 | Small Angle X-Ray Scattering.....  | 176 |
| 6.2.17 | Transmission Electron Microscopy .....   | 177 |
| 6.3    | Synthesis of Zirconium Oxo Clusters.....   | 179 |
| 6.3.1  | Synthesis of $\text{Zr}_6\text{O}_4(\text{OH})_4(\text{OIsob})_{12}(\text{H}_2\text{O}) \cdot 3\text{HOIsob}$ .....    | 179 |
| 6.3.2  | Synthesis of $\text{Zr}_6\text{O}_4(\text{OH})_4(\text{OMc})_8(\text{OIsob})_4(\text{BuOH}) \cdot 4\text{HOOCR}$ ..... | 179 |
| 6.3.3  | Synthesis of $\text{Zr}_6\text{O}_4(\text{OH})_4(5\text{-norbornene-2-carboxylate})_{12}$ .....                        | 180 |
| 6.3.4  | Synthesis of $\text{Zr}_{12}\text{O}_8(\text{OH})_8(\text{OVinac}) \cdot 6\text{HOVinac}$ .....                        | 184 |
| 6.3.5  | Synthesis of $\text{Zr}_{12}\text{O}_8(\text{OH})_8(\text{OMc})_8(\text{OAc})_{16} \cdot 6\text{HOAc}$ .....           | 185 |
| 6.4    | Zirconium Oxo Clusters in Solution .....   | 186 |
| 6.4.1  | $\text{Zr}_4\text{O}_2(\text{OMc})_{12}$ .....   | 186 |
| 6.4.2  | $\text{Zr}_6\text{O}_4(\text{OH})_4(\text{OMc})_{12}$ .....  | 187 |

---

|       |  |     |
|-------|--|-----|
| 6.4.3 | $\text{Zr}_{12}\text{O}_8(\text{OH})_8(\text{OProp})_{24}$ .....   | 188 |
| 6.5   | Considerations about Cluster Formation .....   | 188 |
| 6.5.1 | Deuteration of Methacrylic Acid .....  | 188 |
| 6.5.2 | Synthesis of $\text{Zr}(\text{isoeugenolate})_4$ .....   | 188 |
| 6.6   | Synthesis of Titanium Oxo Clusters.....  | 189 |
| 6.6.1 | Synthesis of $\text{Ti}_6\text{O}_4(\text{OPr})_8(\text{ONorb}_{\text{mix}})_8$ .....                              | 189 |
| 6.6.2 | Synthesis of $\text{Ti}_6\text{O}_4(\text{OEt})_8(\text{OIsob})_8$ .....   | 189 |
| 6.6.3 | Synthesis of $\text{Ti}_6\text{O}_4(\text{OPr})_8(\text{OIsob})_8$ .....   | 190 |
| 6.6.4 | Synthesis of $\text{Ti}_6\text{O}_6(\text{O}^i\text{Pr})_6(\text{OIsob})_6$ .....                                  | 190 |
| 6.6.5 | Synthesis of $\text{Ti}_2(\text{OPr})_6(\text{isoeugenolate})_2$ .....   | 190 |
| 6.7   | Crystallographic Data .....  | 192 |
| 6.8   | Synthesis of Hybrid Polymers .....   | 199 |
| 6.8.1 | Preparation of $\text{Zr}_4\text{O}_2(\text{OMc})_{12}$ Modified Poly(methyl methacrylate) .....                   | 199 |
| 6.8.2 | Preparation of $\text{Zr}_4\text{O}_2(\text{OMc})_{12}$ Modified Polystyrene .....                                 | 200 |
| 6.8.3 | Destroying the Cross-Links with Acetyl Acetone .....   | 202 |
| 6.8.4 | Determination of Residual Zr in Cleaved Polymers.....  | 202 |
| 6.8.5 | Optimization of Polymerization Conditions .....  | 203 |
| 6.8.6 | Optimization of the $\text{Zr}_6\text{O}_4(\text{OH})_4(\text{OMc})_{12}$ - Styrene Polymerization Conditions .... | 205 |
| 6.8.7 | Preparation of $\text{Zr}_6\text{O}_4(\text{OH})_4(\text{OMc})_{12}$ - Styrene Bulk Polymers.....                  | 206 |
| 6.8.8 | Preparation of Polystyrene Doped with Clusters Carrying Less- or Non-Reactive Ligands .....                        | 207 |
| 7     | Summary .....  | 209 |
| 8     | Literature .....   | 216 |

# 1 Introduction

## 1.1 Inorganic-Organic Hybrid Materials

The driving force behind the development of each new material is the demand for new properties. Materials have played an important role in our civilization and have been the milestones of progress. Entire eras have been categorized by the materials they used, the Stone Age, the Bronze Age, etc. Some of these periods lasted for centuries, but in recent times both the rate of major materials breakthroughs and their improvements are increasing ever faster.

The combination of different materials is a well-known concept in materials science and chemistry with the goal to fabricate materials with improved or even new properties. The development of hybrid inorganic-organic materials stems from several different areas of chemistry, including intercalation chemistry [1], but exploded in the 1980's with the birth of soft inorganic chemistry processes, where mild synthetic conditions opened a versatile access to chemically designed hybrid inorganic-organic materials [2-5]. However, the inorganic-organic hybrid materials are not simply physical mixtures between two components but they can be broadly defined as either co-polymers between organic and inorganic building blocks or as nanocomposites with inorganic and organic components intimately mixed. Thus, hybrid materials can either be depicted as homogeneous polymeric systems derived from monomers and miscible inorganic and organic components, or as heterogeneous systems where at least one of the components has a length scale ranging from a few Ångströms to a few tens of nanometers [6]. The properties of the resulting materials are not only the sum of the individual contributions of both phases, but the role of the interfaces and interphases can be predominant. As a consequence, the nature of the interface or the nature of the links and interactions between the organic and inorganic components has been used to categorize the hybrid materials into two main classes [6-8]:

Class I corresponds to all the systems where no covalent or ionic bonds are present between the organic and inorganic components. In such systems, the components undergo only weak interactions such as van der Waals contacts, hydrogen bonding,  $\pi$ - $\pi$  interactions or electrostatic forces.

In Class II materials, the inorganic and organic components are fully or partially linked through strong chemical bonds, such as covalent, ionic or Lewis acid-base bonds.

The combination of inorganic and organic or even bioactive components in a single material at the nanosized level has made accessible an immense new area of materials science that has

implications in the development of multifunctional materials. The chemical nature of this emerging class of hybrid materials varies from molecular and supramolecular adducts to extended solids, mineral or biomineral phases. Inorganic-organic hybrid materials match the characteristics of organic polymers in terms of flexibility and ease of processability and at the same time have the advantages of inorganic compounds such as thermal stability, electrical conductivity and optical or magnetic properties. Thus, many interesting new materials have already been prepared with tuneable properties and are considered as innovative materials with predictable properties and promising applications in many fields such as optics, electronics, ionics, energy storage and conversion, mechanics, membranes, protective coatings, catalysis, sensors, biology, etc (e.g. see [9-13]).

## 1.2 Design Strategies for Inorganic-Organic Hybrid Materials

Next to the classification by the type of chemical interaction between inorganic and organic phases, a second feature concerns the chemical pathway that is used to design the hybrid materials. Generally, 4 types are distinguished in literature [12, 14-16]:

- I Soft chemistry routes
  - A Conventional sol – gel pathways
  - B Bridged precursors
  - C Hydrothermal syntheses
- II Well-defined nano-sized building blocks (NBB)
  - A Assembling
  - B Dispersion
- III Self assembling procedures
  - A Templated growth by organic surfactants
  - B Templated growth by using bridged silsesquioxanes as precursors
  - C Combination of NBB and self-assembling approach
- IV Integrative syntheses

## I Soft Chemistry Routes

Path I corresponds to very convenient soft chemistry routes including sol gel chemistry, the use of specific bridged and polyfunctional precursors, and hydrothermal synthesis.

Amorphous hybrid networks can be obtained by conventional sol-gel pathways (A) through hydrolysis of organically modified (semi)metal alkoxides or (semi)metal halides condensed with or without alkoxides. The solvent used may also contain specific moieties that can interact or be trapped within inorganic components through a large set of interactions (H-bonds,  $\pi$ - $\pi$  interactions, van der Waals). The strategies are simple, low cost and yield amorphous nano-composite hybrid materials that can be transparent and easily shaped as films or bulks. However, the materials are generally locally heterogeneous in chemical composition.

The use of bridged precursors of silsesquioxanes  $X_3Si-R'-SiX_3$  ( $R'$  is an organic spacer,  $X$  is a halide or alkoxide) in Route B allows a preparation of molecular hybrid materials which have a better degree of local organization.

Route C makes use of hydrothermal syntheses in polar solvents in the presence of organic templates. This gave rise to a number of organically modified zeolites for applications in the fields of adsorbents or catalysts.

## II Nano-Sized Building Blocks

In this procedure, the assembling or dispersion of well-defined nano-sized building blocks (NBBs) is used. NBBs are monodisperse preformed objects that keep their integrity in the final materials. Their use is a suitable method to reach a better definition of the inorganic or organic component. These NBBs can be clusters, organically pre- or post-functionalized nanoparticles (metallic oxides, metals, chalcogenides, etc.), core-shell nanoparticles or layered compounds (clays, layered double hydroxides, lamellar phosphates, oxides or chalcogenides). In addition, the NBBs can be capped with polymerizable ligands or be connected through organic spacers. Advantages in using pre-condensed species are:

- A lower reactivity towards hydrolysis or attack of nucleophilic moieties than metal alkoxides
- Monodisperse, perfectly defined structures which facilitate the characterization of the final materials
- A wide range of different architectures and inorganic-organic interfaces
- A high degree of control through step-by-step preparation of the materials

### III Self-Assembling Procedures

In the last years the field of self-assembly has been explored in terms of organization or texturation of growing inorganic or hybrid networks, templated by organic structure directing agents (A). The success of this approach is clearly reasoned in the generation of inorganic-organic interfaces within a whole continuous range of nanocomposites. One of the most striking examples is the synthesis of mesostructured hybrid networks. A recent approach uses the templated growth of mesoporous hybrid materials by using bridged silsesquioxanes as precursors (B). The final porous materials have a high degree of order, and contain organic functionalities within the walls. Furthermore, mesoporosity is available for further organic functionalisation. A third strategy (C) arises from the combination of the NBB approach with the use of organic templates that self-assemble. The combination of NBB and templated assembling probably is closest to the so-called 'Lego-chemistry' approach, i.e. 'synthesis with construction'.

### IV Integrative Syntheses

These synthesis procedures aim at the assembly of structured hybrid materials in the micrometer range. Inspired by natural systems, a combination between these strategies and those described above allows the construction of hierarchically organized materials in terms of structure and functions.

The method applied in this work was based on the nanosized building blocks approach. In a first step, surface modified and well-defined transition metal oxo clusters were prepared by controlled hydrolysis and condensation reactions of transition metal alkoxides in the presence of carboxylic acids. In a second step, the nanosized building blocks were applied as co-monomers in polymerization reactions, acting as cross-linkers with a high density of possible linking points accessible on the cluster surface.

It is necessary, at the beginning of this thesis, to discuss the term 'transition metal oxo cluster'. Following the definition of Cotton [17] a transition metal cluster consists of a finite number of metal atoms which are connected through a major part by metal-metal bonds. At the time the term was proposed, there had been occasional use of the word 'cage' for metals connected together by ligand bridges without metal-metal bonding. However, this term was rejected because it suggested the ideas of containment and encapsulating of something. For example, a triangle of metal atoms being two-dimensional cannot surround anything. Furthermore, metal-metal bonds are often difficult to verify.



Therefore, the term 'cluster' is now used in a broader sense, i.e. for all molecular assemblies having at least three metal atoms, irrespective of the nature of the metal-metal interaction.

For example, molecules such as  $\text{Ti}_6\text{O}_4(\text{OR}')_8(\text{OOCR})$  and  $\text{Zr}_6\text{O}_4(\text{OH})_4(\text{OOCR})_{12}$  ( $\text{OOCR}$  = carboxylate,  $\text{OR}'$  = alkoxide) [18, 19] show typical metal-metal distances in the range of 300-350 pm, making direct bonding between the metal atoms most unlikely. Nevertheless, such compounds are nowadays termed as 'titanium oxo clusters' and 'zirconium oxo clusters', respectively. Very often also the word 'oxo' is omitted. Therefore, it should be pointed out here that all compounds in this work which are termed as 'metal oxo clusters' or only 'clusters', respectively, do not follow the definition of Cotton.

## 1.3 Sol-Gel Process

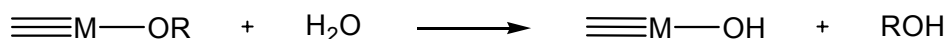
The sol-gel process allows synthesizing ceramic materials of high purity and homogeneity by means of preparation techniques different from the traditional process of solid-state reactions of oxides. In addition, the very mild reaction conditions, particularly the low reaction temperatures, also allow the incorporation of organic moieties into inorganic materials.

Generally, the sol-gel process occurs in the liquid state, with inorganic salts or (semi)metal alkoxides as precursors. Hydrolysis and condensation reactions lead to the formation of a colloidal phase, the so-called sol, which consists of oxidic particles with a size ranging from 1 to a few 10 nanometers. Further hydrolysis and condensation reactions lead to a formation of a network throughout the entire system, a so-called gel. Thus, a gel can be considered a continuous network enclosing a liquid phase.

### 1.3.1 Hydrolytic Sol-Gel Process

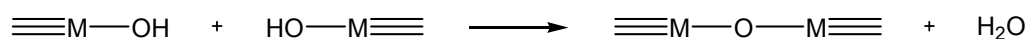
The classic formulation for gel generation by condensation reactions was studied extensively for silicon alkoxides [5] and comprises four components: a silicon alkoxide, water, an acidic or basic catalyst, and, optionally, a solvent to provide compatibility between the usually immiscible silicon alkoxide and water.

The reactivity of metal alkoxides towards water is much higher. The reaction proceeds through hydroxylation that occurs upon hydrolysis [3] (Scheme 1).

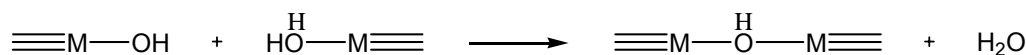


**Scheme 1:** Hydrolysis of metal alkoxides; M = metal atom, ROH = alcohol

The metal hydroxides which are formed in the hydrolysis reaction may condense under water or alcohol elimination, respectively, either through oxo- (oxolation and alkoxolation, Scheme 2) or hydroxo-bridges (Olation, Scheme 3). Under stoichiometric hydrolysis ratios, the alcohol producing condensation reaction is favoured, whereas a water forming condensation is dominant for larger hydrolysis ratios [5]. Olation takes place when solvent-stabilized alkoxides are present in the solution.



**Scheme 2:** Formation of oxo bridges; alkoxolation (elimination of alcohol, top) and oxolation (elimination of water, bottom)



**Scheme 3:** Formation of hydroxo bridges; elimination of alcohol (top) and water (bottom)

Generally, the hydrolysis and condensation reactions involved in the sol-gel process of semi-metal and metal alkoxides tend to occur simultaneously and are partly reversible. The structure and morphology of the resulting networks strongly depends on the relative contribution of each of these reactions.

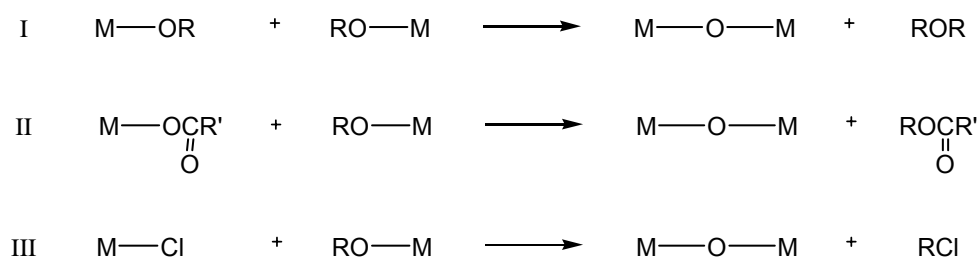
The chemical reactivity of metal alkoxides towards hydrolysis and condensation mainly depends on the positive charge of the metal atom and its ability to increase the coordination number. Thus, the rather low reactivity of  $\text{Si}(\text{OR})_4$  towards hydrolysis and condensation can be related to the low electrophilicity of silicon together with its fully satisfied fourfold coordination which is maintained in the final material. To this end, acid or base catalysts are most widely used in the sol-gel process chemistry of silicon alkoxides to expedite the hydrolysis reactions and to obtain shorter gelation times. As mentioned above, most metal alkoxides are much more reactive than silicon alkoxides [20]. The electronegativity of the metal atoms is much smaller than that of Si, consequentially increasing their positive partial charge. In addition, their coordination number is

higher than their oxidation state and coordination expansion during sol-gel process plays a major role.

An attractive solution to slow down reaction rates of titanium and zirconium alkoxides is to use organic additives which act as coordinating ligands, such as the anions of carboxylic acids,  $\beta$ -diketones or hydrazine derivatives [21, 22]. An alternative strategy is provided by non-hydrolytic sol-gel processes, with different precursors, solvents, experimental conditions, catalysts and reaction mechanisms.

### 1.3.2 Non-Hydrolytic Sol-Gel Processes

The non-hydrolytic sol-gel route involves the reaction of a metal halide with an oxygen donor, such as an alkoxide, an ether, an alcohol, and so forth, under non-aqueous conditions to form an inorganic oxide [23, 24]. The by-products depend on the nature of the oxygen donor molecules. The mechanism differs completely from the hydrolytic sol-gel process: It proceeds through coordination of the oxygen donor to the central metal atom of the halide, followed by cleavage of the carbon-oxygen bond instead of metal-oxygen cleavage. As a consequence, reactivity differences between different metals such as silicon and transition metals may not be the same as those observed in the hydrolytic reaction. Additionally, ligand exchange reactions take place which can change the kinetics and the mechanistic course of the reaction as well as the structure of the products [25]. Examples for non-hydrolytic methods under formation of oxo bridges are shown in Scheme 4. Ether elimination in reaction I is a general possibility, however, it has not been developed to practical applications as the two other ways, ester and alkyl eliminations.

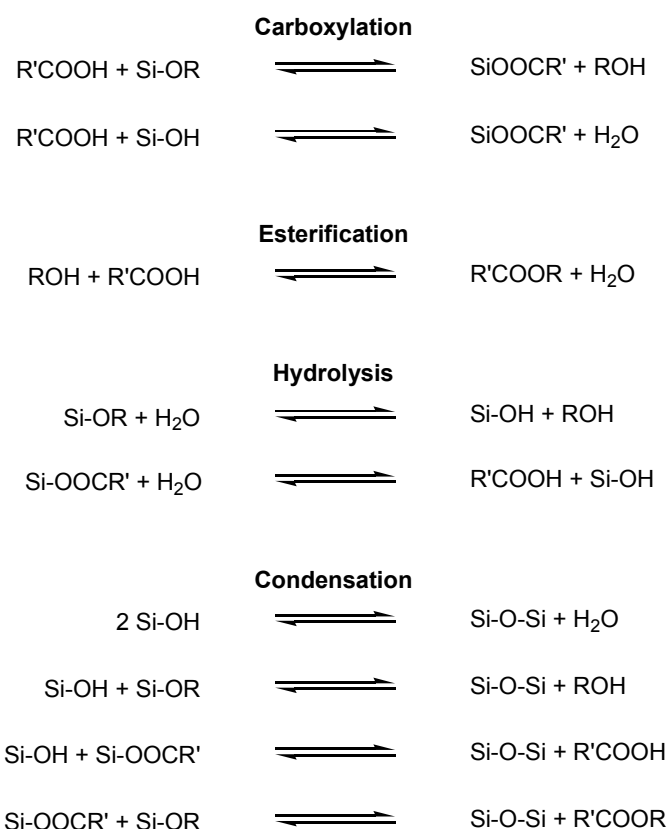


**Scheme 4:** Non-hydrolytic sol-gel route to inorganic oxides

### 1.3.3 Carboxylic Acid Sol-Gel Process

In the hydrolytic sol-gel process several carboxylic acids have been investigated as complexing agents to slow down hydrolysis rates of transition metal alkoxides. The classical formulation consists of four parts, viz. metal alkoxide, solvent, water and a catalyst. Sharp proposed that this four-component mixture can be replaced by just two, originally formic acid and tetraalkoxysilane [26, 27]. The carboxylic acid acts as the solvent, water source and catalyst for both the hydrolytic and condensation reactions. An initial presence of water is not required because the water is generated *in situ* during the reaction. Thus, this procedure can be considered as a combination of the hydrolytic and the non-hydrolytic sol-gel routes, but constitutes an autonomous method.

In a detailed investigation Sharp proposed following reactions included in the formation of a silica network (Scheme 5):



**Scheme 5:** Reactions in the non-aqueous sol-gel process

The overall reaction can be divided into four different sub-reactions, which will not appear consecutively but rather simultaneously: In a first step, the acid coordinates to silicon by reaction

with alkoxysilanes or silanols and generates alcohol or water. Furthermore, water is produced by esterification of the carboxylic acid with alcohol, which is in turn generated in each step of the above scheme, i.e. carboxylation, hydrolysis and condensation. The acid also catalyzes the hydrolysis of Si-OR and Si-OOCR' bonds to form silanols, which then condense by liberating water, alcohol, acid or ester.

The type of alkoxide and carboxylic acid used has a strong influence. Whereas the alkoxide ligands are mainly responsible for miscibility, there is a remarkable difference in the use of strong and weak carboxylic acids, expressed in terms of the pKa value in aqueous solutions. Formic acid (pKa 3.75) and trifluoroacetic acid (pKa 0.23) show rapid gel formation, whereas acetic acid (pKa 4.76) and acrylic acid (pKa 4.25) react two orders of magnitude more slowly.

This method is mostly ascribed to Sharp in the literature. However, already in 1956 Sumrell and Ham reported that the reaction of alkoxysilanes with an excess of carboxylic acid results in the formation of the ester of the carboxylic acid [28]. In addition, many authors applied this method before it was considered an autonomous method [29-32].

In the last 10 years or so the study of transition metal oxo clusters [9, 33] containing carboxylate groups has attracted interest because of their potential as well-defined building blocks for transformation to oxides and inorganic-organic hybrid materials, ultimately leading to an extension of the well-known POSS systems [34-37]. Conceptually, all these compounds were prepared by a non-hydrolytic or a non-aqueous sol-gel pathway or a combination of the two. Whereas the lowered reactivity in these routes is undesired in the formation of gels, it offers great potential for the preparation of intermediate compounds, i.e. primary hydrolysis compounds, because it allows careful control over hydrolysis and condensation reactions.

## 2 Research Goals

Transition metal oxo clusters were functionalized with polymerizable groups such as acrylic acid or methacrylic acid in earlier works. Their use as co-monomers in free radical polymerizations with organic monomers, such as methyl acrylate and methyl methacrylate, resulted in inorganic-organic hybrid polymers which were cross-linked with the inorganic component and showed improved thermal properties. However, these polymerization reactions had more of a proof-of-principle character. Big variations in thermal properties of the resulting materials were obtained, not following a clear trend in terms of the applied cluster concentration and cluster type, i.e. composition and geometry. To this end, a fundamental investigation of the determining factors involved in cluster formation and their use in the preparation of hybrid materials was required.

Zirconium oxo clusters were chosen as model compounds for investigations because the precursors, i.e. zirconium alkoxides, are cheap and readily available. In addition, different cluster geometries are easily accessible by simply changing the molar ratios of the educts.

Therefore, the preparation of zirconium oxo clusters and their application in the preparation of inorganic-organic hybrid materials raised, *inter alia*, the following questions:

- Is there a general relationship between the kind of applied carboxylic acid in the preparation of zirconium oxo clusters and their size and shape? In other words, is there a possibility to predict cluster formation and specific cluster geometries with the simple knowledge of the educts?
- Are polymerization reactions restricted to free radical polymerizations and atom transfer radical polymerization [38], or is there a possibility to introduce functional groups by pre- and post-treatment, respectively?
- What are the optimum conditions to carry out polymerization reactions? Which factors influence the reactivity of surface modified oxo clusters in polymerization reactions and what prerequisites are necessary to obtain homogeneous hybrid polymers?
- What factors determine the properties of the final class II hybrid materials? Is it cross-linking rather than the inorganic filler perception or is it a combination of both?
- Finally, what are the properties of the hybrid materials in terms of thermal, thermomechanical and mechanical behaviour?

### 3 Zirconium Oxo Clusters

Next to the most widely used silicon based nanosized building blocks [34-37], carboxylate-modified metal oxo clusters are one of the most promising candidates in the preparation of inorganic-organic hybrid materials. Many examples have been synthesized until present, such as tin oxo clusters [39], manganese oxo clusters [40, 41], chromium oxo clusters [42], tantalum oxo clusters [43, 44], hafnium oxo clusters [45], niobium oxo clusters [46], vanadium oxo clusters [38], and so forth. Among all the examples the clusters with high valence transition metals point out to be the most easily accessible compounds, offering a wide variety of cluster sizes and geometries. Until present, the most intensely studied carboxylate systems are the titanium oxo clusters which were prepared in different sizes and shapes, ranging from a trimetallic oxo cluster to a  $Ti_9$  structure [33].

Generally, functionalizing groups can be introduced to metal oxo clusters either by grafting to a preformed structure, i.e. a surface modification where an attached ligand is replaced for another, or by an 'in-situ' method, i.e. functional groups are already introduced during formation of the clusters. The latter method is most convenient because synthesis can, in principle, be carried out in one pot without further modification. However, there are reasons to favour the surface modification method, e.g. when a characteristic type of nanosized building block is easily accessible in high yields with just one particular ligand.

A focus was laid on zirconium oxo clusters in this work, because less is known about these compounds in terms of structure-reactivity relationships. Table 1 summarizes the examples which were reported until present, mixed metal oxo clusters [47, 48] are not considered therein.

Apparently, most of the examples were prepared by the carboxylic acid sol-gel route where the ligands, constituting the functional groups, were introduced in situ. A different way in the preparation was investigated by Reza et al. in the latter two examples given in Table 1: Instead of using a zirconium alkoxide as the metal source, zirconium tetrachloride was applied with triethylamine as a buffer. To the best of my knowledge, no other carboxylate substituted zirconium oxo clusters were prepared using this precursor. However, it reveals a basic route to the preparation of cluster compounds which were not accessible with certain ligands by the carboxylic acid.

**Table 1:** Carboxylate modified zirconium oxo clusters; abbreviations are given in the table for clarity

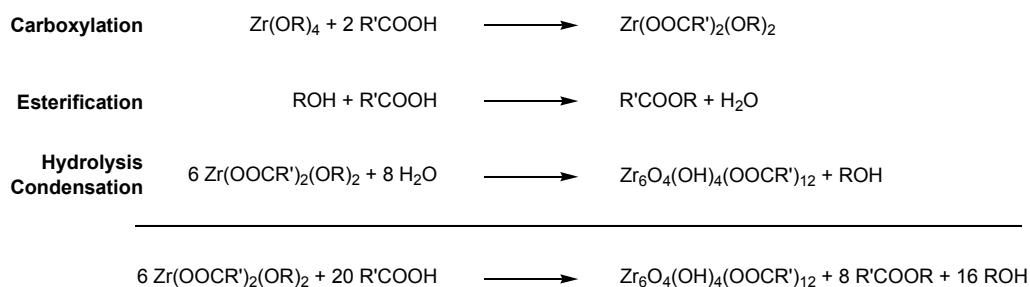
| Cluster  | Precursor                               | Carboxylic Acid  | Remark  | Ref. |
|--|---|--|---|------|
| $\text{Zr}_3\text{O}(\text{OAc})_3(\text{ONep})_7$<br>(HONep = Neopentyl alcohol)  | $\text{Zr}_3\text{O}(\text{ONep})_{10}$ | Acetic acid<br>(HOAc)  | Molar ratio 1:1,<br>toluene; <sup>[a]</sup>   | [49] |
| $\text{Zr}_4\text{O}_2(\text{OFc})_2(\text{O}^i\text{Pr})_{10}$  | $\text{Zr}(\text{O}^i\text{Pr})$        | Formic acid<br>(HOFc)  | Molar ratio 1:1,<br>toluene; <sup>[a]</sup>   | [49] |
| $\text{Zr}_4(\text{OIsob})_4(\text{O}^i\text{Pr})_{12}$  | $\text{Zr}(\text{O}^i\text{Pr})$        | Isobutyric acid<br>(HOIsob)  | Molar ratio 1:1,<br>toluene; <sup>[a]</sup>   | [49] |
| $\text{Zr}_4\text{O}_2(\text{OMc})_{12}$   | $\text{Zr}(\text{OPr})_4$               | Methacrylic acid<br>(HOMc)   | Molar ratio 1:7,<br>propanol; <sup>[a]</sup>  | [19] |
| $\text{Zr}_5\text{O}_4(\text{OIsobBr})_{10}(\text{OPr})_2(\text{PrOH})_4$  | $\text{Zr}(\text{OPr})_4$               | 2-Bromo-isobutyric acid<br>(HOIsobBr)                                      | Molar ratio 1:4,<br>propanol; <sup>[a]</sup>  | [38] |
| $\text{Zr}_5\text{O}_3(\text{OIsob})_6(\text{ONep})_8$   | $\text{Zr}_3\text{O}(\text{ONep})_{10}$ | Isobutyric acid<br>(HOIsob)  | Molar ratio 1:1,<br>toluene; <sup>[a]</sup>   | [49] |
| $\text{Zr}_5\text{O}_3(\text{OAc}^t\text{Bu})_6(\text{ONep})_8$  | $\text{Zr}_3\text{O}(\text{ONep})_{10}$ | Tertiary-butylacetic acid<br>(HOAc <sup>t</sup> Bu)                        | Molar ratio 1:1,<br>toluene; <sup>[a]</sup>   | [49] |
| $\text{Zr}_6\text{O}_2(\text{OBu})_{10}(\text{OMc})_{10}$  | $\text{Zr}(\text{OBu})_4$               | Methacrylic acid<br>(HOMc)   | Molar ratio 1:1.6,<br>butanol; <sup>[a]</sup> | [47] |
| $\text{Zr}_6\text{O}_2(\text{OMe})_4(\text{OBu})_2(\text{OMc})_{14}$   | $\text{Zr}(\text{OBu})_4$               | Methacrylic acid<br>(HOMc),<br>(3-Methacryloxypropyl)-<br>trimethoxysilane | Molar ratio 1:7:1,<br>butanol; <sup>[a]</sup> | [47] |
| $\text{Zr}_6\text{O}_2(\text{OPr})_{16}(\text{O}_2\text{CC}_{10}\text{H}_6\text{O})_2(\text{HOPr})_2$                          | $\text{Zr}(\text{OPr})_4$               | 1-Hydroxy- $\beta$ -naphthoic<br>acid                                      | Molar ratio 1:10,<br>propanol; <sup>[a]</sup> | [50] |
| $\text{Zr}_6\text{O}_4(\text{OH})_4(\text{OMc})_{12}$  | $\text{Zr}(\text{OPr})_4$               | Methacrylic acid<br>(HOMc)   | Molar ratio 1:4,<br>propanol; <sup>[a]</sup>  | [19] |
| $\text{Zr}_6\text{O}_4(\text{OH})_4(\text{OBz})_{12}(\text{PrOH})$   | $\text{Zr}(\text{OPr})_4$               | Benzoic acid<br>(HOBz)   | Molar ratio 1:20,<br>propanol; <sup>[a]</sup> | [51] |
| $\text{Zr}_6\text{O}_4(\text{OH})_4(\text{OMc})_{12}(\text{PrOH})$   | $\text{Zr}(\text{OPr})_4$               | Methacrylic acid<br>(HOMc)   | Molar ratio 1:10,<br>propanol; <sup>[a]</sup> | [51] |
| $\text{Zr}_9\text{O}_6(\text{OPr})_{18}(\text{OAc})_8$   | $\text{Zr}(\text{OPr})_4$               | Acetic acid<br>(HOAc)  | Water; <sup>[a]</sup>                         | [52] |
| $\text{Zr}_{10}\text{O}_6(\text{OH})_4(\text{O}_2\text{CC}_6\text{H}_4\text{O})_8(\text{O}_2\text{CC}_6\text{H}_4\text{OH})_8$ | $\text{Zr}(\text{OPr})_4$               | Salicylic acid   | Molar ratio 1:10,<br>propanol; <sup>[a]</sup> | [50] |



|  |                           |   |   |      |
|--|---------------------------|---|---|------|
| $\text{Zr}_{12}\text{O}_8(\text{OH})_8(\text{OAc})_{24}$                     | $\text{Zr}(\text{OPr})_4$ | Acrylic acid<br>(HOAc)  | Molar ratio 1:10,<br>propanol; <sup>[a]</sup>                                 | [51] |
| $\text{Zr}_{12}\text{O}_8(\text{OH})_8(\text{OAc})_{24}$                     | $\text{Zr}(\text{OBu})_4$ | Acetic acid<br>(HOAc)   | Molar ratio 1:10,<br>butanol, $\text{CH}_2\text{Cl}_2$ ; <sup>[a]</sup>       | [53] |
| $\text{Zr}_{12}\text{O}_8(\text{OH})_8(\text{OProp})_{24}$                   | $\text{Zr}(\text{OBu})_4$ | Propionic acid<br>(HOProp)  | Molar ratio 1:10,<br>butanol; <sup>[a]</sup>                                  | [53] |
| $\text{Zr}_{12}\text{O}_8(\text{OH})_8(\text{OProp})_6(\text{OMc})_{18}$     | $\text{Zr}(\text{OBu})_4$ | Propionic acid (HOProp)<br>Methacrylic acid (HOMc)                | Molar ratio 1:5:2,<br>butanol; <sup>[a]</sup>                                 | [53] |
| $\text{Zr}_{12}\text{O}_8(\text{OH})_8(\text{OAcMe}_2)_{24}$                 | $\text{Zr}(\text{OBu})_4$ | Dimethylacrylic acid<br>(HOAcMe <sub>2</sub> )                    | Molar ratio 1:7,<br>butanol; <sup>[a]</sup>                                   | [53] |
| $\text{Zr}_6(\text{OH})_8(\text{OCH}_3)_4(\text{OAcDP})_{12}$                | $\text{ZrCl}_4$           | Diphenylacetic acid<br>(HOAcDP)                                   | Molar ratio 1:4,<br>triethylamine,<br>$\text{CH}_3\text{CN}$ ; <sup>[c]</sup> | [54] |
| $\text{Zr}_6(\text{OH})_8(\text{OCH}_3)_4(\text{OAcDP})_{10}(\text{phen})_2$ | $\text{ZrCl}_4$           | Diphenylacetic acid<br>(HOAcDP),<br>1,10-Phenanthroline<br>(phen) | Molar ratio 1:4,<br>triethylamine,<br>$\text{CH}_3\text{CN}$ ; <sup>[c]</sup> | [55] |

<sup>[a]</sup> prepared by carboxylic acid route, <sup>[b]</sup> prepared by ligand exchange, <sup>[c]</sup> prepared by non-hydrolytic route

In this work, zirconium oxo clusters were prepared following the ‘in situ’ approach by applying the non-aqueous sol-gel route. According to the mechanisms proposed by Sharp (Scheme 5, p.8), the clusters were formed by carefully operated hydrolysis and condensation reactions [50] of zirconium alkoxides in the presence of carboxylic acids (Scheme 6):



**Scheme 6:** Reactions involved in the formation of zirconium oxo clusters

In a first step, one or more alkoxides are substituted by a carboxylate group. The liberated alcohol undergoes an esterification reaction and produces water which, in turn, hydrolyzes a further part or all of the remaining alkoxide groups and is the source of the oxygen atoms and

hydroxo groups in the cluster. The cluster formed in this example is obtained because there is an optimal balance of charges and coordination numbers, 24 positive charges ( $6 \times \text{Zr}^{\text{IV}}$ ) and 48 coordination sites (each Zr is 8fold coordinated in this structure) are exactly balanced with 24 bidentate carboxylates, 4  $\mu_3\text{-O}$  and 4  $\mu_3\text{-OH}$ . By reducing the stoichiometric ratio between the metal alkoxide and the carboxylic acid, respectively, also the degree of substitution is different, leading to less water produced in an esterification reaction. Therefore, clusters with residual alkoxy groups are formed when the carboxylic acid to alkoxide ratio is low, and a high degree of substitution is achieved at a high carboxylic acid to alkoxide ratio [56].

### 3.1 Preparation of Zirconium Oxo Clusters

Two types of zirconium oxo clusters were obtained when  $\text{Zr}(\text{OBU})_4$  was reacted with various carboxylic acids. The general composition of the first type is  $\text{Zr}_6\text{O}_4(\text{OH})_4(\text{OOCR})_{12}$  (**Zr6**) (Figure 1) and was first reported when  $\text{Zr}(\text{OPr})_4$  was reacted with methacrylic acid in a 1 : 4 ratio [19].

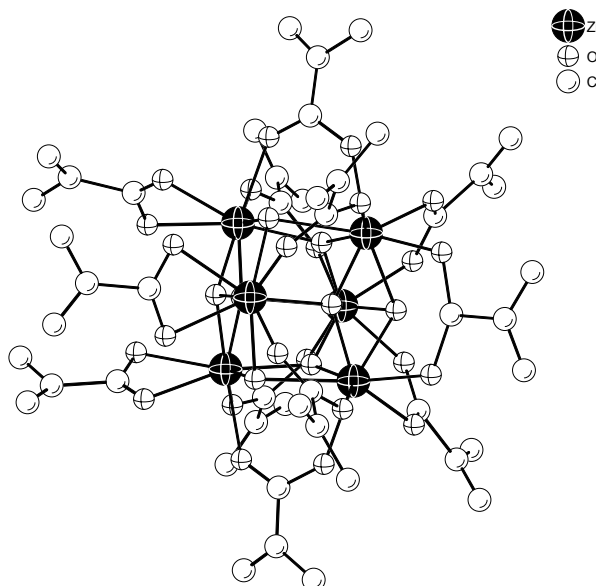


**Figure 1:** Molecular structure of  $\text{Zr}_6\text{O}_4(\text{OH})_4(\text{OMc})_{12}$ , hydrogen atoms are not shown

The structure consists of a  $\text{Zr}_6\text{O}_4(\text{OH})_4$  core in which the faces of the  $\text{Zr}_6$  octahedron are alternatively capped by  $\mu_3\text{-O}$  atoms and  $\mu_3\text{-OH}$  groups, and each zirconium atom is coordinated

by eight oxygen atoms. Three of twelve methacrylates act as chelating ligands at one triangular face, whereas 9 methacrylates bridge two neighbouring Zr atoms each.

The composition of the second cluster type is very similar to the first one, i.e. the  $\text{Zr}_6\text{O}_4(\text{OH})_4$  motif is retained. However, two carboxylate ligands opposite the chelated face do not bridge an edge of the  $\text{Zr}_6$  octahedron as in **Zr6**, but instead link two  $\text{Zr}_6$  cluster units (Figure 2). The  $\text{Zr}_{12}$  cluster can thus be considered as a dimer of **Zr6** in which two  $\text{Zr}_6$  sub-units are connected by four inter-cluster carboxylate bridges. This change of the coordination mode has only little effect on the geometric parameters of the cluster core and the remaining carboxylate ligands.

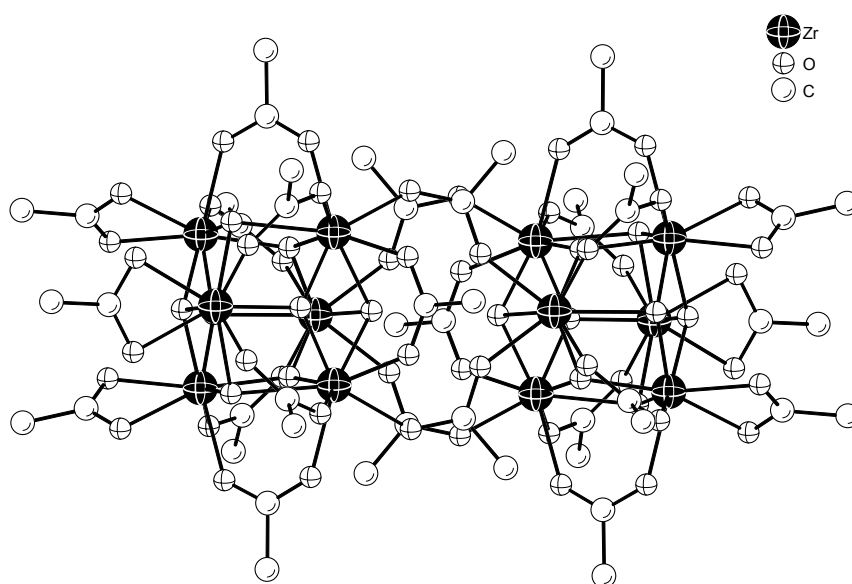


**Figure 2:** Molecular structure of  $\text{Zr}_{12}\text{O}_8(\text{OH})_8(\text{OAc})_{24}$ ; hydrogen atoms are not shown

### 3.1.1 $\text{Zr}_6\text{O}_4(\text{OH})_4(\text{OIsob})_{12}(\text{H}_2\text{O}) \cdot 3\text{HOIsob}$

Crystalline  $\text{Zr}_6\text{O}_4(\text{OH})_4(\text{OIsob})_{12}(\text{H}_2\text{O}) \cdot 3\text{HOIsob}$  (**Zr6-Isob**) was obtained when  $\text{Zr}(\text{O}i\text{Bu})_4$  in butanol (80% solution) was reacted with 7 equivalents of isobutyric acid ( $\text{HOIsob}$ ). The molecule consisted of a  $\text{Zr}_6\text{O}_4(\text{OH})_4$  core, three isobutyrate ligands were chelating and eight bridged two zirconium atoms each. The difference to the prototypical structure of **Zr6** was that one carboxylate ligand switched from a bridging position to a dangling mode opposite the  $\mu_3\text{-O}$  capped face of the  $\text{Zr}_6$  octahedron which was coordinated by chelating ligands [ $\text{Zr}(1)/\text{Zr}(2)/\text{Zr}(3)$ ]. The coordination site vacated by the change of hapticity of the carboxylate ligand was occupied

by a water molecule. This variation of the basic **Zr6** structure had been observed prior for  $\text{Zr}_6\text{O}_4(\text{OH})_4(\text{carboxylate})_{12}(\text{PrOH})$  for methacrylate and benzoate ligands [51] where propanol was coordinated instead of a water molecule. A long  $\text{Zr}(6)\text{-O}(81)$  distance of 224.7 pm excluded the possibility that the ligand was in fact anionic, i.e.  $\text{OH}^-$ . In this case, another ligand had to be protonated, which was excluded by the corresponding  $\text{Zr-O}$  bond length of the monodentate ligand [ $\text{Zr}(4)\text{-O}(63) = 212.5$  pm] which was as expected for anionic carboxylate ligands rather than coordinated carboxylic acids.

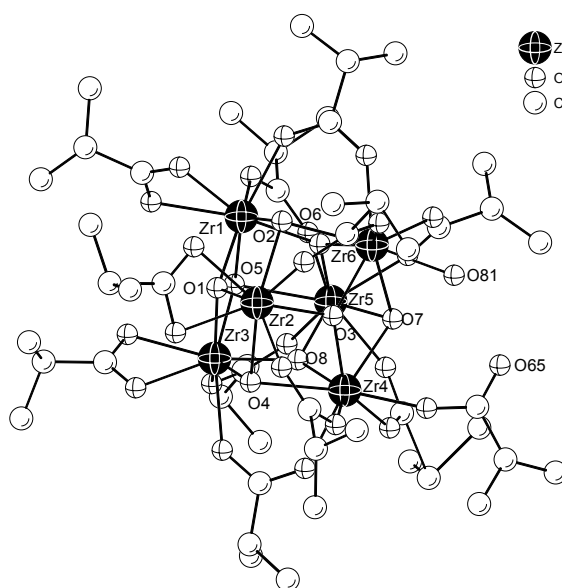


**Figure 3:** Molecular structure of  $\text{Zr}_6\text{O}_4(\text{OH})_4(\text{olsob})_{12}(\text{H}_2\text{O})$ ; hydrogen atoms are omitted for clarity

Judged from the bond lengths, the  $\text{Zr}(1)/\text{Zr}(2)/\text{Zr}(3)$ ,  $\text{Zr}(2)/\text{Zr}(4)/\text{Zr}(6)$ ,  $\text{Zr}(1)/\text{Zr}(5)/\text{Zr}(6)$  and  $\text{Zr}(3)/\text{Zr}(4)/\text{Zr}(5)$  triangles of the  $\text{Zr}_6$  octahedron were bridged by  $\mu_3$ -oxygen atoms, while the other triangles were bridged by  $\mu_3$ -OH groups (Table 2). The bond lengths for the  $\mu_3$ -hydroxo groups were not uniform but distorted, closer to a  $\mu_2$  than to a  $\mu_3$  bonding situation.

**Table 2:** Bond lengths for  $\mu_3$ -oxo atoms and  $\mu_3$ -hydroxo groups in **Zr6-Isob**

| $\mu_3\text{-O}$                                       |                            | $\mu_3\text{-OH}$                                      |                             |
|--|----------------------------|--|-----------------------------|
| $\text{O}(1) - \text{Zr}(1)/\text{Zr}(2)/\text{Zr}(3)$ | 205.0(8)/210.7(8)/211.6(9) | $\text{O}(2) - \text{Zr}(1)/\text{Zr}(2)/\text{Zr}(6)$ | 221.6(9)/221.0(10)/235.9(8) |
| $\text{O}(3) - \text{Zr}(2)/\text{Zr}(4)/\text{Zr}(6)$ | 203.2(8)/206.8(9)/207.1(8) | $\text{O}(4) - \text{Zr}(2)/\text{Zr}(3)/\text{Zr}(4)$ | 222.7(9)/220.8(8)/238.5(9)  |
| $\text{O}(6) - \text{Zr}(1)/\text{Zr}(5)/\text{Zr}(6)$ | 203.6(8)/202.8(8)/206.8(8) | $\text{O}(5) - \text{Zr}(2)/\text{Zr}(3)/\text{Zr}(5)$ | 222.3(8)/220.4(8)/239.1(8)  |
| $\text{O}(8) - \text{Zr}(3)/\text{Zr}(4)/\text{Zr}(5)$ | 203.3(7)/207.2(7)/203.1(7) | $\text{O}(7) - \text{Zr}(4)/\text{Zr}(5)/\text{Zr}(6)$ | 229.5(8)/239.1(8)/224.8(9)  |

From Figure 3 it might not be clear why exactly different modes in the coordination of the carboxylates were present since an all-bridging situation would be much closer to what one expected for a thermodynamic energy minimum. An explanation was given when looking at the hydrogen bond situation (Figure 4): The crystal lattice of **Zr6-Isob** contained three isobutyric acid molecules which were both hydrogen bonded to a  $\mu_3$ -OH group on the one hand and to one oxygen atom of a chelating ligand on the other hand. Furthermore, as denoted in the molecular structure above, the coordinated water molecule formed a hydrogen bridge with the dangling C=O group. Moreover, the second hydrogen atom of the water molecule was hydrogen bonded to the dangling C=O group of a second **Zr6-Isob** molecule which was in close neighbourhood in the crystal lattice. Therefore, this cluster might be considered as a 'quasi-dimeric' structure in the crystalline state rather than as a monomeric. The stabilization of a monodentate carboxylate ligand and a protic ligand occupying the vacated coordination site appeared to play a crucial role in the formation of the cluster, i.e. in the last step of Scheme 6 (p. 13) and has obviously been neglected for polynuclear complexes so far [57].

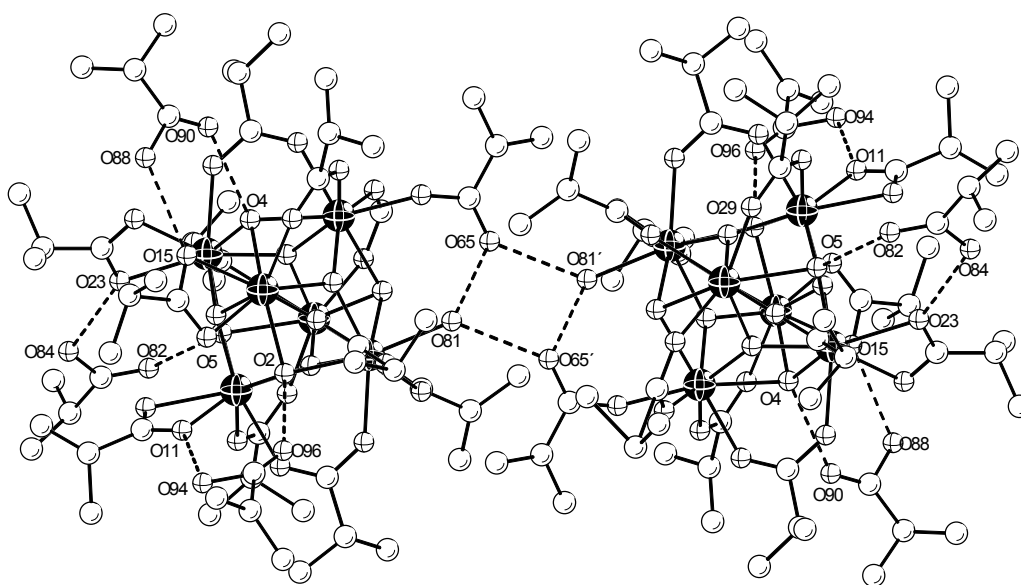


**Figure 4:** Hydrogen bond situation in **Zr6-Isob**

Bond lengths for isobutyric acids hydrogen bonded to the cluster are shown in Table 3. The similarity of the bond lengths between the hydroxy group of the acid to a carbonyl oxygen of the chelated ligands and the carbonyl oxygen of the acid and a  $\mu_3$ -hydroxo group was a proof for the strong acidity of the  $\mu_3$ -hydroxo groups, comparable to the carboxylic acid used ( $pK_a = 4.86$  [58]).

**Table 3:** Bond lengths for isobutyric acids hydrogen bonded to **Zr6-Isob**

| O-H – O [pm]  |          |               |          |               |           |
|---------------|----------|---------------|----------|---------------|-----------|
| O(82) – O(5)  | 274.5(2) | O(88) – O(15) | 259.7(2) | O(94) – O(11) | 267.9(10) |
| O(84) – O(23) | 265.7(2) | O(90) – O(4)  | 269.8(2) | O(96) – O(2)  | 272.6(2)  |

NMR spectroscopy was used to analyze the cluster in solution. It was shown previously that carboxylate ligands bonded to metal oxo clusters undergo mutual exchange in solution, this strategy was also used to exchange a certain carboxylate with another [53, 59-62].

The solvate molecules had to be removed prior measurements. To this end, the compound was dissolved in  $\text{CH}_2\text{Cl}_2$ , and volatiles were removed *in vacuo*. This process was repeated with toluene and once more with  $\text{CH}_2\text{Cl}_2$  as the solvents. The obtained solid was dried at room temperature at  $\sim 10^{-7}$  bar. Measurements were carried out in  $\text{CD}_2\text{Cl}_2$ .

The room temperature  $^1\text{H}$  NMR spectrum showed broad signals due to fast ligand exchange. Therefore, investigations were carried out at  $-80\text{ }^\circ\text{C}$  (Figure 5).

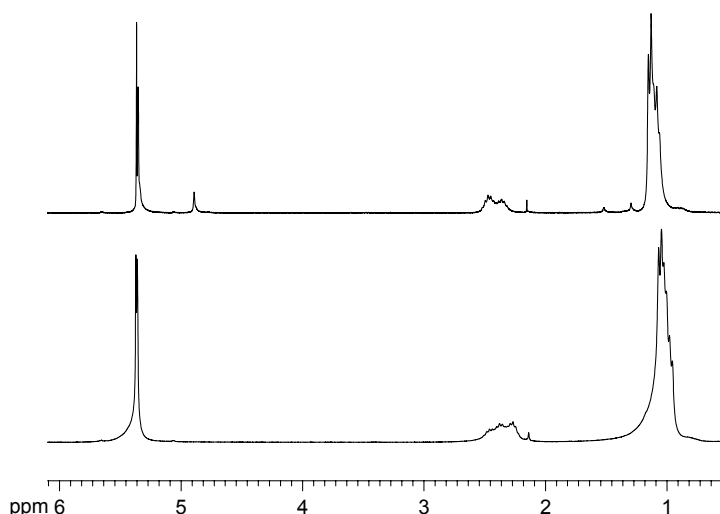


**Figure 5:**  $^1\text{H}$ -NMR spectrum of **Zr6-Isob** in  $\text{CD}_2\text{Cl}_2$ ; top: room temperature, bottom:  $-80\text{ }^\circ\text{C}$ ; OH not shown

The molecular symmetry of the **Zr6-Isob** molecule determined from the crystal structure was  $C_1$ , i.e. all ligands were inequivalent. At room temperature, only two resolved signal sets were observed in 2D NMR experiments ( $^1\text{H} / ^{13}\text{C}$ -HSQC and -HMBC). By cooling the solution to  $-80\text{ }^\circ\text{C}$ , a signal splitting occurred, and three different sets of ligand signals were resolved. This was in contradiction to a  $C_1$  symmetry, where twelve different sets of signals would have been

expected. Such pattern would be expected from a  $C_{3v}$  symmetry, the same as it was observed for the  $Zr_6O_4(OH)_4(OMc)_{12}$  cluster. Therefore, it was assumed that the dangling carboxylate became a bridging ligand in solution and liberated the coordinated water molecule. Figure 6 shows a section of a  $^1H / ^{13}C$ -HMBC spectrum which gives long range correlations from the protons to the carbonyl carbons. The carboxylate ligand at 195.9 ppm was tentatively assigned to chelating isobutyrate and the other two at 182.4 and 180.4 ppm, respectively, to bridging ligands (Table 4). This was in agreement with literature where  $^{13}C$ -NMR spectroscopy was employed to distinguish different binding modes of acetate groups in zinc complexes. Chelating modes were always found to be shifted downfield compared to bidentate or monodentate bridges (chelating > bidentate bridge > monodentate bridge) [63]. Moreover, the shift differences between chelating and bridging ligands in zirconium oxo clusters were always found to be in a range of  $\Delta \approx 15$  ppm [53].

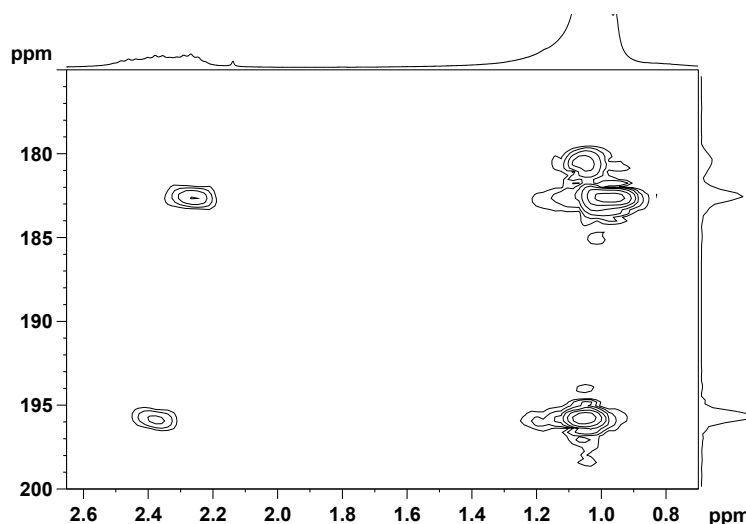


**Figure 6:** Section of a  $^1H / ^{13}C$  HMBC spectrum of **Zr6-Isob** in  $CD_2Cl_2$  at  $-80^\circ C$

**Table 4:**  $^1H / ^{13}C$  NMR chemical shifts [ppm] of the three non-equivalent isobutyrate ligands (Olsob 1-3) of  $Zr_6(OH)_4O_4(Olsob)_{12}$  in  $CD_2Cl_2$  at  $-80^\circ C$ . The labelling of the atoms is as follows:  $OOC^1C^2H(C^3H_3)_2$

|       | Olsob1      | Olsob2      | Olsob3      |
|-------|-------------|-------------|-------------|
| $C^1$ | - / 195.9   | - / 182.4   | - / 180.4   |
| $C^2$ | 2.37 / 35.0 | 2.25 / 35.9 | 2.46 / 33.7 |
| $C^3$ | 1.05 / 17.6 | 0.97 / 19.3 | 1.03 / 18.9 |
| -OH   | 11.55       |             |             |

### 3.1.2 $\text{Zr}_6\text{O}_4(\text{OH})_4(\text{OMc})_8(\text{OIsob})_4(\text{BuOH}) \cdot 4\text{HOOCR}$

When  $\text{Zr}(\text{OBU})_4$  was reacted with about 3.5 molar equivalents of methacrylic and isobutyric acid each, the crystalline mixed-carboxylate cluster  $\text{Zr}_6\text{O}_4(\text{OH})_4(\text{OMc})_8(\text{OIsob})_4(\text{BuOH}) \cdot 4\text{HOOCR}$  (**Zr6-McIsob**) was obtained (Figure 7). Due to the similarity of methacrylate and isobutyrate ligands, and because of disorder, the two kinds of ligands could not be distinguished in the single crystal structure analysis. Thus, the composition was derived from NMR data after removing the solvate molecules and the coordinated butanol. The difference to the prototypical structure of **Zr6** again was that one carboxylate ligand switched from a bridging position to a dangling mode opposite the  $\mu_3\text{-O}$  capped face of the  $\text{Zr}_6$  octahedron coordinated by chelating ligands [Zr(1)/Zr(2)/Zr(4)]. In contrast to the **Zr6-Isob** cluster, where the vacated coordination site was occupied by a water molecule, a coordinated butanol molecule was found in the **Zr6-McIsob** cluster. A long Zr(6)-O(73) distance of 228.7 pm excluded that the ligand was anionic (butoxy), the negative charge was balanced by the monodentate bonded carboxylate ligand [Zr(5)-O(67) distance = 217.3 pm]. Other structural features were as discussed in section 3.1.1.

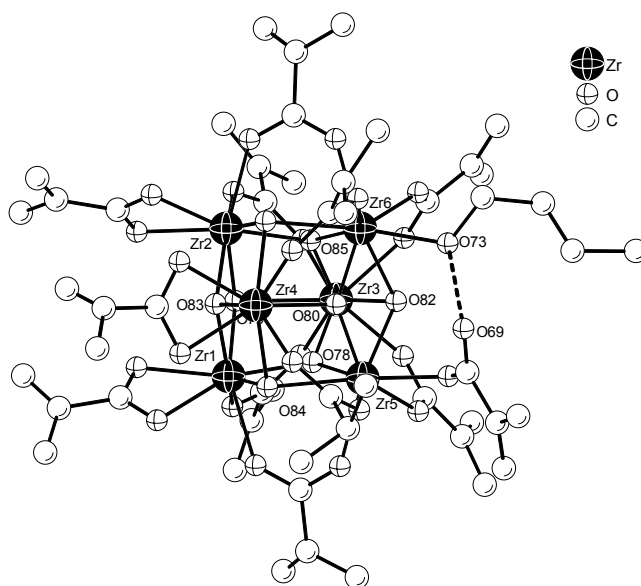


**Figure 7:** Molecular structure of  $\text{Zr}_6\text{O}_4(\text{OH})_4(\text{OMc})_8(\text{OIsob})_4(\text{BuOH})$ ; hydrogen atoms are omitted for clarity

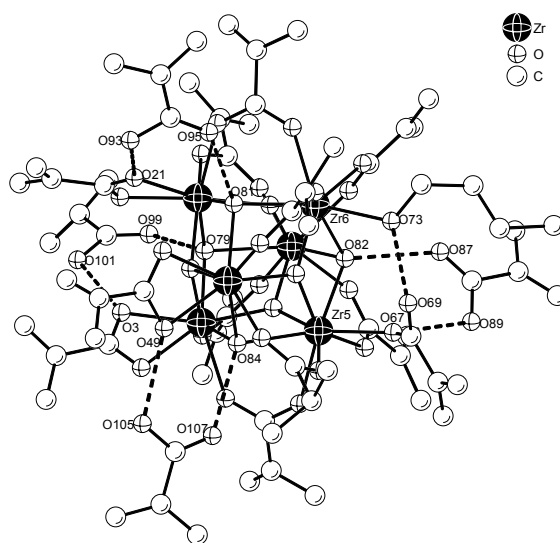
Bond lengths for  $\mu_3\text{-O}$  and  $\mu_3\text{-OH}$  groups are shown in Table 5. Judged therefrom, the Zr(1)/Zr(3)/Zr(5), Zr(4)/Zr(5)/Zr(6), Zr(1)/Zr(2)/Zr(4) and Zr(2)/Zr(3)/Zr(6) triangles of the  $\text{Zr}_6$  octahedron were bridged by  $\mu_3\text{-O}$  groups, while the other triangles were bridged by  $\mu_3\text{-OH}$  groups.



**Table 5:** Bond lengths for  $\mu_3$ -oxo atoms and  $\mu_3$ -hydroxo groups in **Zr6-Mclsob**

| $\mu_3$ -O                |                            | $\mu_3$ -OH               |                            |
|---------------------------|----------------------------|---------------------------|----------------------------|
| O(78) – Zr(1)/Zr(3)/Zr(5) | 204.3(5)/205.4(5)/204.5(5) | O(79) – Zr(1)/Zr(2)/Zr(3) | 220.7(5)/220.1(5)/241.9(5) |
| O(80) – Zr(4)/Zr(5)/Zr(6) | 203.9(5)/208.9(5)/207.0(5) | O(81) – Zr(2)/Zr(4)/Zr(6) | 222.7(5)/221.5(5)/234.9(5) |
| O(83) – Zr(1)/Zr(2)/Zr(4) | 210.0(5)/210.6(5)/209.5(5) | O(82) – Zr(3)/Zr(5)/Zr(6) | 233.2(5)/226.2(5)/225.5(5) |
| O(85) – Zr(2)/Zr(3)/Zr(6) | 203.4(5)/205.0(5)/204.8(5) | O(84) – Zr(1)/Zr(4)/Zr(5) | 222.1(5)/220.3(5)/236.9(5) |

The main difference between the **Zr6-Mclsob** and the **Zr6-Isob** cluster was found in the hydrogen bond situation: The butanol molecule in **Zr6-Mclsob** formed only one hydrogen bond [O(73)–O(69) = 263.2(1) pm] and the structure remained monomeric (Figure 8), whereas in **Zr6-Isob** the coordinated water molecule formed two hydrogen bonds. This situation was stabilized with another, fourth, carboxylic acid molecule which was both hydrogen bonded to a  $\mu_3$ -OH group, O(83), and the coordinated oxygen atom of the monodentate ligand, O(67). Bond lengths for carboxylic acids hydrogen-bonded to the cluster are given in Table 6.

**Figure 8:** Hydrogen bond situation in **Zr6-Mclsob****Table 6:** Bond lengths for carboxylic acids hydrogen-bonded to **Zr6-Mclsob**

| O-H - O [pm]  |          |               |          |                |          |
|---------------|----------|---------------|----------|----------------|----------|
| O(87) – O(82) | 276.3(1) | O(93) – O(21) | 277.5(1) | O(99) – O(79)  | 271.8(0) |
| O(89) – O(67) | 273.7(1) | O(95) – O(81) | 275.3(1) | O(101) – O(3)  | 272.2(0) |
|               |          |               |          | O(105) – O(49) | 270.8(1) |
|               |          |               |          | O(107) – O(84) | 275.6(1) |

After removal of the solvate molecules, the cluster was investigated by NMR spectroscopy. The room temperature  $^1\text{H}$  NMR spectrum in  $\text{CD}_2\text{Cl}_2$  showed broad signals for both the methacrylate and isobutyrate ligands, indicative of fast ligand exchange (Figure 9). Cooling the solution to  $-80\text{ }^\circ\text{C}$  resulted in four resolved sets for the methacrylate ligands and four for the isobutyrate ligands. No butanol signals were found in the spectrum, indicating that the monohapto carboxylate ligand was closed to a bridging bonding with concomitant elimination of butanol. The absence of butanol was further confirmed with a TOCSY experiment at  $-80\text{ }^\circ\text{C}$ .

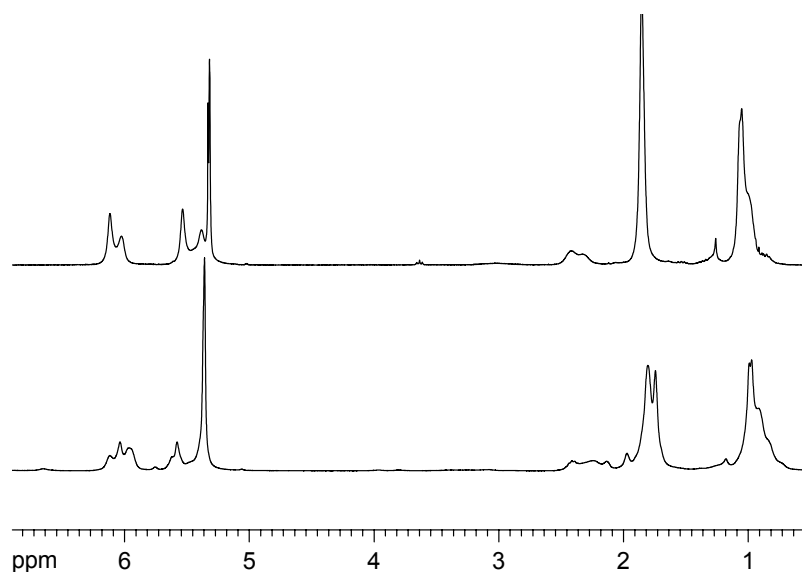


**Figure 9:**  $^1\text{H}$ -NMR spectrum of **Zr6-Mclsob** in  $\text{CD}_2\text{Cl}_2$ ; top: room temperature, bottom:  $-80\text{ }^\circ\text{C}$ ; OH not shown

The symmetry determined from the crystal structure was  $C_1$ , i.e. twelve sets of signals for the carboxylate ligands were expected in NMR experiments. After elimination of the butanol molecule the symmetry might be increased to  $C_{3v}$ . However, both types of ligands occupied chelating and bridging positions because of ligand exchange. Thus, a symmetry between  $C_1$  and  $C_{3v}$  was possible.

Cooling the solution to  $-80\text{ }^\circ\text{C}$  resulted in four resolved sets of signals for the methacrylate and isobutyrate ligands, respectively (Figure 10).  $^1\text{H}$  and  $^{13}\text{C}$  NMR spectroscopic shifts for the different ligands in **Zr6-Mclsob** are given in Table 7. Both types of ligands occupied chelating and bridging positions in the cluster, the carbonyl carbon signals at 183.7 and 183.5 ppm for the methacrylate and 195.5 ppm for the isobutyrate ligands, respectively, were tentatively assigned to the chelating mode, the bridging ligands were found upfield shifted by about 15 ppm.

Next to signals stemming from the methacrylate and isobutyrate ligands, several signals were detected in the  $^1\text{H}$  NMR spectrum at  $-80\text{ }^\circ\text{C}$  which did not show correlations in HMBC and HSQC experiments. They were tentatively assigned as OH.

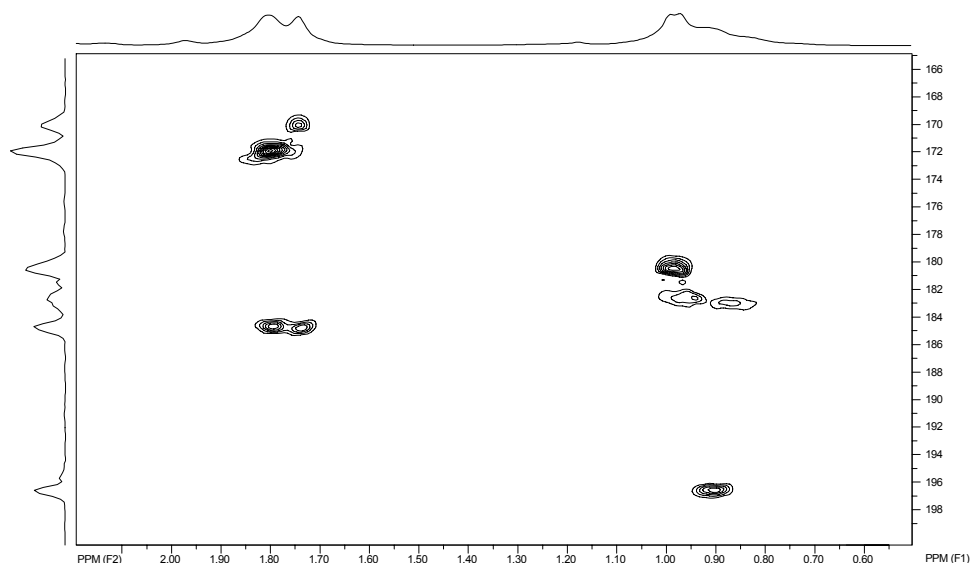


**Figure 10:**  $^1\text{H} / ^{13}\text{C}$  HMBC spectrum of **Zr6-Mclsob** in  $\text{CD}_2\text{Cl}_2$  at  $-80\text{ }^\circ\text{C}$

**Table 7:**  $^1\text{H} / ^{13}\text{C}$  NMR chemical shifts [ppm] of the four non-equivalent methacrylate (OMc1-4) and isobutyrate ligands (Olsob1-4) of **Zr6-Mclsob** in  $\text{CD}_2\text{Cl}_2$  at  $-80\text{ }^\circ\text{C}$ . The labelling of the atoms is as follows:  $\text{OOC}^1\text{C}^2(\text{C}^4\text{H}_3)=\text{C}^3\text{H}_2$  and  $\text{OOC}^1\text{C}^2\text{H}(\text{C}^3\text{H}_3)_2$

|               | $\text{C}^1$            | $\text{C}^2$ | $\text{C}^3$       | $\text{C}^4$ |
|---------------|-------------------------|--------------|--------------------|--------------|
| <b>OMc1</b>   | - / 183.7               | - / 135.2    | 6.03, 5.54 / 125.9 | 1.73 / 17.4  |
| <b>OMc2</b>   | - / 183.5               | - / 136.2    | 6.10, 5.57 / 123.4 | 1.78 / 17.9  |
| <b>OMc3</b>   | - / 170.9               | - / 138.4    | 5.92, 5.33 / 123.2 | 1.79 / 17.9  |
| <b>OMc4</b>   | - / 168.8               | - / 135.2    | 6.03, 5.54 / 125.9 | 1.73 / 17.4  |
| <b>Olsob1</b> | - / 195.5               | 2.28 / 34.9  | 0.89 / 17.4        | -            |
| <b>Olsob2</b> | - / 182.0               | 2.20 / 35.0  | 0.85 / 18.2        | -            |
| <b>Olsob3</b> | - / 181.5               | 2.28 / 34.9  | 0.93 / 17.8        | -            |
| <b>Olsob4</b> | - / 179.4               | 2.37 / 32.5  | 0.97 / 17.8        | -            |
| <b>OH</b>     | 11.36, 8.08, 7.94, 6.61 |              |                    |              |

### 3.1.3 $\text{Zr}_6\text{O}_4(\text{OH})_4(5\text{-Norbornene-2-carboxylate})_{12}$

The use of bicyclic compounds possessing unsaturated bonds, such as norbornene and its derivatives, allows access to ring opening metathesis polymerization (ROMP). Metathesis polymerization has attracted considerable attention in the last years due to the development of well-defined polymers with controlled architectures, molecular weights, polydispersities and terminal functionalities [64]. As a consequence, many monomers are readily available, such as 5-norbornene-2-carboxylic acid (bicyclo[2.2.1]hept-5-ene-2-carboxylic acid), which was used in a first attempt to prepare zirconium oxo clusters.

#### $\text{Zr}_6\text{O}_4(\text{OH})_4(\text{ONorb}_{\text{mix}})_{12} \cdot 3\text{HONorb}_{\text{mix}}$

When  $\text{Zr}(\text{OBU})_4$  was reacted with 7 equivalents of 5-norbornene-2-carboxylic acid (enantiomeric and isomeric mixture of 81% endo and 19% exo acid, 'HONorb<sub>mix</sub>'), the crystalline cluster  $\text{Zr}_6\text{O}_4(\text{OH})_4(\text{ONorb}_{\text{mix}})_{12} \cdot 3\text{HONorb}_{\text{mix}}$  (**Zr6-Norb<sub>mix</sub>**) was obtained in quantitative yields within three weeks. Due to the use of isomeric and enantiomeric acids, the ligands showed strong disorder in the crystal structure and a clear assignment of endo and exo ligands was not possible (Figure 11). A determination of the endo/exo ratio by NMR spectroscopy was not possible either because of broad and overlapping signals in the  $^1\text{H}$  spectra.

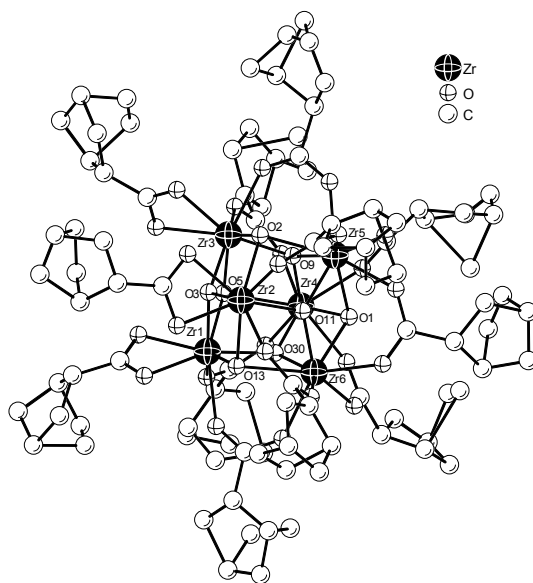


**Figure 11:** Molecular structure of  $\text{Zr}_6\text{O}_4(\text{OH})_4(\text{ONorb}_{\text{mix}})_{12}$ ; hydrogen atoms are omitted for clarity

The molecule consisted of a  $Zr_6$  core where the faces were alternatively capped with  $\mu_3$ -oxo atoms and  $\mu_3$ -hydroxo groups. Three ligands were in a chelating mode and were stabilized with hydrogen bonded solvate acids, the other nine carboxylates bridged two neighbouring Zr atoms each. Thus, this structure showed exactly the same features as the prototypical **Zr6** cluster.

According to the bond lengths, the Zr(1)/Zr(3)/Zr(4), Zr(1)/Zr(2)/Zr(6), Zr(2)/Zr(3)/Zr(5) and Zr(4)/Zr(5)/Zr(6) triangles of the  $Zr_6$  octahedron were bridged by  $\mu_3$ -hydroxo groups, while the other triangles, Zr(1)/Zr(2)/Zr(3), Zr(1)/Zr(4)/Zr(6), Zr(2)/Zr(5)/Zr(6) and Zr(3)/Zr(4)/Zr(5), were capped by  $\mu_3$ -O atoms (Table 8).

**Table 8:** Bond lengths for  $\mu_3$ -oxo atoms and  $\mu_3$ -hydroxo groups in **Zr6-Norb<sub>mix</sub>**

| $\mu_3$ -O                |                            | $\mu_3$ -OH               |                            |
|---------------------------|----------------------------|---------------------------|----------------------------|
| O(3) – Zr(1)/Zr(2)/Zr(3)  | 210.8(4)/209.5(4)/208.9(4) | O(5) – Zr(1)/Zr(3)/Zr(4)  | 220.6(5)/221.6(5)/236.5(5) |
| O(30) – Zr(1)/Zr(4)/Zr(6) | 203.5(4)/206.4(4)/204.7(4) | O(13) – Zr(1)/Zr(2)/Zr(6) | 221.1(5)/220.2(4)/242.1(5) |
| O(11) – Zr(2)/Zr(5)/Zr(6) | 203.3(4)/206.2(4)/204.7(4) | O(2) – Zr(2)/Zr(3)/Zr(5)  | 220.4(5)/221.5(4)/241.0(4) |
| O(9) – Zr(3)/Zr(4)/Zr(5)  | 203.1(4)/205.8(4)/205.2(4) | O(1) – Zr(4)/Zr(5)/Zr(6)  | 227.2(5)/226.9(5)/226.5(5) |

As obvious from Table 8, the bond lengths for the  $\mu_3$ -hydroxo groups were not uniform. For the hydroxo groups, which were additionally hydrogen bonded to solvate acids, the bonding situation was closer to a  $\mu_2$  than to a  $\mu_3$  situation, whereas the non-hydrogen bonded hydroxo group, O(1), showed symmetric bond lengths to Zr(4)/Zr(5)/Zr(6).

The hydrogen bond situation is shown in Figure 12. In contrast to the examples described before, viz **Zr6-Isob** and **Zr6-McIsob**, the three solvate molecules were not bonded symmetrically to the  $\mu_3$ -OH group and one oxygen atom of a chelating ligand each, but one chelating ligand was stabilized by two acids [O(22) – O(34), O(10) – O(38)]. As a consequence, one acid became distorted because the hydrogen bridge was shared with the chelating ligand showing no or little hydrogen bonding [O(34) – O(29)] (Table 9).

**Table 9:** Bond lengths for carboxylic acids hydrogen-bonded to **Zr6-Norb<sub>mix</sub>**

| O-H – O [pm]  |          |               |          |               |          |
|---------------|----------|---------------|----------|---------------|----------|
| O(5) – O(33)  | 274.7(0) | O(13) – O(35) | 282.1(1) | O(2) – O(37)  | 278.3(1) |
| O(22) – O(34) | 275.8(0) | O(24) – O(36) | 258.7(1) | O(10) – O(38) | 272.3(1) |
| O(29) – O(34) | 292.4(1) |               |          |               |          |

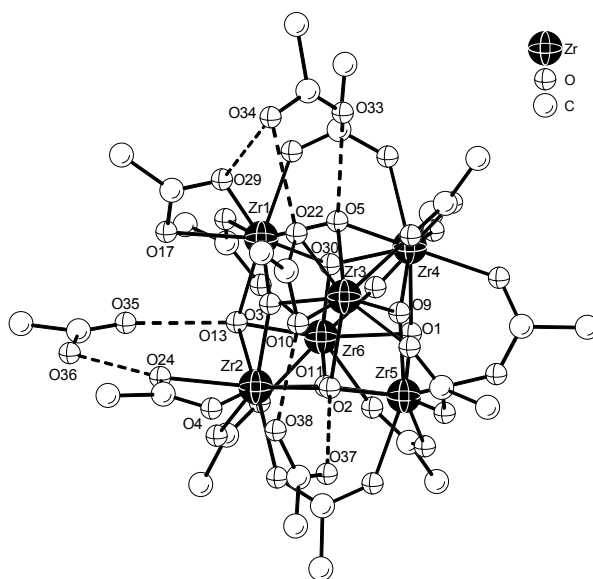


**Figure 12:** Hydrogen bond situation in **Zr6-Norb<sub>mix</sub>**; acetate ligands are shown instead of norbornene carboxylates for purposes of clarity

The solvate acids had to be removed. Since norbornene carboxylic acid has a boiling point of  $\sim 270\text{ }^{\circ}\text{C}$  it could not be removed as a volatile compound. Thus, a precipitation process was applied: The cluster was dissolved in  $\text{CH}_2\text{Cl}_2$  and double the volume of n-heptane was added. About 3/4 of the solvents was removed carefully *in vacuo* until the cluster precipitated from the solution, which additionally cooled because of solvent evaporation. After sedimentation, the less volatile solvent (n-heptane) was decanted and the solid was washed with n-heptane. This procedure was repeated once, after that the solid was washed with n-heptane and dried *in vacuo*.

Figure 13 shows the  $^1\text{H}$  NMR spectra of **Zr6-Norb<sub>mix</sub>** in  $\text{CD}_2\text{Cl}_2$  at room temperature and at  $-80\text{ }^{\circ}\text{C}$ . Next to the signals stemming from the cluster, additional signals were identified as the butyl ester of the corresponding acid (n-butyl-5-norbornene-2-carboxylate) which was formed as a by-product in cluster synthesis and could not be removed fully with the precipitation and washing processes.

The symmetry of the cluster in the crystalline state was  $C_1$ , i.e. twelve inequivalent signals for the carboxylates were expected in NMR experiments when the symmetry was retained in solution. In principle,  $C_{3v}$  symmetry was possible when considering all ligands as acetates. However, the use of enantiomeric acids in the cluster preparation led to diastereomers. Thus, the highest symmetry observable was  $C_{3v}$ , many signals were possible for the diastereomers. 2D NMR experiments (COSY, TOCSY, HSQC and HMBC) revealed only one set of signals for the norbornene carboxylates. When the solution was cooled to  $-80\text{ }^{\circ}\text{C}$  the signals broadened, but again only one set of signals was observed in the NMR experiments (Table 10).

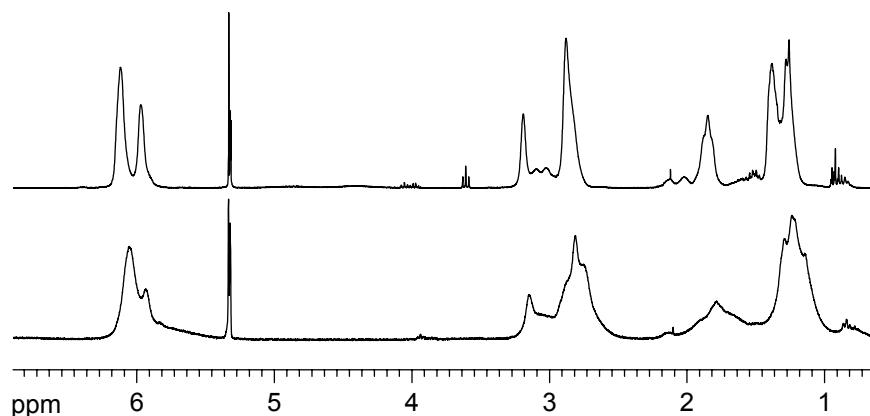


**Figure 13:**  $^1\text{H}$  NMR spectrum of **Zr6-Norb<sub>mix</sub>** in  $\text{CD}_2\text{Cl}_2$ ; top: room temperature, bottom:  $-80\text{ }^\circ\text{C}$ ; OH not shown

**Table 10:**  $^1\text{H}$  /  $^{13}\text{C}$  NMR chemical shifts [ppm] of the norbornene carboxylate ligands of **Zr6-Norb<sub>mix</sub>** in  $\text{CD}_2\text{Cl}_2$  at room temperature and  $-80\text{ }^\circ\text{C}$

|                      | RT                | $^1\text{H}$ / $^{13}\text{C}$ | $-80\text{ }^\circ\text{C}$ $^1\text{H}$ / $^{13}\text{C}$ | Labelling |
|----------------------|-------------------|--------------------------------|--|-----------|
| <b>C<sup>1</sup></b> | 3.22 / 45.6       |                                | 3.14 / 44.7  |           |
| <b>C<sup>2</sup></b> | 2.87 / 45.8       |                                | 2.81 / 41.7  |           |
| <b>C<sup>3</sup></b> | 1.90, 1.33 / 29.5 |                                | 1.79, 1.28 / 28.1  |           |
| <b>C<sup>4</sup></b> | 2.87 / 42.6       |                                | 2.81 / 41.6  |           |
| <b>C<sup>5</sup></b> | 6.13 / 138.0      |                                | 6.06 / 136.9   |           |
| <b>C<sup>6</sup></b> | 5.97 / 132.7      |                                | 5.93 / 132.1   |           |
| <b>C<sup>7</sup></b> | 1.42, 1.32 / 49.4 |                                | 1.37, 1.22 / 48.6  |           |
| <b>C<sup>8</sup></b> | - / 180.2         |                                | n.d.*  |           |
| <b>OH</b>            | 10.55             |                                | 11.8, 6.9  |           |

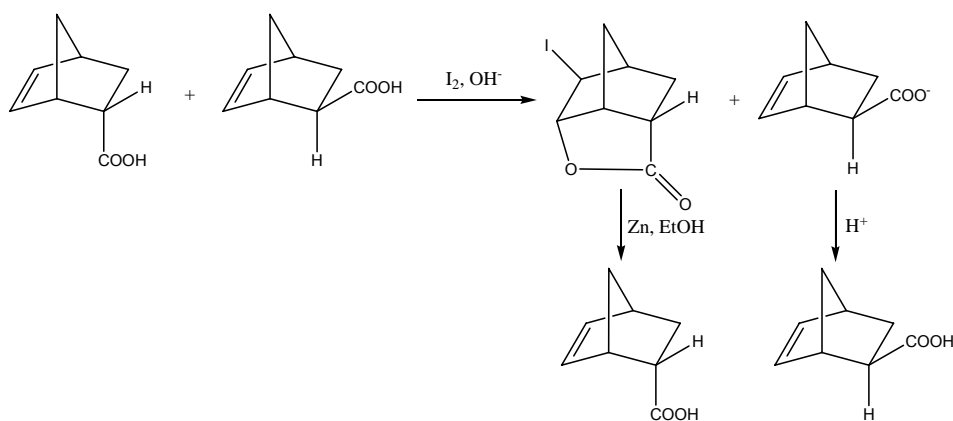
\* not detected

In order to obtain crystal structures with better defined ligands, pure endo and exo isomers were applied in cluster syntheses. Unfortunately, these isomers were not commercially available and thus had to be separated. For the separation of these isomers chemical ways were necessary, namely lactonization methods, because crystallization and distillation were insufficient.

Generally, lactonization can be carried out by several synthetic routes:

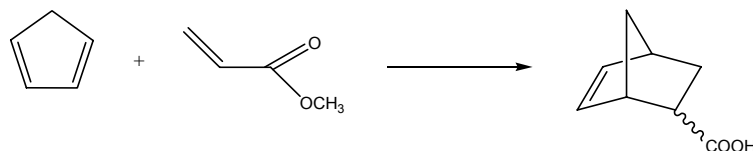
- Treatment with cold sulphuric acid [65] leads to rearrangements of the ring and thus new isomers are produced [66].
- Bromination forms the desired lactone, but the reaction is very fast and again leads to rearrangements. Moreover, the exo isomer reacts to a dibromo product which must be reduced again [67].
- Iodolactonization is the mildest procedure reported to obtain a lactone from the endo isomer, the exo isomer remains unaffected [68].

The latter method was favoured and iodolactonization of endo-5-norbornene-2-carboxylic acid was carried out modifying somewhat the procedures described in literature [69-71] (Scheme 7).



**Scheme 7:** Iodolactonization of 5-norbornene-2-carboxylic acid in basic medium

Judged from  $^1\text{H}$  NMR spectra, the reaction gave 100 % pure endo and exo products. However, the yield for the endo-product was rather poor (~30 %). Therefore, 5-norbornene-2-carboxylic acid was prepared in higher amounts by reaction of freshly cracked cyclopentadiene with methyl acrylate [72]. The reaction was almost quantitative with the expected dominance of the endo product [73]. The following endo/exo separation was carried out as described above resulting in comparable yields.



**Scheme 8:** Diels-Alder cycloaddition of cyclopentadiene and methyl acrylate



$$\text{Zr}_6\text{O}_4(\text{OH})_4(\text{ONorb}_{\text{endo}})_{12} \cdot 3\text{HONorb}_{\text{endo}}$$

Reaction of 7 equivalents of endo-5-norbornene-2-carboxylic acid with  $\text{Zr}(\text{O}i\text{Bu})_4$  resulted in the crystalline cluster  $\text{Zr}_6\text{O}_4(\text{OH})_4(\text{ONorb}_{\text{endo}})_{12} \cdot 3\text{HONorb}_{\text{endo}}$  (**Zr6-Norb<sub>endo</sub>**) in quantitative yields. The molecular structure had the same features as described above for **Zr6-Norb<sub>mix</sub>**: The zirconium atoms formed an octahedron and the faces were alternatively capped with  $\mu_3\text{-O}$  atoms and  $\mu_3\text{-OH}$  groups, respectively. Three norbornene carboxylate ligands were chelating and the other nine bridged two neighbouring Zr atoms each. The ligands in the crystal structure (Figure 14) were again strongly disordered because of the use of enantiomeric acids.

The Zr(1)/Zr(3)/Zr(5), Zr(1)/Zr(4)/Zr(6), Zr(2)/Zr(3)/Zr(4) and Zr(2)/Zr(5)/Zr(6) triangles of the  $\text{Zr}_6$  octahedron were bridged by  $\mu_3\text{-hydroxo}$  groups, while the other triangles, Zr(1)/Zr(3)/Zr(4), Zr(1)/Zr(5)/Zr(6), Zr(2)/Zr(3)/Zr(5) and Zr(2)/Zr(4)/Zr(6), were bridged by  $\mu_3\text{-O}$  atoms (Table 11).

**Table 11:** Bond lengths for  $\mu_3\text{-oxo}$  atoms and  $\mu_3\text{-hydroxo}$  groups in **Zr6-Norb<sub>endo</sub>**

| $\mu_3\text{-O}$         |                            |  | $\mu_3\text{-OH}$        |                            |  |
|--------------------------|----------------------------|--|--------------------------|----------------------------|--|
| O(2) – Zr(1)/Zr(3)/Zr(4) | 209.5(4)/209.6(4)/211.0(5) |  | O(1) – Zr(2)/Zr(3)/Zr(4) | 239.7(4)/223.0(5)/220.4(4) |  |
| O(5) – Zr(1)/Zr(5)/Zr(6) | 202.8(4)/205.5(4)/206.1(4) |  | O(3) – Zr(1)/Zr(3)/Zr(5) | 220.5(4)/221.2(4)/242.1(4) |  |
| O(6) – Zr(2)/Zr(3)/Zr(5) | 205.5(4)/203.4(4)/206.4(4) |  | O(4) – Zr(1)/Zr(4)/Zr(6) | 220.8(5)/220.9(4)/236.2(4) |  |
| O(8) – Zr(2)/Zr(4)/Zr(6) | 205.4(4)/202.5(4)/206.5(4) |  | O(7) – Zr(2)/Zr(5)/Zr(6) | 226.2(4)/227.0(5)/226.0(4) |  |

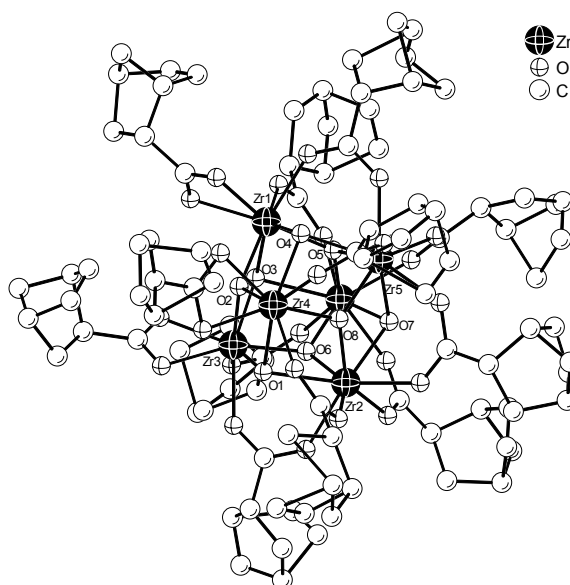


**Figure 14:** Molecular structure of  $\text{Zr}_6\text{O}_4(\text{OH})_4(\text{ONorb}_{\text{endo}})_{12}$ ; hydrogen atoms are omitted for clarity

The hydrogen bond situation is shown in Figure 15. The three solvate molecules were both hydrogen bonded to an oxygen atom of a chelating ligand and a  $\mu_3$ -OH group each (Table 12). This bonding situation was the reason why the Zr -  $\mu_3$ -OH bond lengths in the Zr(1)/Zr(3)/Zr(5), Zr(1)/Zr(4)/Zr(6) and Zr(2)/Zr(3)/Zr(4) triangles were closer to a  $\mu_2$  situation than to a  $\mu_3$ . The remaining, fourth  $\mu_3$ -OH group, O(7), showed uniform distances to the neighbouring Zr atoms (Table 12).

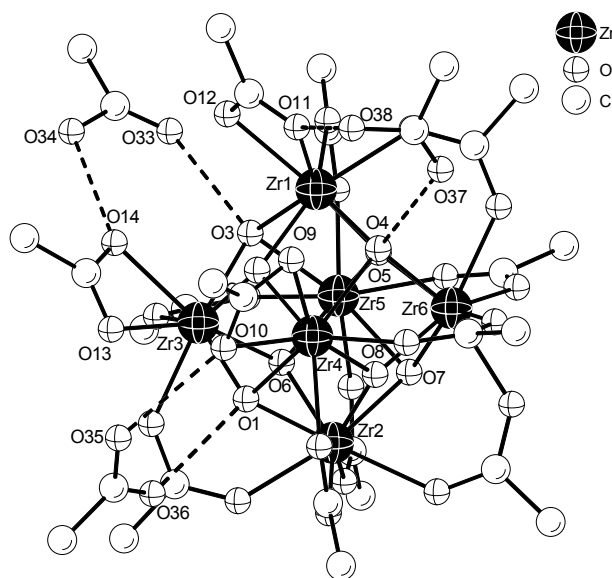


**Figure 15:** Hydrogen bond situation in **Zr6-Norb<sub>endo</sub>**; acetate ligands are shown instead of norbornene carboxylates for purposes of clarity

**Table 12:** Bond lengths for carboxylic acids hydrogen-bonded to **Zr6-Norb<sub>endo</sub>**

| O-H – O [pm]  |          |               |          |               |          |
|---------------|----------|---------------|----------|---------------|----------|
| O(33) – O(3)  | 282.1(1) | O(35) – O(10) | 269.1(1) | O(37) – O(4)  | 275.8(0) |
| O(34) – O(14) | 264.6(1) | O(36) – O(1)  | 279.4(1) | O(38) – O(11) | 285.7(1) |

For NMR investigations, the solvate acids were removed by a precipitation process. The symmetry of the cluster determined from the crystalline state was  $C_1$ . The highest symmetry possible in the liquid state was  $C_{3v}$  as it was discussed above for the **Zr6-Norb<sub>mix</sub>** cluster.  $^1\text{H}$  NMR spectra of **Zr6-Norb<sub>endo</sub>** are shown in Figure 16. The signals at room temperature were broad and unresolved and only one set of signals was observed. Additionally, n-butyl-ester was present which was formed as a by-product during cluster formation and could not be removed in the purification steps. Cooling the solution to  $-80\text{ }^\circ\text{C}$  resulted in further broadening of the signals

and again only one set of signals was observed. The signals (Table 13) were assigned with the help of COSY, TOCSY, HSQC, and HMBC experiments. The OH signal at room temperature was very broad and appeared at ~10.2 ppm, it sharpened when the solution was cooled to -80 °C and shifted to 11.7 ppm. Additionally, a second signal was observed at 6.9 ppm which did not show correlations in 2D experiments and was assigned as OH.

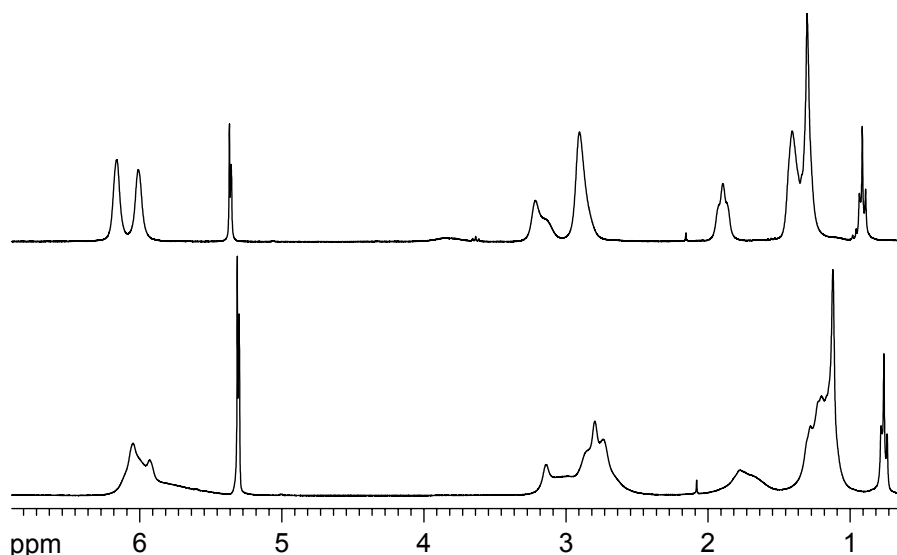


**Figure 16:**  $^1\text{H}$  NMR spectrum of **Zr6-Norb<sub>endo</sub>** in  $\text{CD}_2\text{Cl}_2$ ; top: room temperature, bottom: -80 °C; OH not shown

**Table 13:**  $^1\text{H}$  /  $^{13}\text{C}$  NMR chemical shifts of **Zr6-Norb<sub>endo</sub>** at room temperature and -80 °C in  $\text{CD}_2\text{Cl}_2$

|                      | RT | $^1\text{H}$ / $^{13}\text{C}$ | -80 °C $^1\text{H}$ / $^{13}\text{C}$ | Labelling |
|----------------------|----|--------------------------------|---------------------------------------|-----------|
| <b>C<sup>1</sup></b> |    | 3.18 / 45.4                    | 3.15 / 44.7                           |           |
| <b>C<sup>2</sup></b> |    | 2.84 / 45.5                    | 2.75 / 45.4                           |           |
| <b>C<sup>3</sup></b> |    | 1.86, 1.34 / 29.4              | 1.84, 1,34 / 28.8                     |           |
| <b>C<sup>4</sup></b> |    | 2.86 / 42.4                    | 2.81 / 41.8                           |           |
| <b>C<sup>5</sup></b> |    | 6.12 / 138.8                   | 6.06 / 136.9                          |           |
| <b>C<sup>6</sup></b> |    | 5.97 / 132.9                   | 5.94 / 132.1                          |           |
| <b>C<sup>7</sup></b> |    | 1.37, 1.25 / 49.2              | n.r. *, 1.27 / 49.4                   |           |
| <b>C<sup>8</sup></b> |    | 180.2                          | 179.4                                 |           |
| <b>OH</b>            |    | 10.18                          | 11.68, 6.91                           |           |

\* n.r. = not resolved

$$\text{Zr}_6\text{O}_4(\text{OH})_4(\text{ONorb}_{\text{exo}})_{12}(\text{BuOH}) \cdot 3\text{HONorb}_{\text{exo}}$$

$\text{Zr}_6\text{O}_4(\text{OH})_4(\text{ONorb}_{\text{exo}})_{12}(\text{BuOH}) \cdot 3\text{HONorb}_{\text{exo}}$  (**Zr6-Norb<sub>exo</sub>**) was obtained when  $\text{Zr}(\text{OBu})_4$  was reacted with seven equivalents of *exo*-5-norbornene-2-carboxylic acid. In contrast to the clusters prepared with an *endo*/*exo* mixture or pure *endo* acid, the structure did not show a ‘symmetric’ behaviour of the bridging ligands, but one ligand switched to a monohapto mode and the free coordination site was occupied with a coordinated butanol molecule (Figure 17) as described for the **Zr6-Mclsob** cluster. A long  $\text{Zr}(6)\text{-O}(25)$  distance of 228.7 pm excluded that the ligand was anionic (butoxy), the negative charge was balanced by the monodentate bonded carboxylate ligand [ $\text{Zr}(5)\text{-O}(23)$  distance = 217.3 pm]. Other structural features were as described in previous sections: Six zirconium atoms formed an octahedron and the faces were alternatively capped with  $\mu_3\text{-O}$  atoms or  $\mu_3\text{-OH}$  groups (Table 14).

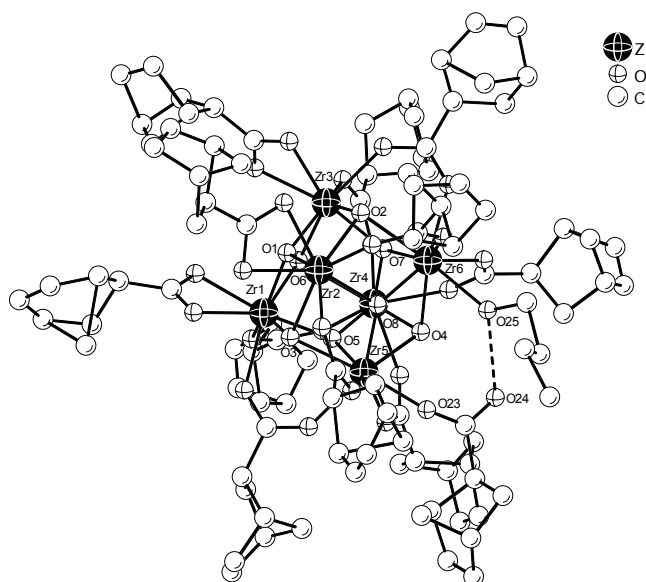


**Figure 17:** Molecular structure of  $\text{Zr}_6\text{O}_4(\text{OH})_4(\text{ONorb}_{\text{exo}})_{12}(\text{BuOH})$ ; hydrogen atoms are omitted for clarity

**Table 14:** Bond lengths for  $\mu_3\text{-oxo}$  atoms and  $\mu_3\text{-hydroxo}$  groups in **Zr6-Norb<sub>exo</sub>**

| $\mu_3\text{-O}$                                       |                            | $\mu_3\text{-OH}$                                      |                            |
|--|----------------------------|--|----------------------------|
| $\text{O}(1) - \text{Zr}(1)/\text{Zr}(2)/\text{Zr}(3)$ | 210.3(6)/209.0(6)/209.3(6) | $\text{O}(3) - \text{Zr}(1)/\text{Zr}(2)/\text{Zr}(5)$ | 221.1(6)/223.6(6)/236.8(6) |
| $\text{O}(5) - \text{Zr}(1)/\text{Zr}(4)/\text{Zr}(5)$ | 204.3(6)/202.8(6)/206.8(6) | $\text{O}(6) - \text{Zr}(1)/\text{Zr}(3)/\text{Zr}(4)$ | 218.4(6)/220.0(6)/242.7(6) |
| $\text{O}(8) - \text{Zr}(2)/\text{Zr}(5)/\text{Zr}(6)$ | 204.7(5)/208.4(6)/205.4(6) | $\text{O}(2) - \text{Zr}(2)/\text{Zr}(3)/\text{Zr}(6)$ | 219.2(6)/222.5(7)/237.1(6) |
| $\text{O}(7) - \text{Zr}(3)/\text{Zr}(4)/\text{Zr}(6)$ | 204.0(6)/205.7(6)/205.3(6) | $\text{O}(4) - \text{Zr}(4)/\text{Zr}(5)/\text{Zr}(6)$ | 236.4(6)/225.5(6)/229.0(6) |

As expected, the three solvate acids formed hydrogen bonds with a  $\mu_3$ -OH group and an oxygen atom of a chelated carboxylate each (Table 15). Additionally, the butanol molecule formed a hydrogen bond with the monohapto bonded carboxylate [O(24) - O(25) = 268.0(8) pm].

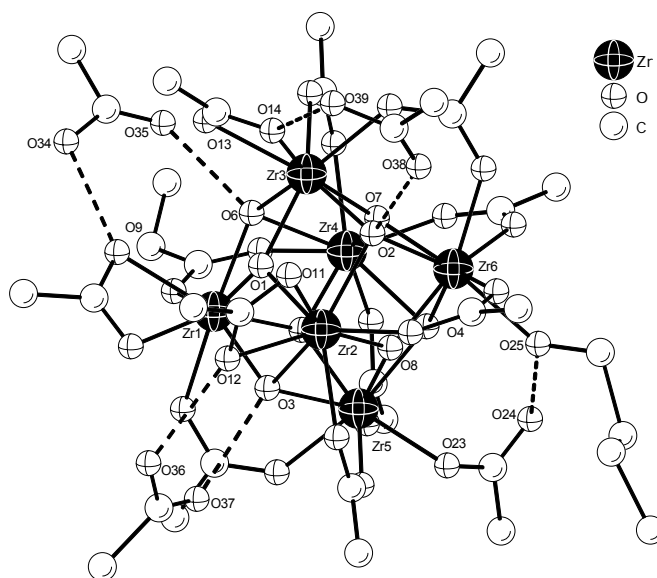


**Figure 18:** Hydrogen bond situation in **Zr6-Norb<sub>exo</sub>**; norborneate ligands are shown as acetates for clarity

**Table 15:** Bond lengths for carboxylic acids and butanol hydrogen-bonded to **Zr6-Norb<sub>exo</sub>**

| O-H – O [pm] |          |               |          |               |          |
|--------------|----------|---------------|----------|---------------|----------|
| O(34) – O(9) | 262.4(7) | O(36) – O(12) | 261.2(1) | O(38) – O(2)  | 273.3(1) |
| O(35) – O(6) | 276.2(5) | O(37) – O(3)  | 273.2(1) | O(39) – O(14) | 262.7(9) |

The solvate acids were removed by a precipitation process for NMR investigations. The room temperature  $^1\text{H}$  NMR spectrum (Figure 19) showed broad signals and in 2D experiments (COSY, TOCSY, HSQC, HMBC) only one set of signals for cluster-bonded norbornene carboxylates was detected. Next to the signals stemming from the carboxylates, also n-butyl ester was observed, but no butanol could be identified in a TOCSY experiment. This indicated that the monohapto ligand was closed with elimination of butanol, as it was the case for the **Zr6-McIsob** cluster. The assignment of the signals is shown in Table 16.



**Figure 19:**  $^1\text{H}$  NMR spectrum of **Zr6-Norb<sub>exo</sub>** in  $\text{CD}_2\text{Cl}_2$  at room temperature; OH not shown

**Table 16:**  $^1\text{H}$  /  $^{13}\text{C}$  NMR chemical shifts of Zr6-ONorb<sub>exo</sub> at room temperature in CD<sub>2</sub>Cl<sub>2</sub>

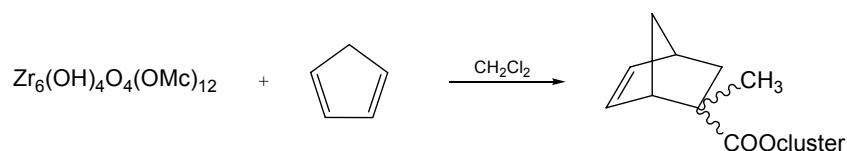
## Diels-Alder Reactions

The latter three examples of zirconium oxo clusters showed that bicyclic compounds could be used in the preparation of such compounds. Both, the endo and exo isomer, formed  $\text{Zr}_6$  structures, the same as it was observed for the prototypical  $\text{Zr}_6\text{O}_4(\text{OH})_4(\text{OMc})_{12}$  cluster, when neglecting the structural variation of a coordinated butanol molecule in the **Zr6-Norb<sub>exo</sub>** example. Thus, an attempt was made to react the **Zr6** cluster with cyclopentadiene in order to follow the post-synthesis modification approach in cluster preparation.

So far, several approaches were made to post-modify zirconium oxo clusters with the aim to introduce new functional groups or to block reactive groups on the cluster surface in order to adjust the ratio of functional and non-functional groups. To this end, the **Zr6** cluster was reacted with acetyl acetone, but no crystalline structures were obtained [53], whereas  $\text{Zr}_4\text{O}_2(\text{OMc})_{12}$  (**Zr4**) was degraded to a monomeric unit. Reaction of the **Zr4** cluster with trimethylsilane or triphenylsilane in the presence of a platinum catalyst, led to a decomposition of the cluster [53, 74], the same was observed when the **Zr4** cluster was reacted with m-chloro-perbenzoic acid in order to introduce epoxy-groups [75]. The only successful procedure of post-synthesis modifying cluster bonded carboxylates was the exchange for other carboxylic acids in solution [53]. The zirconium oxo clusters were obviously very sensitive to rough reaction conditions and the fact that they were moisture sensitive additionally limited the accessible reactions.

In contrast to most of the reactions described above, Diels-Alder [4+2] cycloadditions [72] are very mild reactions and products are formed in high yields at low temperatures, provided that the electronic conditions between the reaction partners, viz alkene and conjugated diene, are suitable [76].

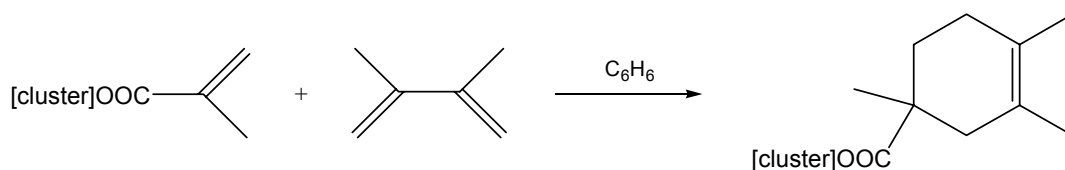
In an attempt to modify the methacrylate ligands of **Zr6**, the cluster was dissolved in dichloromethane and freshly cracked cyclopentadiene was added. The solution was heated to reflux for 24 hours and the solvent was removed *in vacuo*. The expected product, which would have differed from the **Zr6-Norb<sub>mix</sub>** structure in one additional methyl group at the 2 position, is shown in Scheme 9.



**Scheme 9:** Possible Diels-Alder cycloaddition of **Zr6** and cyclopentadiene

$^1\text{H}$  NMR spectra of the obtained product showed many signals which could be assigned to dimerized cyclopentadiene. After several washing procedures with n-heptane and drying at  $10^{-7}$  bar, the product was identified as the **Zr6** cluster, i.e. a reaction did not occur between the cluster as the dienophile alkene and cyclopentadiene.

In a second approach, harsher reaction conditions were applied: cyclopentadiene was replaced for 2,3-dimethyl butadiene and benzene was used as the solvent. The solution was refluxed for 24 hours at  $\sim 80^\circ\text{C}$ . By doing so, a cyclic product would be obtained instead of a bicyclic (Scheme 10). However, the higher reaction temperatures and the use of a more reactive diene led to polymerization of butadiene and no product could be isolated for NMR measurements.



**Scheme 10:** Possible Diels-Alder cycloaddition of **Zr6** and 2,3-dimethyl butadiene

The failure in these approaches had several reasons:

First of all, it is known that Diels-Alder reactions are sterically highly demanding reactions and the fact that the ligands on the cluster surface underwent fast ligand exchange in solution might have hindered appropriate reaction conditions. The second fact considered electronic reasons and appeared to be the most reasonable one. As mentioned above, a cycloaddition will give high yields at low temperatures and ambient pressure when using an electron-poor alkene and an electron-rich diene. Both of the applied dienes fulfilled the criterion of electron-rich dienes. The methacrylic unit, however, switched from a 'good' dienophile in the ester or acid form to a less reactive molecule because of coordination.

### 3.1.4 $\text{Zr}_{12}\text{O}_8(\text{OH})_8(\text{OVinac})_{24} \cdot 6\text{HOVinac}$

Crystalline  $\text{Zr}_{12}\text{O}_8(\text{OH})_8(\text{OVinac})_{24} \cdot 6\text{HOVinac}$  (**Zr12-Vinac**) was obtained when  $\text{Zr}(\text{OBU})_4$  was reacted with 7 equivalents of vinylacetic acid (HOVinac). After 5 minutes of reaction, a microcrystalline precipitate was obtained which formed colourless crystals after another two days which were suitable for single crystal measurements.

The molecule consisted of two carboxylate connected  $\text{Zr}_6\text{O}_4(\text{OH})_4$  cores (Figure 20). Three vinylacetate ligands on each core were chelating, 7 ligands bridged two neighbouring zirconium atoms each, and two ligands were no longer bound to the same  $\text{Zr}_6$  core, but formed bridges between the two  $\text{Zr}_6$  cores. Thus, the difference to the prototypical structure of **Zr6** was that two carboxylate ligands of each core switched from an edge-bridging to an inter-cluster bridging mode [O(57)/O(84A), O(62)/O(83A), O(62)/O(83A), O(84)/O(57A)]. As described for other variations of the **Zr6** structure above, this variation occurred opposite the  $\mu_3\text{-O}$  capped face of the  $\text{Zr}_6$  octahedron coordinated by chelating ligands [Zr(2)/Zr(3)/Zr(6)] and the inversion related atoms [Zr(2A)/Zr(3A)/Zr(6A)]. This variation of the basic **Zr6** structure was observed prior for clusters carrying acrylate, propionate, mixed methacrylate and propionate, and acetate ligands [51, 53].



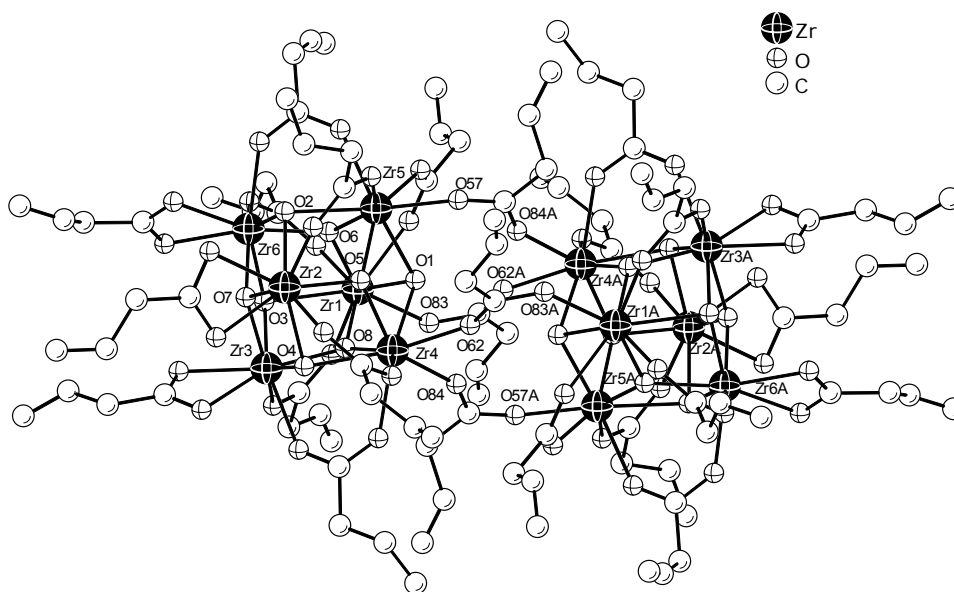


**Figure 20:** Molecular structure of  $\text{Zr}_{12}\text{O}_8(\text{OH})_8(\text{OVinac})_{24}$ ; hydrogen atoms are omitted for clarity

Judged from the bond lengths, the  $\text{Zr}(1)/\text{Zr}(5)/\text{Zr}(6)$ ,  $\text{Zr}(1)/\text{Zr}(3)/\text{Zr}(4)$ ,  $\text{Zr}(2)/\text{Zr}(3)/\text{Zr}(6)$  and  $\text{Zr}(2)/\text{Zr}(4)/\text{Zr}(5)$  triangles of the  $\text{Zr}_6$  octahedra were bridged by  $\mu_3$  oxygen atoms, while the other triangles were bridged by  $\mu_3$ -hydroxo groups (Table 17).

**Table 17:** Bond lengths for  $\mu_3$ -oxo atoms and  $\mu_3$ -hydroxo groups in **Zr12-Vinac**; inversion related atoms are not given

| $\mu_3\text{-O}$                                       |                            | $\mu_3\text{-OH}$                                      |                            |
|--|----------------------------|--|----------------------------|
| $\text{O}(5) - \text{Zr}(2)/\text{Zr}(4)/\text{Zr}(5)$ | 205.5(2)/206.3(4)/208.9(2) | $\text{O}(1) - \text{Zr}(1)/\text{Zr}(4)/\text{Zr}(5)$ | 230.1(2)/230.1(2)/229.8(2) |
| $\text{O}(6) - \text{Zr}(1)/\text{Zr}(5)/\text{Zr}(6)$ | 204.9(2)/205.4(1)/203.5(2) | $\text{O}(2) - \text{Zr}(2)/\text{Zr}(5)/\text{Zr}(6)$ | 218.3(3)/239.1(2)/221.7(2) |
| $\text{O}(7) - \text{Zr}(2)/\text{Zr}(3)/\text{Zr}(6)$ | 210.3(2)/210.8(2)/209.0(3) | $\text{O}(3) - \text{Zr}(1)/\text{Zr}(3)/\text{Zr}(6)$ | 239.0(2)/219.4(3)/221.7(2) |
| $\text{O}(8) - \text{Zr}(1)/\text{Zr}(3)/\text{Zr}(4)$ | 208.6(2)/205.5(2)/206.2(2) | $\text{O}(4) - \text{Zr}(2)/\text{Zr}(3)/\text{Zr}(4)$ | 220.4(2)/221.5(2)/233.1(2) |

The bond lengths for the  $\mu_3$ -hydroxo groups were not uniform but distorted, closer to a  $\mu_2$  than to a  $\mu_3$  bonding situation. Again, this was reasoned by hydrogen bonded vinylacetic acid ligands which stabilized the chelating mode of six ligands (Figure 21). Hydrogen bond lengths are summarized in Table 18.

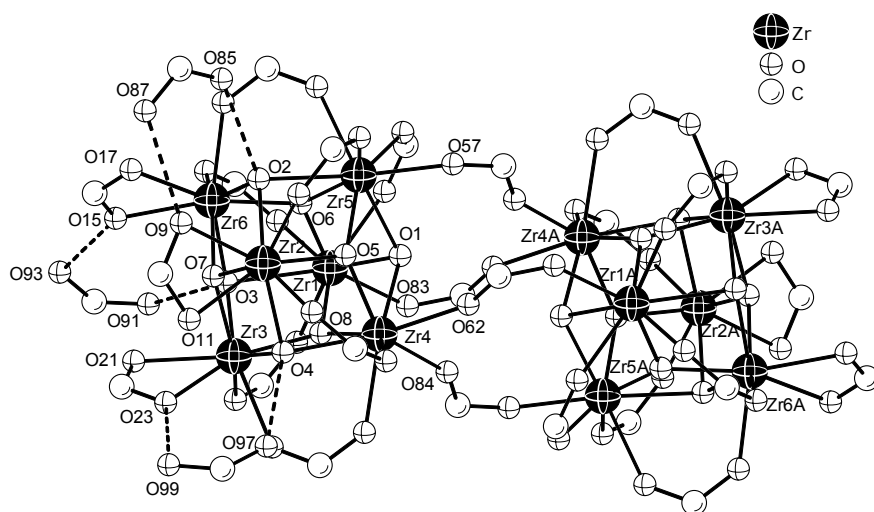


**Figure 21:** Hydrogen bond situation in **Zr12-Vinac**, vinylacetate ligands are set as formates for clarity

**Table 18:** Bond lengths for vinylacetic acids hydrogen bonded to **Zr12-Vinac**

| O-H – O [pm] |          |               |          |               |          |
|--------------|----------|---------------|----------|---------------|----------|
| O(85) – O(2) | 271.8(1) | O(91) – O(3)  | 275.0(2) | O(97) – O(4)  | 273.1(1) |
| O(87) – O(9) | 265.8(0) | O(93) – O(15) | 262.9(2) | O(99) – O(23) | 263.8(1) |

The solvate molecules were removed as described for the **Zr6-Isob** cluster for NMR measurements. The room temperature  $^1\text{H}$  NMR spectrum showed surprisingly sharp signals (Figure 22), and long range correlations to the carbonyl carbon atoms in an HMBC experiment were observed. The symmetry of the cluster in the crystalline state was  $C_i$  with seven inequivalent ligand positions. Neglecting a slight perturbation of the symmetry by crystal packing or slightly different conformations of the ligands, the molecular symmetry was in fact  $C_{2h}$ . This should result in seven sets of signals with a ratio of 1:1:2:2:2:2:2. In the case of a  $C_i$  symmetry there are, in principle, twelve inequivalent ligand positions, leading to twelve sets of signals in the  $^1\text{H}$  NMR spectrum. In fact, six different signals were observed in HSQC and HMBC experiments at room temperature, indicating that the symmetry was actually  $\sim C_{2h}$  at room temperature because the ligand conformations were averaged on the NMR time scale. At lower temperatures ( $-40\text{ }^\circ\text{C}$ ), an additional one or two signals occurred and the  $^1\text{H}$  NMR spectra became broad and unstructured, therefore clear assignment was not possible due to signal overlapping. This means that the symmetry was reduced to  $C_i$  or even  $C_1$  at low temperatures. Signals for the inequivalent ligands at room temperature are summarized in Table 19. The OH signal was broad at 11.55 ppm, other signals at 7.37, 7.32 and 6.88 ppm gave neither long

range correlations in an HMBC experiment nor correlations in an HSQC and were thus tentatively assigned as OH. This was further reasoned with the shifts these signals underwent in temperature-dependent experiments.

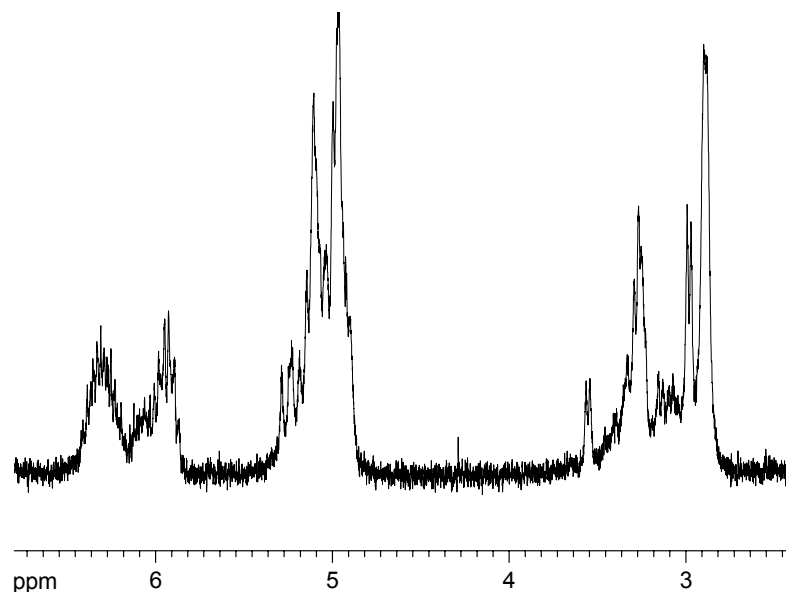


**Figure 22:**  $^1\text{H}$ -NMR spectrum of **Zr12-Vinac** in  $\text{d}_8$ -toluene at room temperature

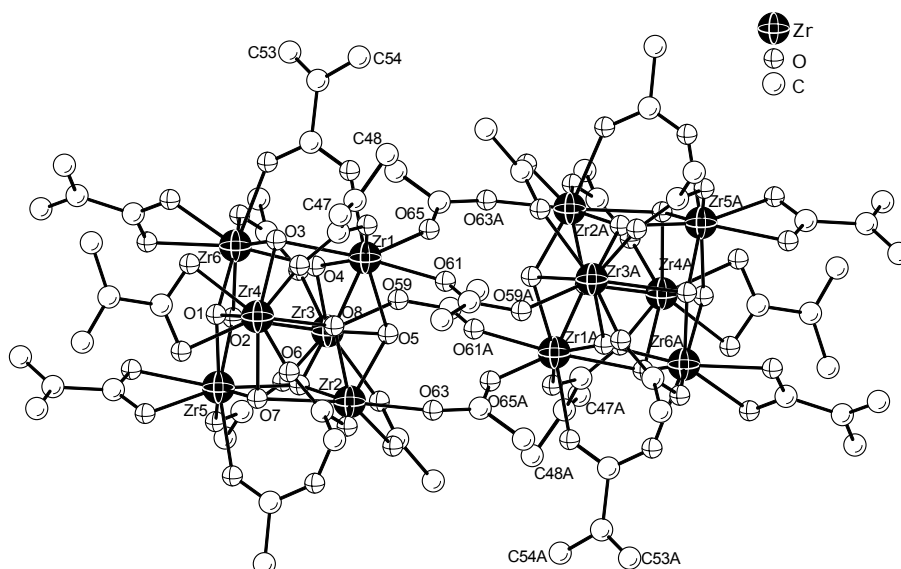
**Table 19:**  $^1\text{H}$  /  $^{13}\text{C}$  NMR chemical shifts [ppm] of the six non-equivalent vinylacetate ligands (OVinac1-6) of **Zr12-Vinac** in  $\text{d}_8$ -toluene at RT. The labelling of the atoms is as follows:  $\text{C}^1\text{H}_2\text{C}^2\text{HC}^3\text{H}_2\text{C}^4\text{OO}$

|                | $\text{C}^1$            | $\text{C}^2$ | $\text{C}^3$      | $\text{C}^4$ |
|----------------|-------------------------|--------------|-------------------|--------------|
| <b>OVinac1</b> | 5.17, 5.26 / 115.8      | 6.43 / 135.1 | 3.61, 3.30 / 42.1 | - / 176.9    |
| <b>OVinac2</b> | 5.27, 5.11 / 117.1      | 6.34 / 133.7 | 3.57, 3.27 / 42.1 | - / 182.5    |
| <b>OVinac3</b> | 5.30, 5.14 / 117.1      | 6.32 / 133.7 | 3.33, 3.17 / 41.8 | - / 182.7    |
| <b>OVinac4</b> | 5.23, 5.09 / 117.1      | 6.30 / 133.7 | 3.28, 3.14 / 41.6 | - / 178.7    |
| <b>OVinac5</b> | 5.27, 5.12 / 117.1      | 6.30 / 133.7 | 3.29, 3.14 / 41.6 | - / 182.3    |
| <b>OVinac6</b> | 5.04, 4.96 / 118.5      | 5.94 / 131.0 | 3.00, 2.90 / 39.5 | n.d. *       |
| <b>OH</b>      | 11.55, 7.36, 7.32, 6.88 |              |                   |              |

\* n.d. = not detected

### 3.1.5 $\text{Zr}_{12}\text{O}_8(\text{OH})_8(\text{OAc})_{16}(\text{OMc})_8 \cdot 6\text{HOAc}$

A mixed acetate - methacrylate substituted cluster  $\text{Zr}_{12}\text{O}_8(\text{OH})_8(\text{OAc})_{16}(\text{OMc})_8 \cdot 6\text{HOAc}$  (**Zr12-AcMc**) cluster was obtained when  $\text{Zr}(\text{OBU})_4$  was reacted with about 3.5 equivalents of acetic acid and 1.5 equivalents of methacrylic acid. The molecule (Figure 23) showed the characteristic features of a  $\text{Zr}_{12}$  structure: Two  $\text{Zr}_6\text{O}_4(\text{OH})_4$  cores were connected with four inter-bridging acetate ligands [O(59)/O(61A), O(61)/O(59A), O(63)/O(65A), O(65)/O(63A)] opposite the  $\mu_3\text{-O}$  capped faces of the  $\text{Zr}_6$  octahedra [Zr(4)/Zr(5)/Zr(6) and Zr(4A)/Zr(5A)/Zr(6A)]. Six methacrylate ligands were in a chelating mode and the other four positions on the 'cluster-belts' were half occupied by methacrylates [C(47)/C(48), C(53)/C(54) and the inversion related atoms C(47A)/C(48A) and C(53A)/C(54A)] and acetates, respectively. All other coordination sites were occupied by intra-cluster bridging acetate ligands.

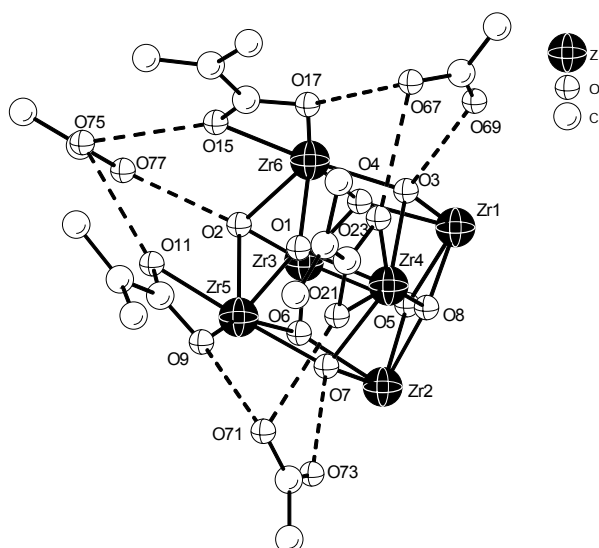


**Figure 23:** Molecular structure of  $\text{Zr}_{12}\text{O}_8(\text{OH})_8(\text{OAc})_{16}(\text{OMc})_8$ ; hydrogen atoms are omitted for clarity

According to the bond lengths, the Zr(1)/Zr(2)/Zr(4), Zr(1)/Zr(3)/Zr(6), Zr(2)/Zr(3)/Zr(5) and Zr(4)/Zr(5)/Zr(6) triangles of the  $\text{Zr}_6$  octahedra were bridged by  $\mu_3$ -oxygen atoms, while the other triangles were bridged by  $\mu_3$ -hydroxo groups (Table 20). The triangle capped with the O(5)-hydroxo group showed uniform bond lengths to the zirconium atoms, whereas distances in the other three hydroxo-capped triangles were distorted. This was again reasoned by hydrogen bonding of the solvate acids with the  $\mu_3\text{-OH}$  groups and one oxygen atom of a chelating methacrylate ligand each (Figure 24).

**Table 20:** Bond lengths for  $\mu_3$ -oxo atoms and  $\mu_3$ -hydroxo groups in **Zr12-AcMc**; inversion related atoms are not given

| $\mu_3$ -O               |                            | $\mu_3$ -OH              |                            |
|--------------------------|----------------------------|--------------------------|----------------------------|
| O(1) – Zr(4)/Zr(5)/Zr(6) | 210.5(4)/208.1(1)/210.5(6) | O(2) – Zr(3)/Zr(5)/Zr(6) | 239.1(5)/222.4(6)/218.9(6) |
| O(4) – Zr(1)/Zr(3)/Zr(6) | 206.0(5)/208.0(5)/206.4(5) | O(3) – Zr(1)/Zr(4)/Zr(6) | 232.6(5)/220.9(6)/220.2(6) |
| O(6) – Zr(2)/Zr(3)/Zr(5) | 205.1(6)/205.8(6)/202.3(5) | O(5) – Zr(1)/Zr(2)/Zr(3) | 230.1(5)/229.0(5)/229.4(5) |
| O(8) – Zr(1)/Zr(2)/Zr(4) | 205.6(5)/208.2(5)/206.5(5) | O(7) – Zr(2)/Zr(4)/Zr(5) | 239.1(5)/221.3(6)/221.1(6) |

**Figure 24:** Hydrogen bond situation in **Zr12-AcMc**; ligands taking place in hydrogen bonding are shown for just one  $\text{Zr}_6$  subunit

The hydrogen bond situation differed slightly from the examples described above: Whereas in most of the previous examples the free acids were bound to one chelating ligand and a  $\mu_3$ -OH group each, the hydrogen bonds in this structure were located between two chelating ligands each. Thus, the second hydrogen bond of each acid molecule was shared with two oxygen atoms of the chelating ligands, leading to more or less homogeneous bond lengths (Table 21). A similar situation was indicated in the **Zr6-Norb<sub>mix</sub>** structure (Figure 12, p. 26), where one of three acid molecules was located between two oxygen atoms of a chelating norborneate ligand.

**Table 21:** Bond lengths for hydrogen bonded acetic acids in **Zr12-AcMc**

| O-H – O [pm]  |          |               |          |               |          |
|---------------|----------|---------------|----------|---------------|----------|
| O(67) – O(17) | 289.3(0) | O(71) – O(9)  | 299.5(0) | O(75) – O(11) | 301.1(0) |
| O(67) – O(23) | 285.9(0) | O(71) – O(21) | 285.7(2) | O(75) – O(15) | 285.9(2) |
| O(69) – O(3)  | 268.1(1) | O(73) – O(7)  | 271.1(1) | O(77) – O(2)  | 271.7(1) |

For NMR investigations, the solvate molecules were removed as described for **Zr6-Isob**. The  $^1\text{H}$  NMR spectra at room temperature and  $-80\text{ }^\circ\text{C}$  in  $\text{CD}_2\text{Cl}_2$  showed broad and overlapping signals (Figure 25). Additional signals from toluene were present.

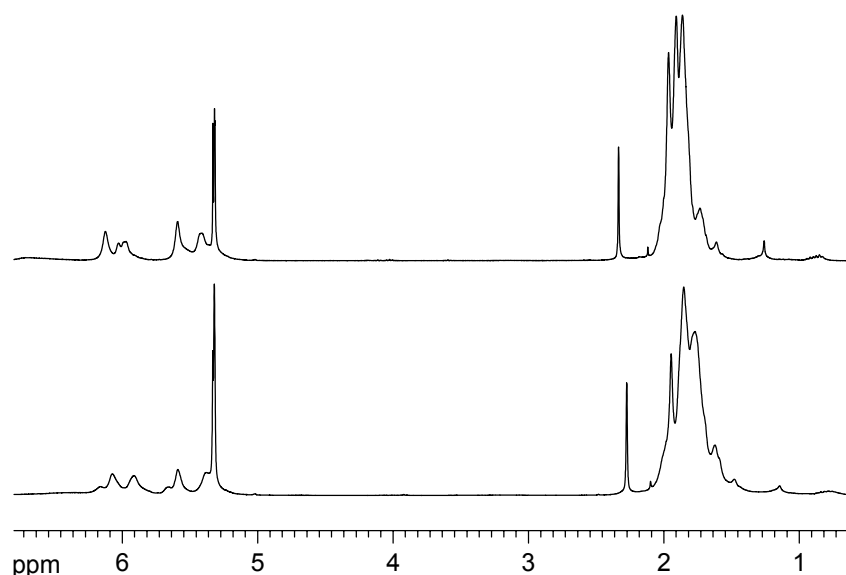


**Figure 25:**  $^1\text{H}$ -NMR spectra of **Zr12-AcMc** in  $\text{CD}_2\text{Cl}_2$ ; top: room temperature, bottom:  $-80\text{ }^\circ\text{C}$ ; OH are not shown

The symmetry of the cluster in the crystalline state was  $C_i$ , corresponding to seven inequivalent ligand positions. Taking into account that in solution ligand exchange took place and all ligands, acetates and methacrylates, occupied both chelating and bridging positions, the symmetry could be reduced to  $C_1$ , which could in turn lead to 24 signals for acetates and methacrylates. In fact, four different signals for the methacrylate and seven for the acetate ligands were observed in HSQC and HMBC experiments at  $-80\text{ }^\circ\text{C}$ , indicating that the symmetry, as determined from the crystal structure, was more or less retained in solution. A broad OH signal occurred at 9.8 ppm at room temperature and shifted to 11.5 ppm at  $-80\text{ }^\circ\text{C}$ .

**Table 22:**  $^1\text{H}$  /  $^{13}\text{C}$  NMR chemical shifts [ppm] of the four non-equivalent methacrylate (OMc1-4) and 7 acetate ligands (OAc1-7) of **Zr12-AcMc** in  $\text{CD}_2\text{Cl}_2$  at  $-80\text{ }^\circ\text{C}$ . The labelling of the atoms is as follows:  
 $\text{OOC}^1\text{C}^2(\text{C}^4\text{H}_3)=\text{C}^3\text{H}_2$  and  $\text{OOC}^1\text{C}^2\text{H}_3$

|             | <b>C<sup>1</sup></b> | <b>C<sup>2</sup></b> | <b>C<sup>3</sup></b> | <b>C<sup>4</sup></b> |
|-------------|----------------------|----------------------|----------------------|----------------------|
| <b>OMc1</b> | - / 183.5            | - / 135.7            | 6.06, 5.59 / 127.2   | 1.75 / 16.6          |
| <b>OMc2</b> | - / 183.3            | - / 135.9            | 6.17, 5.66 / 127.1   | 1.82 / 16.6          |
| <b>OMc3</b> | - / 180.1            | - / 135.6            | 6.08, 5.59 / 126.9   | 1.68 / 16.6          |
| <b>OMc4</b> | - / 171.1            | - / 138.5            | 5.92, 5.39 / 123.8   | 1.77 / 17.8          |
| <b>OAc1</b> | - / 189.5            | n.r. *               | -                    | -                    |
| <b>OAc2</b> | - / 189.5            | n.r. *               | -                    | -                    |
| <b>OAc3</b> | - / 180.1            | 1.47 / 22.9          | -                    | -                    |
| <b>OAc4</b> | - / 180.1            | 1.62 / 22.9          | -                    | -                    |
| <b>OAc5</b> | - / 176.4            | n.r. *               | -                    | -                    |
| <b>OAc6</b> | - / 175.4            | 2.00 / 23.1          | -                    | -                    |
| <b>OAc7</b> | - / 174.1            | 1.95 / 20.5          | -                    | -                    |
| <b>OH</b>   | 11.48                | -                    | -                    | -                    |

\* n.r. = not resolved

## 3.2 Zirconium Oxo Clusters in Solution

The final goal in preparing surface modified zirconium oxo clusters was their use as co-monomers in polymerization reactions. Therefore, knowledge about their behaviour in solution was required because it was shown in the above investigations that the symmetry determined from the crystal structures was not always observed in solution.

To this end, a fundamental NMR spectroscopic characterization was carried out to learn more about the clusters in solution. The clusters  $\text{Zr}_4\text{O}_2(\text{OMc})_{12}$  (**Zr4**),  $\text{Zr}_6\text{O}_4(\text{OH})_4(\text{OMc})_{12}$  (**Zr6**) and  $\text{Zr}_{12}\text{O}_8(\text{OH})_8(\text{OProp})_{24}$  (**Zr12**) were chosen as model compounds.

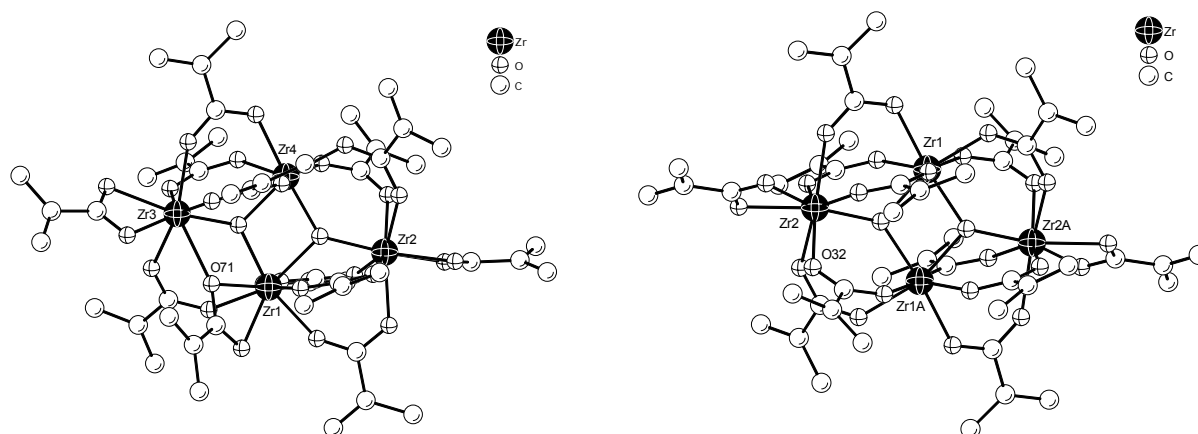
### 3.2.1 $\text{Zr}_4\text{O}_2(\text{OMc})_{12}$

The discussion starts with the simpler case, i.e. the **Zr4** cluster, because it was obtained in high yields within a short time and the molecule did not possess hydroxo groups.

Two different kinds of crystal structures were reported for this cluster type, depending on the type of zirconium alkoxide used in the preparation [19, 77]. When the precursor zirconium propoxide was reacted with a 15fold excess of methacrylic acid, the 'asymmetric' **Zr4** cluster was obtained. A cluster with the same composition was formed when zirconium butoxide was reacted with seven equivalents of methacrylic acid. The main difference between these two structures was that the  $^2\eta$ ,  $\mu_2$  - coordinated methacrylate ligand  $[\text{Zr}(1)-\text{O}(71)-\text{Zr}(3)]$  in the left isomer in Figure 26 was converted into a symmetric  $\mu_2$  bridge, i.e. the cluster became symmetric with a crystallographic inversion symmetry. It was also reported that the solution NMR spectra of these two structures were the same, indicating that the structures interconverted in solution.

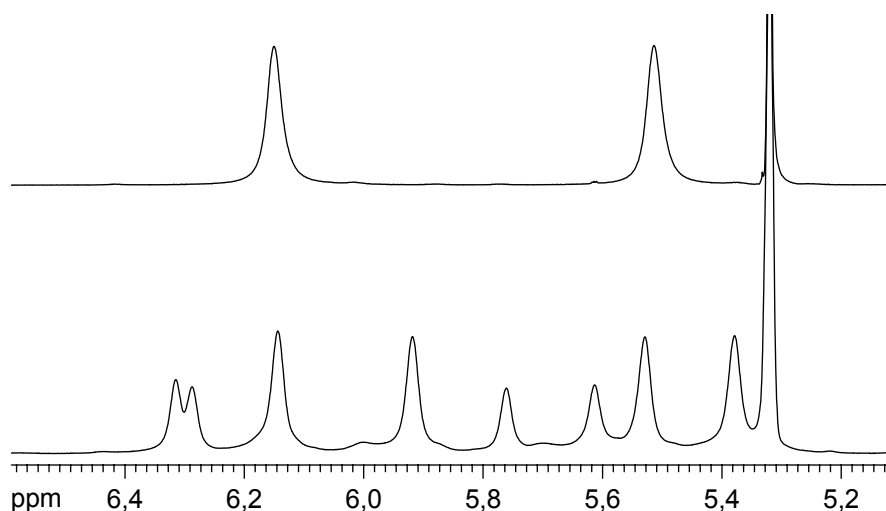
In an extended investigation, the **Zr4** cluster was prepared five times independently with both precursors,  $\text{Zr}(\text{OPr})_4$  and  $\text{Zr}(\text{OBu})_4$ , and cell parameters were determined for 5-10 crystals of each product. In fact, there was no general relation between the precursor used and the crystallographic symmetry of the structure obtained. Both structures, asymmetric and symmetric, were found in the attempts. However, no mixture of the two types was observed in a single attempt, i.e. either the whole product consisted of the asymmetric or the symmetric form, respectively. NMR measurements revealed that both structures indeed showed the same signal pattern in solution.





**Figure 26:** Asymmetric (left) and symmetric (right) isomers of  $\text{Zr}_4\text{O}_2(\text{OMc})_{12}$ ; hydrogen atoms are not shown

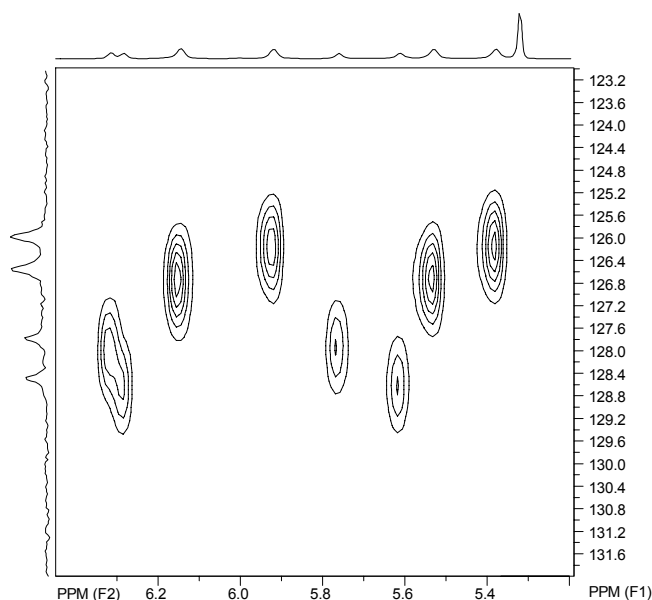
The symmetry of the ‘symmetric’ **Zr4** isomer in the crystalline state was  $C_i$  with six inequivalent ligand positions. Neglecting a slight perturbation of the symmetry by crystal packing or slightly different conformations of the ligands, the molecular symmetry was in fact  $C_{2h}$ . This should result in four sets of signals with a ratio of 1:1:2:2. However, only one set of broad signals was observed in the  $^1\text{H}$  NMR spectra at room temperature, indicative of a fast ligand exchange. At  $-80\text{ }^\circ\text{C}$ , four discrete sets of signals were observed for the methacrylate ligands (Figure 27, Table 23). Thus, the molecular structure of the **Zr4** cluster was retained in solution. The assignment of the signals was done with 2D NMR experiments ( $^1\text{H}/^{13}\text{C}$  -HSQC, -HMBC) in which four inequivalent sets of signals were confirmed (Figure 28).



**Figure 27:**  $^1\text{H}$  NMR spectra for the methylene protons of **Zr4** in  $\text{CD}_2\text{Cl}_2$ ; top: RT, bottom:  $-80\text{ }^\circ\text{C}$

**Table 23:**  $^1\text{H}$  /  $^{13}\text{C}$  NMR chemical shifts [ppm] of the four non-equivalent methacrylate ligands (OMc1-4) of **Zr4** in  $\text{CD}_2\text{Cl}_2$  at  $-80^\circ\text{C}$ . The labelling of the atoms is as follows:  $\text{OOC}^1\text{C}^2(\text{C}^4\text{H}_3)=\text{C}^3\text{H}_2$ 

|             | $\text{C}^1$ | $\text{C}^2$ | $\text{C}^3$       | $\text{C}^4$ |
|-------------|--------------|--------------|--------------------|--------------|
| <b>OMc1</b> | - / 186.4    | - / 136.1    | 6.32, 5.77 / 127.9 | 1.55 / 16.8  |
| <b>OMc2</b> | - / 180.4    | - / 136.4    | 6.29, 5.62 / 128.6 | 1.78 / 17.5  |
| <b>OMc3</b> | - / 173.5    | - / 138.1    | 5.93, 5.39 / 126.1 | 1.57 / 17.8  |
| <b>OMc4</b> | - / 172.6    | - / 137.5    | 6.16, 5.54 / 126.7 | 1.82 / 17.7  |
| <b>OH</b>   | 12.96        |              |                    |              |

**Figure 28:** Section of a  $^1\text{H}$  /  $^{13}\text{C}$  NMR HSQC spectrum of **Zr4** in  $\text{CD}_2\text{Cl}_2$  at  $-80^\circ\text{C}$  showing four different signals for the methylene carbons

The  $^1\text{H}$  NMR spectra of **Zr4** changed significantly after several measurements at  $-80^\circ\text{C}$ . Since decomposition of the compound at low temperatures was most unlikely, these changes were ascribed to water which condensed into the NMR tube at low temperatures. It was already assumed in previous works that zirconium oxo clusters were water sensitive. However, an investigation was missing. Therefore, the **Zr4** cluster was reacted with stoichiometric amounts of water-saturated  $\text{CD}_2\text{Cl}_2$  in the NMR tube, and a  $^1\text{H}$  NMR spectrum was recorded immediately (Figure 29). It was not surprising that the addition of water led to the same changes of the signal pattern as it was observed by accident. By adding  $\text{H}_2\text{O}$  to the solution, a signal at  $\sim 13$  ppm also

became more pronounced, which was ascribed to an acidic OH. To compare: Integration of this signal at  $-80\text{ }^{\circ}\text{C}$  of freshly dissolved **Zr4** in  $\text{CD}_2\text{Cl}_2$  gave a signal intensity of 0.12 protons, whereas the sample reacted with 3 equivalents of water gave 3.6 protons. Pure **Zr4** should, in principle, not show an OH signal. It was ascribed to traces of water which were still present in the NMR solvent and could not be removed through drying with  $3\text{ \AA}$  zeolite.

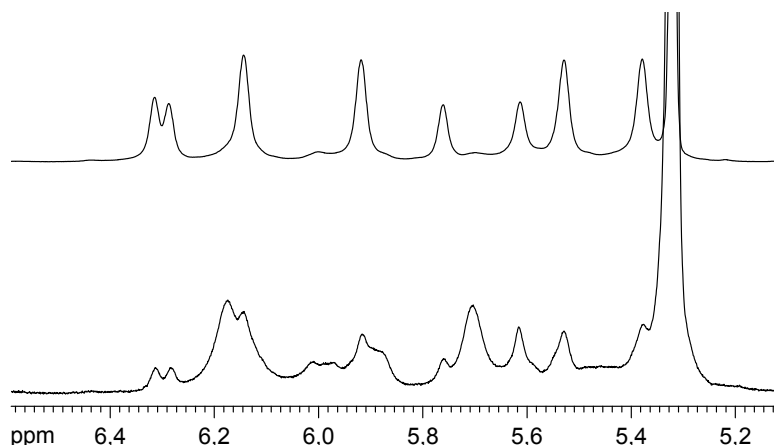


**Figure 29:**  $^1\text{H}$  NMR spectra at  $-80\text{ }^{\circ}\text{C}$  in  $\text{CD}_2\text{Cl}_2$ ; top: **Zr4**, bottom: **Zr4** + 3 equ. of  $\text{H}_2\text{O}$ ; the methylene proton region is shown

Next to OH signals arising from the contact of **Zr4** with water, some signals occurred which were identified as butyl methacrylate which was formed as a by-product during the cluster formation. Removal of both acidic compounds and ester was possible when **Zr4** was re-crystallized from a mixture of benzene and triethylamine. By doing so, the **Zr4** cluster crystallized with benzene as a crystal solvate and only the symmetric isomer was obtained.

For further NMR investigations, the **Zr4** cluster was re-crystallized from benzene and the crystal solvate was removed by dissolving the crystals in  $\text{CH}_2\text{Cl}_2$  and evaporating volatile compounds *in vacuo*. Moreover, common NMR tubes were replaced for Young tubes which allowed gas-tight closing through Teflon sealing. As a consequence, the signal patterns of the **Zr4** cluster remained unchanged, even during long periods of low temperature measurements.

Temperature dependent  $^1\text{H}$  NMR spectra for the methylene proton region are shown in Figure 30. When the solution was cooled gradually, a splitting of the broad signals, as observed at room temperature, occurred, indicating that also the symmetry changed on the NMR time scale. At  $-80\text{ }^{\circ}\text{C}$  four sets of signals were observed in accordance with the molecular symmetry.

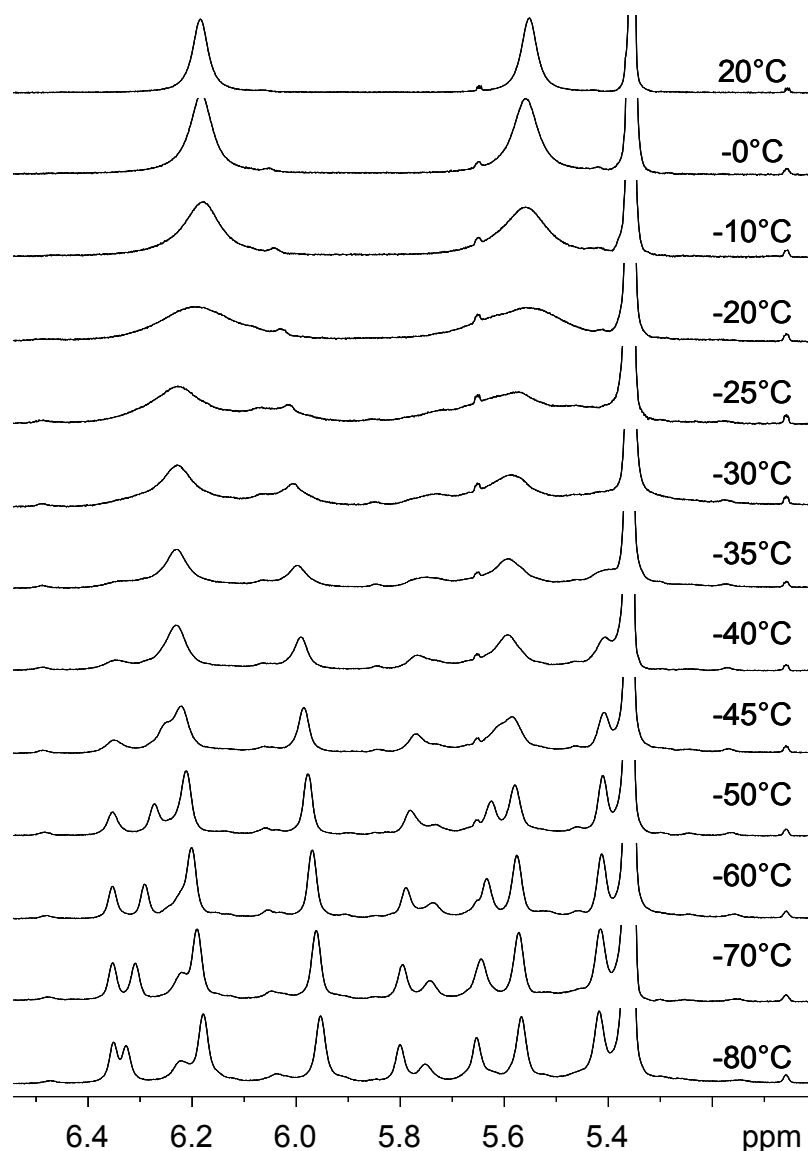


**Figure 30:** Temperature dependent  $^1\text{H}$  NMR spectra of **Zr4** in  $\text{CD}_2\text{Cl}_2$ ; the methylene proton region is shown

Parallel to  $^1\text{H}$  NMR spectra, also EXSY spectra were recorded to learn more about the exchange processes of the ligands. From room temperature to  $-50^\circ\text{C}$  all of the methacrylate ligands exchanged with each other. At  $-80^\circ\text{C}$  only dipolar coupling occurred, i.e. exchange was not observed on the NMR time scale. At  $-60^\circ\text{C}$  and  $-70^\circ\text{C}$ , respectively, the picture was somehow different: At  $-70^\circ\text{C}$  a ligand exchange between two inequivalent methacrylate ligands was observed. The corresponding  $^1\text{H}$  spectrum and the ligands taking place in the exchange process are shown in Figure 31 (left). At  $-60^\circ\text{C}$  three distinct exchange processes were observed (Figure 31, right).

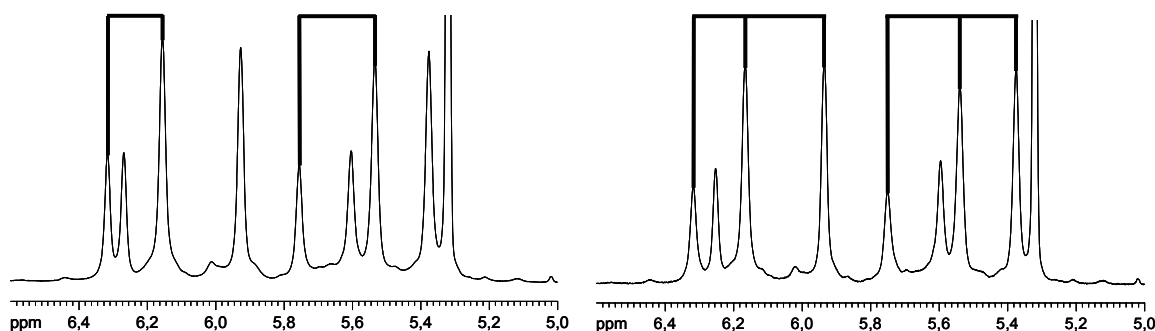


**Figure 31:**  $^1\text{H}$  NMR spectra of **Zr4** at  $-70\text{ }^\circ\text{C}$  (left) and  $-60\text{ }^\circ\text{C}$  (right) in  $\text{CD}_2\text{Cl}_2$ ; the ligands taking place in the exchange processes are highlighted; only the methylene proton region is shown

Generally, the effects on the NMR spectra are the same whether an intramolecular or an intermolecular exchange process is involved [78]. Thus, it could not be distinguished whether the observed exchange processes were intra- or intermolecular. However, in a typical experiment about 2 mg of **Zr4** cluster was dissolved in 0.5 ml of  $\text{CD}_2\text{Cl}_2$ , corresponding to a concentration of about  $3\text{ mmol l}^{-1}$ , thus making intermolecular exchange rather unlikely. Moreover, in all  $^1\text{H}$  NMR spectra, a signal for an acidic OH was observed and tentatively assigned as free acid. Nevertheless, some additional information of how the first exchange process at  $-70\text{ }^\circ\text{C}$  might proceed was obtained from crystal structures: The asymmetric and symmetric isomers of the **Zr4** cluster are shown in Figure 26 (p. 45). To repeat, the basic difference between these two structures was that one bridging ligand in the symmetric isomer became partly chelating in the asymmetric one, i.e. one oxygen of a carboxylate switched from a 'normal' bridging to a  $^2\eta, \mu_2$  mode. Furthermore, both crystal structures were obtained in high yields within a short time, indicating that both structures have comparable energy minima. The exchange process at  $-70\text{ }^\circ\text{C}$  took place between a bridging and a chelating ligand, respectively. Judged from molecular symmetry and the  $^1\text{H}$  NMR integral, the signal at 6.16 ppm (OMc4) was assigned as a bridging carboxylate, whereas the signal at 6.32 ppm (OMc1) belonged to the ligand showing a shift of 186.4 ppm for the carbonyl carbon which was characteristic for a chelating ligand [63]. Therefore, a chelating ligand was converted into a bridging ligand in the exchange process and vice versa, all other ligands remained unaffected at that temperature. Looking at the two isomers of the **Zr4** cluster this might give a good indication of how the exchange mechanism might proceed.

No information was provided from crystal structures for the other exchange processes at  $-60\text{ }^\circ\text{C}$ . For this reason, and for reasons of reliability, no mechanisms were formulated. However, as mentioned above, it could not be excluded that intermolecular processes, such as cluster - acid exchange, were involved.

### 3.2.2 $\text{Zr}_6\text{O}_4(\text{OH})_4(\text{OMc})_{12}$

The crystal structure of  $\text{Zr}_6\text{O}_4(\text{OH})_4(\text{OMc})_{12}$  (**Zr6**) contained disordered methacrylic acid molecules and n-butyl methacrylate, which was formed as a by-product during cluster formation. These compounds had to be removed for NMR investigations, because free acid causes mutual exchange with coordinated carboxylates. To this end, the cluster was dissolved in  $\text{CH}_2\text{Cl}_2$  and volatiles were removed *in vacuo*. This was repeated with toluene and once more with  $\text{CH}_2\text{Cl}_2$  as the solvents, and the solid was dried at  $10^{-7}$  bar.

In contrast to **Zr4**, the  $^1\text{H}$  NMR spectrum of **Zr6** showed a signal splitting of the methylene protons at room temperature, indicating that the coalescence temperature for the complete exchange of all methacrylate ligands of this cluster was somewhat higher (Figure 32).

The symmetry of **Zr6** in the crystalline state was  $P6_3mc$  with strongly disordered solvate molecules. Thus, the cluster had  $\text{C}_{3v}$  symmetry, resulting in three non-equivalent methacrylate ligands with a ratio of 1:1:2. In a  $^1\text{H} / ^{13}\text{C}$  HMBC experiment at  $-80^\circ\text{C}$  indeed three non-equivalent ligands were observed (Figure 33), proving that the symmetry of **Zr6** was retained in solution. Next to signals stemming from the methacrylate ligands, traces of n-butyl methacrylate were present which were not fully removed.

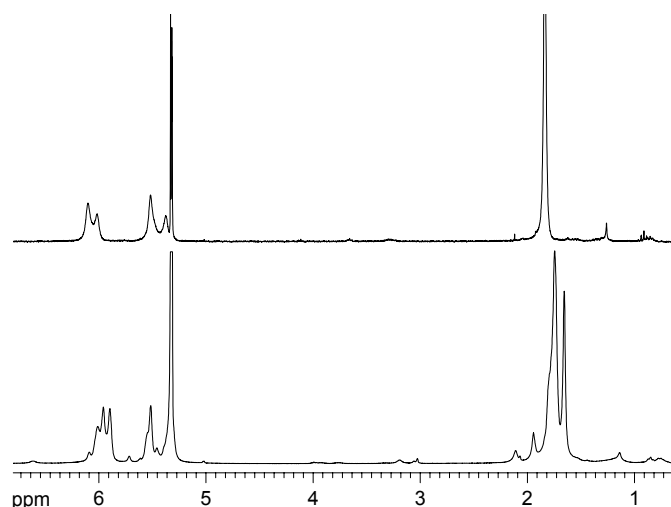


**Figure 32:**  $^1\text{H}$  NMR spectra of **Zr6** in  $\text{CD}_2\text{Cl}_2$ ; top: room temperature, bottom:  $-80^\circ\text{C}$ ; OH not shown

The proton signals of the methyl groups were overlapping and the signal ratio of the olefinic protons could not be determined exactly because of partial overlap but was approximately 1:1:2. Methacrylate ligand OMc1 (Table 24) was tentatively assigned as a chelating ligand because of the chemical shift of the carbonyl carbon (183.7 ppm) and the corresponding methylene proton intensity at 6.03 ppm. OMc2 and OMc3 constituted bridging methacrylates.

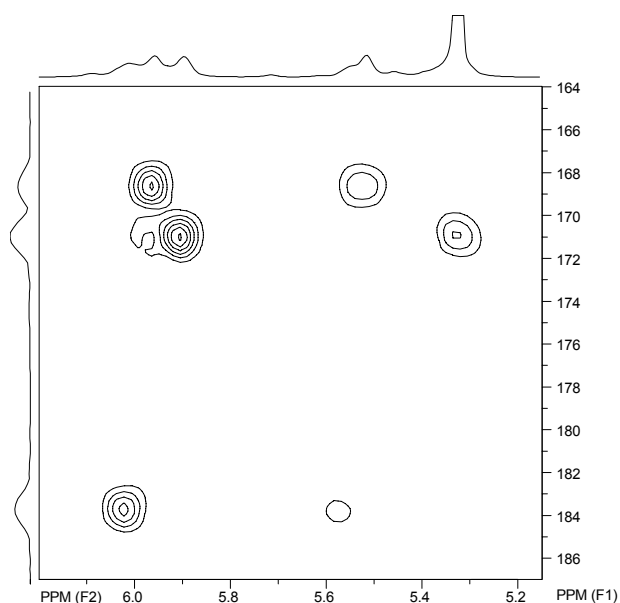


**Figure 33:**  $^1\text{H} / ^{13}\text{C}$  NMR HMBC spectrum of the carbonyl region of **Zr6** at  $-80\text{ }^\circ\text{C}$  in  $\text{CD}_2\text{Cl}_2$ ; ( $=\text{CH}_2/\text{COO}^-$ )

**Table 24:**  $^1\text{H} / ^{13}\text{C}$  NMR chemical shifts [ppm] of the three non-equivalent methacrylate ligands (OMc1-3) of **Zr6** in  $\text{CD}_2\text{Cl}_2$  at  $-80\text{ }^\circ\text{C}$ . The labelling of the atoms is as follows:  $\text{OOC}^1\text{C}^2(\text{C}^4\text{H}_3)=\text{C}^3\text{H}_2$

|             | <b>C<sup>1</sup></b> | <b>C<sup>2</sup></b> | <b>C<sup>3</sup></b> | <b>C<sup>4</sup></b> |
|-------------|----------------------|----------------------|----------------------|----------------------|
| <b>OMc1</b> | - / 183.7            | - / 135.9            | 6.03, 5.57 / 126.7   | 1.75 / 16.5          |
| <b>OMc2</b> | - / 171.0            | - / 138.5            | 5.91, 5.33 / 123.6   | 1.76 / 17.9          |
| <b>OMc3</b> | - / 168.7            | - / 135.2            | 5.97, 5.53 / 125.8   | 1.66 / 16.3          |
| <b>OH</b>   | 11.34, 11.21         |                      |                      |                      |

The presence of acidic OH groups in the molecule raised the question whether these could catalyze transesterification reactions. In the case of methacrylate ligands polymerized with methyl methacrylate the educt and product of course would be the same. However, reaction of a different cluster, such as **Zr6-Isob**, with MMA would transform an unreactive cluster into a reactive one.

To this end, **Zr6** was dissolved in  $\text{CHCl}_3$  and the same volume of ethyl acetate was added. After heating the solution to reflux for one hour, the volatiles were removed *in vacuo* and  $^1\text{H}$  and  $^1\text{H} / ^{13}\text{C}$  HMBC NMR spectra were recorded. The absence of coordinated acetate ligands in the product proved that no transesterification took place. In fact, only signals for methacrylate ligands were observed in the  $^1\text{H}$  NMR spectrum.

### 3.2.3 $\text{Zr}_{12}\text{O}_8(\text{OH})_8(\text{OProp})_{24}$

The symmetry of  $\text{Zr}_{12}\text{O}_8(\text{OH})_8(\text{OProp})_{24}$  (**Zr12**) in the crystalline state was  $C_i$  (Figure 34). Assuming unrestricted ligand motion in solution, the symmetry was in fact  $C_{2h}$ , this should result in seven sets of ligand resonances in the  $^1\text{H}$  NMR spectrum with a ratio of 1:1:2:2:2:2:2. The room temperature  $^1\text{H}$  spectrum (Figure 35) showed surprisingly sharp signals, the same picture as it was observed for **Zr12-Vinac**.

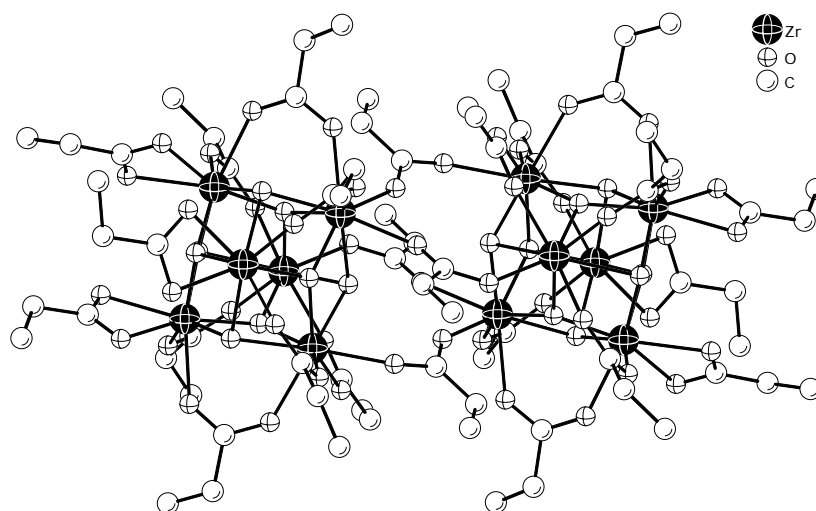


**Figure 34:** Molecular structure of  $\text{Zr}_{12}\text{O}_8(\text{OH})_8(\text{OProp})_{24}$ ; hydrogen atoms are omitted for clarity

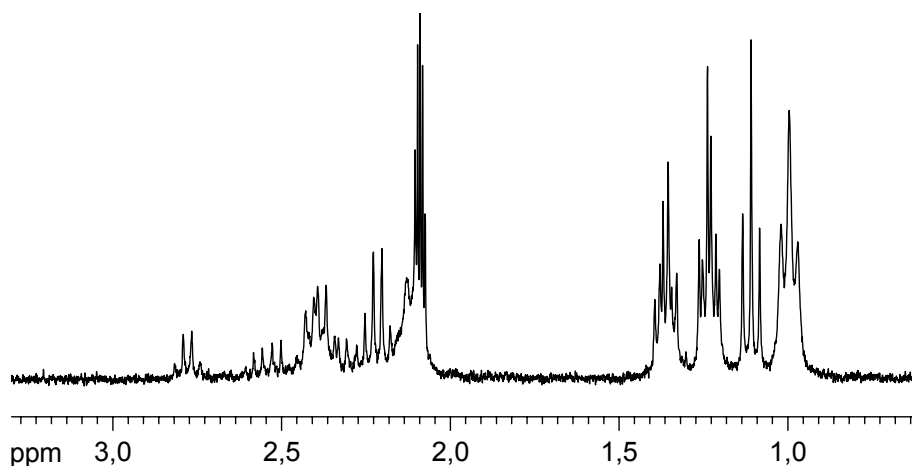


**Figure 35:**  $^1\text{H}$  NMR spectrum of **Zr12** in  $\text{C}_7\text{D}_8$  at room temperature; OH not shown



Six inequivalent sets of ligand signals were observed in 2D NMR experiments at room temperature, indicating that **Zr12** had approximately  $C_{2h}$  symmetry in solution. The signals were assigned with HSQC, HMBC and COSY NMR spectra and are given in Table 25. Next to a broad OH signal at 11.76 ppm, there were three signals which did not give correlations in HSQC, HMBC and COSY spectra. Therefore, and because of the shift these proton signals underwent in temperature dependent experiments, they were tentatively assigned as OH.

**Table 25:**  $^1\text{H}$  /  $^{13}\text{C}$  NMR chemical shifts [ppm] of the seven non-equivalent propionate ligands (OProp1-7) of **Zr12** in  $d_8$ -toluene at room temperature. The labelling of the atoms is as follows:  $\text{OOC}^1\text{C}^2\text{H}_2\text{C}^3\text{H}_3$

|               | $\text{C}^1$            | $\text{C}^2$ | $\text{C}^3$ |
|---------------|-------------------------|--------------|--------------|
| <b>OProp1</b> | - / 184.0               | 2.59 / 29.9  | 1.39 / 9.9   |
| <b>OProp2</b> | - / 184.0               | 2.32 / 29.9  | 1.40 / 9.9   |
| <b>OProp3</b> | - / 180.0               | 2.25 / 30.3  | 1.14 / 9.7   |
| <b>OProp4</b> | - / 179.7               | 2.42 / 30.4  | 1.26 / 9.4   |
| <b>OProp5</b> | - / 178.4               | 2.82 / 30.1  | 1.39 / 9.9   |
| <b>OProp6</b> | - / n.o.*               | 2.16 / 28.4  | 1.03 / 8.4   |
| <b>OH</b>     | 11.76, 7.67, 7.43, 6.21 |              |              |

\* n.o. = not observed

Temperature dependent measurements are shown in Figure 36. The use of  $d_8$ -toluene as the NMR solvent allowed covering a wide temperature range (-100 °C - 100 °C) which was not possible for **Zr4** and **Zr6** because of poor solubility at low temperatures. As apparent, the  $^1\text{H}$  NMR spectra underwent dramatic changes with temperature. At -20 °C seven resonances were observed for the carbonyl carbons. At -40 °C nine different carbonyl carbons were identified, indicating that symmetry was lowered from  $C_{2h}$  to  $C_i$  or  $C_s$  at low temperatures. Further cooling to -100 °C resulted in broad and unstructured spectra because all ligands became inequivalent.

The sharp pattern of the  $^1\text{H}$  NMR signals at room temperature successively coalesced when the sample was heated. However, at 100 °C one propionate ligand was still well separated, i.e. full coalescence was not observed. Further heating was not possible because of solvent limitations.

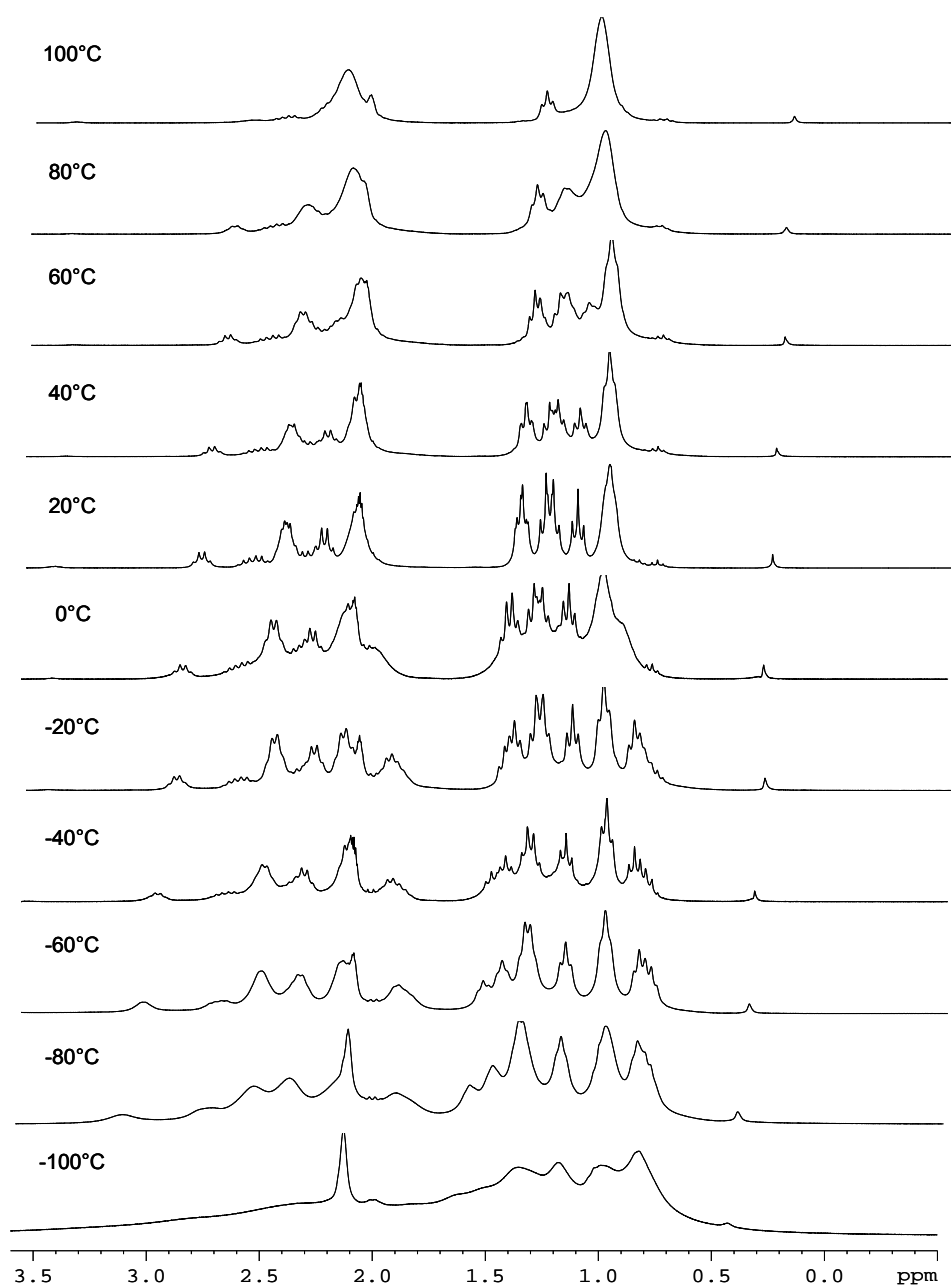


**Figure 36:** Temperature dependent  $^1\text{H}$  NMR spectra of **Zr12** in  $d_8$ -toluene; OH are not shown

### 3.2.4 Conclusion

In summary, it was ascertained that the symmetry of different types of zirconium oxo clusters, viz. **Zr4**, **Zr6** and **Zr12**, was retained in solution and that the clusters were stable. Carboxylate ligands on the cluster surface were not static but showed fast mutual exchange. The **Zr4** cluster showed the fastest exchange processes because the signals coalesced at room temperature. Cooling a  $\text{CD}_2\text{Cl}_2$  solution to  $-80\text{ }^\circ\text{C}$  resulted in four resolved sets of ligand signals which was in accordance with the molecular symmetry in the crystalline state. Judged from EXSY experiments at this temperature, no exchange processes took place on the NMR time scale. At  $-70\text{ }^\circ\text{C}$  a chelating ligand exchanged with a bridging ligand. At  $-60\text{ }^\circ\text{C}$  three inequivalent ligands were found to exchange with each other whereby intermolecular exchange of ligands between cluster and free acid could not be neglected. In titration experiments, the sensitivity of the cluster towards water was proven. Stoichiometric amounts of water in form of water saturated  $\text{CD}_2\text{Cl}_2$  were added successively to a solution containing **Zr4**. Changes in the  $^1\text{H}$  NMR spectra indicated that the cluster indeed was decomposed by water. Addition of three equivalents of water led to a precipitation of a white solid which was insoluble in organic solvents and water and was ascribed to  $\text{ZrO}_2$ .

The **Zr6** molecule had  $\text{C}_{3v}$  symmetry in the crystalline state. The  $^1\text{H}$  NMR spectrum showed signal splitting at room temperature, indicating that the coalescence temperature was somewhat higher when compared to **Zr4**. Cooling a  $\text{CD}_2\text{Cl}_2$  solution to  $-80\text{ }^\circ\text{C}$  resulted in three resolved sets of ligand signals, as it was expected from molecular symmetry. The presence of acidic OH groups in close neighbourhood to cluster-bonded methacrylate ligands in the molecule raised the question whether transesterification of methacrylates with ester molecules in solution was catalyzed. To this end, **Zr6** was dissolved in  $\text{CHCl}_3$ , ethyl acetate was added and the solution was refluxed for 1 hour.  $^1\text{H}$  NMR spectra of the product revealed no indication for transesterification.

The **Zr12** cluster showed sharp signals in  $^1\text{H}$  NMR spectra at room temperature. In good agreement with molecular symmetry ( $\text{C}_{2h}$ ), 6 sets of signals were observed in 2D NMR experiments. The good solubility of **Zr12** in toluene allowed covering a wide temperature range. From room temperature to  $-20\text{ }^\circ\text{C}$  the cluster showed  $\sim\text{C}_{2h}$  symmetry. Further cooling resulted in broad and unstructured  $^1\text{H}$  signals, indicative of a lowering of the symmetry to  $\text{C}_i$  or  $\text{C}_1$ . When the solution was heated, the signals broadened successively. At  $100\text{ }^\circ\text{C}$  all ligands except one coalesced, indicating fast ligand exchange on the NMR time scale as it was observed for the **Zr4** cluster at room temperature.

### 3.3 Considerations about Cluster Formation

Generally, three aspects have to be considered in the formation of zirconium oxo clusters by the carboxylic acid sol-gel route: The type of zirconium alkoxide, the type of carboxylic acid and the stoichiometric ratio applied in syntheses. The interplay between these factors decides on whether a cluster crystallizes from the reaction solution or not and which type of cluster is formed. Characterization of compounds with IR and NMR spectroscopy without a single crystal structure is difficult because of ligand exchange in solution and associated symmetry reasons (see above).

#### 3.3.1 Type of Zirconium Alkoxide

The type of alkoxide, ' $\text{Zr}(\text{OR})_4$ ', used in the preparation of zirconium oxo clusters is an important point. Commonly, transition metal alkoxides in solution are oligomeric compounds and/or solvent adducts in order to satisfy the coordination requirements of the metal atom. Apart from physical parameters, such as concentration and temperature, aggregation depends on the size of the metal atom, the size of the alkoxide groups and the type of the solvent [3, 79].

Dimeric solvent adducts were postulated for zirconium alkoxides with  $\text{R} = \text{O}^i\text{Pr}$ ,  $\text{O}^n\text{Pr}$  and  $\text{O}^n\text{Bu}$ . In the case of  $\text{Zr}(\text{O}^i\text{Pr})_4$  this suggestion was confirmed with a single crystal structure [80], the precursor  $\text{Zr}_2(\mu\text{-O}^i\text{Pr})_2(\text{O}^i\text{Pr})_6(\text{HO}^i\text{Pr})_2$  is commercially available. EXAFS measurements of  $\text{Zr}(\text{O}^n\text{Pr})_4$  in propanol solution indicated this dimeric structure [81], molecular weight determination revealed an average aggregate size of 2.44. However, in single crystal measurements Day et al. observed a tetrameric species,  $\text{Zr}_4(\mu_3\text{-OPr})_2(\mu_2\text{-OPr})_4(\text{OPr})_{10}$ , which kept its integrity in hydrocarbon solution [82]. In the case of zirconium butoxide a degree of association was determined to 1.77 and  $\text{Zr}(\text{OBu})_4(\text{HOBu})_2$  was postulated [79] which is in equilibrium with oligomers.

The presence of dimeric or tetrameric alkoxides as the precursors raised the question whether oxo clusters are assembled from pre-formed units. Most of the compounds obtained from the precursors  $\text{Zr}(\text{OPr})_4$  and  $\text{Zr}(\text{OBu})_4$ , respectively, indeed showed even numbers of zirconium atoms. The formation of the clusters with odd numbers, such as  $\text{Zr}_5\text{O}_4(\text{OIsobPr})_{10}(\text{OPr})_2(\text{HOPr})_4$ , indicated that mono- or trimetallic species were incorporated in the formation process. The same was the case for the clusters  $\text{Zr}_6\text{O}_2(\text{OBu})_{10}(\text{OMc})_{10}$  and  $\text{Zr}_6\text{O}_2(\text{OMe})_4(\text{OBu})_2(\text{OMc})_{14}$ . Although the overall number of Zr atoms is even, in fact these clusters consist of two  $\text{Zr}_3$  subunits rather which are connected with two  $\mu_2$ -alcoholates each.

### 3.3.2 Type of Carboxylic Acid

In this work,  $\text{Zr}(\text{OBu})_4$  as the precursor was reacted with various carboxylic acids in order to prepare oxo cluster compounds, the successful syntheses were already described in section 3. However, many of the carboxylic acids used did not form the desired compounds, to be more correctly, no crystalline products were obtained. For instance, bifunctional acids, such as itaconic acid, lactic acid, alanine and aminobenzoic acids (o-, m-, p-isomers) immediately led to a precipitation of amorphous white solids when they were reacted with  $\text{Zr}(\text{OBu})_4$  in various amounts, typically 1:1, 1:4, 1:7 and 1:10. An additional factor in these attempts probably was the use of additional solvent because the solid acids were not sufficiently soluble in the alkoxide. Therefore, saturated solutions of acids in butanol were applied in the syntheses. Replacing the alcohol for  $\text{CH}_2\text{Cl}_2$  and toluene, if possible, also led to a precipitation.

When formic acid was reacted with  $\text{Zr}(\text{OBu})_4$  in various stoichiometric amounts, the solution formed a gel within a short time. When a mixture of formic acid and methacrylic acid was reacted with the alkoxide, the cluster  $\text{Zr}_6\text{O}_4(\text{OH})_4(\text{OMc})_{12}(\text{BuOH})$  was obtained which showed the same structural features as **Zr6-McIsob**, i.e. one bridging ligand opposite the chelated face of the  $\text{Zr}_6$  octahedron switched to a dangling mode and the free coordination site was occupied with a coordinated butanol molecule. Unfortunately, this compound could not be reproduced in several attempts. However, no coordinated formates were found in the crystal structure, indicating that methacrylates were favoured as the ligands when compared to formates. Several other carboxylic acids, such as 2-phenyl-propionic acid, crotonic acid and allylacetic acid did not form the desired structures either, probably because of steric reasons.

As a proof of principle, the bidentate carboxylic acids were replaced by 2-methoxy-4-propenylphenol (isoeugenol). Phenolic OH-groups are known to replace alkoxy groups in metal alkoxides [79] and this bidentate ligand was already used in the sol-gel process to lower the reactivity of zirconium alkoxides [83, 84]. Reaction of 7.6 equivalents of isoeugenol with 1 equivalent of  $\text{Zr}(\text{OBu})_4$  resulted in the crystalline monomeric zirconium complex  $\text{Zr}(\text{isoeugenolate})_4$  (Figure 37) instead of a cluster compound. Although isoeugenol was employed for the synthesis that contained about 9% of the *syn* isomer, only the isomer with the *anti* propenyl group was found in single crystal structures. Selected bond lengths are given in Table 26.

When mixtures of isoeugenol and carboxylic acids such as acetic acid and methacrylic acid were applied in syntheses, no crystalline compounds were obtained. Therefore, investigations with this type of chelating ligand were not further continued.

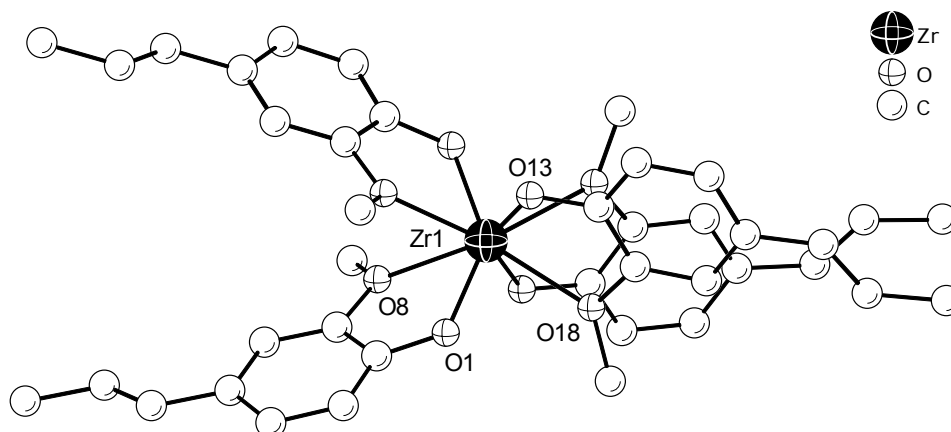


**Figure 37:** Molecular structure of  $\text{Zr}(\text{isoeugenolate})_4$ ; hydrogen atoms are omitted for clarity

**Table 26:** Zr - O bond lengths in  $\text{Zr}(\text{isoeugenolate})_4$

| Zr – O [pm]  |            |               |            |
|--------------|------------|---------------|------------|
| Zr(1) – O(1) | 205.26(23) | Zr(1) – O(13) | 206.15(31) |
| Zr(1) – O(8) | 239.22(31) | Zr(1) – O(18) | 240.57(30) |

Generally, the carboxylic acid has several tasks in oxo cluster formation: First of all the carboxylate must substitute OR groups of the alkoxide and thus liberate alcohol. In a second step water must be produced through esterification reaction of the excess acid with liberated alcohol to enable condensation to a cluster compound (Scheme 6, p.13). It was shown recently that the formation rate of ester plays an important role and thus influences the size and shape of the obtained clusters [53]. To this end, the formation of the cluster  $\text{Zr}_{12}\text{O}_8(\text{OH})_8(\text{OProp})_6(\text{OMc})_{18}$  was followed by NMR spectroscopy starting from  $\text{Zr}(\text{O}i\text{Bu})_4$ , propionic acid and methacrylic acid. After 6 hours only the formation of butyl propionate was observed, whereas no butyl methacrylate was detected in the reaction solution. It was concluded that reaction of  $\text{Zr}(\text{O}i\text{Bu})_4$  with acids showing fast ester formation, such as acetic acid and propionic acid, results in dimeric  $\text{Zr}_{12}$  structures, whereas slow ester formation favours  $\text{Zr}_6$  structures. As a conclusion, another factor which strongly determines the ability of cluster formation is the pK value of the carboxylic acid. Table 27 summarizes several carboxylic acids which were successfully applied in cluster syntheses and some where no crystalline clusters were obtained.

**Table 27:** Selection of successfully and unsuccessfully applied carboxylic acids for oxo cluster syntheses and their corresponding pKa values

| Successful       |      | Unsuccessful        |            |
|------------------|------|---------------------|------------|
| Acetic acid      | 4.76 | Itaconic acid       | 3.85, 5.45 |
| Propionic acid   | 4.88 | Lactic acid         | 3.86       |
| Methacrylic acid | 4.66 | o-Aminobenzoic acid | 4.98       |
| Vinylacetic acid | 4.42 | Alanine             | 2.35       |
| Isobutyric acid  | 4.86 | Formic acid         | 3.77       |

A proof for the strong influence of the pK value was observed in a deuteration experiment. The primary idea was to replace the  $\mu_3$ -OH groups in  $\text{Zr}_6\text{O}_4(\text{OH})_4(\text{OMc})_{12}$  for  $\mu_3$ -OD groups. By doing so, the cluster would be easily detectable in the hybrid polymers by solid state NMR. Therefore, the OH groups of methacrylic acid were replaced for OD groups through exchange reaction with  $\text{D}_2\text{O}$ , and the OD - deuterated acid was then applied in the preparation of **Zr6**. However, crystallization times were considerably longer (3 weeks instead of 1 week for **Zr6**), very low yields were obtained and the  $^1\text{H}$  NMR spectra differed very much from the pattern of **Zr6**. Moreover, in single crystal measurements the cell parameters could not be determined because of the bad quality of the obtained crystals. Since the experimental conditions were the same as they were applied for the protonated acid, this was explained with the change in the pK value because of the isotopic effect. Literature search revealed that the isotopic effect increases with increasing pK, being larger for weaker acids. Several authors reported correlations between the  $\text{pK}_\text{H}$  and the  $\text{pK}_\text{D}$  values of dissociation constants in  $\text{H}_2\text{O}$  and  $\text{D}_2\text{O}$ , respectively. The most recent and most reliable correlation was reported by Delgado et al. by analyzing dozens of compounds [85]. Correlation of these data led to the empiric equation  $\text{pK}_\text{D} = 0.32 + 1.044 \text{ pK}_\text{H}$ . On account of this, the pK value of methacrylic acid was shifted from 4.66 for the protonated to 5.19 for the deuterated species, leading to a different behaviour in the reaction with zirconium butoxide.

Taking into account the above remarks about carboxylic acids, a rough rule of thumb was derived concerning the requirements of a carboxylic acid towards cluster formation:

Reaction of a sterically modest, monofunctional carboxylic acid with a pK value in the range of about 4 - 5 with zirconium butoxide and propoxide, respectively, results in the formation of crystalline zirconium oxo clusters.

However, there exist exceptions: For instance, when  $\text{Zr}(\text{OPr})_4$  was reacted with 2-bromo-isobutyric acid ( $\text{pK} = 2.91$ ), a  $\text{Zr}_5$  structure was obtained [38], and when  $\text{Zr}(\text{OBu})_4$  was reacted with the bifunctional acid 3-mercaptopropanoic acid ( $\text{pK} = 4.34$ ), a  $\text{Zr}_{12}$  structure was obtained [86].

### 3.3.3 Stoichiometric Ratio of Alkoxide and Carboxylic Acid

A third main point in cluster formation is the stoichiometric ratio in which the carboxylic acid is reacted with the alkoxide. Three different cluster geometries were obtained for the system consisting of  $\text{Zr}(\text{OBU})_4$  and methacrylic acid when they were reacted in various amounts (Figure 38).

A carboxylic acid to alkoxide ratio of 1.6 : 1 resulted in the formation of the cluster  $\text{Zr}_6\text{O}_2(\text{OBU})_{10}(\text{OMc})_{10}$  within one month in poor yield [47]. The low ratio applied in the synthesis provided a very open cluster with unsubstituted OR groups and with a low degree of condensation because little water was produced in the esterification reaction. When the ratio was increased to 4 : 1, the cluster  $\text{Zr}_6\text{O}_4(\text{OH})_4(\text{OMc})_{12}$  was obtained in quantitative yields within one week [19]. All alkoxide groups were substituted for methacrylate ligands, and sufficient water was produced in an esterification reaction which allowed condensation to a compact cluster core. A very high methacrylic acid to alkoxide ratio of 7 : 1 resulted in the formation of the cluster  $\text{Zr}_4\text{O}_2(\text{OMc})_{12}$  within one day [19]. A high degree of substitution was achieved, i.e. three carboxylates per zirconium atom. As a consequence, a rather open cluster was obtained because most of the coordination sites of the zirconium atoms were already occupied by the methacrylate ligands.

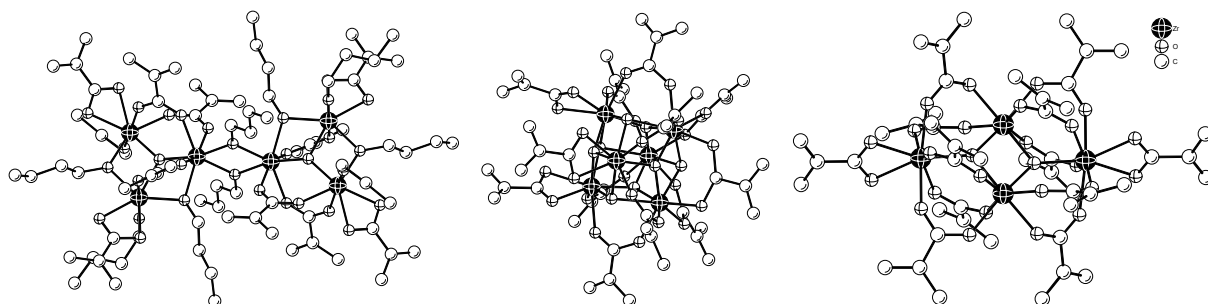


**Figure 38:** Molecular structures of  $\text{Zr}_6\text{O}_2(\text{OBU})_{10}(\text{OMc})_{10}$  (left),  $\text{Zr}_6\text{O}_4(\text{OH})_4(\text{OMc})_{12}$  (middle) and  $\text{Zr}_4\text{O}_2(\text{OMc})_{12}$  (right); hydrogen atoms are omitted for clarity

Conceptually, methacrylic acid and  $\text{Zr}(\text{OBU})_4$  was the only system which formed three main types of cluster geometries. However, this showed the general possibility of tuning the cluster sizes and shapes and the degrees of substitution by a simple variation of the stoichiometric ratios in cluster syntheses.



### 3.3.4 Conclusion

By summarizing the above considerations it was concluded that several factors influence the cluster formation.

A first important point was the type of alkoxide used in cluster preparation. Transition metal alkoxides usually are oligomeric compounds and/or solvent adducts and dimeric solvent adducts were postulated for some zirconium alkoxides in solution. In the case of  $\text{Zr}(\text{O}^i\text{Pr})_4$  this was confirmed by a single crystal structure [80], whereas  $\text{Zr}(\text{OPr})_4$  was found to be tetrameric in the crystalline state [82]. On account of this, the question rose whether clusters are assembled of pre-formed alkoxide adducts. Most of the clusters obtained indeed showed an even number of zirconium atoms, however, clusters such as  $\text{Zr}_5\text{O}_4(\text{OIsobBr})_{10}(\text{OPr})_2(\text{HOPr})_4$  and  $\text{Zr}_6\text{O}_2(\text{OBu})_{10}(\text{OMc})_{10}$  prove that odd units, monomeric or trimeric, were incorporated in cluster formation. Although the overall number of zirconium atoms in the latter case was even, the structure consisted of two  $\mu_3\text{-O} - \text{Zr}_3$  subunits rather.

Another, main factor was the type of carboxylic acid which was applied in the preparation of oxo clusters. In this work, bi-functional acids, where the second functionality was a hydroxo, an amino or a carboxylato group, formed precipitates when they were reacted with  $\text{Zr}(\text{OBu})_4$ . Apart from that, the pK value played a crucial role. Acids with a pK in the range of ~4 - 5 formed clusters in many cases. For instance, formic acid with a pK of 3.77 led to fast gel formation when it was mixed with  $\text{Zr}(\text{OBu})_4$  in various amounts. When a mixture of formic acid and methacrylic acid was applied in the synthesis, only methacrylate ligands were coordinated to a  $\text{Zr}_6$  cluster, and no formates were present in a crystal structure. A more pronounced influence of the pK was observed when  $\text{Zr}(\text{OBu})_4$  was reacted with OD deuterated methacrylic acid in the same conditions as they were applied in the preparation of **Zr6**. Crystallization times were very long, and  $^1\text{H}$  NMR spectra indicated a structure different from **Zr6**. This was attributed to the isotopic effect upon replacing the proton for a deuterium. According to an empiric formula, the pK value of methacrylic acid changed from 4.66 to 5.19.

A third factor which strongly determined cluster formation was the stoichiometric ratio between alkoxide and carboxylic acid. In the system  $\text{Zr}(\text{OBu})_4$  and methacrylic acid, three different cluster types were obtained in terms of geometry and degree of substitution.

## 4 Titanium Oxo Clusters

In contrast to zirconium oxo clusters, many structurally characterized carboxylate substituted titanium oxo clusters were reported. Depending on the titanium alkoxides used in the syntheses, the carboxylic acids, their stoichiometric ratio and the reaction conditions, several cluster geometries were obtained, ranging from  $Ti_3$  up to  $Ti_9$  structures (for a recent review see reference [33]).

In a proof of principle approach, different titanium alkoxides, viz ethoxide, propoxide and isopropoxide, were reacted with 5-norbornene-2-carboxylic acid or isobutyric acid. By doing so, titanium oxo clusters carrying carboxylate groups which are, in principle, accessible to ROMP or with non-reactive carboxylate groups, were obtained.

### 4.1 $Ti_6O_4(OPr)_8(ONorb_{mix})_8$

When titanium propoxide was reacted with 5-norbornene-2-carboxylic acid in the presence of propanol, the crystalline cluster  $Ti_6O_4(OPr)_8(ONorb_{mix})_8$  (**Ti6-Norb<sub>mix</sub>**) was obtained in high yields. Clusters of the same structural type were previously obtained for several combinations of OR (OEt, OPr, OBu, O<sup>i</sup>Pr) and OOCR (acetate, acrylate, methacrylate, benzoate, 2-bromoisobutyrate) [18, 38, 87-90]. The main structural features are shown in Figure 39. All Ti atoms were located in a planar arrangement and revealed an octahedral coordination by oxygen atoms. The oxygen atoms originated from five different types of ligands:  $\mu_2$ - and  $\mu_3$ - oxo bridges [O(1), O(2)], bridging [O(3)] and terminal [O(7), O(11), O(15)] propoxides and bridging norbornene carboxylate ligands [O(19)-O(21), O(29)-O(31), O(39)-O(41), O(49)-O(51)].

The asymmetric unit of **Ti6-Norb<sub>mix</sub>** contained two halves of the molecule which had nearly identical structural parameters (Figure 40). The overall structure of the hexanuclear cluster was centrosymmetric, three crystallographically independent titanium atoms [Ti(1), Ti(2), Ti(3) and Ti(4), Ti(5), Ti(6), respectively] formed a sub-unit.

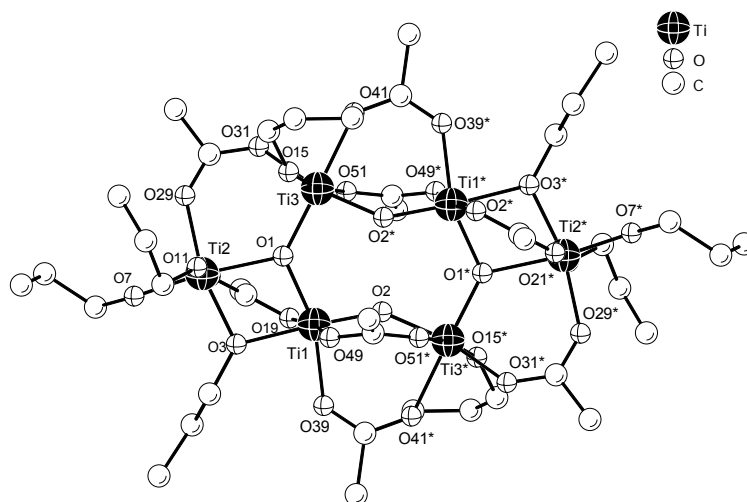


**Figure 39:** Molecular structure of  $\text{Ti}_6\text{O}_4(\text{OPr})_8(\text{ONorb}_{\text{mix}})_8$ ; only the  $\alpha$ -atom of the norbornenyl group is shown and hydrogen atoms are omitted for clarity

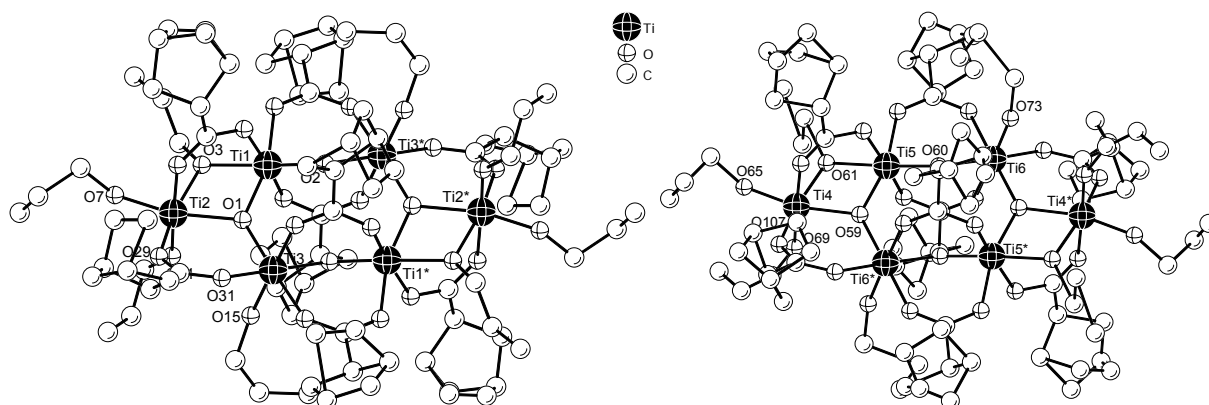


**Figure 40:** Molecular structures of the two molecules of **Ti6-Norb<sub>mix</sub>** in the crystal unit, hydrogen atoms are omitted for clarity

Selected bond lengths are given in Table 28. The Ti - O bond lengths were found between 175 and 217 pm. This large variation resulted from the different kind of oxygen donors and was additionally influenced by the nature of the trans ligand. The longest Ti - O distances were generally found trans to a terminal propoxy ligand. For example, the distance of the  $\mu_3$ -O atom O(1) to Ti(2) was significantly longer than to Ti(1) and Ti(3), respectively. Ti(2) had a propoxide ligand in the trans position whereas Ti(1) and Ti(3) had a norborneate ligand.

**Table 28:** Ti – O bond lengths in **Ti6-Norb<sub>mix</sub>**

| Ligand Type          | Bond lengths [pm] |          | Bond lengths [pm] |          |
|----------------------|-------------------|----------|-------------------|----------|
|                      | Molecule 1        |          | Molecule 2        |          |
| $\mu_3$ -Oxo         | O(1) – Ti(1)      | 190.7(3) | O(59) – Ti(4)     | 208.3(4) |
|                      | O(1) – Ti(2)      | 207.0(3) | O(59) – Ti(5)     | 189.8(5) |
|                      | O(1) – Ti(3)      | 189.5(3) | O(59) – Ti(6)*    | 189.7(4) |
| $\mu_2$ -Oxo         | O(2) – Ti(1)      | 175.3(3) | O(60) – Ti(5)     | 175.8(4) |
|                      | O(2)* – Ti(3)     | 187.7(3) | O(60) – Ti(6)     | 187.1(4) |
| Propoxide bridging   | O(3) – Ti(1)      | 204.9(4) | O(61) – Ti(4)     | 196.2(5) |
|                      | O(3) – Ti(2)      | 193.9(4) | O(61) – Ti(5)     | 208.6(4) |
| Propoxide terminal   | O(7) – Ti(2)      | 179.6(4) | O(65) – Ti(4)     | 177.9(5) |
|                      | O(11) – Ti(2)     | 176.6(4) | O(69) – Ti(4)     | 176.8(5) |
|                      | O(15) – Ti(3)     | 175.2(4) | O(73) – Ti(6)     | 180.0(5) |
| Norborneate bridging | O(19) – Ti(1)     | 199.4(3) | O(77) – Ti(4)     | 211.4(5) |
|                      | O(21) – Ti(2)     | 217.0(4) | O(79) – Ti(5)     | 197.9(5) |
|                      | O(29) – Ti(2)     | 202.1(5) | O(87) – Ti(5)     | 203.4(6) |
|                      | O(31) – Ti(3)     | 205.6(4) | O(89) – Ti(6)     | 207.0(6) |
|                      | O(39) – Ti(1)     | 202.9(4) | O(97) – Ti(5)     | 197.9(4) |
|                      | O(41)* – Ti(3)    | 208.1(4) | O(99) – Ti(6)     | 206.9(5) |
|                      | O(49) – Ti(1)     | 200.1(4) | O(107) – Ti(4)    | 199.9(7) |
|                      | O(51)* – Ti(3)    | 207.7(4) | O(109) – Ti(6)*   | 203.4(5) |

\* = inversion related atoms

## 4.2 $\text{Ti}_6\text{O}_4(\text{OEt})_8(\text{Olsob})_8$ and $\text{Ti}_6\text{O}_4(\text{OPr})_8(\text{Olsob})_8$

Reaction of isobutyric acid with titanium ethoxide or propoxide, dissolved in the corresponding alcohol, resulted in the formation of the clusters  $\text{Ti}_6\text{O}_4(\text{OEt})_8(\text{Olsob})_8$  and  $\text{Ti}_6\text{O}_4(\text{OPr})_8(\text{Olsob})_8$  (Figure 41). They showed the same structural features as the **Ti6-Norb<sub>mix</sub>** cluster described above: All Ti atoms were located in a planar arrangement and revealed an octahedral coordination by oxygen atoms. The oxygen atoms originated from five different types of ligands, the bond lengths to the titanium atoms are summarized in Table 29.

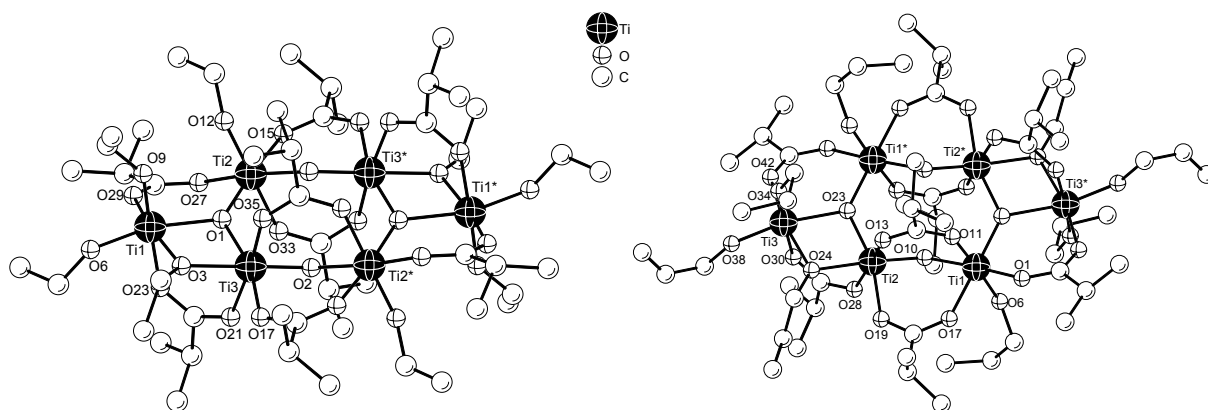


**Figure 41:** Molecular structures of  $\text{Ti}_6\text{O}_4(\text{OEt})_8(\text{OLSob})_8$  (left) and  $\text{Ti}_6\text{O}_4(\text{OPr})_8(\text{OLSob})_8$  (right); hydrogen atoms are omitted for purposes of clarity

**Table 29:** Ti - O distances in  $\text{Ti}_6\text{O}_4(\text{OEt})_8(\text{OLSob})_8$  and  $\text{Ti}_6\text{O}_4(\text{OPr})_8(\text{OLSob})_8$

| Ligand Type                   | Bond lengths [pm] in<br>$\text{Ti}_6\text{O}_4(\text{OEt})_8(\text{OLSob})_8$ |            | Bond lengths [pm] in<br>$\text{Ti}_6\text{O}_4(\text{OPr})_8(\text{OLSob})_8$ |            |
|-------------------------------|---|------------|---|------------|
| $\mu_3$ -Oxo                  | O(1) – Ti(1)  | 206.50(27) | O(23) – Ti(1)*  | 190.06(24) |
|                               | O(1) – Ti(2)  | 189.16(27) | O(23) – Ti(2)   | 189.42(24) |
|                               | O(1) – Ti(3)  | 190.54(27) | O(23) – Ti(3)   | 209.41(23) |
| $\mu_2$ -Oxo                  | O(2)* – Ti(2)   | 187.37(26) | O(10) – Ti(1)   | 188.06(24) |
|                               | O(2)* – Ti(3)   | 175.22(27) | O(10) – Ti(2)   | 175.61(23) |
| Ethoxide / Propoxide bridging | O(3) – Ti(1)  | 195.19(31) | O(24) – Ti(2)   | 207.17(24) |
|                               | O(3) – Ti(3)  | 206.08(30) | O(24) – Ti(3)   | 196.23(26) |
| Ethoxide / Propoxide terminal | O(6) – Ti(1)  | 179.80(32) | O(6) – Ti(1)  | 176.01(27) |
|                               | O(9) – Ti(1)  | 178.20(33) | O(34) – Ti(3)   | 176.32(28) |
|                               | O(12) – Ti(2)   | 176.56(32) | O(38) – Ti(3)   | 181.08(26) |
| Isobutyrate bridging          | O(15) – Ti(2)   | 209.56(31) | O(1) – Ti(1)  | 205.21(28) |
|                               | O(17)* – Ti(3)*   | 203.90(30) | O(42) – Ti(3)   | 201.29(28) |
|                               | O(21) – Ti(3)   | 199.63(29) | O(11) – Ti(1)   | 208.57(27) |
|                               | O(23) – Ti(1)   | 215.06(30) | O(13) – Ti(2)   | 203.08(27) |
|                               | O(27) – Ti(2)   | 204.83(30) | O(17) – Ti(1)   | 208.83(26) |
|                               | O(29) – Ti(1)   | 204.53(33) | O(19) – Ti(2)   | 204.42(25) |
|                               | O(33) – Ti(2)   | 208.68(30) | O(28) – Ti(2)   | 200.57(27) |
|                               | O(35)* – Ti(3)*   | 201.47(30) | O(30)* – Ti(3)  | 207.83(28) |
|                               |   |            |   |            |
|                               |   |            |   |            |

\* = inversion related atoms

### 4.3 $\text{Ti}_6\text{O}_6(\text{O}^i\text{Pr})_6(\text{OIsob})_6$

A  $\text{Ti}_6$  cluster with a different geometry, when compared to the examples given above, was obtained when isobutyric acid was reacted with titanium isopropoxide in the presence of isopropanol. The cluster  $\text{Ti}_6\text{O}_6(\text{O}^i\text{Pr})_6(\text{OIsob})_6$  (Figure 42) showed the same structural features as the examples reported in literature [91-94]. The core of this molecule consisted of two six-membered rings of alternating Ti and O atoms  $[\text{Ti} - (\mu_3\text{-O})]_3$  that were stacked offset to each other. Each Ti central atom was surrounded by the three  $\mu_3\text{-O}$  atoms, two oxygen atoms of bridging isobutyrate, and one oxygen of a terminal isopropoxide ligand in a distorted octahedron. The observation of a  $\text{Ti}_6\text{O}_6$  core instead of a  $\text{Ti}_6\text{O}_4$  structure were attributed to a kinetic effect caused by the different size of the alkoxo ligands or the degree of aggregation of the parent alkoxides [33] (titanium ethoxide and propoxide are trimeric in solution, while titanium isopropoxide is monomeric [79]), or by a different ratio of substitution- and esterification reactions.

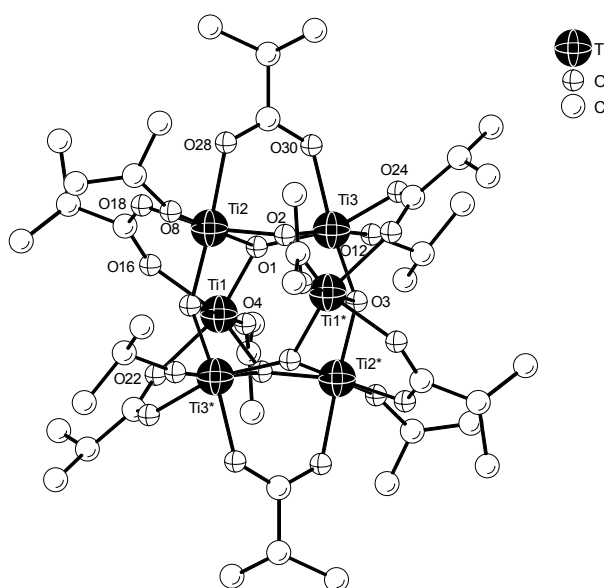


**Figure 42:** Molecular structure of  $\text{Ti}_6\text{O}_6(\text{O}^i\text{Pr})_6(\text{OIsob})_6$ , hydrogen atoms are omitted for clarity

Ti – O distances are given in Table 30. The  $\mu_3\text{-O}$  - Ti distances showed differences because of the trans ligands. Taking the O(1) - Ti(1)/Ti(2)/Ti(3) unit as an example, the distance O(1) - Ti(2) was 216 pm whereas the other two bond lengths, O(1) - Ti(1)/Ti(3), were 189 pm. This was again reasoned by the trans effect. Ti(1) and Ti(2) had an isobutyrate ligand in trans position, whereas Ti(2) had an isopropoxide ligand trans to the Ti -  $\mu_3\text{-O}$  bond, which resulted in a longer Ti - O distance.

**Table 30:** Ti - O bond lengths in  $\text{Ti}_6\text{O}_6(\text{OPr})_6(\text{OIsob})_6$ 

| Ligand Type  | Bond length [pm]                                     |                                  |
|--------------|--|----------------------------------|
| $\mu_3$ -Oxo | O(1) – Ti(1)/Ti(2)/Ti(3)                             | 188.78(21)/216.06(22)/189.04(22) |
|              | O(2) – Ti(1) <sup>*</sup> /Ti(2)/Ti(3)               | 190.42(23)/188.48(23)/214.62(22) |
|              | O(3) – Ti(1) <sup>*</sup> /Ti(2) <sup>*</sup> /Ti(3) | 215.01(23)/188.57(22)/190.84(23) |
| Isopropoxide | O(4) – Ti(1)   | 176.71(24)                       |
|              | O(8) – Ti(1)   | 176.98(23)                       |
|              | O(12) – Ti(2)  | 175.99(24)                       |
| Isobutyrate  | O(16) – Ti(1)  | 205.64(25)                       |
|              | O(18) – Ti(2)  | 205.58(25)                       |
|              | O(22) – Ti(1)  | 205.80(24)                       |
|              | O(24) <sup>*</sup> – Ti(3) <sup>*</sup>              | 206.15(24)                       |
|              | O(28) – Ti(2)  | 206.21(23)                       |
|              | O(30) – Ti(3)  | 203.60(24)                       |

\* = inversion related atoms

## 4.4 $\text{Ti}_2(\text{OPr})_6(\text{isoeugenolate})_2$

When titanium propoxide was reacted with 2.3 equivalents of isoeugenol, the centrosymmetric dimer  $\text{Ti}_2(\text{OPr})_6(\text{isoeugenolate})_2$  was obtained. Of course, this compound did not represent an oxo cluster. However, for the sake of completeness it is mentioned here. Such a compound was previously prepared by the reaction of  $\text{Ti}(\text{O}^i\text{Pr})_4$  with isoeugenol [95]. The derivative was spectroscopically characterized and used for the preparation of sol-gel materials with polymerizable organic groups. In this work it was possible to confirm the postulated structure with the preparation of the crystalline n-propyl derivative.

The asymmetric unit contained two halves of the molecule. Both had nearly identical structural parameters (Figure 43). The bond lengths of both the bridging and the terminal propoxide ligands were influenced by the corresponding trans ligand (Table 31). The shortest Ti - O distance was that trans to the bridging propoxide group [O(13) and O(41)], and the longest that of the bridging propoxide group trans to the terminal propoxide ligand [O(21)<sup>\*</sup> and O(37)<sup>\*</sup>].

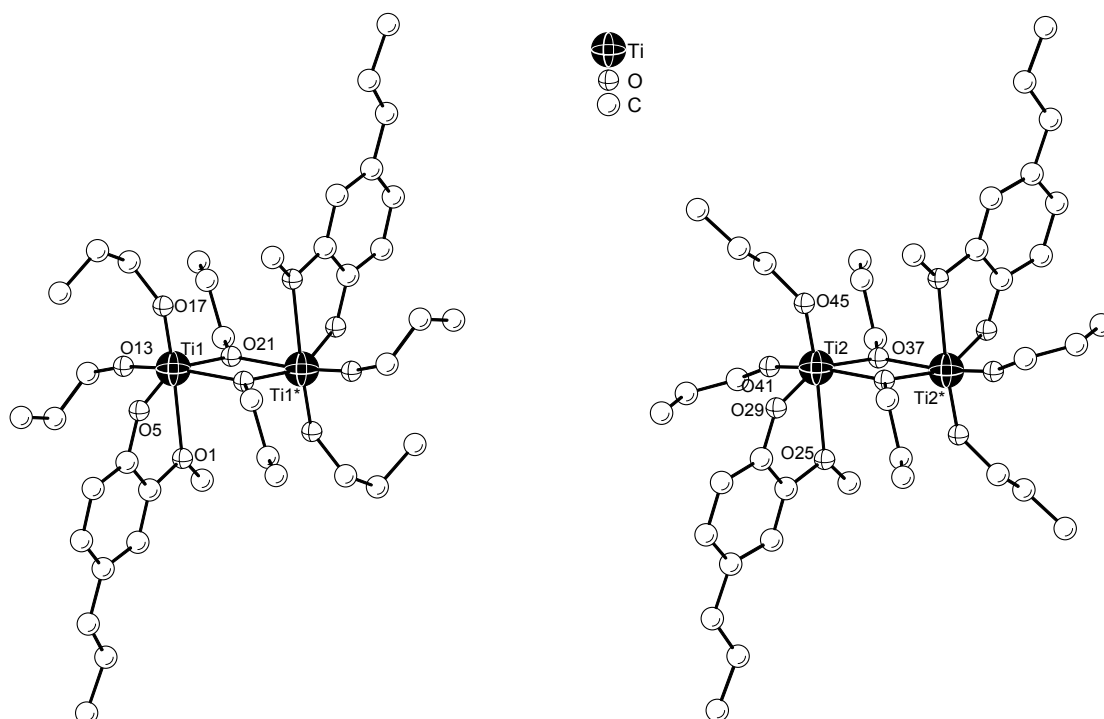


**Figure 43:** Molecular structure of the two molecules of  $\text{Ti}_2(\text{OPr})_6(\text{isoeugenolate})_2$  in the asymmetric unit, hydrogen atoms are omitted for clarity

**Table 31:** Ti – O bond lengths of  $\text{Ti}_2(\text{OPr})_6(\text{isoeugenolate})_2$

| Ligand Type        | Bond lengths [pm] |            | Bond lengths [pm] |            |
|--------------------|-------------------|------------|-------------------|------------|
|                    | Molecule 1        |            | Molecule 2        |            |
| Propoxide bridging | O(21) – Ti(1)     | 200.21(30) | O(37) – Ti(2)     | 199.43(31) |
|                    | O(21) – Ti(1)*    | 204.87(30) | O(37) – Ti(2)*    | 205.57(34) |
| Propoxide terminal | O(13) – Ti(1)     | 177.26(33) | O(41) – Ti(2)     | 177.49(38) |
|                    | O(17) – Ti(1)     | 178.05(33) | O(45) – Ti(2)     | 178.65(33) |
| Isoeugenolate      | O(1) – Ti(1)      | 238.55(32) | O(25) – Ti(2)     | 238.02(31) |
|                    | O(5) – Ti(1)      | 191.63(30) | O(29) – Ti(2)     | 192.08(31) |

\* = inversion related atoms



## 5 Hybrid Polymers

### 5.1 $\text{Zr}_4\text{O}_2(\text{OMc})_{12}$ Modified Polymers

Radical-initiated co-polymerization of the **Zr4** cluster with methyl methacrylate or styrene as the organic monomers resulted in materials showing improved thermal properties. The cross-linked polymers were insoluble in organic solvents such as benzene or ethyl acetate but showed swelling instead. Moreover, thermal depolymerization was retarded or even inhibited by the cluster cross-linking [77].

However, the thermal decomposition temperatures of the thus prepared hybrid polymers showed differences and did not follow a clear trend when the cluster proportion was increased. Moreover, NMR investigations of the **Zr4** cluster revealed a strong sensitivity to water. Thus, the monomers as well as the used solvents had to be desiccated very carefully [96] in a new attempt to improve the polymer properties by cluster cross-linking.

#### 5.1.1 $\text{Zr}_4\text{O}_2(\text{OMc})_{12}$ Modified Poly(methyl methacrylate)

To overcome problems with reproducibility of the previous obtained materials, polymerizations were carried out with methyl methacrylate which was distilled twice from  $\text{CaH}_2$  to remove both inhibitors and water.

The polymerization was difficult to control because of fast gel formation and auto-acceleration. The gel point corresponds to the incipient formation of an infinite network. All the polymerization steps may be assumed reaction-controlled prior to the gel point, which implies that the reaction rates constants are indeed constant. After the gel point this assumption is not valid for the cross-linking, the termination, and chain transfer to pendent vinyl group steps, because they become diffusion-controlled [97]. Consequently, the temperature in the solution, which cannot be released in time, is higher than the applied temperature and leads to heterogeneous polymerization. This behaviour is reflected in the short gelation times (e.g. less than 5 minutes)

and also in porous polymers with many bubbles incorporated. To this end, necessity was given to slow down the polymerization and to prolong gelation time, respectively.

In a first research direction, this was achieved by reducing the previously applied initiator concentrations and by using more solvent in the polymerization reactions, which might act as an efficient heat dissipation agent.

### Polymerizations with Initiator Variation

Three samples with the same cluster concentration in the monomer, viz ~1 mol%, were initiated with different amounts of benzoyl peroxide and polymerized at 70 °C for 24 hours to prolong the gelation times. The methyl methacrylate to benzene ratio was kept constant at 1 : 2.4, the lowest level possible to ensure complete dissolution of the **Zr4** cluster. After drying the samples *in vacuo*, the polymers were milled and extracted two times with ethyl acetate for three days each to remove residual benzene, followed by a repeated drying *in vacuo*, that time at 100 °C. The hybrid polymers were characterized by TGA and DSC.

The TGA curves in Figure 44 evidenced that there was a clear shift of the onset temperature of thermal decomposition in the cluster doped samples, but also that there was little influence of the initiator concentration on the thermal properties.

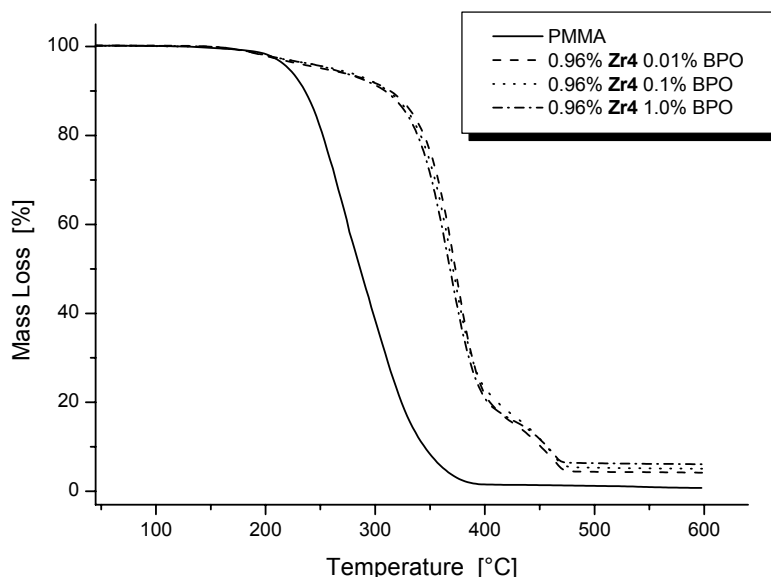


**Figure 44:** TGA curves of PMMA doped with 0.96 % of **Zr4** cluster; variation of the initiator concentration

Values for onset temperatures of each step and the related mass losses are summarized in Table 32.

**Table 32:** Thermal data of **Zr4** doped PMMA prepared with benzene as the solvent and varying initiator concentrations

| Sample                                       | Onset 1<br>[°C] | Mass<br>loss 1<br>[%] | Onset 2<br>[°C] | Mass<br>loss 2<br>[%] | Onset 3<br>[°C] | Mass<br>loss 3<br>[%] | Residual<br>mass<br>[%] | Residual<br>mass<br>calc. [%] | Gelation<br>time<br>[min] |
|--|-----------------|-----------------------|-----------------|-----------------------|-----------------|-----------------------|-------------------------|-------------------------------|---------------------------|
| PMMA 1%<br>BPO                               | -               | -                     | 245             | -                     | -               | -                     | -0.19                   | 0.00                          | 70                        |
| PMMA +<br><b>Zr4</b> + solv.<br>0.01%<br>BPO | 165             | 5.11                  | 346             | 79.29                 | 442             | 11.55                 | 4.03                    | 4.18                          | 40                        |
| PMMA +<br><b>Zr4</b> + solv.<br>0.1% BPO     | 162             | 4.03                  | 341             | 78.46                 | 447             | 12.49                 | 4.95                    | 4.18                          | 30                        |
| PMMA +<br><b>Zr4</b> + solv.<br>1% BPO       | 164             | 3.74                  | 338             | 80.80                 | 446             | 9.27                  | 4.93                    | 4.18                          | 7                         |

Neat PMMA did not exhibit appreciable mass loss below thermal decomposition, where 100 % of mass was lost due to thermo-oxidative degradation of the polymer chains. For cluster doped samples the behaviour was different, where two additional mass loss steps were at hand. The first mass loss, namely Mass loss 1 with the associated onset temperature Onset 1, was related to a loss of species with low molecular weights such as solvent (benzene, ethyl acetate), residual monomers or oligomers. By increasing the amount of initiator by two orders of magnitude from 0.01 % to 1 %, the Mass loss 1 decreased from 5.1 % to 3.7 %, indicating that either polymerization was more complete because less unreacted monomers were volatilized or that most of the solvent was removed in the latter samples. However, a mass loss below thermal decomposition of the main polymer should, in general, be avoided or kept as small as possible. To this end, industrial polymers undergo further treatment after polymerization which allows for improvements of the materials properties. Cross-linked polymers can only be extracted, dried and heated, which was applied in this case anyway.

Mass loss 2 with its onset temperature of thermal decomposition, Onset 2, took place between 300 and 420 °C and originated from a degradation of the main polymer chains and was also the stage where char formation took place. Onset 2 showed higher values when less benzoyl peroxide was used in the initiation of the polymerization.

Finally, the produced organic char was oxidatively volatilized at temperatures between 400 and 470 °C (Mass loss 3, Onset 3). It must be pointed out that values for Onset 3 are given just for

completeness and could not be determined accurately because they were very much influenced by Mass loss 2, which strongly determined a following onset.

To sum up, the overall mass loss of the **Zr4** hybrid polymers took place in three stages:

1. Mass loss below 150 °C which was related to species with low molecular weights, such as solvent, residual monomer or oligomers.
2. Major mass loss between 300 and 420 °C because of the degradation of the main polymer chains and char formation.
3. A mass loss between 400 and 470 °C originating from oxidative volatilization of organic char produced in step 2.

By reducing the amount of initiator in the polymerizations, more volatile residues were present in the systems, but also the onset temperature of thermal decomposition shifted to higher values.

An explanation for Mass loss 3 and the production of organic char in step 2 was found in the literature when comparing results from thermoset systems or fire retarding polymers. Correlations between cross-link density and thermal stability or fire resistance of polymers were studied extensively with controversial results, and it appeared to be no general relation.

For example, Nyden et al. [98] investigated the influence of the cross-linking density on the flammability of modified thermoplastics. The authors cross-linked polyethylene by  $\gamma$ -irradiation and showed increases in the char yields and in times of ignition by cone calorimetry.

Zaikov and Aseeva [99] studied the thermal degradation of cross-linked poly(methacrylates), but no increase in thermal stability was detected relative to that of pure poly(methyl methacrylate).

Levchik et al. cross-linked polystyrene with divinylbenzene and observed that cross-linked samples commenced degradation at higher temperatures than PS, while the onset of degradation for PMMA cross-linked with various dimethacrylates was at lower temperatures than for neat PMMA [100].

Nevertheless, there was a clear correlation between cross-linking and char formation which derived from a hindered degradation through unzipping of the polymer chains: When the unzipping or depropagation process reached a cross-linking point, it is necessary to simultaneously break two or more bonds, depending on the effective cross-link functionality, to liberate a fragment. An unzipping will stop at this point for the time being since such simultaneous breaking is most improbable as long as there are other mechanisms possible. This was a first reason in the production of organic char. A second aroused from the inorganic filler perception: The burning of polymeric materials can be viewed as a two step process whereby volatile fragments produced in the thermal degradation of the condensed phase mix with the

ambient oxygen in the gas phase where they are combusted. Much of the energy released in this process is absorbed and thermalized by the residual polymer. The cycle continues as long as there is sufficient heat to further pyrolyze the polymer into combustible products. The activity of fire retardants, such as metal oxides, is due to the ability to inhibit reactions which propagate gas-phase combustion or to their capacity to depress the rate of evolution of volatile compounds from the condensed phase [98]. Thus, the cluster might have acted as both a cross-linking point preventing a thermo-oxidative induced unzipping of polymer chains and as inorganic filler inhibiting the propagation of combustion.

Conceptually, this fact described the thermo-oxidative behaviour in almost all of the transition metal oxo cluster doped hybrid polymers (for examples see [44, 77, 101-104]). However, it was never discussed from the perspective of char formation. Of course, this was not only limited to transition metal oxo clusters, but was found in many systems, such as the POSS doped polymers [105-107].

From Table 32 it can also be seen that gelation times prolonged significantly when less initiator was applied. Apart from thermal properties this had also effects on the hybrid materials shapes. For instance, the polymer prepared with 0.01 wt% of benzoyl peroxide was obtained as a bulk polymer after drying, whereas the samples prepared with 0.1 and 1 wt% initiator, respectively, were obtained as porous pieces with many bubbles incorporated. The preparation of bulk polymers was of paramount importance for mechanical characterizations where holes in a specimen would make the results worthless.

In addition to TGA measurements, the samples were also characterized by DSC (Figure 45). Onset temperatures of thermal combustion appeared at lower temperatures than they were found in TGA measurements. However, onset temperatures determined by TGA and by DSC could not be compared because different heating rates were programmed (3 °C/min in DSC and 5 °C/min in TGA, respectively) and different atmospheres were applied: Whereas a dynamic air atmosphere was applied in TGA and the sample was located in an 'open pan', air atmosphere was static in DSC and a little hole in the pan was not sufficient for unhampered release of the gaseous products. Therefore, char formation and volatilization became an important issue.

The DSC curve for neat PMMA showed an awkward endothermic event that stretched from 200 to 350 °C. Thermal degradation of PMMA took place in this temperature region by chain radical reaction of depolymerization [108, 109]. A subsequent exothermic event at higher temperatures was thus less pronounced.

A different picture was observed in the cluster doped samples. Depolymerization reactions were hindered by incorporation of **Zr4** and onset temperatures of thermal combustion were also shifted. Remarkably, the latter event took place in at least two stages, indicating again that char

was formed during main polymer degradation which was then oxidatively volatilized at higher temperatures.

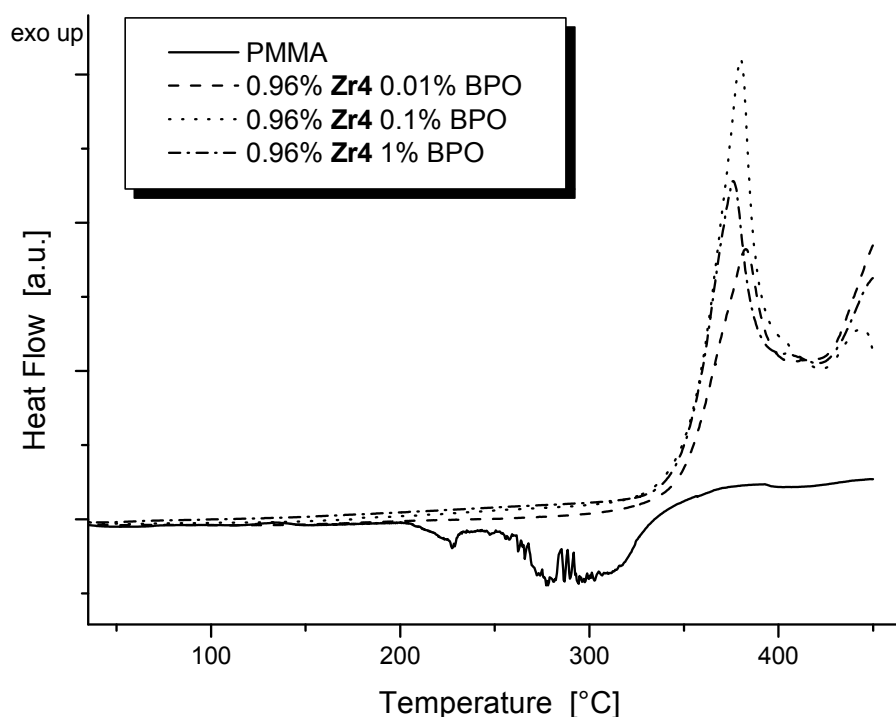


**Figure 45:** DSC thermographs of **Zr4** doped PMMA; variation of initiator concentration

Comparable to TGA results, no differences were obtained in DSC by changing the initiator concentrations in the preparation of hybrid polymers. It was tried to determine glass transition temperatures ( $T_g$ ) by removing the thermal history of the samples in a first heating scan at a ramp of 2 °C/min and taking  $T_g$  from a second run at a ramp of 40 °C/min. However, in none of the samples a transition was observed. Either the cross-linking density was too high that a  $T_g$  was not observed anymore [110], or the molecular weight distributions, i.e. polydispersities, of the thus prepared hybrid polymers were too large that a distinct glass transition was lost again.

The hybrid polymers were no longer soluble in organic solvents such as ethyl acetate, THF or benzene but showed swelling, i.e. solvent uptake, instead. A characteristic specification in polymer chemistry is the molecular weight and its distribution which is determined by size exclusion chromatography (SEC). In SEC, the polymers need to be dissolved in preferentially THF or DMF. Therefore, direct access was not possible for the cross-linked hybrid polymers. An alternative way to determine the molecular weights of the polymer chains was possible by considering the following facts:

- The **Zr4** cluster is degraded by acetyl acetone according to [111]



- The structure of  $\text{Zr(acac)}_4$  was reported by Wakeshima et al. [112]
- Doped polymers swelled in acetyl acetone
- PMMA is soluble in acetyl acetone

Taking use of the facts listed above, the cluster cross-linking was destroyed by adding a 1 : 1 mixture of ethyl acetate and acetyl acetone to milled polymers and stirring for several weeks at room temperature. Ethyl acetate was added to dissolve the polymers faster. Further treatments included the separation of the formed Zr-compounds by centrifugation and by various precipitation and re-dissolving steps from methanol and THF, respectively.

Molecular weights and polydispersities were thus accessible by SEC (Table 33). The molecular weights of the doped polymers decreased with increasing initiator concentration and thus with the gelation time from 3700 kg/mol to 200 kg/mol. The polydispersities were very large in all of the cases.

**Table 33:** Molecular weights and polydispersities of undoped and doped PMMA; variation of the initiator concentration

| Sample                              | $M_n$ [kg mol <sup>-1</sup> ] | $P_d$ | $t_g$ [min] |
|-------------------------------------|-------------------------------|-------|-------------|
| PMMA 1% BPO                         | 37.7                          | 2.16  | 70          |
| PMMA + 0.96% <b>Zr4</b> , 0.01% BPO | 3668.3                        | 4.04  | 40          |
| PMMA + 0.96% <b>Zr4</b> , 0.1% BPO  | 1687.6                        | 4.35  | 30          |
| PMMA + 0.96% <b>Zr4</b> , 1% BPO    | 202.5                         | 1.93  | 7           |

## Polymerizations with Solvent Variation

Next to varying the initiator concentrations, gelation times and thus molecular weights and polydispersities may be influenced by a variation of the solvent concentration whereby the solvent acts as a heat dissipation agent. This was investigated by polymerizing three samples with the same proportion of **Zr4** (1 mol%) and the same amount of initiator (0.1 wt% BPO), but with different amounts of solvent. After 24 hours at 70 °C the polymers were milled and extracted with ethyl acetate to remove residual benzene, followed by drying *in vacuo* at 100 °C.

The TGA measurements in Figure 46 revealed no influences of the solvent concentration on thermal properties. Mass losses took place in three distinct stages (Table 34) and were not different to the values obtained from initiator variation. Solely the gelation time was prolonged from 30 min for an MMA : benzene ratio of 1 : 2.4 to 120 min for a ratio of 1 : 10.3. Further increase of the solvent proportion prevented the polymerization solution from gelation and thus led to a precipitation of the polymer during polymerization.

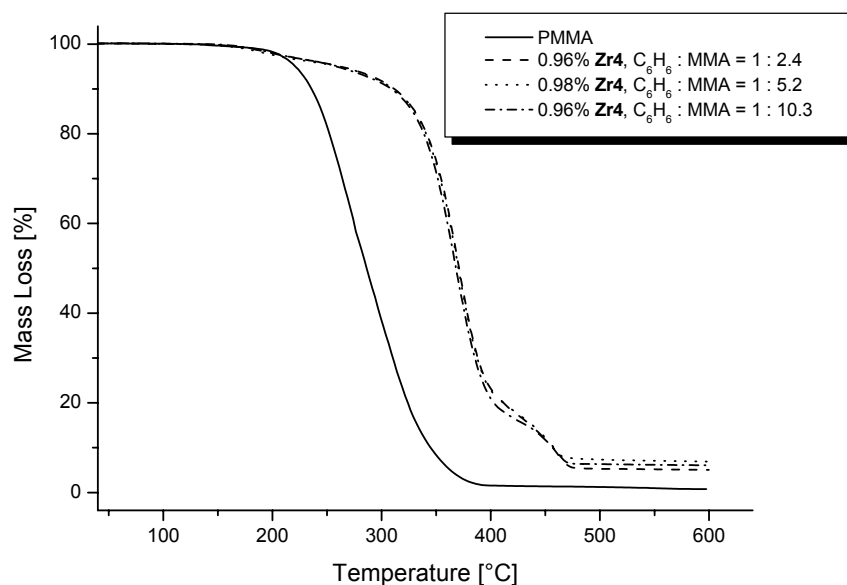


**Figure 46:** TGA curves of PMMA doped with ~1 mol% of **Zr4**; variation of the solvent concentration

The residual masses were too high when compared to values which were calculated theoretically by assuming that polymerization yield was 100 %, and that the entire **Zr4** proportion decomposed to  $\text{ZrO}_2$  during combustion. This was ascribed to non-crosslinked species which were extracted by ethyl acetate, and thus increased the proportion of **Zr4** in the hybrid polymers. A mass loss below thermal decomposition was ascribed to residual low molecular weight



species, mainly to the solvent. However, the loss of solvent was small enough that no thermal effect was observed by DSC (Figure 47).

**Table 34:** Thermal data of **Zr4** doped PMMA prepared with various amounts of benzene

| Sample                                | Onset 1 [°C] | Mass loss 1 [%] | Onset 2 [°C] | Mass loss 2 [%] | Onset3 [°C] | Mass loss 3 [%] | Residual mass [%] | Residual mass calc. [%] | Gelation time [min] |
|---------------------------------------|--------------|-----------------|--------------|-----------------|-------------|-----------------|-------------------|-------------------------|---------------------|
| PMMA                                  | -            | -               | 245          | -               | -           | -               | -0.59             | 0.00                    | 70                  |
| PMMA + <b>Zr4</b> + solv.<br>1 : 2.4  | 162          | 4.03            | 341          | 78.46           | 447         | 12.49           | 4.95              | 4.18                    | 30                  |
| PMMA + <b>Zr4</b> + solv.<br>1 : 5.2  | 160          | 4.22            | 340          | 77.85           | 447         | 10.70           | 6.81              | 4.26                    | 38                  |
| PMMA + <b>Zr4</b> + solv.<br>1 : 10.3 | 153          | 3.12            | 339          | 83.58           | 442         | 7.63            | 5.42              | 4.18                    | 120                 |

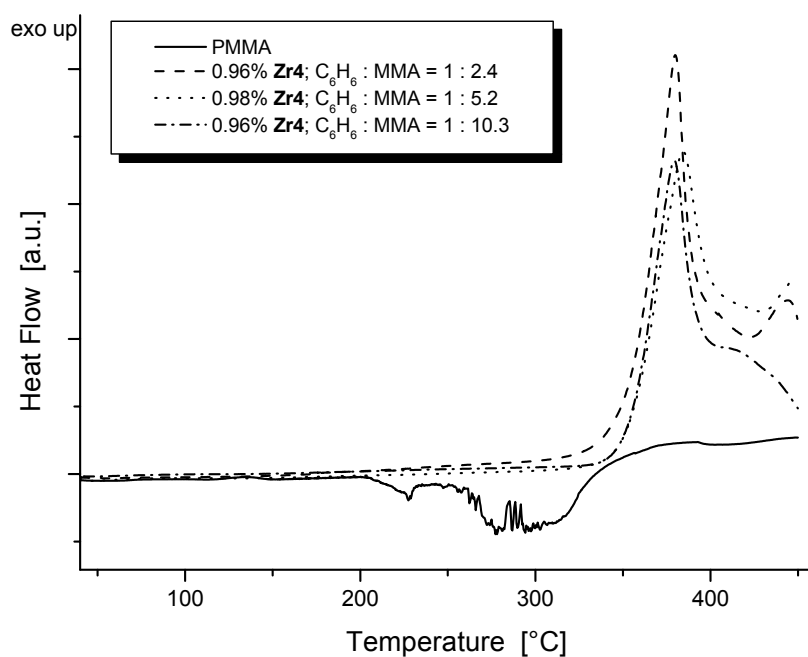


**Figure 47:** DSC curves of PMMA doped with ~1 % of **Zr4**; variation of the solvent concentration

Molecular weights were determined after treatment of the milled samples with acetyl acetone (Table 35).  $M_n$  was very high (1700 kg/mol) when the gelation time was prolonged up to two hours. By applying a solvent ratio of 1 : 2.5 and 1 : 5, respectively, no significant changes in the

gelation times and thus in the molecular weights were observed. Polydispersities seemed to be independent from the gelation times.

**Table 35:** Molecular weights and polydispersities of undoped and doped PMMA; solvent variation

| Sample                             | $M_n$ [kg mol <sup>-1</sup> ] | $P_d$ | $t_g$ [min] |
|------------------------------------|-------------------------------|-------|-------------|
| PMMA 1% BPO                        | 37.7                          | 2.16  | 70          |
| PMMA + <b>Zr4</b> + solv. 1 : 2.4  | 324.2                         | 2.64  | 30          |
| PMMA + <b>Zr4</b> + solv. 1 : 5.2  | 294.9                         | 1.92  | 38          |
| PMMA + <b>Zr4</b> + solv. 1 : 10.3 | 1687.6                        | 4.35  | 120         |

### Polymerizations without Solvent

All of the above described materials still contained some solvent after drying *in vacuo*. The residual benzene was removed for the most part by repeated extraction with ethyl acetate and subsequent drying at elevated temperatures *in vacuo*. However, this procedure was feasible for small polymer pieces or powders but not for bulk samples because the benzene could not be removed completely, neither by extraction with ethyl acetate for long times, nor by drying *in vacuo* at elevated temperatures.

Samples without residual solvent were prepared by making a saturated solution of **Zr4** in the monomer. After removal of undissolved cluster the polymerization was carried out by adding 1 % BPO as the radical initiator to this solution and heating to 70 °C for 24 hours. The polymers were then dried *in vacuo* at 100 °C.

The **Zr4** cluster amount in saturated solutions of MMA at room temperature was determined to 0.17 mol% by weighing back undissolved **Zr4** after removal of residual monomer. This was confirmed by elemental analysis results where the residual mass of ZrO<sub>2</sub> in the hybrid polymers was determined, and the initial **Zr4** concentration was calculated to 0.16 mol%.

A 0.16 mol% concentration of **Zr4** was significantly smaller than that applied before and this was also reflected in thermal measurements (Figure 48) where the first (low molecular residues) and the third (related to the cluster) mass losses could not be determined because of the very small values. The absence of a clear mass loss at temperatures below thermal decomposition proved the absence of unreacted monomers, thus an almost complete consumption took place and the monomers were removed by drying *in vacuo*.

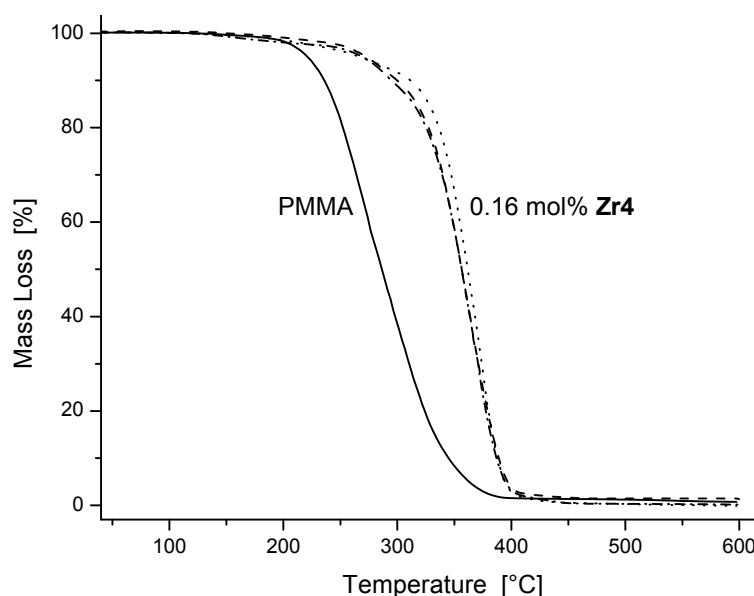


**Figure 48:** TGA curves of PMMA doped with 0.16 mol% of **Zr4**; polymerization without solvent

The onset temperatures of thermal decomposition of the main polymer chains (Table 36) were 10 °C lower when compared to the samples doped with 1 mol% of **Zr4**. Nevertheless, an improvement was obvious and quite remarkable when taking into account the small proportions of cluster which were applied.

**Table 36:** Thermal data for **Zr4** doped PMMA prepared from a saturated solution

| Sample                     | Onset | Residual mass [%] | Residual mass expected [%] | $t_g$ [min] |
|----------------------------|-------|-------------------|----------------------------|-------------|
| PMMA + <b>Zr4</b> sat. (1) | 323   | 1.10              | 0.78                       | 5           |
| PMMA + <b>Zr4</b> sat. (2) | 331   | -0.25             | 0.78                       | 5           |
| PMMA + <b>Zr4</b> sat. (3) | 325   | 0.07              | 0.78                       | 3           |

DSC measurements (Figure 49) revealed that small cluster proportions could not prevent the polymers from thermal depolymerization, but the endothermic signal in the doped sample was shifted to higher temperatures and was less broad than that of neat PMMA which was prepared under the same conditions. The exothermic peak of combustion of the main polymer was well defined and the peak of oxidative char volatilization formed only a shoulder at 430 °C due to the small cluster proportion.

The gelation times of the thus prepared polymers were very short, hence molecular weights were small as well (Table 37). Further attempts for improvement by variation of the initiator concentration were not conducted because the small cluster amounts did not prevent the

polymers from thermal depolymerization and also the onset temperature of thermal decomposition was not at an optimum.

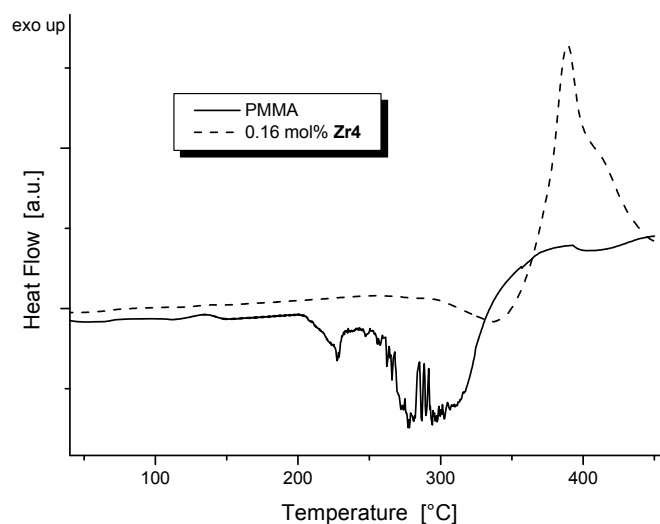


**Figure 49:** DSC curves of undoped and doped PMMA; polymerizations without additional solvent

**Table 37:** Molecular weights and polydispersities of undoped and doped PMMA; polymerizations without solvent

| Sample              | $M_n$ [kg mol <sup>-1</sup> ] | $P_d$ | $t_g$ [min] |
|---------------------|-------------------------------|-------|-------------|
| PMMA 1% BPO         | 37.7                          | 2.16  | 70          |
| <b>Zr4</b> PMMA (1) | 23.6                          | 2.58  | 5           |
| <b>Zr4</b> PMMA (3) | 23.8                          | 2.37  | 3           |

### 5.1.2 $Zr_4O_2(OMc)_{12}$ Modified Polystyrene

Investigations of the MMA-**Zr4** systems were extended to styrene. By reasoning the lower reactivity of styrene [113] when compared to methyl methacrylate [114], the differences between these two monomers had to be figured out when they were co-polymerized with the **Zr4** cluster. By applying the same polymerization procedures as for MMA, differences in the gelation times and molecular weights were expected.

## Polymerizations with Initiator Variation

Three samples with the same cluster concentration in the monomer (~1 mol%) were initiated with different amounts of BPO and polymerized at 70 °C for 24 hours. After drying the samples *in vacuo*, the polymers were milled and extracted two times with ethyl acetate for three days each to remove residual benzene, followed by a drying *in vacuo* at 100 °C.

TGA measurements (Figure 50) revealed that the thermal shifts were less reproducible when compared to PMMA samples, albeit a characteristic shift of the onset temperatures of thermal decomposition due to the cluster incorporation was obvious. Polystyrene had a thermal decomposition temperature 100 °C higher than that of PMMA. Therefore, the shift caused by cluster incorporation was less pronounced.

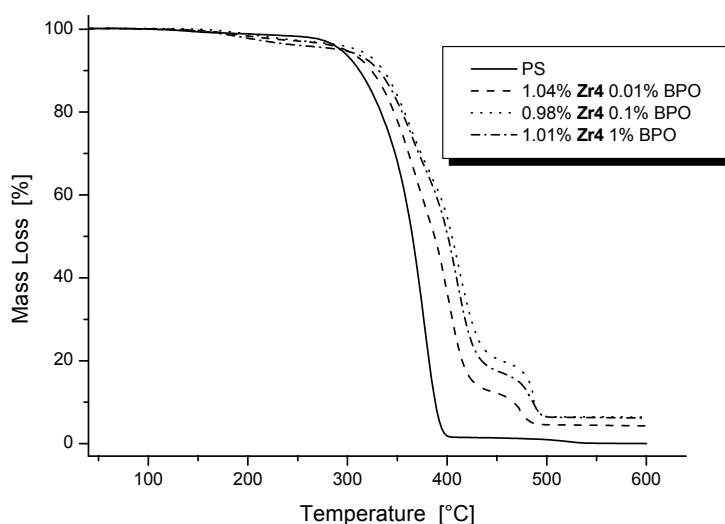


**Figure 50:** TGA curves of PS doped with 1 mol% of **Zr4**; variation of the initiator concentration

The mass loss took place in three stages which are summarized in Table 38.

The onset temperatures of thermal decomposition shifted from 340 °C for pure PS to 20 °C higher values for the doped samples. Volatile compounds were released with an onset temperature of about 160 °C and showed a mass loss which was in the same range as in the MMA case. The third mass loss, i.e. the loss related to char volatilization, was shifted from 445 °C for the PMMA samples to about 480 °C in the polystyrene samples.

Gelation times behaved predictable and were prolonged from 20 min for 1 wt% of initiator to 100 min for 0.01 wt% of BPO.

**Table 38:** Thermal data of **Zr4** doped PS prepared with benzene; initiator variation

| Sample                             | Onset 1<br>[°C] | Mass<br>loss 1<br>[%] | Onset 2<br>[°C] | Mass<br>loss 2<br>[%] | Onset3<br>[°C] | Mass<br>loss 3<br>[%] | Residual<br>mass<br>[%] | Residual<br>mass<br>calc. [%] | Gelation<br>time<br>[min] |
|------------------------------------|-----------------|-----------------------|-----------------|-----------------------|----------------|-----------------------|-------------------------|-------------------------------|---------------------------|
| PS<br>1% BPO                       | -               | -                     | 340             | '100'                 | -              | -                     | -0.13                   | 0.00                          | 135                       |
| PS+ <b>Zr4</b> +solv.<br>0.01% BPO | 163             | 3.19                  | 358             | 77.31                 | 480            | 13.25                 | 6.24                    | 4.37                          | 100                       |
| PS+ <b>Zr4</b> +solv.<br>0.1% BPO  | 157             | 2.86                  | 356             | 84.83                 | 481            | 4.92                  | 4.24                    | 4.12                          | 50                        |
| PS+ <b>Zr4</b> +solv.<br>1% BPO    | 153             | 4.39                  | 363             | 78.48                 | 475            | 10.94                 | 6.04                    | 4.24                          | 20                        |

By adding a mixture of 50 vol% of ethyl acetate and 50 vol% of acetyl acetone to the milled polymer samples, the cross-linking cluster units were destroyed and the polymer chains were released. After separating the polymers from zirconium compounds, the molecular weights and polydispersities were determined by SEC (Table 39). The molecular weights correlated to the gelation times and increased from 77 kg/mol to 175 kg/mol. However, also the polydispersities increased.

**Table 39:** Molecular weights and polydispersities of undoped and doped PS; initiator variation

| Sample                                  | $M_n$ [kg mol <sup>-1</sup> ] | $P_d$ | $t_g$ [min] |
|---|-------------------------------|-------|-------------|
| PS 1% BPO                               | 77.2                          | 1.8   | 70          |
| PS + 1.04% <b>Zr4</b> + solv. 0.01% BPO | 175.3                         | 3.5   | 100         |
| PS + 0.98% <b>Zr4</b> + solv. 0.1% BPO  | 96.7                          | 2.3   | 50          |
| PS + 1.01% <b>Zr4</b> + solv. 1% BPO    | 77.2                          | 1.8   | 20          |

DSC measurements revealed no signals other than exothermic combustion in the doped samples (Figure 51). PS is known to undergo thermal degradation by the chain radical mechanism [109] at elevated temperatures. This mechanism was hindered because of cross-linking and gave the explanation why there was an exothermic peak of combustion in the doped polymer, whereas in neat PS two signals compensated, i.e. exothermic combustion and endothermic degradation.

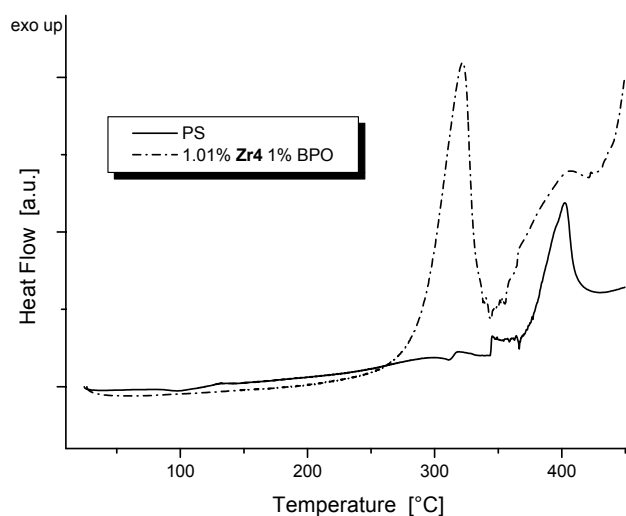


**Figure 51:** DSC curves of undoped and doped PS; polymerization with initiator variation

## Polymerizations with Solvent Variation

Polystyrene samples were also prepared by varying the solvent amount in the polymerizations with the objective to prolong gelation times. This was achieved by polymerizing three samples with the same proportion of **Zr4** in the monomer (1 mol%) and the same amount of initiator (0.1 wt% of BPO), but with different amounts of solvent. After 24 hours at 70 °C, the polymers were milled and extracted two times with ethyl acetate for three days each to remove residual benzene, followed by a drying *in vacuo* at 100 °C.

TGA measurements (Figure 52) revealed some influence of the solvent amount on thermal properties. The mass losses took place in three stages (Table 40) where Mass loss 1, i.e. the loss of solvent and unreacted monomers or oligomers, increased slightly with increasing solvent amount. The onset temperatures of thermal decomposition decreased when more solvent was applied. The residual masses differed very much from the values calculated by assuming that polymerization conversion was 100 %. This was a strong indication that polymerization was not complete when bigger amounts of solvent were applied in polymerizations. Unreacted monomers and oligomers were not incorporated into the cross-linked network and were dissolved in the swelling steps. As a consequence, the values for residual masses were much higher than expected.

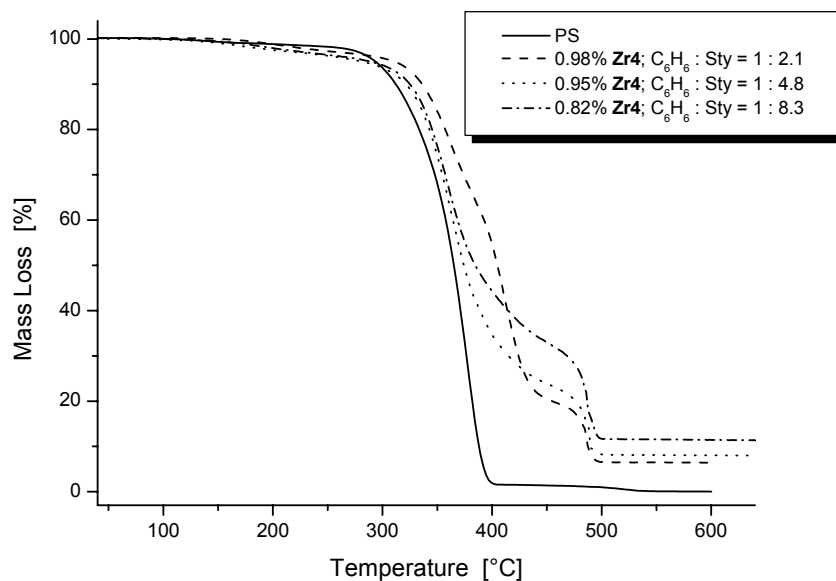


**Figure 52:** TGA curves of undoped and **Zr4** doped PS samples, polymerization with solvent variation

**Table 40:** Thermal data of **Zr4** doped PS; solvent variation

| Sample                | Onset 1 [°C] | Mass loss 1 [%] | Onset 2 [°C] | Mass loss 2 [%] | Onset 3 [°C] | Mass loss 3 [%] | Residual mass [%] | Residual mass calc. [%] | Gelation time [min] |
|-----------------------|--------------|-----------------|--------------|-----------------|--------------|-----------------|-------------------|-------------------------|---------------------|
| PS                    | -            | -               | 340          | '100'           | -            | -               | -0.59             | 0.00                    | 70                  |
| Sty :solv.<br>1 : 2.1 | 157          | 2.86            | 350          | 84.83           | 467          | 4.92            | 4.24              | 4.12                    | 50                  |
| Sty :solv.<br>1 : 4.8 | 138          | 3.0             | 332          | 73.46           | 481          | 15.46           | 7.95              | 3.99                    | 145                 |
| Sty :solv.<br>1 : 8.3 | 151          | 3.76            | 331          | 63.7            | 480          | 21.13           | 11.22             | 3.44                    | 260                 |

DSC measurements exhibited no signal apart from exothermic combustion (Figure 53) and glass transition temperatures were not observed.

Table 41 shows molecular weights and polydispersities of undoped and doped samples determined after destroying the cross-linking cluster units by acetyl acetone and purification of the polymers. For the sample prepared with a solvent to monomer ratio of 4.8 : 1, the data were not determined.



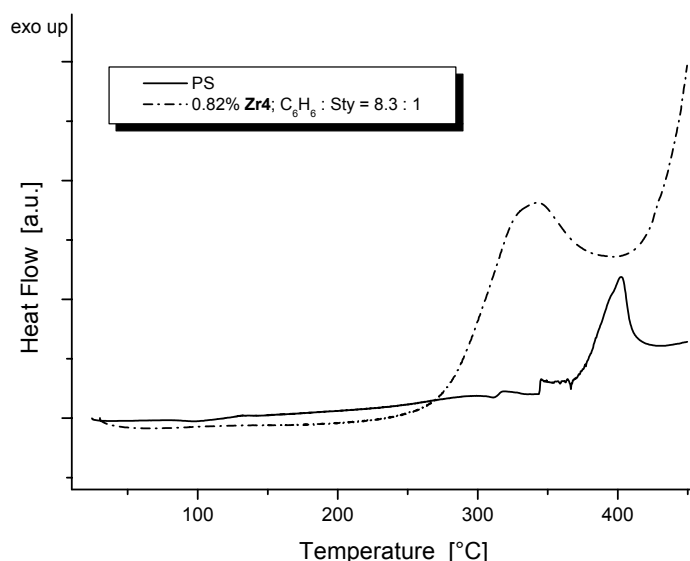


**Figure 53:** DSC curves of undoped and **Zr4** doped PS; polymerization with solvent variation

**Table 41:** Molecular weights and polydispersities of undoped and doped PS; initiator variation

| Sample                          | $M_n$ [kg mol <sup>-1</sup> ] | $P_d$ | $t_g$ [min] |
|---------------------------------|-------------------------------|-------|-------------|
| PS                              | 77.2                          | 1.8   | 70          |
| PS + <b>Zr4</b> + solv. 1 : 2.1 | 175.3                         | 3,5   | 50          |
| PS + <b>Zr4</b> + solv. 1 : 4.8 | -                             | -     | 145         |
| PS + <b>Zr4</b> + solv. 1 : 8.3 | 55.5                          | 1,87  | 260         |

## Polymerizations without Solvent

Apparently, the use of solvent was a crucial factor in styrene systems. Therefore, samples without additional solvent were prepared. The solubility of the **Zr4** cluster in styrene at room temperature was determined to 0.08 mol% by weighing back undissolved **Zr4** after preparing a saturated solution of the cluster in styrene and removal of residual monomer. This was confirmed by elemental analysis results, where the residual mass of  $ZrO_2$  in the hybrid polymers was determined, and the initial **Zr4** concentration was calculated to 0.08 mol%.

Two polymerizations were started by the addition of 1 wt% of BPO as the radical initiator to saturated solutions and were carried out at 70 °C for 24 hours. The polymers were then dried *in vacuo* at 100 °C.

TGA measurements (Figure 54, Table 42) showed little thermal shifts upon doping with 0.08 mol% of **Zr4** cluster when compared to samples doped with higher cluster proportions. Nevertheless, thermal degradation was shifted by about 20 °C when compared to neat PS.

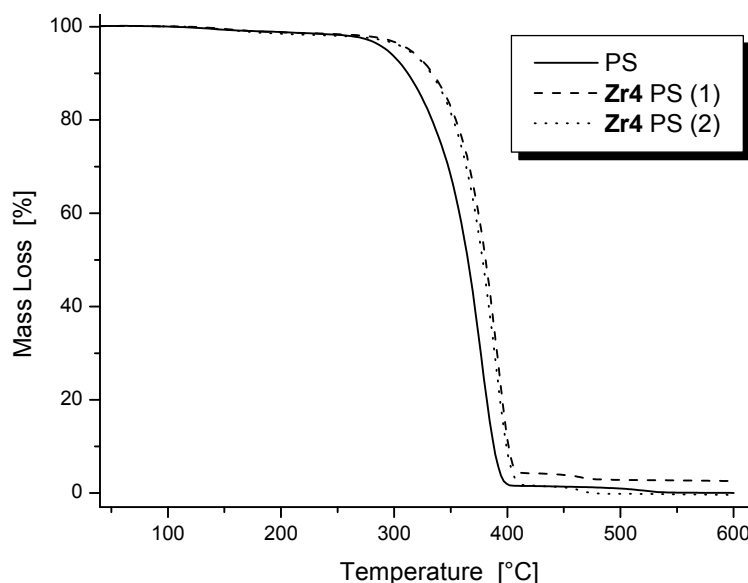


**Figure 54:** TGA curves of PS doped with 0.08 mol% of **Zr4**; polymerization without solvent

**Table 42:** Thermal data for PS doped with **Zr4**; polymerization without solvent

| Sample                   | Onset<br>[°C] | Residual mass<br>[%] | Residual mass expected<br>[%] | $t_g$<br>[min] |
|--------------------------|---------------|----------------------|-------------------------------|----------------|
| PS + <b>Zr4</b> sat. (1) | 359           | 2.49                 | 0.38                          | 150            |
| PS + <b>Zr4</b> sat. (2) | 355           | -0.50                | 0.38                          | 130            |
| PS + <b>Zr4</b> sat. (3) | 358           | -0.07                | 0.38                          | 130            |

DSC thermographs did not reveal any differences when compared to neat polystyrene. Molecular weights and polydispersities were determined from samples which were degraded by acetyl acetone. The dissolution time of the polymers was much shorter when compared to samples with higher cluster loadings. The results (Table 43) showed that the molecular weights of the hybrid polymers prepared without additional solvent were lower when compared to neat polystyrene. Polydispersities were in a range which was acceptable for free radical polymerization.

**Table 43:** Molecular weights and polydispersities of undoped and **Zr4** doped PS; without solvent

| Sample                   | $M_n$ [kg mol <sup>-1</sup> ] | $P_d$ | $t_g$ [min] |
|--------------------------|-------------------------------|-------|-------------|
| PS                       | 77.2                          | 1.80  | 135         |
| PS + <b>Zr4</b> sat. (1) | 22.1                          | 1.76  | 150         |
| PS + <b>Zr4</b> sat. (2) | 21.7                          | 3.13  | 130         |
| PS + <b>Zr4</b> sat. (3) | 21.8                          | 2.00  | 130         |

### 5.1.3 Determination of Residual Zr in the Cleaved Polymers

Several assumptions were made when the cluster cross-links were destroyed with acetyl acetone. First of all, it was assumed that the cluster decomposed according to [111]



If the degradation stopped at that point, there was still the possibility of obtaining a polymer chain with a zirconium atom in the backbone because two methacrylate groups were attached. However, this was unlikely for some reasons:

First of all, acetyl acetone was not applied stoichiometrically as depicted in the reaction above, but in big excess. By doing so, the chance of obtaining a molecular zirconium complex carrying four acetyl acetonates, as it was reported by Wakeshima et al. [112], was reasoned. Secondly, the degradation reactions were carried out at ambient atmosphere and the solvents applied, ethyl acetate and acetyl acetone, were not purified from water. Therefore, in all probability the reaction did not stop at the  $\text{Zr}(\text{acac})_4$  stage, but proceeded to  $\text{ZrO}_2$  instead. This was reasoned by a non-soluble, fine, white precipitate which was present in all of the samples after the degradation step. Nevertheless, the zirconium fraction in the cleaved polymers had to be determined to rule out possible intermediate products during decomposition.

TGA was not sensitive enough to determine traces of zirconium in the polymers. Therefore, samples for optical emission spectroscopy were prepared. The method applied was inductively coupled plasma optical emission spectroscopy (ICP-OES), where the samples had to be dissolved in aqueous solution. Since neither PS nor PMMA are soluble in water, they were combusted in annealing liners and a possible residue, consisting of  $\text{ZrO}_2$ , was dissolved afterwards by microwave assisted digestion in acidic solution.

For the dissolution of  $\text{ZrO}_2$ , pressure decomposition in PTFE vessels with HF,  $\text{H}_2\text{SO}_4$  or HF/HCl/ $\text{HNO}_3$  for more than 16 hours was most often applied [115, 116]. The use of HF made dissolution faster, but instrumental limitations required a shortening of the digestion time to 30 minutes. Reference samples, consisting of pure  $\text{ZrO}_2$ , were digested to determine the recovery (Table 44). The entire measurements were corrected to this recovery.

**Table 44:** Recovery from microwave assisted digestion of pure  $\text{ZrO}_2$

| $\text{ZrO}_2$ [mg] | Mass Zr in $\text{ZrO}_2$ [%] | Vol [ml] | Expected [ppm] | Measurement [ppm] | Dilution | Value [ppb] | Recovery     |
|---------------------|-------------------------------|----------|----------------|-------------------|----------|-------------|--------------|
| 57.47               | 0.7403                        | 0.01     | 4254.52        | 3276.74           | 1906.19  | 1719        | <b>0.770</b> |
| 30.27               | 0.7403                        | 0.01     | 2240.89        | 1736.08           | 2042.45  | 850         | <b>0.774</b> |

For the blank value, an empty annealing liner underwent the same procedures as the samples. Non-precipitated samples were combusted and tested for their Zr-content as well. Reference polymer samples of neat PS and PMMA were measured to determine the initial Zr-concentration in the doped polymers originating from the Zr content in the monomers and solvents which were applied the syntheses.

**Table 45:** Zr contents in undoped and doped polymers

| Sample                      | Found Zr-Conc. [mg/g] | Initial Zr-Conc. [mg/g] |
|-----------------------------|-----------------------|-------------------------|
| PMMA prec.                  | $0.031 \pm 0.002$     | 0                       |
| <b>Zr4</b> PMMA 0.52% prec. | $0.95 \pm 0.03$       | 17.6                    |
| <b>Zr4</b> PMMA 0.52% prec. | $0.914 \pm 0.006$     | 17.6                    |
| <b>Zr4</b> PMMA 0.92% prec. | $0.70 \pm 0.01$       | 31.1                    |
| <b>Zr4</b> PMMA 0.92% prec. | $0.614 \pm 0.007$     | 31.1                    |
| <b>Zr4</b> PMMA 0.70% pure  | $25.4 \pm 1.0$        | 23.6                    |
| <b>Zr4</b> PMMA 1.12% pure  | $40.3 \pm 0.7$        | 37.8                    |
| PS prec.                    | $0.144 \pm 0.003$     | 0                       |
| PS prec.                    | $0.174 \pm 0.009$     | 0                       |
| <b>Zr4</b> PS 0.48% prec.   | $0.60 \pm 0.04$       | 16.201                  |

Results of the measurements are shown in Table 45 and Figure 55. For comparison, the values of the initial Zr concentration are also shown. Deviations of the determined and the calculated values were small and derived from weighing errors in the preparation of the hybrid polymers and also from extracting unreacted monomers and oligomers with ethyl acetate. Therefore, the concentrations from ICP-OES measurements depicted the most exact values.

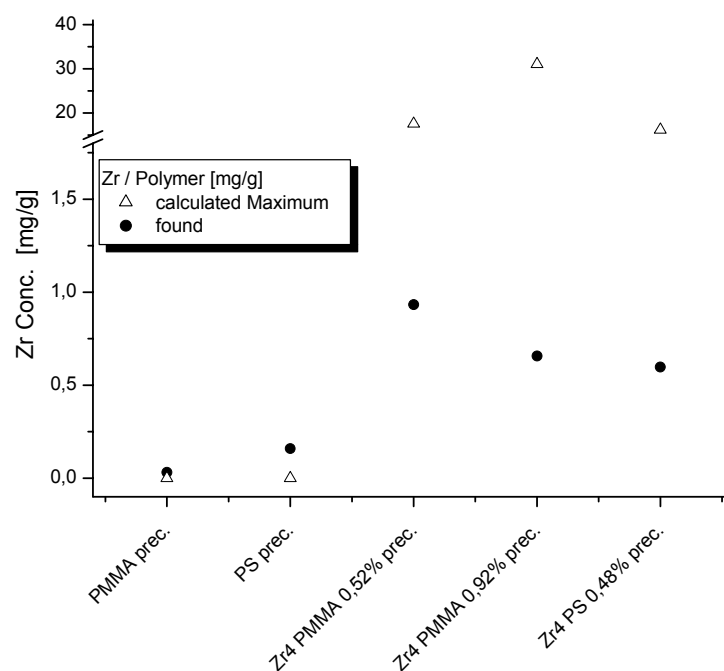


**Figure 55:** Zr concentration in untreated and treated polymers; note the different scales in the y-axis

In summary, it was ascertained that networks of poly(methyl methacrylate) and polystyrene cross-linked with the **Zr4** cluster were decomposed by selectively destroying the cluster with acetyl acetone. Degradation did not stop at the reported compound  $\text{Zr}(\text{acac})_2(\text{OMc})_2$  but proceeded to species carrying not more than one methacrylate ligand, such as  $\text{Zr}(\text{acac})_4$  and  $\text{ZrO}_2$ , respectively. On account of this, no zirconium atoms were found in the backbone of polymer chains which were liberated from the cross-linked networks.

### 5.1.4 Optimization of the Polymerization Conditions

Despite the rather poor improvements in the **Zr4** systems upon changing the solvent or initiator concentrations, a further attempt was made to optimize the polymerization conditions with regard to improvements in the thermal properties of the resulting materials. This was reasoned by the investigations in the **Zr6** cluster systems (see section 5.2), where remarkable improvements in thermal properties were obtained by adjusting the polymerization conditions properly [74, 117, 118].<sup>a</sup>

The optimizations of the **Zr4** systems described in this sub-chapter follow, in principle, the conditions which were applied for the **Zr6** case and will be described in more detail in the following chapter. The main objective in tuning the polymerization conditions was again to avoid auto-acceleration which would result in heterogeneous polymers. To this end, the previously employed initiator benzoyl peroxide [77, 87, 103, 119-121] was replaced by lauroyl peroxide, which has a lower decomposition temperature. Moreover, a step-wise polymerization procedure was applied.

#### Optimization of the System $\text{Zr}_4\text{O}_2(\text{OMc})_{12}$ - Methyl Methacrylate

The previously employed **Zr4** cluster concentration of 1 mol% was reduced to 0.5 mol% to additionally prolong the gelation times without using more solvent. The preparation of the hybrid polymers was as following: **Zr4** cluster was dissolved in benzene and the corresponding amount of MMA was added. The solution was then heated to 80 °C, i.e. close to the boiling point, and then polymerization was started by the addition of lauroyl peroxide. The solution was kept at this temperature for 3 or 5 minutes, and was then immediately quenched to 0 °C in an ice-water bath. Polymerization was then continued at 40 °C and, after removal of benzene *in vacuo*, post-polymerization was carried out at 100 °C. The hybrid polymer was then dried *in vacuo* and residual benzene was removed by extracting the milled samples two times with ethyl acetate. Afterwards the polymers were heated to 120 °C in high vacuum to remove volatile compounds.

---

<sup>a</sup> The structuring of the work in this document does not follow the chronology in which the experiments were performed in the lab. However, for purposes of clarity, it is more meaningful to present results of the **Zr4** system in this chapter.

The optimizations were conducted with regard to thermal properties, in particular onset temperatures of thermal degradation and glass transition temperatures ( $T_g$ ). The amounts of lauroyl peroxide which were added to start the polymerizations was varied as well as the time of the pre-polymerization step at 80 °C.

Table 46 shows the variations which were applied, the sample 'PMMA' constitutes cluster-free polymer which was prepared without solvent. In the samples **MMA1** and **MMA2** the amount of initiator was kept constant at 0.1 wt% relative to the mass of methyl methacrylate, and the time of the pre-polymerization step at 80 °C was 3 or 5 minutes. In the samples **MMA3** and **MMA4** the time of pre-polymerization was also 3 or 5 minutes, but the initiator concentration was reduced to 0.05 wt%.

**Table 46:** Polymerization conditions for optimization of the system **Zr4** - MMA

| Sample      | LPO<br>[wt %] <sup>a</sup> | Reaction Conditions |            |            | Gelation<br>Time <sup>b</sup><br>[min] |
|-------------|----------------------------|---------------------|------------|------------|--|
|             |                            | Step 1              | Step 2     | Step 3     |  |
| <b>PMMA</b> | 0.1                        | 80°C / 3min         |            |            | 60                                     |
| <b>MMA1</b> | 0.1                        | 80°C / 5min         |            |            | 30                                     |
| <b>MMA2</b> | 0.1                        | 80°C / 3min         | 40°C / 48h | 100°C / 2h | 50                                     |
| <b>MMA3</b> | 0.05                       | 80°C / 5min         |            |            | 60                                     |
| <b>MMA4</b> | 0.05                       | 80°C / 3min         |            |            | 120                                    |

<sup>a</sup> relative to the mass of MMA; <sup>b</sup> counted from the 40 °C heating period on

By comparing the samples **MMA1** with **MMA2** and **MMA3** with **MMA4**, respectively, it was obvious that the gelation times were prolonged by either lowering the initiator concentration or by shortening the period of the pre-polymerization step. The results from TGA measurements (Figure 56) showed clear shifts in the onset temperatures of thermal decompositions for the hybrid polymers when compared to neat PMMA. However, there were almost no differences between the samples prepared at different conditions, solely sample **MMA2**, which was prepared with 0.1 wt% of initiator and a pre-polymerization time of 3 minutes, exhibited less mass loss due to volatile compounds below thermal decomposition. A detailed description of the thermal decomposition process is given in Table 47.

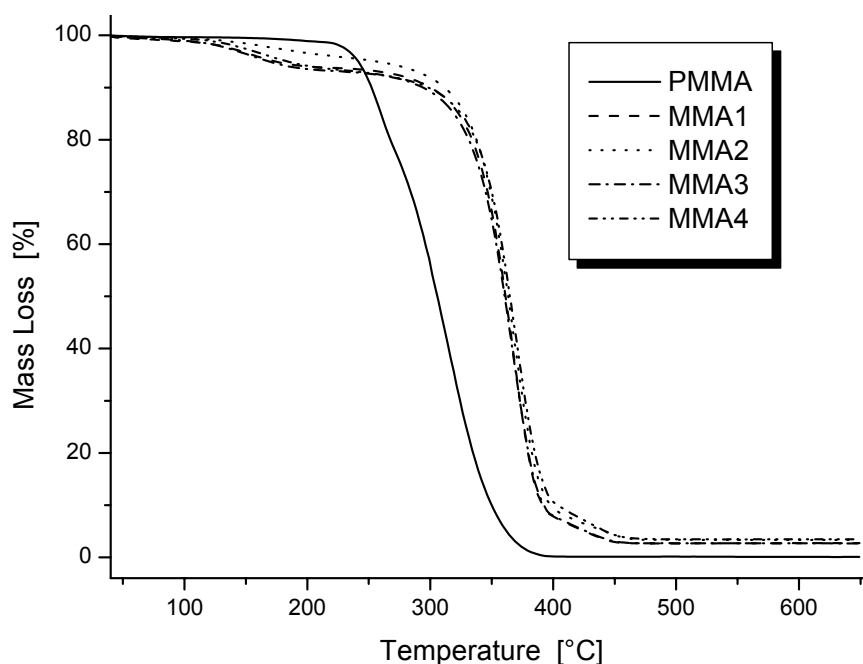


**Figure 56:** TGA curves of undoped and **Zr4** doped PMMA samples; variation of initiator concentration and pre-polymerization times

**Table 47:** Thermal data of **Zr4** doped PMMA; variation of initiator concentrations and polymerization times

| Sample | Onset 1<br>[°C] | Mass<br>loss 1<br>[%] | Onset 2<br>[°C] | Mass<br>loss 2<br>[%] | Onset 3<br>[°C] | Mass<br>loss 3<br>[%] | Residual<br>mass<br>[%] | Residual<br>mass calc.<br>[%] |
|--------|-----------------|-----------------------|-----------------|-----------------------|-----------------|-----------------------|-------------------------|-------------------------------|
| PMMA   |                 |                       | 257             | '100'                 | -               | -                     | 0.1                     | 0                             |
| MMA1   | 124             | 5.29                  | 337             | 91.42                 | -               | 7.5                   | 2.72                    | 2.31                          |
| MMA2   | 129             | 3.88                  | 338             | 92.69                 | -               | 8.37                  | 3.34                    | 2.31                          |
| MMA3   | 122             | 6.20                  | 336             | 90.65                 | -               | 11.93                 | 2.66                    | 2.31                          |
| MMA4   | 129             | 5.56                  | 341             | 90.71                 | -               | 6.52                  | 3.47                    | 2.31                          |

In contrast to neat PMMA, the hybrid polymers showed non-negligible mass losses between 130 °C and 250 °C. This was attributed to residual benzene, monomer or oligomers. The major mass loss due to degradation of the main polymer was shifted from 257 °C for neat PMMA by about 80 °C to higher values. Mass loss 3 between 400 °C and 470 °C was related to oxidative volatilization of char which was produced in step 2 and had no clear onset. Therefore, the value was arbitrarily determined as the difference in masses between the changes of the slopes in the corresponding temperature region. The residual masses were higher when compared to values which were calculated theoretically with the assumption that polymerization yield was 100 %, and the entire **Zr4** proportion decomposed to  $\text{ZrO}_2$  during combustion. This was attributed to



species which were not incorporated into the cross-linked networks and thus were removed in the extraction steps with ethyl acetate.

Even though there was a pronounced mass loss below thermal decomposition of the hybrid materials, this was not reflected in the DSC thermographs (Figure 57). No signal was observed below 300 °C. At 320 °C, an endothermic event took place which was related to depolymerization reactions [109]. It was already shown earlier works that such reactions were inhibited by applying higher proportions of the **Zr4** cluster [77] and also in the previous section, where the cluster loading was 1 mol%, no depolymerization occurred. Above 350 °C, a pronounced exothermic event took place because of thermal combustion of the polymer. Again, this exotherm consisted of two signals in which the latter formed a shoulder at 440 °C and was ascribed to the combustion of char.

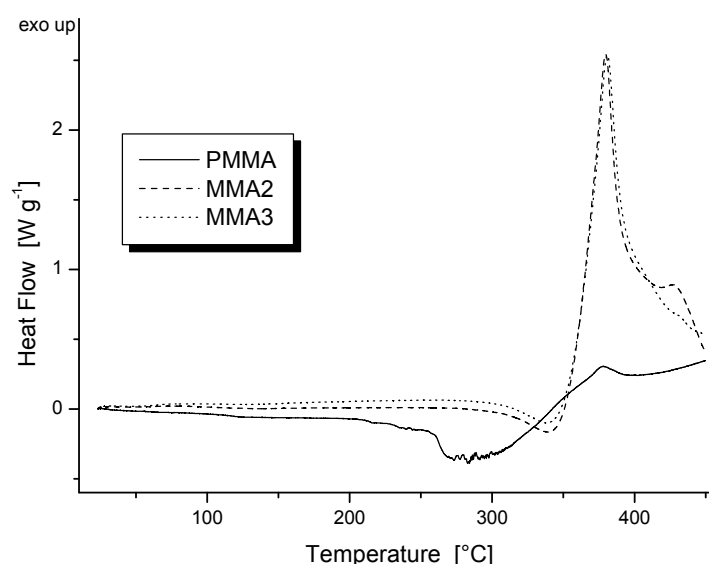


**Figure 57:** DSC thermographs of undoped and doped PMMA samples

A surprising finding in these newly prepared samples was the observation of a defined glass transition temperature, which was not observed in the samples prepared with benzoyl peroxide as the initiator and a cluster loading of 1 mol%. Glass transition temperatures were determined by heating the samples once to 200 °C in order to remove the thermal history, and then take the onset temperature of the event in a second heating scan at a ramp of 40 °C/min.

Additionally, the molecular weights and polydispersities were determined by SEC after degradation of the cross-linking cluster units by acetyl acetone. The results are presented in Table 48.

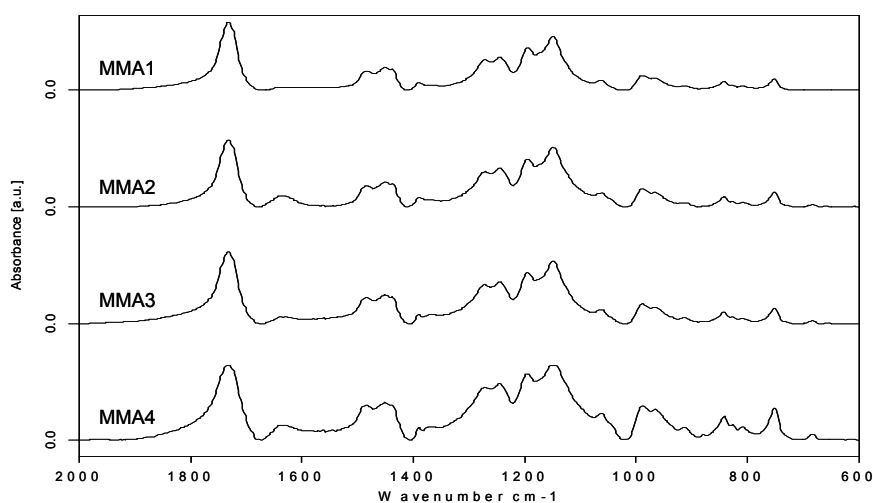
**Table 48:** Molecular weights, polydispersities and glass transition temperatures for optimized PMMA samples

| Sample | Gelation Time [min] | Onset 2 [°C] | T <sub>g</sub> [°C] | M <sub>n</sub> [kg mol <sup>-1</sup> ] | P <sub>d</sub> |
|--------|---------------------|--------------|---------------------|--|----------------|
| PMMA   | 60                  | 257          | 115                 | 784.6                                  | 1.52           |
| MMA1   | 30                  | 337          | 129                 | 87.4                                   | 7.62           |
| MMA2   | 50                  | 338          | 126                 | 515.3                                  | 9.70           |
| MMA3   | 60                  | 336          | 126                 | 643.2                                  | 2.86           |
| MMA4   | 120                 | 341          | 122                 | 714.3                                  | 8.84           |

The molecular weights of the polymers increased with increasing gelation times. Unfortunately, the polydispersities were large in all of the polymers except for neat PMMA. The glass transition temperatures were shifted to higher values when compared to pure PMMA and seemed to correlate with the gelation times.

### Spectroscopic Characterization

Infrared spectroscopy was used to determine the functional groups present in the polymers. The spectra of the hybrid polymers and that of the pure PMMA were very similar. In order to compare the band intensities on a qualitative scale, potassium ferricyanide was added as an internal standard in the preparation of the KBr pellets.

**Figure 58:** FTIR spectra of Zr<sub>4</sub> - MMA hybrid polymers

All FTIR spectra (Figure 58) were dominated by the broad bands of PMMA. The band at  $1634\text{ cm}^{-1}$  was assigned to the C=C stretching vibration and stemmed from unreacted methyl methacrylate or unreacted methacrylate ligands bonded to the **Zr4** cluster. A differentiation was not possible because of the broad bands. Depending on the applied preparation procedure, this band was more pronounced in the samples **MMA2** and **MMA4** whereas in **MMA1** and **MMA3** almost all of the monomers were consumed because weak or no signals were observed in the FTIR spectra.

In summary, a step-wise polymerization of **Zr4** with MMA resulted in materials which showed improved thermal properties. However, the influence of the polymerization conditions was weakly pronounced. Similar results were observed in a PMMA system cross-linked with the **Zr6** cluster [74, 117]. Therefore, investigations were extended to styrene as the monomer, where improvements in the **Zr6** case were more pronounced.

### Optimization of the System $\text{Zr}_4\text{O}_2(\text{OMc})_{12}$ - Styrene

Polystyrene has a higher decomposition temperature than poly(methyl methacrylate). Thus, the improvements in thermal properties, caused by a cross-linking with the **Zr4** cluster, were expected to be lower than in the MMA case.

Optimizations were again investigated by replacing benzoyl peroxide for lauroyl peroxide as the initiator and by applying a step-wise polymerization. Since styrene is less reactive than methyl methacrylate, the variations were carried out in a wider range.

The procedure was similar to the systems described above: The **Zr4** cluster was dissolved in benzene at room temperature, and styrene was added in an amount, that the **Zr4** concentration was 0.5 mol%. After heating to  $80\text{ }^{\circ}\text{C}$ , lauroyl peroxide was added and the solution was kept at this temperature between 2.5 and 15 minutes. One sample was also prepared without this pre-polymerization step. The solution was quenched to  $0\text{ }^{\circ}\text{C}$  immediately after this step, and then polymerization was carried out at  $60\text{ }^{\circ}\text{C}$  for one day. After removal of benzene, the sample was heated to  $80\text{ }^{\circ}\text{C}$  for one day and an additional day at  $120\text{ }^{\circ}\text{C}$ . The sample was then dried *in vacuo*. After milling, the residual benzene was extracted two times with ethyl acetate, followed by drying in high vacuum at elevated temperatures.

Table 49 shows the variations of the pre-polymerization step periods at  $80\text{ }^{\circ}\text{C}$ , PS constituted cluster-free polystyrene. The gelation times decreased by increasing the  $80\text{ }^{\circ}\text{C}$  heating period. In

sample **St5** no pre-polymerization was applied, but polymerization was started at 60 °C without cooling of the solution. Therefore, gelation time was shorter when compared to other samples.

**Table 49:** Optimization of **Zr4** + styrene through pre-polymerization time variation

| Sample     | LPO<br>[wt %] <sup>a</sup> | Reaction Conditions |            |            |             | Gelation<br>Time <sup>b</sup><br>[min] |
|------------|----------------------------|---------------------|------------|------------|-------------|--|
|            |                            | Step 1              | Step 2     | Step 3     | Step 4      |  |
| <b>PS</b>  | 0.05%                      | 80°C / 5min         |            |            |             | >240                                   |
| <b>St1</b> | 0.10%                      | 80°C / 2.5min       |            |            |             | 135                                    |
| <b>St2</b> | 0.10%                      | 80°C / 5min         | 60°C / 24h | 80°C / 24h | 120°C / 24h | 110                                    |
| <b>St3</b> | 0.10%                      | 80°C / 10min        |            |            |             | 90                                     |
| <b>St4</b> | 0.10%                      | 80°C / 15min        |            |            |             | 70                                     |
| <b>St5</b> | 0.10%                      | 0min                |            |            |             | 25                                     |

<sup>a</sup> relative to the mass of styrene; <sup>b</sup> counted from the 60 °C heating period on

Selected TGA curves are shown in Figure 59. The thermal properties of polystyrene were not improved through a cross-linking with the **Zr4** cluster. The onset temperatures of thermal decomposition (Table 50) were even shifted to values below 340 °C, the temperature at which neat PS decomposed. This was attributed to the different slopes of tangents in this particular region. In fact, the thermal decomposition temperature was slightly improved for the hybrid polymers, as obvious in Figure 59.

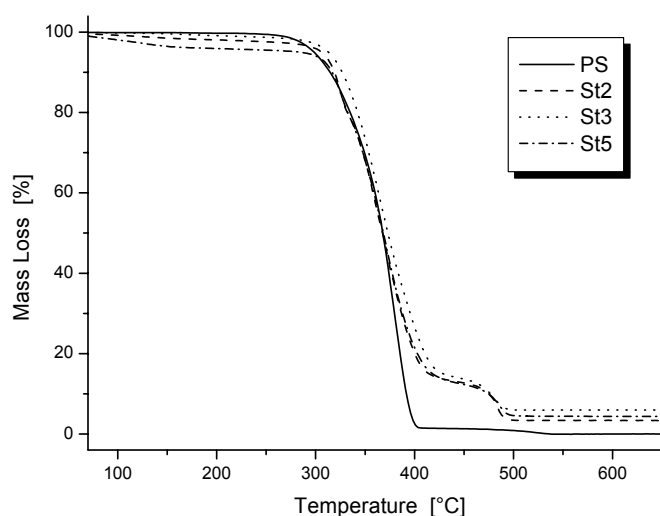


**Figure 59:** TGA curves of undoped and doped PS samples; variation of the pre-polymerization periods

A mass loss below thermal decomposition was apparent in all of the hybrid polymers and was most pronounced for the sample where no pre-polymerization step was applied. Generally, the formation of char was clearer in the polystyrene case when compared to **Zr4** cross-linked PMMA.

**Table 50:** Thermal data of **Zr4** doped PS; variation of the pre-polymerization periods

| Sample | Onset 1<br>[°C] | Mass<br>loss 1<br>[%] | Onset 2<br>[°C] | Mass<br>loss 2<br>[%] | Onset 3<br>[°C] | Mass<br>loss 3<br>[%] | Residual<br>mass<br>[%] | Residual<br>mass calc.<br>[%] |
|--------|-----------------|-----------------------|-----------------|-----------------------|-----------------|-----------------------|-------------------------|-------------------------------|
| PS     | -               | -                     | 340             | '100'                 | -               | -                     | 0.01                    | 0                             |
| St1    | -               | 2.22                  | 319             | 84.4                  | 476             | 9.57                  | 3.83                    | 2.22                          |
| St2    | -               | 2.46                  | 322             | 84.38                 | 474             | 9.77                  | 3.38                    | 2.22                          |
| St3    | -               | 1.37                  | 328             | 85.04                 | 468             | 7.67                  | 5.98                    | 2.22                          |
| St4    | -               | 3.21                  | 323             | 84.00                 | 479             | 9.27                  | 3.53                    | 2.22                          |
| St5    | -               | 4.00                  | 327             | 83.53                 | 475             | 7.83                  | 4.34                    | 2.22                          |

DSC measurements of the hybrid polymers which were prepared by different pre-polymerization times did not show signals apart from thermal decomposition (Figure 60), although a mass loss below 300 °C was observed in TGA measurements. Glass transition temperatures were determined at a ramp of 40 °C/min and are presented in Table 51 together with results from SEC measurements, where the molecular weights and the polydispersities were determined after decomposition of the cross-linking units by acetyl acetone.

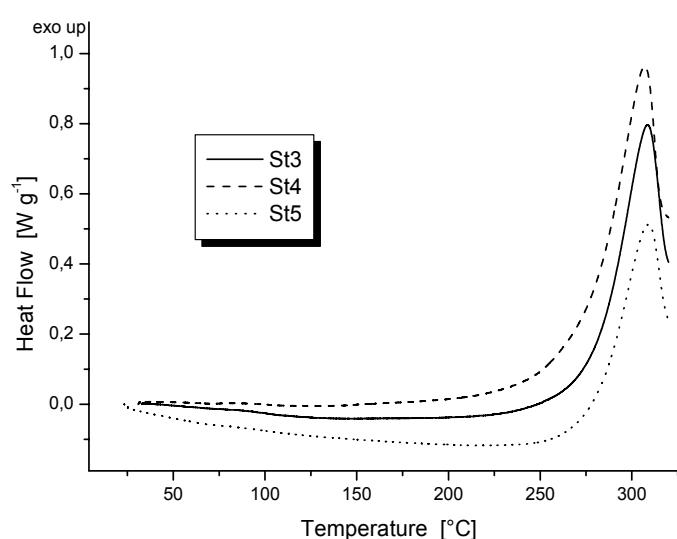


**Figure 60:** DSC curves of undoped and doped PS samples; variation of the pre-polymerization periods

**Table 51:** Glass transition temperatures, molecular weights and polydispersities for PS samples with different initiator concentrations

| Sample | Gelation Time [min] | Onset 2 [°C] | T <sub>g</sub> [°C] | M <sub>n</sub> [kg mol <sup>-1</sup> ] | P <sub>d</sub> |
|--------|---------------------|--------------|---------------------|--|----------------|
| PS     | >240                | 340          | 100                 | 34.7                                   | 2.64           |
| St1    | 135                 | 319          | 109                 | 241.1                                  | 3.16           |
| St2    | 110                 | 322          | 106                 | 89.1                                   | 5.36           |
| St3    | 90                  | 328          | 109                 | 101.6                                  | 4.36           |
| St4    | 70                  | 323          | 109                 | 77.9                                   | 5.17           |
| St5    | 25                  | 327          | 108                 | 55.7                                   | 11.57          |

Generally, the glass transition temperatures were shifted to higher values through cross-linking with **Zr4** when compared to neat PS, but no correlation with the gelation times and thus with the pre-polymerization step was observed. Polymers with higher molecular weights were obtained through prolonging the gelation times and also high polydispersities were observed.

The initiator concentrations were also varied. To this end, the pre-polymerization period at 80 °C was kept constant at 5 minutes and the amount of lauroyl peroxide was varied between 0.05 and 0.50 wt%. Again, polymerization was carried out in 4 steps (Table 52).

The gelation times shortened when the initiator concentrations were increased. TGA measurements (Figure 61) revealed that a mass loss below thermal decomposition, i.e. the volatilization of solvent or unreacted monomer, was related to the amount of initiator. The more initiator was used in the polymerizations, the more pronounced was the mass loss below 300 °C.

**Table 52:** Optimization of the system **Zr4** + styrene; variations of the initiator concentration

| Sample | LPO [wt %] <sup>a</sup> | Reaction Conditions |            |            |             | Gelation Time tg <sup>b</sup> [min] |
|--------|-------------------------|---------------------|------------|------------|-------------|-------------------------------------|
|        |                         | Step 1              | Step 2     | Step 3     | Step 4      |                                     |
| PS     | 0.05%                   |                     |            |            |             | >240                                |
| St6    | 0.05%                   |                     |            |            |             | 125                                 |
| St2    | 0.10%                   | 80°C / 5min         | 60°C / 24h | 80°C / 24h | 120°C / 24h | 110                                 |
| St7    | 0.25%                   |                     |            |            |             | 50                                  |
| St8    | 0.50%                   |                     |            |            |             | 40                                  |

<sup>a</sup> relative to the mass of styrene; <sup>b</sup> counted from the 60 °C heating period on

Table 53 summarizes the events which took place in TGA. As mentioned, mass losses below thermal decomposition increased with increasing initiator concentration and simultaneously Mass Loss 3 decreased, i.e. the amount of char produced in step 2, which was related to cross-linking. On account of this it was assumed that the use of higher initiator concentrations led to hybrid materials containing higher amounts of unreacted monomers and a less degree of cross-linking.

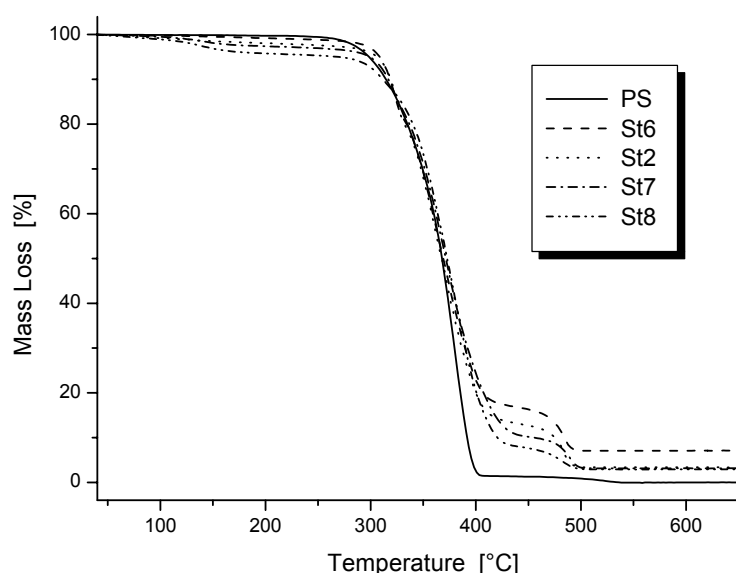


**Figure 61:** TGA curves of undoped and doped PS samples; variation of initiator concentrations

Onset temperatures of thermal decomposition were again lower than that of neat PS because of different slopes of the tangents during combustion in step 2.

**Table 53:** Thermal data for **Zr4** doped PS; variation of the initiator concentrations

| Sample | Onset 1<br>[°C] | Mass<br>loss 1<br>[%] | Onset 2<br>[°C] | Mass<br>loss 2<br>[%] | Onset 3<br>[°C] | Mass<br>loss 3<br>[%] | Residual<br>mass<br>[%] | Residual<br>mass<br>calc.<br>[%] |
|--------|-----------------|-----------------------|-----------------|-----------------------|-----------------|-----------------------|-------------------------|----------------------------------|
| PS     |                 |                       | 340             | '100'                 |                 |                       | 0.01                    | 0                                |
| St6    |                 | 1.24                  | 330             | 82.15                 | 472             | 9.55                  | 7.11                    | 2.22                             |
| St2    |                 | 2.46                  | 322             | 84.38                 | 474             | 9.77                  | 3.38                    | 2.22                             |
| St7    |                 | 2.73                  | 328             | 87.06                 | 479             | 7.09                  | 3.15                    | 2.22                             |
| St8    |                 | 4.32                  | 335             | 87.99                 | 469             | 4.71                  | 2.9                     | 2.22                             |

DSC measurements at a ramp of 3 °C/min revealed no signals apart from thermal combustion and are thus not shown. Glass transition temperatures were determined at a ramp of 40 °C/min and are presented in Table 54 together with GPC results.

**Table 54:** Glass transition temperatures, molecular weights and polydispersities for PS samples with different initiator concentrations

| Sample | Gelation Time<br>[min] | Onset 2<br>[°C] | T <sub>g</sub><br>[°C] | M <sub>n</sub><br>[kg mol <sup>-1</sup> ] | P <sub>d</sub> |
|--------|------------------------|-----------------|------------------------|---|----------------|
| PS     | >240                   | 340             | 100                    | 34.7                                      | 2.67           |
| St6    | 125                    | 330             | 108                    | 394.4                                     | 2.64           |
| St2    | 110                    | 322             | 106                    | 89.1                                      | 5.36           |
| St7    | 50                     | 328             | 104                    | 89.8                                      | 4.13           |
| St8    | 40                     | 335             | 106                    | 65.6                                      | 3.71           |

### Spectroscopic Characterization

FTIR spectra of selected **Zr4** doped polystyrene samples are shown in Figure 62. Potassium ferricyanide was used as an internal standard to allow for qualitative comparison of the spectra. The spectra were dominated by the strong polymer bands. The band at 1642 cm<sup>-1</sup> represented the C=C stretching vibration and was related to unreacted monomers. A close look revealed that in the samples **St5** (not shown) and **St6**, polymerizations were most complete because the C=C band was only visible as a small hump in the spectra, whereas in samples **St3** and **St8** (not shown) clear bands at 1642 cm<sup>-1</sup> were observed, indicative of residual vinyl groups in the polymer. Next to the bands which were assigned to PS, signals originating from the **Zr4** cluster were visible. The asymmetric stretching vibration at 1550 cm<sup>-1</sup> was covered by the PS matrix, but the symmetric carboxylate stretching vibration at 1370 cm<sup>-1</sup> and the band at 1244 cm<sup>-1</sup> (COC stretching) was clearly related to carboxylate groups.



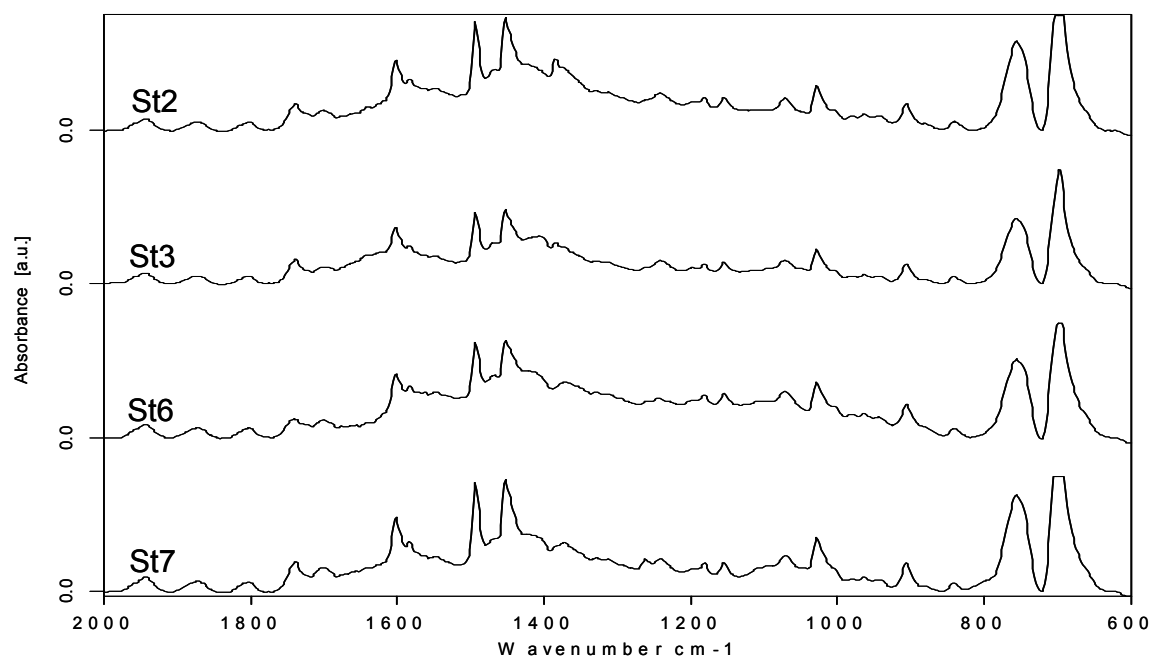


**Figure 62:** FTIR spectra of selected **Zr4** doped PS samples

In conclusion, the cross-linking of styrene with the **Zr4** cluster did not change the onset temperatures of thermal combustion, but glass transition temperatures were increased up to 9 °C. The amount of initiator which was used in the polymerizations was much more important than the time of the pre-polymerization period at 80 °C. Therefore, it was assumed that sample **St6**, which was initiated with 0.05 wt% lauroyl peroxide for 5 minutes at 80 °C, was polymerized under the most ideal conditions: With a gelation time of more than two hours auto-acceleration was avoided and  $T_g$  was shifted by 8 °C. Furthermore, this sample showed least residual double bonds, exhibited the highest molecular weight of the polymer chains and at the same time had the lowest polydispersity.

### 5.1.5 Conclusion

In summary, the use of the **Zr4** cluster as a cross-linking co-monomer in polymerization reactions with methyl methacrylate or styrene resulted in hybrid materials which mostly showed improved thermal properties when compared to the neat thermoplastics. In the case of cross-linked PMMA also depolymerization reactions were inhibited. The main problem in the preparation of **Zr4** doped hybrid polymers was the short gelation time due to cross-linking of the multifunctional cluster. By prolonging the gelation time, which was connected to the auto-acceleration problem, the polymers were prepared in bulk whereas polymers exhibiting short gelation times were always obtained as porous solids with many bubbles incorporated and thus were useless for testing the mechanical properties.

The molecular weights were tuned by prolonging the gelation times. This was possible either by reducing the amount of the initiator benzoyl peroxide, or by reducing the monomer concentration through adding more solvent to the polymerization solution. Small or no influence on the thermal properties was observed by doing so. Solely very high solvent concentrations (ratio of solvent / monomer > 10) led to a precipitation of the polymers during the polymerization rather than to a gelation. In a second approach, the initiator lauroyl peroxide was used and a step-wise polymerization was applied. The gelation times were prolonged by reducing the amount of initiator and by reducing the time of the pre-polymerization period. However, the influence on the thermal properties was again small.

Polymer properties, such as molecular weight and polydispersity, could not be determined from cross-linked samples. Therefore, the cross-linking cluster units were destroyed with acetyl acetone. Atomic emission spectroscopy investigations confirmed that all of the **Zr4** units were selectively destroyed. The released polymer chains were characterized by SEC and showed large polydispersities. However, Hild et al. [122, 123] investigated the network formation in free radical co-polymerizations of styrene with bi-unsaturated co-monomers such as divinylbenzene and ethylene dimethacrylate in detail. To this end, the authors studied properties of the networks at defined times after the gelation point. They found that shortly after the gel point a considerably high proportion of the macromolecules was not yet connected to the network. By extracting these non-linked polymers they made a rough investigation of the molecular weight and the polydispersity by SEC. In early stages of gelation, the polydispersity of the extracted polymers was quite high (~4.5) but decreased by time with concomitant increase of molecular weight. They concluded that pendent double bonds attached to these species were potential linking points and that the higher the average molecular weight of these polymers, the higher was also the probability of bond formation. Similar considerations might be applied in cluster cross-linked polymers: In early stages only one methacrylate group of **Zr4** was attached to a growing polymer chain and a second, third, etc. double bond was consumed at higher rates of conversion.

## 5.2 $\text{Zr}_6\text{O}_4(\text{OH})_4(\text{OMc})_{12}$ Modified Polystyrene

### 5.2.1 Optimization of the Polymerization Conditions

The investigations of the **Zr4** hybrid polymers revealed that the molecular weight distribution and the polydispersities were difficult to control. The main problem was a short gelation time even with very small cluster proportions. From this point on, the so-called Trommsdorff-Norrish-Smith or gel effect [124], the reaction heat was difficult to release and the exothermic polymerization reaction shifted the temperature to higher values than applied. This resulted in heterogeneous polymers with relatively high proportions of unreacted double bonds, which was consequentially reflected in the thermal properties, such as in a mass loss below thermal decomposition temperature. Possible solutions to prolong the gelation time and thus to obtain more homogeneous polymers were the use of chain transfer agents, e.g. 2-mercaptoethanol [125], or to apply a step-wise polymerization reaction [126].

In contrast to **Zr4**, the **Zr6** cluster showed considerable solubility in monomers such as styrene and methyl methacrylate. The use of solvent, which was always a crucial factor in the final cluster doped polymers due to its incorporation into the networks, was renounced and conditions had to be developed for the system consisting of a monomer, the **Zr6** cluster and an initiator. Another advantage of using the **Zr6** cluster was the remarkably higher chemical stability of the hybrid polymers. Whereas the **Zr4** cluster doped polymers were degraded by acetyl acetone, the **Zr6** doped polymers have been stable in a solution containing acetyl acetone and ethyl acetate for more than 18 months.

Since this work was published with MMA and styrene as the monomers [74, 117, 118], solely the optimization of the styrene system with respect to thermal properties is described here, because it was applied in the preparation of hybrid polymers used for thermomechanical and mechanical characterization. Styrene was favoured as the monomer because it is less reactive than MMA and thus allowed better control in co-polymerization reactions with the cross-linking cluster.

In order to optimize the system consisting of styrene as the monomer and the **Zr6** cluster as the co-monomer, the previously employed initiator benzoyl peroxide [77, 87, 103, 119-121] was replaced by lauroyl peroxide which had a lower decomposition temperature. A second modification was the introduction of a pre-polymerization step at 80 °C for several minutes. Many monomers were initiated at this temperature, but the system could release the reaction

heat in time to avoid heterogeneous polymerization. Polymerization parameters were varied in a way so that the cluster proportion was kept constant at 0.5 mol%. The period of the pre-polymerization step as well as the initiator concentration was varied independently. Experimental details are given in Table 55.

**Table 55:** Variation of the polymerization conditions for 0.5 mol% of **Zr6** in styrene

| Sample     | wt %<br>LPO <sup>a</sup> | Reaction conditions |            |             | Gelation<br>Time <sup>b</sup><br>[min] | T <sub>d</sub><br>[°C] | T <sub>g</sub><br>[°C] |
|------------|--------------------------|---------------------|------------|-------------|--|------------------------|------------------------|
|            |                          | Step 1              | Step 2     | Step 3      |  |                        |                        |
| <b>PS</b>  | 0.05                     | 80°C / 5min         | 60°C / 24h | 120°C / 24h | > 240                                  | 341                    | 104                    |
| <b>St1</b> | 0.05                     | -                   | 60°C / 48h | 120°C / 1h  | 36                                     | 355                    | 115                    |
| <b>St2</b> | 0.05                     | 80°C / 5min         | 60°C / 48h | 120°C / 24h | 130                                    | 337                    | 112                    |
| <b>St3</b> | 0.05                     | 80°C / 5min         | 60°C / 24h | 120°C / 24h | 126                                    | 390                    | 121                    |
| <b>St4</b> | 0.05                     | 80°C / 10min        | 60°C / 24h | 120°C / 24h | 62                                     | 374                    | 116                    |
| <b>St5</b> | 0.05                     | 80°C / 15min        | 60°C / 24h | 120°C / 24h | 28                                     | 347                    | 115                    |
| <b>St6</b> | 0.10                     | 80°C / 5min         | 60°C / 24h | 120°C / 24h | 90                                     | 367                    | 116                    |
| <b>St7</b> | 0.10                     | 80°C / 10min        | 60°C / 24h | 120°C / 24h | 45                                     | 371                    | 118                    |

<sup>a</sup> relative to the mass of styrene; <sup>b</sup> gelation times were counted from the 60 °C heating period on

In the polymerizations, 0.5 mol% of **Zr6** was dissolved in styrene and the reactions were started by adding the initiator, followed by heating to 80 °C. The reaction conditions were modified in a way that the solutions were pre-polymerized at 80 °C for several minutes. The systems were then quenched in an ice-water bath. Polymerizations were carried out at 60 °C for one or two days. Finally, post-polymerizations were carried out at 120 °C for one day to consume the residual monomers completely. Afterwards the samples were dried *in vacuo*.

The data in Table 55 show that the gelation times of the polymers were shortened by a longer pre-polymerization period, which was in turn linked to the auto-acceleration problem.

The thermal stabilities of the doped polymers were investigated by TGA in synthetic air atmosphere and a heating rate of 5 °C/min. Glass transition temperatures were determined by DSC by heating the samples once at a ramp of 2 °C/min in static air atmosphere to remove thermal history and, after cooling the sample, taking the onset temperature of the transition in a second heating scan at a ramp of 40 °C/min.

TGA curves of **Zr6** cross-linked PS (Figure 63) showed that the total mass loss of the cluster cross-linked polymers occurred in two distinct stages. Only in sample **St1**, where no pre-polymerization step was applied, there was also some mass loss at temperatures below 300 °C,

very likely due to the volatilization of unreacted monomers or small oligomers. The absence of this loss in the pre-polymerized samples showed that polymerization was complete and all monomers were consumed. The major mass loss was between 300 and 420 °C due to degradation of the main polymer chains and char formation. It is worth mentioning here that polymerization conditions which resulted in higher onset temperatures of thermal degradation also resulted in higher char yields. The thus produced organic char underwent complete oxidative volatilization between 420 and 470 °C, and only an inorganic residue, consisting of  $\text{ZrO}_2$ , was retained. Since char yield was related to both inorganic filler and cross-linking [100], the TGA data showed that the amount of cross-linking was increased by tuning the polymerization conditions.

When comparing the thermographs of sample **St1** with **St3**, a clear improvement due to pre-polymerization was obvious. The polymer with the highest thermal stability (onset of thermal decomposition 390 °C) was **St3**. In addition, the polymerization appeared to be complete as there was almost no mass loss below 300 °C. DSC measurements of the prepared samples showed no transition next to glass transition. Sample **St3**, i.e. the sample which the best thermal characteristics in TGA, also had the highest glass transition temperature among other variations.

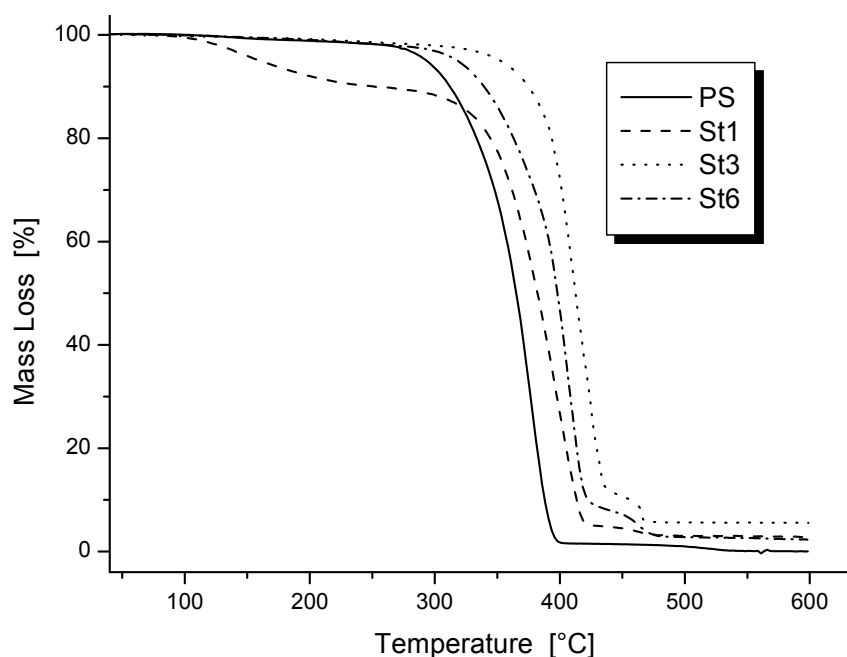


**Figure 63:** TGA curves of selected Zr6 PS hybridise; sample PS is an undoped reference sample

In conclusion, it was assumed that the reaction conditions for sample **St3**, i.e. 80 °C for 5 min / 60 °C for 1 day / 120 °C for 1 day, were the optimal conditions for the particular precursor combination.

### 5.2.2 Preparation of $\text{Zr}_6\text{O}_4(\text{OH})_4(\text{OMc})_{12}$ Doped Bulk Polymers

Bulk samples with bigger dimensions were required for testing the mechanical and thermomechanical properties. For example, a cylindrical sample with the required dimensions had to be prepared on a 30 grams scale. To this end, the previously developed polymerization conditions had to be modified somehow because of upscaling. Due to time and material consuming reasons, the polymerizations on that scale could not be evaluated as accurately as before and not for each concentration. In fact, modifications were figured out for a **Zr6** concentration of 0.43 mol%. The initiator concentration and the post-polymerization step were not changed. A focus was laid on the initiation step. Samples were previously prepared by adding lauroyl peroxide to a solution containing the **Zr6** cluster and monomer and then starting the polymerization by heating the Schlenk tube to 80 °C. However, by increasing the monomer volume significantly, 5 minutes were not even sufficient to heat the solutions to the desired temperature of 80 °C. Thus, the polymerization solution was heated prior to the addition of the initiator and as a consequence was kept at this temperature for a shorter time. It was found that maintaining the polymerization solution for half the time applied previously before quenching, i.e. 2.5 min instead of 5 min, resulted in gelation times which were most comparable, but still shorter than those obtained for polymerizations on a smaller scale. Furthermore, step 2 was modified by introducing a 24 hours heating period at 80 °C. The final reaction conditions for the preparation of bulk samples were thus: Heating at 80 °C for 2.5 min, quenching to 0 °C, heating to 60 °C for 24 hours, heating to 80 °C for 24 hours and, finally, heating to 120 °C for 36 hours. After polymerization, the sample was freed from the Schlenk tube and dried *in vacuo* at elevated temperatures for 8 hours. This procedure was applied in the preparation of cluster doped polystyrene samples with **Zr6** concentrations of 0.24, 0.43, 0.70 and 0.87 mol%.

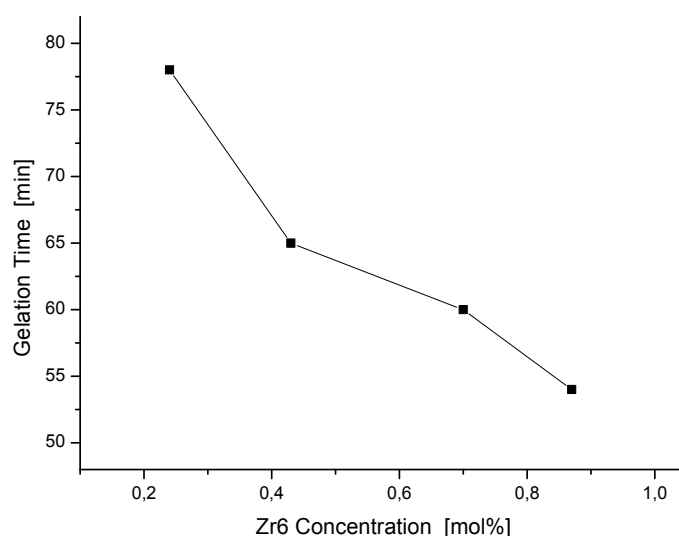


**Figure 64:** Gelation time versus **Zr6** concentration

The gelation times which were observed in the polymerization reactions are shown in Figure 64. Whereas the gelation time for the undoped polystyrene sample was longer than 4 hours, it decreased to 78 minutes for the sample doped with 0.24 mol% of **Zr6** cluster. In addition, there was a clear correlation between cluster proportions applied and the gelation times, indicating that the clusters took part in the polymerizations and acted as cross-linkers.

The samples prepared under these conditions were used in the measurements described in the following sub-chapters.

### 5.2.3 Thermal Properties

#### Thermogravimetric Analysis

The TGA measurements of the **Zr6** hybrid polymers were carried out in dynamic synthetic air atmosphere from room temperature to 650 °C, the curves are shown in Figure 65.

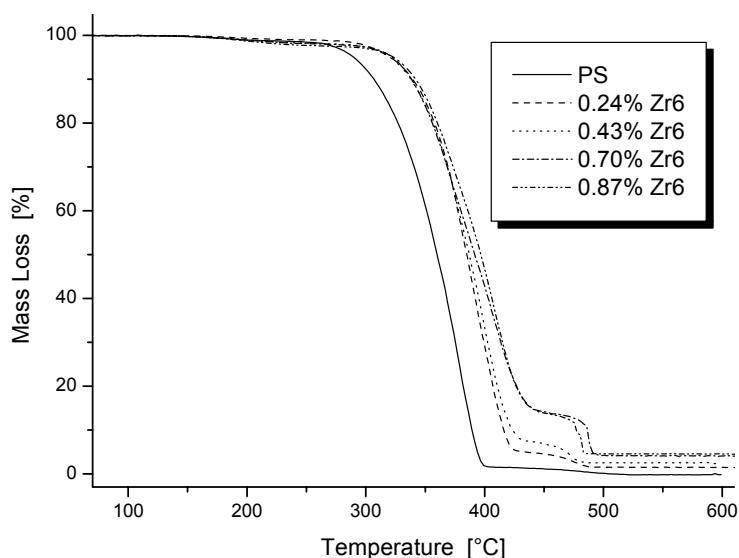


**Figure 65:** TGA curves of undoped and doped polystyrene samples

As apparent in Table 56, the onset temperatures of thermal decomposition of the main polymer chains were shifted to slightly lower values when compared to the optimized samples described in section 5.2.1. This was attributed to the preparation of the samples in bulk, where heat

transfer during polymerization became a much more important factor. On account of this, also some mass loss below thermal decomposition, which originated from volatile compounds with low molecular weights, such as unreacted monomer or oligomers, was observed.

**Table 56:** Thermal data of undoped and **Zr6** doped polystyrene

| <b>Zr6 Conc.</b><br>[mol%] | <b>Onset 1</b><br>[°C] | <b>Mass loss 1</b><br>[%] | <b>Onset 2</b><br>[°C] | <b>Mass loss 2</b><br>[%] | <b>Onset 3</b><br>[°C] | <b>Mass loss 3</b><br>[%] | <b>Residual mass</b><br>[%] | <b>Residual mass calc.</b><br>[%] |
|----------------------------|------------------------|---------------------------|------------------------|---------------------------|------------------------|---------------------------|-----------------------------|-----------------------------------|
| 0                          | 148                    | 1.78                      | 321                    | 96.37                     | 473                    | 1.97                      | -0.12                       | 0.00                              |
| 0.24                       | 164                    | 1.58                      | 345                    | 93.05                     | 461                    | 3.77                      | 1.62                        | 1.64                              |
| 0.43                       | 167                    | 1.68                      | 345                    | 90.84                     | 466                    | 4.91                      | 2.57                        | 2.86                              |
| 0.70                       | 157                    | 2.17                      | 342                    | 84.16                     | 484                    | 9.14                      | 4.43                        | 4.40                              |
| 0.87                       | 168                    | 2.30                      | 351                    | 82.81                     | 474                    | 10.05                     | 4.88                        | 5.34                              |

The TGA curves of **Zr6** cross-linked polystyrene samples showed that the total mass loss of the cluster-crosslinked polymers occurred in three distinct stages:

Onset 1 and Mass loss 1, respectively, were used to describe the volatilization of low molecular weight species. For undoped polystyrene this loss could, in principle, be avoided when applying some post-treatment procedure such as precipitation or melting. However, this was not performed in order to obtain comparable values for doped samples, which could not be processed after cross-linking anymore with the exception of heating and evacuating, which was applied to all of the samples anyway.

The major mass loss was shifted from 320 °C for neat polystyrene to values about 25 °C higher for the doped samples (Onset 2). Mass loss 2 decreased from 96 % for neat polystyrene gradually to 83 % for the sample doped with 0.87 mol% of cluster. This was contributed to char formation in this step which became more pronounced with higher cluster loadings and with a higher degree of cross-linking. Although samples were placed in an open pan, hampered oxygen diffusion into the samples occurred which might give an explanation for a small char formation in the undoped sample. The shift by about 25 °C upon doping with **Zr6** cluster was observed for all concentrations and there was no further increase in onset temperature when bigger cluster proportions were applied. This indicated that a saturation in thermal properties was already reached.

Onset 3 and Mass loss 3 described the oxidative volatilization of organic char which was produced in the step 2. A trend in the amount of formed char was clearly visible: By increasing the cluster proportion in the samples and thus the loading of inorganic moieties and the amount of cross-linking, respectively, also the char yield increased.



Finally, it is needless to mention that the residual mass determined from TGA increased with increasing cluster proportion. A theoretical value was calculated by assuming that zirconium dioxide was the only remaining residue after combustion. The values found and calculated, respectively, agreed well for all cluster concentrations.

## Differential Scanning Calorimetry

DSC measurements of the hybrid polymers were conducted in static air atmosphere in aluminum pans, the sample mass was kept between 2 and 4 mg. Glass transition temperatures were determined by first removing thermal history of the samples in a heating run with a ramp of 2 °C/min. After cooling the samples, they were heated with a ramp of 40 °C/min. In order to see transitions other than glass transition, samples were also measured up to 450 °C at a ramp of 3 °C/min, i.e. where thermal combustion took place. In this case, no prior heating scan was applied. A hole was made into the pans to keep the pressure at a constant, ambient level.

In Figure 66 the thermographs of the **Zr6** hybrid polymers and of neat PS are shown. Since no prior heating scan was applied, the glass transitions in the temperature region of about 100 °C were visible. Due to cross-linking, this effect was less pronounced for the hybrid polymers bearing higher cluster loadings. Apart from glass transitions, a pronounced exothermic signal was observed from thermal combustion of the polymers.

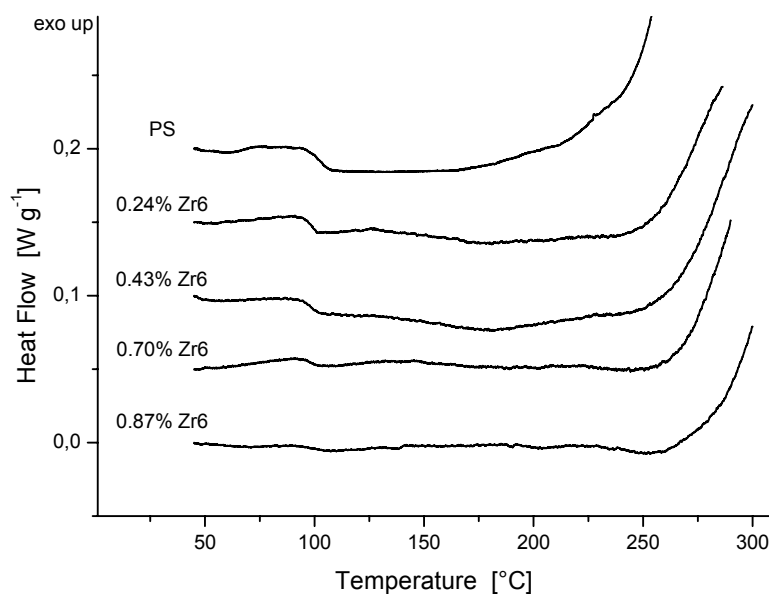


**Figure 66:** DSC thermographs of PS and **Zr6** doped PS; the position on the vertical axis was shifted by 50 mW/g to distinguish between the different curves.

The exothermic event in DSC started at a lower temperature when compared to TGA, but was not yet finished at a temperature of 450 °C. To illustrate this finding, the full DSC scan of the polymer doped with 0.87 mol% of **Zr6** is shown in Figure 67. The first exothermic peak with a maximum at around 335 °C was ascribed to the degradation of the main polymer chains and the production of char, as discussed for TGA. A second exothermic event was then expected for the oxidative volatilization of organic char. Indeed, a peak with a maximum at around 420 °C was observed. However, the DSC signal did not decline to zero, as it was expected if all material was combusted, but showed a further increase in the exothermic signal instead. This indicated that not all organic residues were combusted at this temperature and that the diffusion of oxygen into the aluminum pan determined the kinetics of oxidative degradation.

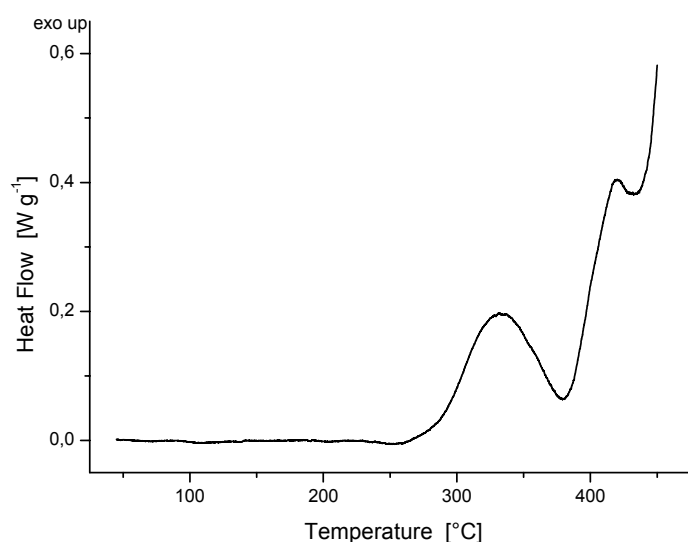


**Figure 67:** DSC scan over the full temperature range for PS doped with 0.87 mol% of **Zr6** cluster

However, the most important fact which was concluded from DSC investigations was the absence of additional signals apart from glass transition and thermal combustion, such as volatilization of low molecular species and a curing of the polymers. Additional signals were observed previously when PMMA was cross-linked with the **Zr4** cluster in the presence of benzene [59] and post-curing was evidenced in a PMMA sample cross-linked with an octafunctional methacrylate substituted titanium oxo cluster, where a pronounced exotherm at 118 °C was ascribed to the polymerization of unreacted species [102].

Glass transition temperatures of the polymers were determined at a heating rate of 40 °C/min where  $T_g$  was taken as the onset point of the transition. The transition was furthermore characterized by an endset temperature,  $T_+$ , and a temperature in the middle of the transition,

$T_{mid}$ . At the beginning of the curves, a pronounced drift was observed because of rapid heating (Figure 68). The values of the  $T_g$ 's are shown in the inset and are also given in Table 57.

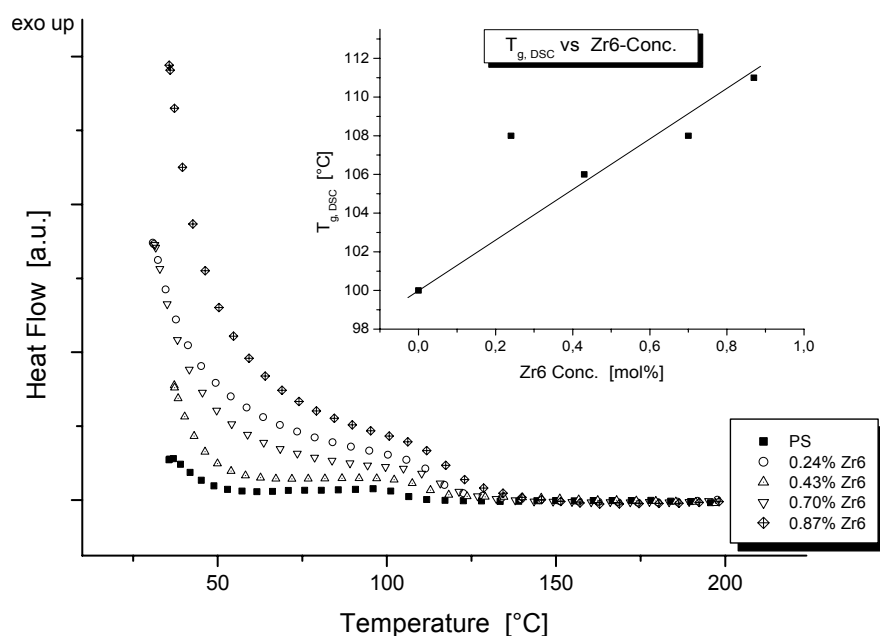


**Figure 68:** DSC heating scans of **Zr6** doped PS samples at a rate of 40 °C/min; values are graphically presented in the inset.

**Table 57:** Glass transition data of **Zr6** doped PS determined by DSC

| Zr6 Concentration [mol%] | $T_g$ [°C] | $T_{mid}$ [°C] | $T_+$ [°C] | $\Delta T$ [°C] |
|--------------------------|------------|----------------|------------|-----------------|
| 0                        | 100        | 103            | 105        | 5               |
| 0.24                     | 108        | 114            | 120        | 12              |
| 0.43                     | 105        | 110            | 116        | 11              |
| 0.70                     | 108        | 117            | 124        | 16              |
| 0.87                     | 111        | 120            | 126        | 15              |

The glass transition temperatures shifted from 100 °C for neat polystyrene to 111 °C for the sample doped with 0.87 mol% of **Zr6** cluster. The values showed good correlation with the cluster concentration and followed a linear trend (a line is drawn to guide the eye in Figure 68). The sample doped with 0.24 mol% cluster was a reproducible outlier.

The breadth of the transition, which is given as a  $\Delta T$ , increased from 5 °C for pure polystyrene to values between 11 and 16 °C, respectively, by doping with **Zr6** cluster. A broadening of the transition was explained by an increased heterogeneity of the polymer matrix [127]. However,

since large heating ramps were applied in this investigation, one could only draw the conclusion that broadening occurred and originated from cluster incorporation. A quantification was not possible. A more reliable value for  $\Delta T$  was obtained from modulated differential scanning calorimetry.

### Modulated Differential Scanning Calorimetry

Modulated DSC (MDSC) has become a well-established thermal analysis method and was initially developed by Reading et al. [128] who showed that by adding a periodic temperature oscillation to the conventional, mostly linear, DSC thermal programs the resulting heat flow signal can be separated into time dependent and time independent components [129]. With this method, reversible effects such as melting or glass transitions can be separated from irreversible effects, such as cross-linking, decomposition or evaporation. It is also possible to separate superimposed signals or to detect consecutive signals within a short range [130].

A typical modulated DSC heating signal showing a linear ramp which is superposed with a sinusoidal signal is presented in Figure 69.

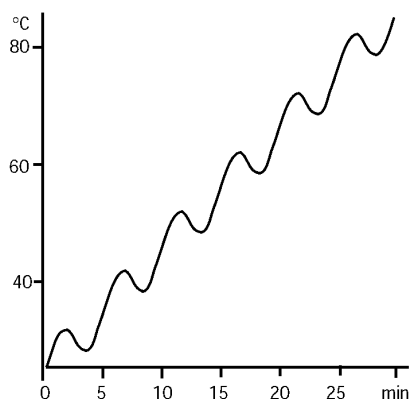


**Figure 69:** MDSC ramp superposed with a sinusoidal signal

Measurements of the **Zr6** doped samples were carried out from room temperature to 150 °C in dynamic nitrogen atmosphere. The thermal history of the samples was removed in a first heating and cooling run, the curves and analyses presented here result from the second heating run.

Glass transition temperatures were determined from the reversible heat flow versus temperature curves, which are shown in Figure 70. The glass transition temperature  $T_g$  in this analysis was characterized by three parameters,  $T_-$ ,  $T_g$ ,  $T_+$ , representative of the minimum, middle and

maximum of the transition. The  $T_g$  value was determined as the temperature corresponding to the half-height of the transition step, as commonly used for determining  $T_g$  [131]. Similar to the DSC results, the  $T_g$  shifted upon doping with the **Zr6** cluster from 101.5 °C for neat polystyrene to 107.1 °C for the sample doped with 0.87 mol% of **Zr6**. By looking at the reversible heat flow curves, a broadening of the transition was in evidence. However, the height of the transition, i.e. the heat flow determined between the onset and endset point, remained unaffected. Values for  $T_g$ 's, the broadnesses of the transitions and their heights are given in Table 58.

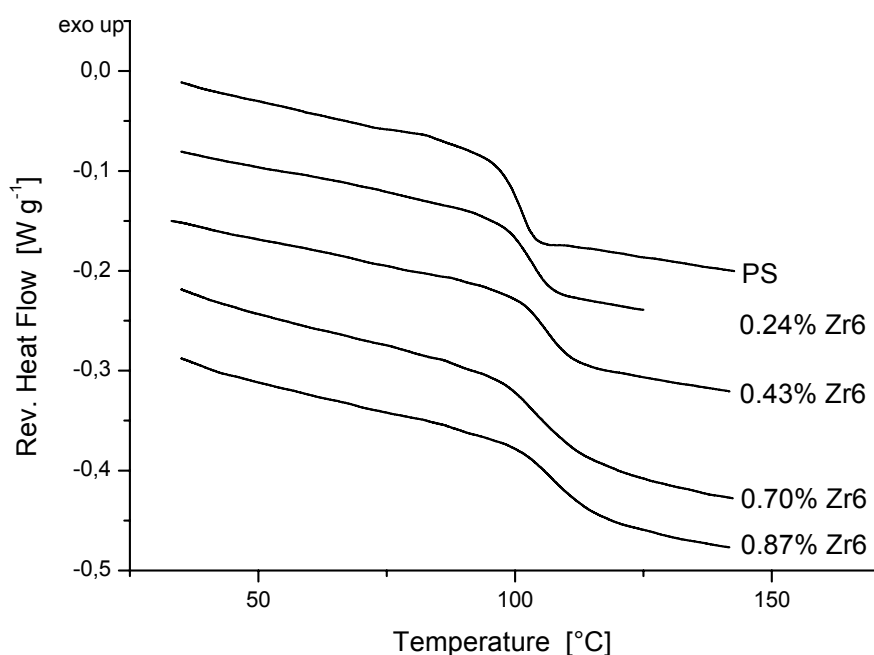


**Figure 70:** MDSC thermograms of polystyrene and the cluster doped polymers; the positions on the vertical axis were shifted by 70 mW/g to distinguish between the different curves

**Table 58:** Glass transition data of undoped and doped PS; determined by MDSC

| Zr6 Concentration<br>[mol%] | $T_g$ [°C] | $T_-$ [°C] | $T_+$ [°C] | $\Delta T$ [°C] | Height<br>[mW/g] |
|-----------------------------|------------|------------|------------|-----------------|------------------|
| 0                           | 101.5      | 96.7       | 103.6      | 6.9             | 16.8             |
| 0.24                        | 103.4      | 98.0       | 107.1      | 9.1             | 16.7             |
| 0.43                        | 106.1      | 100.2      | 111.2      | 13.2            | 16.6             |
| 0.70                        | 103.6      | 97.6       | 113.2      | 15.6            | 17.3             |
| 0.87                        | 107.1      | 100.4      | 114.1      | 13.7            | 16.9             |

Generally, an increased  $T_g$  is always caused by a hindered mobility of the polymer chains, in this case by the incorporation of the **Zr6** cluster and, as a consequence, by cross-linking. Since inorganic-organic hybrid polymers in many cases show phase separation from a certain critical concentration on (e.g. see [105, 106, 132]), which might be reflected in a second (glass-) transition, selected samples were measured from -30 °C to 200 °C. However, no transition next to the glass transition of the polymer matrix was observed, again indicating a homogeneous distribution of the cluster molecules in the polymer matrix because each glass transition reflects a distinct segmental relaxation environment [133]. Thus, the existence of a single  $T_g$  in the hybrid polymers indicates homogeneity on a scale of about 10 - 30 nm, while multiple  $T_g$ 's reflect macrophase separation [134]. For example, Abad et al. [135] prepared epoxy networks containing up to 50 wt% of a monofunctional cubic silsesquioxane. By doing so, the  $T_g$  decreased slightly when compared to the neat polymer, and an additional second transition was observed by MDSC which was attributed to amorphous, POSS-rich domains.

The thermographs of the non-reversible heat flow in the glass transition region are shown in Figure 71. The area of the peak in the glass transition region decreased with increasing cluster loading, showing a hindered chain mobility caused by cluster incorporation into the polymer matrix. The sample doped with 0.43 mol% of **Zr6** appeared to be an outlier.

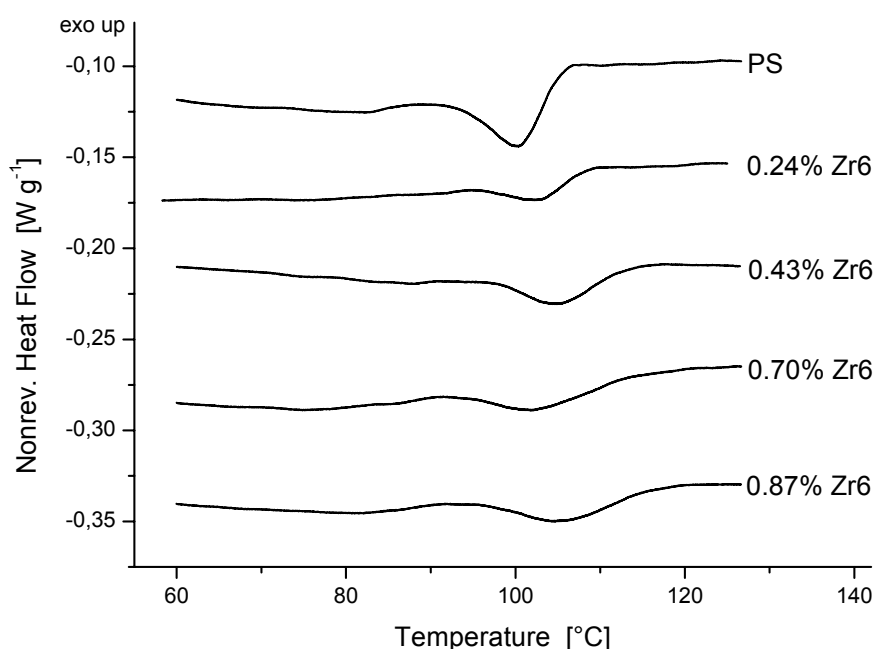


**Figure 71:** Nonreversible heat flow from MDSC measurements for PS and **Zr6** doped PS; the position on the vertical axis is shifted by 70 mW/g to distinguish between the different curves.

Values for  $T_g$ 's determined from MDSC measurements depend on many factors such as heating rate, modulation amplitude, modulation time and number of modulation cycles during the

transition [136, 137]. Values for polystyrene determined from these studies agreed very well with literature values. A broadening of transitions was observed by several other authors. For example, Porter and Blum [127] studied the glass transition behaviour of adsorbed polystyrene on silica and observed a broadening of the transitions in dependence of the adsorbed polymer, where  $T_g$  and the transition breadth increased with decreasing amount of polymer adsorbed.

### 5.2.4 Infrared Spectroscopy

Infrared spectroscopy was used to determine the presence of residual double bonds in the **Zr6** doped polystyrene samples. The spectra were dominated by the polymer matrix (Figure 72). In the samples doped with 0.87 and 0.70 mol% of **Zr6** cluster, a signal at  $1645\text{ cm}^{-1}$  was observed, indicating that unreacted double bonds were present in the polymer. In the samples polymerized with lower cluster concentrations, i.e. 0.24 and 0.43 mol%, no bands were present or were covered by the background.

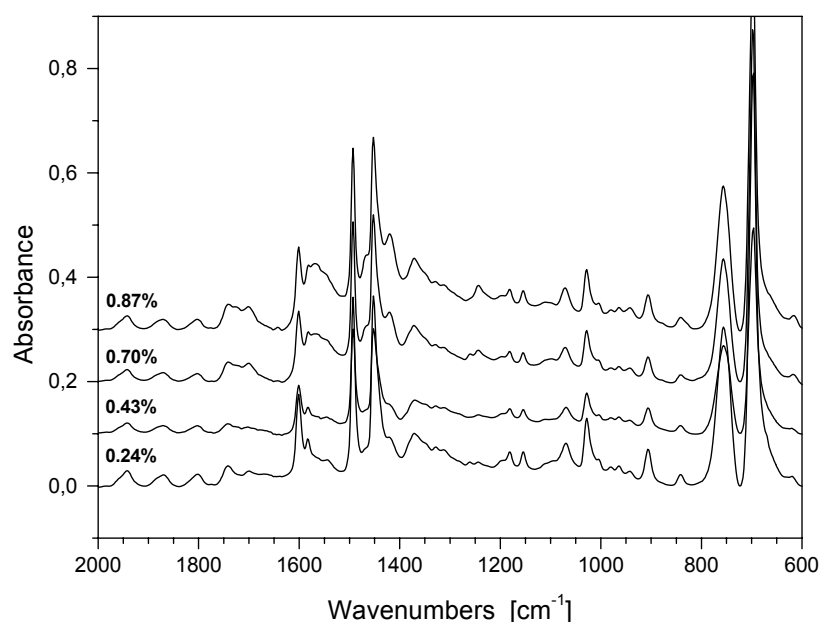


**Figure 72:** FTIR spectra of **Zr6** doped hybrid polymers; the position on the vertical axis was shifted

Apart from the signals of the polystyrene matrix, also signals originating from the **Zr6** cluster were observed. Bands of the asymmetric carboxylate stretching vibration were clearly visible at  $1571$  and  $1547\text{ cm}^{-1}$ . Moreover, the symmetric stretching vibration at  $1417\text{ cm}^{-1}$  was apparent.

Depending on the cluster concentration, also a band at  $1700\text{ cm}^{-1}$  was observed which was assigned to the carbonyl vibration of a carboxylic acid, stemming from the **Zr6** cluster, which was not applied solvate-free in these polymerizations.

### 5.2.5 Swelling Behaviour

Cluster cross-linked polymers are not soluble in organic solvents, such as toluene or ethyl acetate, but show swelling instead [77, 138].

The equilibrium degree of swelling was determined by swelling the crack-free polymer pieces in ethyl acetate at room temperature. To this end, pre-weighed polymer pieces were placed in a beaker with ethyl acetate and periodically weighed until weight constancy was reached.

The degree of swelling,  $d_{sw}$ , was determined according to

$$d_{sw} = \frac{m_{sw} - m_{dry}}{m_{dry}} \cdot 100\%$$

where  $m_{sw}$  and  $m_{dry}$  were the masses of the polymer in the swollen and in the dry state, respectively.

With increasing cluster proportion, i.e. an increasing amount of possible cross-link functionalities, the solvent uptake decreased (Figure 73, Table 59). This was a clear proof for network formation.

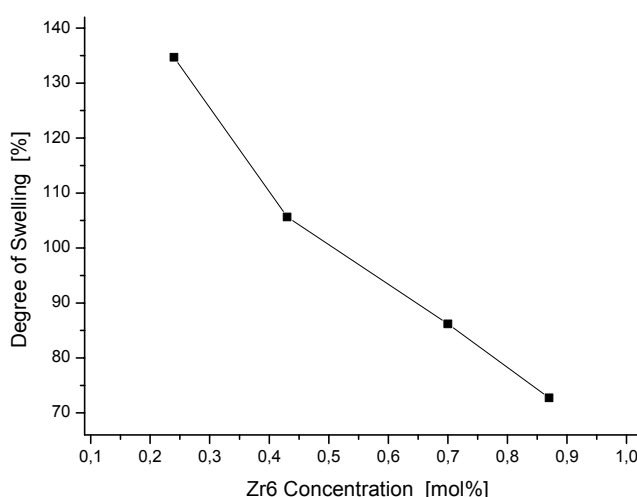


**Figure 73:** Swelling of **Zr6** doped polystyrene samples in ethyl acetate



**Table 59:** Swelling behaviour of **Zr6** doped PS samples in ethyl acetate

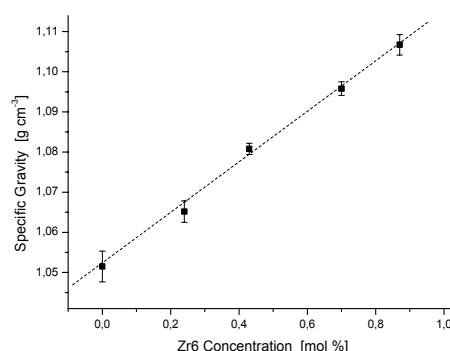
| <b>Zr6 Concentration [mol%]</b> | <b>Degree of Swelling [%]</b> |
|---------------------------------|-------------------------------|
| 0                               | -                             |
| 0.24                            | 135                           |
| 0.43                            | 106                           |
| 0.70                            | 86                            |
| 0.87                            | 73                            |

It might be useful to compare values obtained from other cross-link sources:

Sundell et al. cross-linked styrene with various divinyl monomers, among them the most frequently used divinylbenzene (DVB) [139]. Cross-linked polymers were swollen in toluene and a saturation in solvent uptake was observed for about 10 mol% of divinylbenzene. When compared to cluster cross-linked PS, a solvent uptake of 135 % would correspond to a cross-linking with 2 mol% of DVB and an uptake of 73 % to a cross-linking with 4 mol% of DVB, keeping in mind the use of a different solvent, i.e. ethyl acetate instead of toluene.

### 5.2.6 Specific Gravity

Densities of undoped and doped polystyrene samples were determined on a hydrostatic balance using the Archimedean principle. The samples were weighed in air and in water at a known temperature, and the specific gravity was calculated from buoyancy. It is needless to mention that with increasing **Zr6** proportion the specific gravity also increased. The data obtained are presented in Figure 74 and Table 60, respectively. The value for pure polystyrene was in agreement with literature values for atactic polystyrene [140].

**Figure 74:** Densities of pure and cluster doped polystyrene samples

**Table 60:** Densities ( $\rho$ ) and standard errors for pure PS and the hybrid polymers

| Zr6 Concentration [mol%] | $\rho$ @ 25.5 °C [g cm <sup>-3</sup> ] |
|--------------------------|--|
| 0                        | 1.052 $\pm$ 0.004                      |
| 0.24                     | 1.065 $\pm$ 0.003                      |
| 0.43                     | 1.081 $\pm$ 0.001                      |
| 0.70                     | 1.096 $\pm$ 0.002                      |
| 0.87                     | 1.107 $\pm$ 0.003                      |

### 5.2.7 Thermal Mechanical Analysis

Polymers encounter a wide variation in temperature when they are used in the everyday world. Thus, the dimensional and mechanical stability of the materials is of paramount importance and must be determined [11].

Thermal mechanical analysis (TMA) can be defined as the measurement of a specimen's dimensions (length or volume) as a function of temperature whilst it is subjected to a constant mechanical stress. Thermal expansion coefficients can be determined in this way and changes in this property with temperature monitored. Polymers deform with increasing temperature under the applied stress at a particular temperature which is connected either to a melting or a glass transition temperature. A specimen also may possess some residual stress, resulting from preparation, which is released at a certain temperature [141]. Measurement of thermal expansion provides information about the average linear,  $\alpha$ , or cubic,  $\beta$ , coefficient of thermal expansion [130].

The undoped and doped polystyrene samples were measured from room temperature to 135 °C, i.e. from below to above glass transition temperature. The samples were heated once with a heating rate of 1 °C/min in dynamic nitrogen atmosphere to remove the thermal history of the polymers and to ensure plane surfaces. Thermal expansion coefficients were then determined from a second or third heating run. Since the polymers underwent a glass-to-rubber transition in the region of 100 °C - 120 °C, two different expansion coefficients had to be considered, one below the glass transition temperature, and another one above  $T_g$ . The values were determined from the slope of the relative length changes versus temperature curves by performing a linear regression of the data in the range of 30 - 40 °C (below  $T_g$ ) and 110 - 120 °C (above  $T_g$ ), respectively. Measurements of the hybrid polymers are shown in Figure 75. The thermograms

were characterized by a change of the slope of the graphs at a temperature which corresponded to the glass transition temperature.

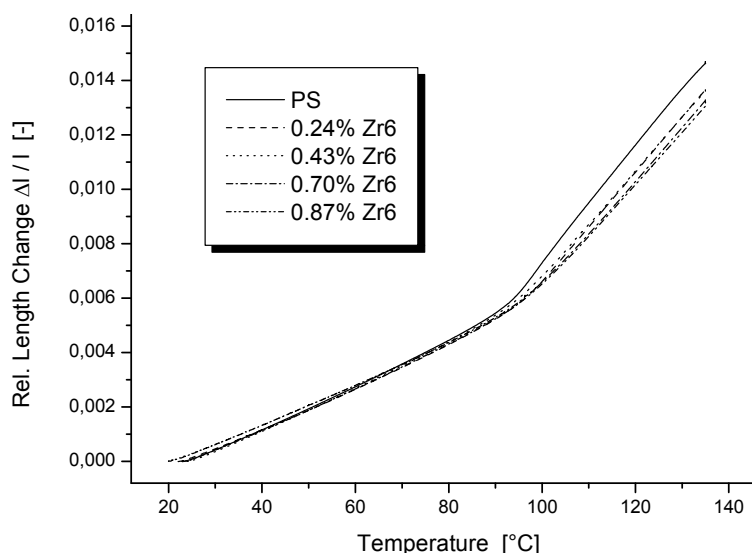


**Figure 75:** Relative length change versus temperature for undoped and doped polystyrene samples

The data of the thermal expansion coefficients are given in Table 61 and are graphically presented in Figure 76. The linear thermal expansion coefficient for pure polystyrene below glass transition temperature was 74 ppm/°C and agreed well with literature values [140]. Doping with various proportions of the **Zr6** cluster did not change the values of thermal expansion coefficients in the glassy state, a fact which was found for polystyrene samples cross-linked with organic co-monomers [142], but also for epoxides cross-linked with an octafunctional cubic silsesquioxane [106]. Above  $T_g$ , the hybrid polymers became rubber-like and properties were determined by the network structure. On account of this, the linear thermal expansion coefficients decreased with increasing **Zr6** proportion and thus with increasing degree of cross-linking [143, 144].

**Table 61:** Thermal expansion coefficients determined below and above glass transition temperature

| Zr6 Conc. [mol%] | $\alpha$ (30 – 40 °C) [ $10^{-6} \text{ }^{\circ}\text{C}^{-1}$ ] | $\alpha$ (110 – 120 °C) [ $10^{-6} \text{ }^{\circ}\text{C}^{-1}$ ] |
|------------------|---|---|
| 0                | 74  | 213   |
| 0.24             | 70  | 202   |
| 0.43             | 74  | 197   |
| 0.70             | 70  | 192   |
| 0.87             | 71  | 190   |

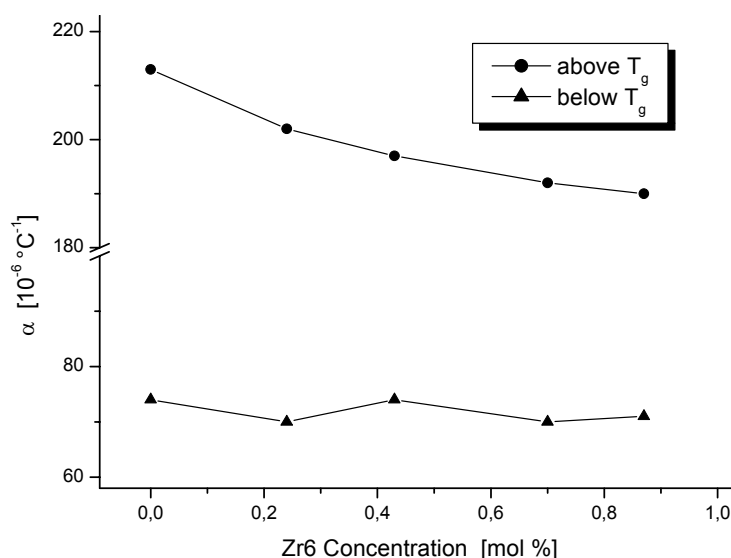


**Figure 76:** Thermal expansion coefficients below and above  $T_g$ ; take notice of the break in the y-axis

### 5.2.8 Dynamic Mechanical Properties

Dynamic Mechanical Analysis (DMA) is one of the main techniques used in studying polymer hybrid materials. In DMA, the mechanical properties are measured as a function of temperature [141, 145, 146]. It can be described as applying an oscillating force to a sample and measuring the materials response to that force. From this, one calculates properties like the tendency to flow (the viscosity), the phase lag, and the stiffness (the modulus) from the sample recovery. These properties are related to the molecular mobility within materials. Thus, DMA is often used to determine the glass transition and other transitions in macromolecular materials, or to follow changes in the chemical properties brought about by chemical reactions.

Dynamic mechanical measurements of polystyrene samples were carried out at 1 Hz from room temperature to 220 °C. Dynamic moduli at room temperature were determined for each sample in single cantilever clamping mode. The modulus of elasticity for the PS sample was 2.9 GPa and agreed well with literature values [140]. Doping with the **Zr6** cluster shifted the dynamic moduli to values which were about 400 MPa higher when compared to pure PS. However, small influences of the cluster concentration to the moduli were observed (Figure 77, Table 62).

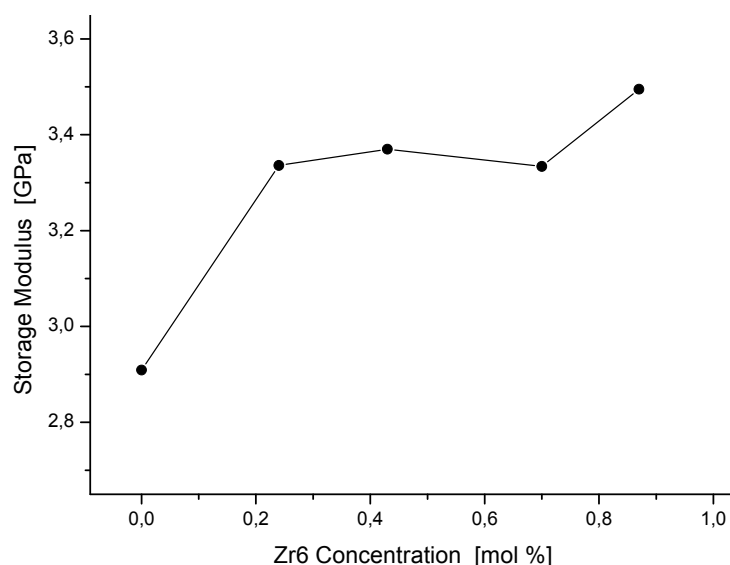


**Figure 77:** Dynamic moduli of polystyrene samples determined at room temperature in single cantilever clamping

**Table 62:** Dynamic moduli of undoped and **Zr6** doped polystyrene samples

| Zr6 Concentration [mol %] | Dynamic Modulus [GPa] |
|---------------------------|-----------------------|
| 0                         | 2.91                  |
| 0.24                      | 3.34                  |
| 0.43                      | 3.37                  |
| 0.70                      | 3.33                  |
| 0.87                      | 3.50                  |

The dynamic moduli as functions of temperatures for varying **Zr6** proportions were recorded in tension mode and are shown in Figure 78. The polystyrene samples exhibited dynamic mechanical response which was characteristic for thermoplastic materials: At room temperature, the storage modulus was relatively high and, with increasing temperature, this modulus gradually decreased. At the glass transition temperature, which was reflected in a maximum of the  $\tan \delta$  versus temperature curves (Figure 80), a sharp decrease in the dynamic modulus was observed because the polymer chains obtained segmental mobility and their state changed from glassy to rubbery. By increasing the temperature above the glass transition temperature, the  $\tan \delta$  value reduced again and the decay in the modulus attenuated. In this so-called rubber plateau, the polymer chains had full segmental mobility and the properties were determined by the entangled network [147].

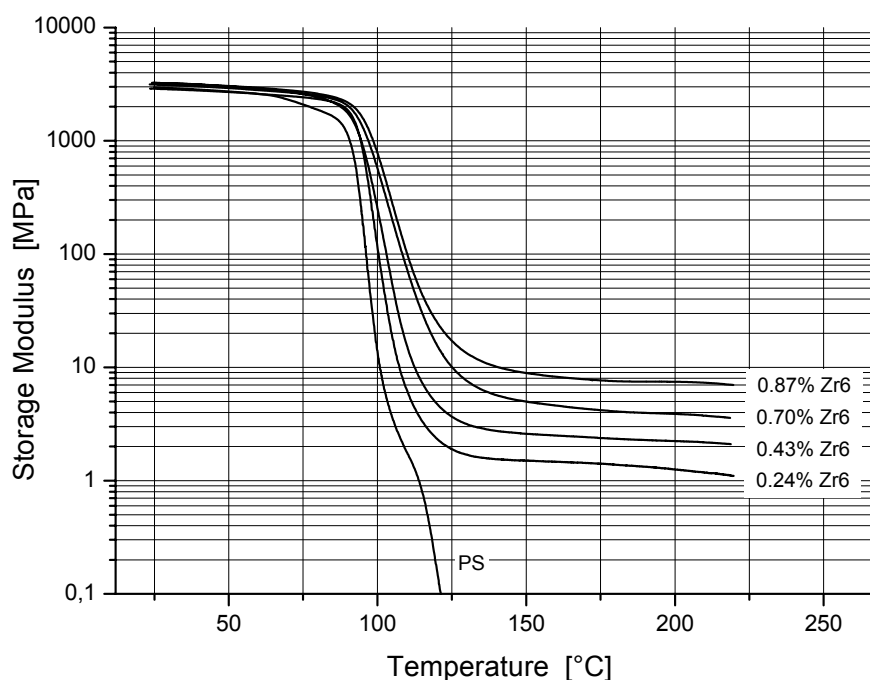


**Figure 78:** Dynamic moduli as functions of temperatures for undoped and doped polystyrene samples

Over the whole temperature range, all hybrid polymers showed storage moduli which were increased when compared to that of neat polystyrene. In addition, the glass transition temperatures shifted gradually with increasing **Zr6** concentration, which was seen from the temperature where the decay from glassy to rubbery took place, i.e. where  $\tan \delta$  reached a maximum. It was reported that polystyrene possesses a second transition,  $T_{\beta}$ , near 50 °C [148] which was a result of phenyl group rotation about the main chains [149]. However, this weakly pronounced transition was neither observed in neat polystyrene nor in the hybrid polymers.

The modulus of elasticity at room temperature shifted significantly from 2.9 GPa for pure polystyrene by about 20 % to 3.5 GPa for the sample doped with 0.87 mol% of **Zr6** cluster. Within the series, no pronounced changes of the moduli with increasing cluster proportion were observed. This was different to other comparable inorganic-organic hybrid materials:

Trabelsi et al. polymerized dimethacryloxy-tetraethoxylated bisphenol A and 2-hydroxyethyl methacrylate in the presence of a titanium oxo cluster bearing eight methacrylate groups [104]. The modulus of elasticity OF the pure co-polymer was increased from 0.7 GPa to 1.8 GPa by doping with 2.5 wt% of cluster (to compare: 0.24 mol% **Zr6** cluster in polystyrene corresponded to 3.8 wt%). However, by increasing the amount of Ti-cluster to 5.0 and 7.5 wt%, respectively, the stiffness of the matrix decreased again to 1.6 and 1.0 GPa, respectively. The increase in dynamic modulus upon doping with small amounts of Ti cluster was explained by an increase of the cross-linking density of the matrix. Decreases of the moduli at higher cluster loadings were

explained by the aggregation of the Ti clusters, and by self-reaction and sterical hindrance caused by these aggregates.

Epoxy-type systems which were cross-linked with octafunctional polyhedral oligomeric silsesquioxane (POSS) in the amounts of 7 wt% to 32 wt% POSS [106] showed the same behaviour. Doping with 7 wt% of POSS increased the dynamic modulus when compared with the neat matrix. By further increasing the amount of cross-linker, the stiffness shifted to values below the neat matrix. Remarkably, a shift to lower values was directly related to the POSS content, i.e. the higher the POSS content, the lower the modulus.

In contrast to that, Li et al. characterized polystyrene copolymers cross-linked with a tetrafunctional POSS unit with DMA in bending mode [150]. The bending modulus at 40 °C for pure polystyrene was 0.8 GPa and increased to 1.7 GPa or 1.75 GPa upon doping with 0.42 mol% or 0.88 mol% of POSS as the cross-linker. Again, this remarkable increase in modulus was attributed to cross-linking. However, whereas doping with 0.42 mol% of cross-linker increased the modulus by more than 100 %, a doubling of the POSS concentration did not cause significant changes anymore.

The effect of post-curing in thermosets consisting of poly(methyl methacrylate) cross-linked with an oxotantalum cluster was shown by Basch et al. [151]. The dynamic modulus for pristine PMMA was determined to 1.6 GPa, a value far below literature reports of ~3 GPa [140]. A doping with 1 mol% of tetrafunctional oxotantalum cluster shifted the value to 1.4 GPa and by further increasing the cluster proportion to 2 mol%, the modulus decreased to 0.8 GPa. The authors attributed this to residual, unreacted monomer, which was volatilized or polymerized at higher temperatures, an assumption which was reasoned because of the broad  $\tan \delta$  curves.

Recapitulating the findings from literature systems, cross-linking mostly, but not necessarily, led to an increase in dynamic moduli in the glassy state of class II hybrid materials. In the majority of cases, an increase of stiffness was observed when thermoplastic materials were cross-linked with an inorganic-organic co-monomer, such as surface modified transition metal oxo clusters or modified POSS. However, no linear correlation between the amount of cross-linker and the increases in stiffness were reported. In fact, the systems tended to show saturation or even a decrease in this property instead. In the underlying system, i.e. polystyrene cross-linked with the **Zr6** cluster, an increase in dynamic modulus was still obtained, indicating that the saturation level in this property was not reached yet. This finding was quite remarkable because the hybrid polymers had a cluster proportion up to 0.87 mol%, which corresponded to 12.5 wt%.

The glass transition temperatures were determined from the maxima of the  $\tan \delta$  curves (Figure 80) and increased with the cluster proportion from 100 °C for pure polystyrene to 110 °C for the doped samples, the results are shown in Figure 79 and in Table 63. The trend was similar to that obtained for dynamic moduli, but less pronounced. Whereas doping with 0.24 mol% of **Zr6** shifted the modulus by about 20 %, the glass transition increased only by 4 °C. Up to cluster

contents of 0.70 mol%, the correlation between glass transition temperature and cluster concentration was linear. Further increasing the concentration of cluster did not influence the  $T_g$  anymore, indicating that a plateau was reached.

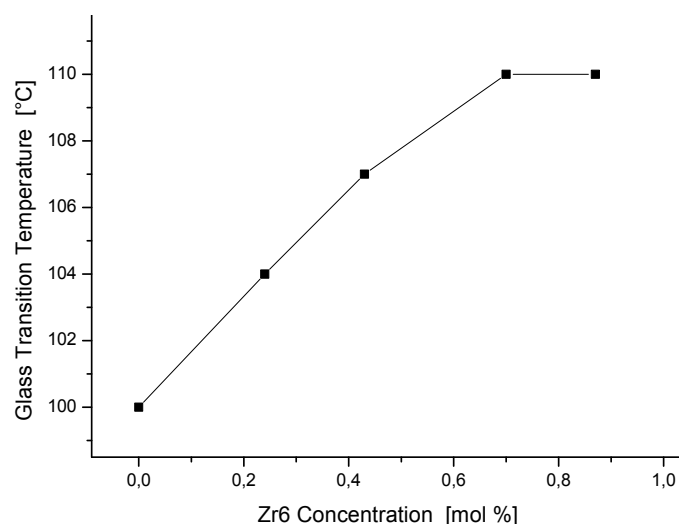


**Figure 79:**  $T_g$ 's of undoped and doped PS determined from the maxima of  $\tan \delta$  curves in tension mode

**Table 63:** Glass transition temperatures and full width at half maximum values of polystyrene samples determined from  $\tan \delta$  curves

| Zr6 Concentration<br>[mol %] | Glass Transition<br>Temperature [°C] | $\Delta T$ - Tan $\delta$ Full Width at<br>Half Maximum [°C] |
|------------------------------|--------------------------------------|--|
| 0                            | 100                                  | 11   |
| 0.24                         | 104                                  | 14   |
| 0.43                         | 107                                  | 17   |
| 0.70                         | 110                                  | 27   |
| 0.87                         | 110                                  | 26   |

Similar observations were also made in the above described system prepared by Trabelsi et al. [104], i.e. a system consisting of a titanium oxo cluster cross-linked co-polymer. Whereas doping with small amounts of cluster shifted the dynamic modulus significantly, the shift in  $T_g$  was small. By comparing the moduli and glass transition temperatures, the authors assumed that there might be other than cross-linking mechanisms responsible for increases in stiffness and in  $T_g$ , originating from the heterogeneity of the system. Therefore, properties such as the degree of dispersion or physical interactions between clusters and polymer chains might have been responsible for the measured property, the value of which represented the sum of interactions.



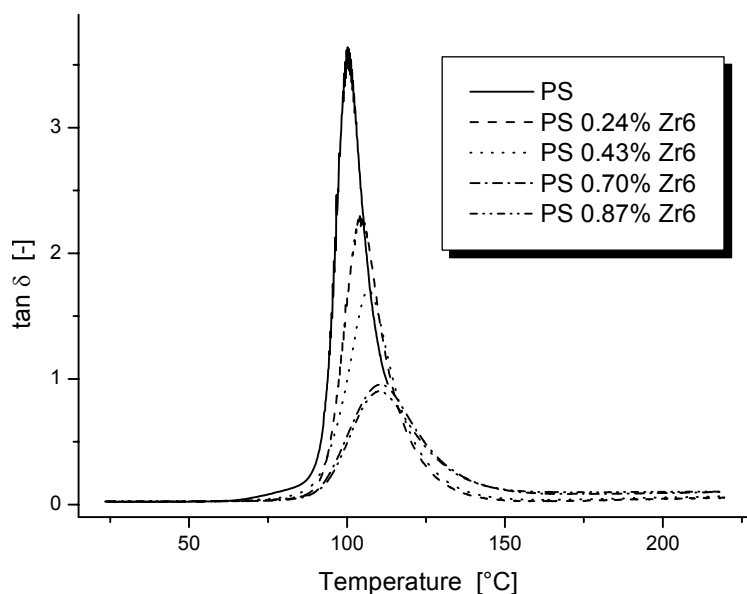


**Figure 80:** Tan  $\delta$  as functions of temperatures with varying **Zr6** concentration

The loss tangent maximum decreased gradually with increasing cluster proportions from  $\tan \delta = 3.6$  for neat polystyrene to  $\tan \delta = 0.9$  for the sample doped with 0.87 mol% of **Zr6** cluster (Figure 80). The decrease in damping was not serious because polymeric materials with damping factors bigger than 0.3 are still considered to possess good damping properties when they are applied in the respective temperature region. The peak of the glass transition broadened simultaneously with the decrease in the loss factor. The values were determined from the full width at half maximum of the loss factor peaks and are given in Table 63 as a  $\Delta T$ , which was linked to the distribution of mobility of polymer segments and thus may be taken as a measure of the structural inhomogeneity of the polymer network [105, 152]. As a consequence, the increase of  $\Delta T$  from 11 °C for neat polystyrene up to 27 °C for the hybrid polymers proved that the degree of heterogeneity was for the most part determined by the incorporation of the **Zr6** cluster.

Whereas the moduli of elasticity were shifted by about 20 % for cluster cross-linked samples in the glassy state, the situation was even more pronounced in the rubbery state, i.e. above  $T_g$ . As apparent in Figure 78, the rubbery plateau moduli,  $E_N^0$ , for doped samples shifted gradually to values of 8 MPa for the sample doped with 0.87 mol% of **Zr6**. Gradual increases in moduli by almost one order of magnitude again indicated that a saturation level was not reached yet.

The absence of a minimum in the  $\tan \delta$  curve for pure PS resulted from the modulus of elasticity which was zero at this temperature. A weakly pronounced plateau or the missing of that is typical for polymers with broad distributions in their molecular weights [153]. In this work, polystyrene was prepared by free radical polymerization in the same conditions as required for

the cluster doped samples and had a polydispersity of 2.6, as determined from SEC. Thus, for following calculations, literature values for the plateau modulus ( $E_N^0$ ) of PS were consulted which were determined to 0.6 MPa at 140 °C [154].

## NETWORK DENSITY

The polymer chains have full segmental mobility in the rubber plateau and the properties are determined by the entangled network [147]. Once a polymer reached this viscoelastic state, the shear modulus can be deduced from the modulus of elasticity by using the equation

$$G = \frac{E}{2(1 + \nu)}$$

where  $\nu$  represents the so-called Poisson's ratio as the ratio of the lateral and axial strains [130]. In the rubber-elastic state, which is on hand for thermoplastic and thermoset materials above  $T_g$ , Poisson's ratio is 0.5. Thus the equation given above reduces to

$$G = \frac{E}{3}.$$

According to Lomellini et al. [155], approximate plateau moduli ( $G_N^0$ ) were determined by using the convention

$$G_N^0 = G'_{\tan \delta \rightarrow \min}$$

where the plateau modulus was taken as the point in the storage modulus where the loss tangent

$$\log(\tan \delta) = \frac{G''}{G'}$$

passed through a minimum. The values for the hybrid polymers were determined by taking the minima obtained from a simple second order curve fit of the measured data in the respective plateau area. They are shown in Figure 81 and were found between 160 °C and 170 °C. Since

the neat polystyrene sample did not show a plateau and, as a consequence, no minimum. Thus, a plateau modulus  $E_N^0$  of 0.6 MPa at 140 °C was considered [154]. The plateau values are shown in Table 64.

**Table 64:**  $T_{\tan\delta-\min}$  and rubber moduli at this temperature for undoped and doped polystyrene samples

| Zr6 Concentration [mol%] | $T_{\tan\delta-\min}$ [°C] | $E_N^0$ [MPa] | $G_N^0$ [MPa] |
|--------------------------|----------------------------|---------------|---------------|
| 0                        | 140 *                      | 0.60 *        | 0.200 *       |
| 0.24                     | 164                        | 1.457         | 0.486         |
| 0.43                     | 162                        | 2.484         | 0.828         |
| 0.70                     | 163                        | 4.496         | 1.499         |
| 0.87                     | 171                        | 7.805         | 2.602         |

\* value taken from reference [154]

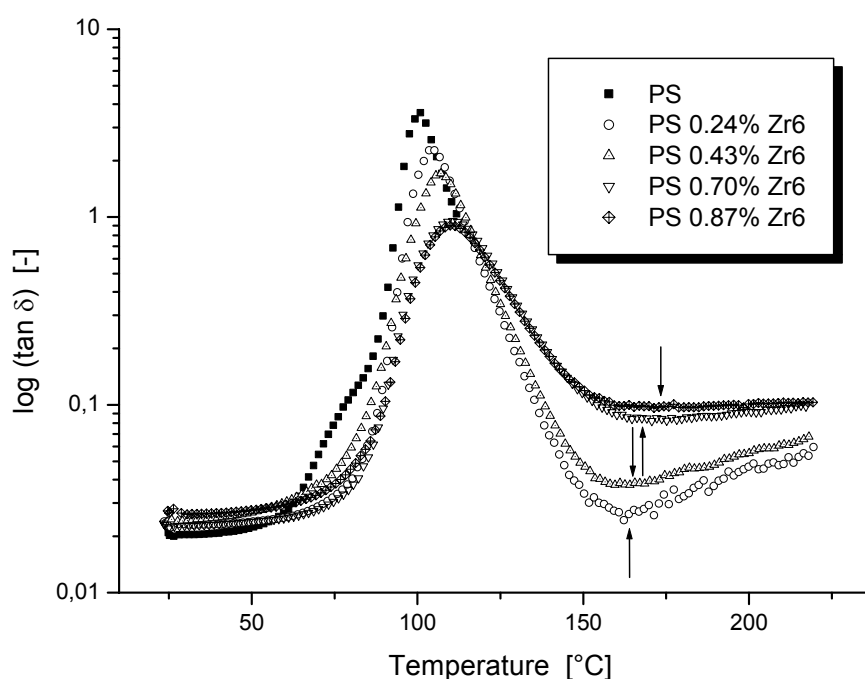


**Figure 81:** Damping factor versus temperature, the minima are highlighted with arrows

Values for moduli of elasticity and, as a consequence, shear moduli, were increased with increasing cluster proportion. In contrast to similar systems discussed above, e.g. reference [104], no saturation level was observed. In fact, rather the opposite situation was at hand. The

moduli showed a correlation with the cluster concentration which was more than linear, showing a polynomial growth in the present cluster concentration range rather (Figure 82).

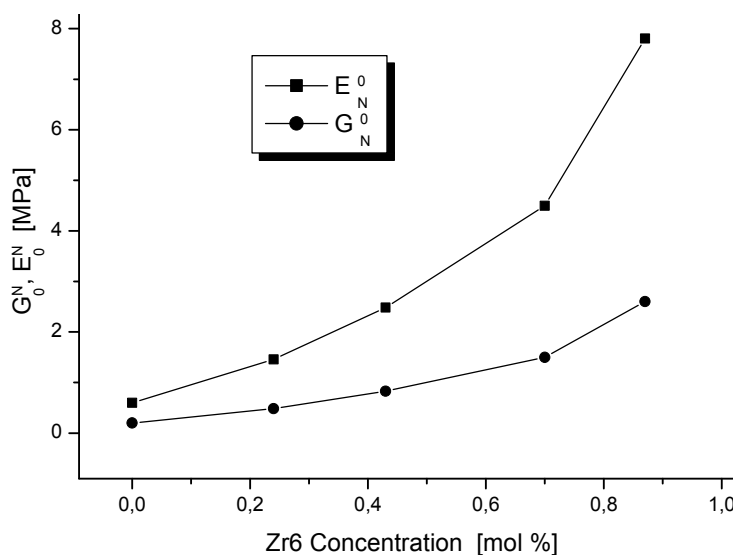


**Figure 82:** Moduli of elasticity and shear moduli versus **Zr6** concentration

The theory of rubber elasticity predicts a relationship between the shear modulus and the concentration of the network strands. This relationship was used to evaluate  $M_e$ , the equivalent molecular weight of a strand in the entangled network, which is called the entanglement molecular weight [156]

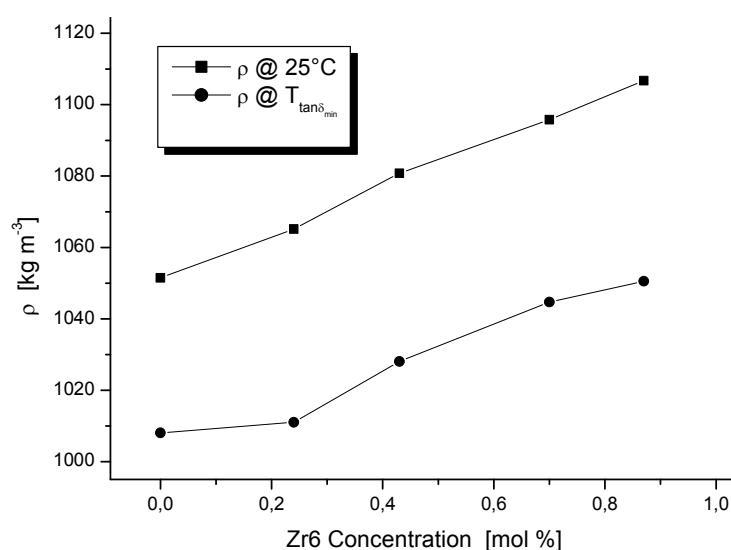
$$M_e = g \rho_r \frac{RT}{G_N^0}$$

where  $\rho_r$  is the density of the polymer in the rubbery state,  $R$  the ideal gas constant and  $T$  the absolute temperature. Kopesky et al. performed these calculations for polyhedral oligomeric silsesquioxanes (POSS) doped poly(methyl methacrylate)s [157]. They considered the factor  $g$ , which described the difference between dynamic and static behaviour and was calculated to 4/5, but is commonly taken as 1. Specific gravities of the hybrid polymers at room temperature were corrected to plateau temperatures using the thermal expansion coefficients as determined by TMA measurements. The calculations are summarized in Table 65 and are graphically presented in Figure 83.

**Table 65:** Polymer densities corrected to  $T = T_{\tan\delta-\min}$ 

| Zr6 Concentration<br>[mol%] | $\rho$ @ 25°C<br>[kg/m <sup>3</sup> ] | $\beta=3\alpha$ [10 <sup>-6</sup> /°C] < $T_g$<br>$\beta=3\alpha$ [10 <sup>-6</sup> /°C] > $T_g$ | $T_g$<br>[°C] | $T$ @ $\tan\delta_{\min}$<br>[°C] | $V/V_0^*$ @ $T_g$<br>[m <sup>3</sup> ] | $V/V_0^*$ @ $T_{\tan\delta-\min}$<br>[m <sup>3</sup> ] | $\rho$ @ $T_{\tan\delta-\min}$<br>[kg/m <sup>3</sup> ] |
|-----------------------------|---------------------------------------|--|---------------|-----------------------------------|--|--|--|
| 0                           | 1051.5                                | 222<br>639   | 100           | 140                               | 1.0171                                 | 1.0431   | <b>1008.1</b>  |
| 0.24                        | 1065.2                                | 210<br>606   | 104           | 164                               | 1.0166                                 | 1.0536   | <b>1011.0</b>  |
| 0.43                        | 1080.8                                | 222<br>591   | 107           | 162                               | 1.0182                                 | 1.0513   | <b>1028.1</b>  |
| 0.70                        | 1095.8                                | 210<br>576   | 110           | 163                               | 1.0179                                 | 1.0489   | <b>1044.7</b>  |
| 0.87                        | 1106.7                                | 213<br>570   | 110           | 171                               | 1.0181                                 | 1.0535   | <b>1050.5</b>  |

\*  $V_0$  = volume at room temperature (arbitrary set as 1)

**Figure 83:** Polymer densities corrected to  $T_{\tan\delta-\min}$ 

The entanglement molecular weights were calculated with the corrected densities and were found to decrease with increasing cluster proportion (Figure 84), a situation which was very close to what one might have expected. For instance, by increasing the cluster concentration from 0.24 mol% to 0.70 mol%, i.e. by a factor of about three, the molecular weight between two entanglement points, which is connected to a certain distance, decreased from 7.6 kg/mol to 2.5 kg/mol, also by a factor of three. The  $M_e$  value of pure polystyrene did not fit into this linear

relationship. However, it is necessary to point out again that this value was taken from literature, representing a polymer prepared differently than the hybrid materials.

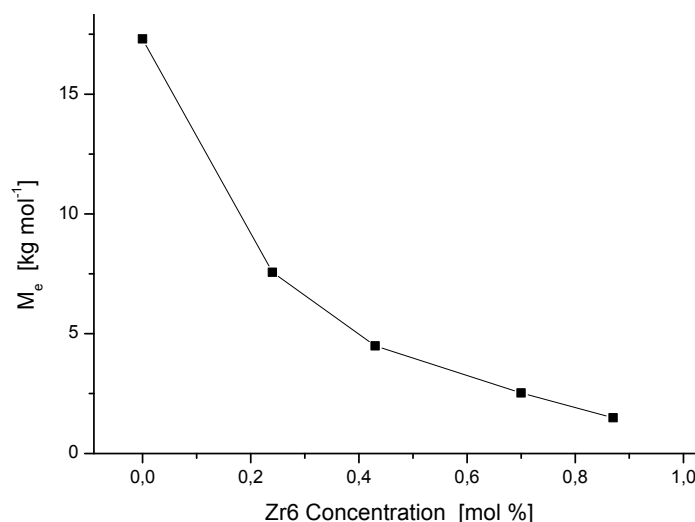


**Figure 84:** Molecular weight between entanglements in undoped and doped PS

The molecular weight between entanglements,  $M_e$ , is inversely proportional to the network density,  $\nu_e$ , according to

$$\nu_e = \frac{\rho_g N_L}{M_e}$$

where  $\rho_g$  is the density of the polymer in the glassy state and  $N_L$  the Loschmidt number. In this way, the distance between two entanglement points,  $\xi$ , is given by [158]

$$\xi = (\sqrt[3]{\nu_e})^{-1}$$

Network densities for the hybrid polymers were calculated by combining properties from the rubbery state, the plateau modulus, and from the glassy state, the density below glass transition temperature. By doing so, a correlation was observed not exhibiting any saturation effects in the investigated cluster proportion range (Figure 85). The distances between the entanglement points,  $\xi$ , were calculated from the inverse cubic root of the network densities and showed a clear correlation with the cluster proportion. The results of the calculations are summarized in Table 66.

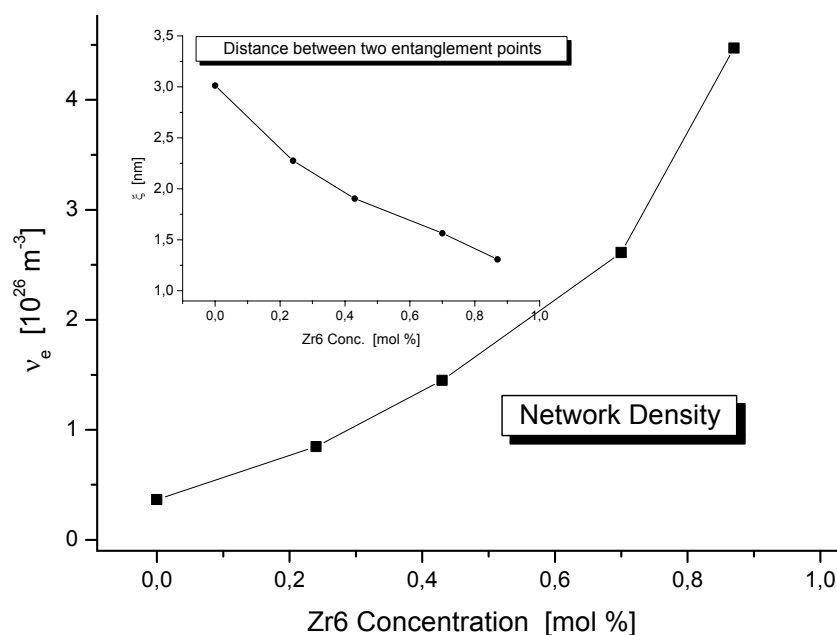


**Figure 85:** Network densities and distances between two entanglement points versus **Zr6** concentration

**Table 66:** Network parameters of the hybrid polymers calculated from storage moduli and densities

| Zr6 Concentration [mol %] | Plateau Modulus $G_N^0$ [MPa] | Entanglement Molecular Weight $M_e$ [kg/mol] | Network Density $v_e$ [ $10^{26}/\text{m}^3$ ] | Distance between two Entanglement Points $\xi$ [nm] |
|---------------------------|-------------------------------|--|--|---|
| 0                         | 0.200                         | 17.308                                       | 0.366  | 3.01  |
| 0.24                      | 0.486                         | 7.564  | 0.848  | 2.28  |
| 0.43                      | 0.828                         | 4.491  | 1.450  | 1.90  |
| 0.70                      | 1.499                         | 2.527  | 2.611  | 1.56  |
| 0.87                      | 2.602                         | 1.491  | 4.471  | 1.31  |

For a deeper understanding on the origin of the factors which influenced the materials properties in the rubbery state, it might be useful to compare systems different from cluster cross-linked polymers:

Van Melick et al. [147] cross-linked styrene with a bifunctional methacrylate-type monomer in amounts up to 5 wt%. Upon cross-linking, the rubber plateau moduli,  $G_N^0$ , were increased from 0.15 MPa for pure polystyrene to 0.51 MPa for the sample cross-linked with 5 wt% of bifunctional monomer. Apart from the pure polystyrene sample, a linear relation was found for rubber plateau moduli versus the concentration of the cross-linking agent. The network densities

followed the same trend: An increase in the rubber plateau modulus to 0.51 MPa would correspond to a **Zr6** cluster proportion of about 0.25 % in the hybrid polymers, i.e. very small cluster concentration.

Strachota et al. cross-linked epoxy-type polymers with POSS systems carrying 2, 4 and 8 reactive groups [105]. To keep the stoichiometric ratio of functional groups in the system constant, they increased the POSS concentration with decreasing functionality. By doing so, the rubber moduli decreased but also increased, depending on the number of functionalities and, at the same time, on the applied POSS concentration. This was reasoned by a pronounced aggregation of the POSS units.

In conclusion, many factors determine the dynamic rubbery behaviour of the hybrid polymers. Cross-linking of polymers with organic monomers usually increased the rubber modulus because network-formation occurred. In POSS doped polymers it was shown that their incorporation mostly caused a decrease in the rubber modulus. On the other hand, the modulus increased again with increasing proportion of unreactive POSS. This was very likely due to the higher stiffness caused by the rigid Si-O cubes. Moreover, a strong dependence derived from the interactions between the molecular network and the functionalities provided by the inorganic-organic cross-linker. By applying this to the inorganic-organic systems consisting of a polystyrene matrix cross-linked with the **Zr6** cluster, two factors appeared to be crucial: First of all, the cluster with twelve methacrylate ligands per unit acted as an efficient cross-linker and secondly, the cluster acted as rigid inorganic filler, additionally increasing the stiffness of the network.



## 5.2.9 Mechanical Properties

### TENSION TESTS

These tests can be used to ascertain several mechanical properties of materials that are important to design, such as modulus of elasticity or tensile strength [130, 159]. A specimen is deformed, usually to fracture, with a gradually increasing tensile load that is applied uniaxially along the axis of the specimen. The output is recorded as engineering stress  $\sigma$  (load or force) versus the engineering strain  $\varepsilon$  (elongation) where strain is unitless, but commonly expressed as a percentage. When the strain exceeds the elastic region of the polymer, the sample either breaks or is plastically deformed.

Tension tests of doped and undoped polystyrene samples were performed at room temperature until break on standardized specimens in 'dog-bone' geometry with a parallel tension range of 12 mm. For each **Zr6** proportion in the polymer, the number of samples was between 8 and 12. Typical stress-strain diagrams for undoped and doped polystyrene are shown in Figure 86. An elongation at break in the region of a few percent is typical for brittle polymers, such as polystyrene.

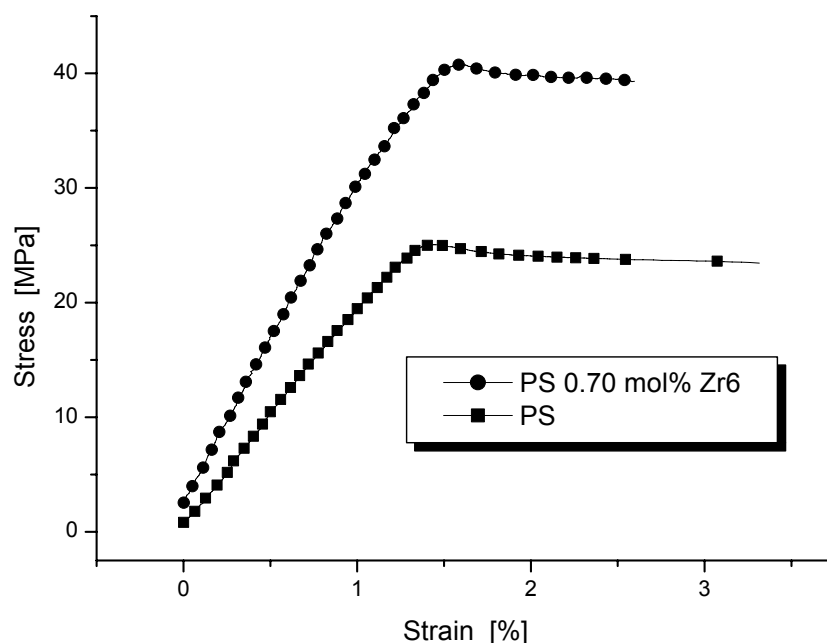


**Figure 86:** Stress-strain curves for polystyrene and a sample doped with 0.70 mol% of **Zr6** cluster

A higher modulus of elasticity was observed in the cluster cross-linked samples. Moreover, the tensile strength, which is defined by the maximum stress on the engineering stress-strain curve, increased. The results of the measurements are summarized in Figure 87 and Table 67.

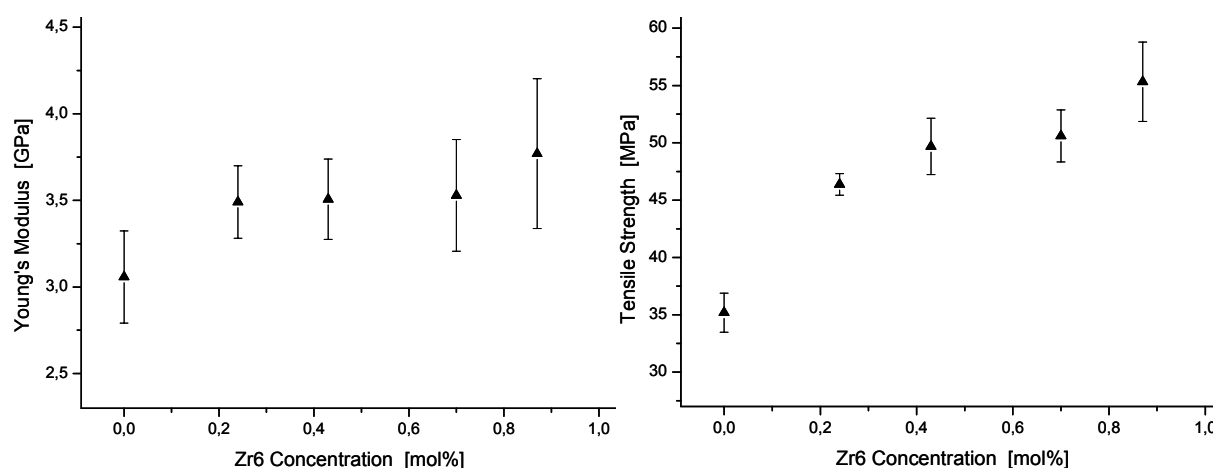


**Figure 87:** Young's moduli (left) and tensile strengths (right) of PS and **Zr6** doped PS

**Table 67:** Mechanical data of undoped and doped polystyrene samples obtained from tensile tests

| Zr6-Conc. [mol%] | Young's Modulus [GPa] | Tensile Strength [MPa] |
|------------------|-----------------------|------------------------|
| 0                | 3.06 ± 0.27           | 35.1 ± 1.7             |
| 0.24             | 3.49 ± 0.21           | 46.4 ± 0.9             |
| 0.43             | 3.51 ± 0.23           | 49.7 ± 2.5             |
| 0.70             | 3.53 ± 0.32           | 50.6 ± 2.3             |
| 0.87             | 3.77 ± 0.43           | 55.3 ± 3.5             |

Cross-linking changes and generally improves the mechanical properties, where improvements are most significant above the glass transition temperature [160]. The Young's modulus in the tensile tests was determined far below glass transition temperature to 3 GPa for undoped and about 3.5 to 3.8 GPa for doped polystyrene samples. The changes in the moduli with increasing cluster proportion were not pronounced. This was in accordance with results for thermosetting resins in the glassy state, where the modulus did not change significantly with the degree of cross-linking [161].

The improvements in the tensile strengths from 35 MPa for neat PS to 55 MPa for the sample doped with 0.87 mol% of **Zr6** were clearer and seemed to show a correlation with the cluster proportion. This finding was attributed to a degree of cross-linking which was low enough to still exhibit plastic yielding in tension [162] (see Figure 86) because highly cross-linked thermosets

usually have a much lower fracture toughness and exhibit brittle failure in tension. For example, Sundell et al. prepared polystyrene samples cross-linked with various cross-linking agents, such as divinylbenzene, and found an increase in the stress at break at 1–5 % cross-linking, followed by a rapid decrease due to brittle failure [139].

It is necessary to mention that neat polystyrene can exhibit tensile strengths up to 65 MPa. However, this property strongly depends on a post-treatment of the polymer, i.e. on the processing parameters, but also on the tacticity and, to a certain extent, on the molecular weights and polydispersities [140]. In addition, the testing conditions which were applied in this work did not follow the ISO norm in every respect because the traverse speed was half the velocity as set by the ISO norm.

## COMPRESSION TESTS

### Compressive behaviour of glassy polymers

The macroscopic response to deformation of glassy polymers in tension appears brittle below the glass transition temperature. Polystyrene is such a material, which fractures at a few percent of strain under most loading conditions. When performing tensile tests, necking and crack-like defects appear in a tensile bar already in the apparent elastic region [163, 164]. The predominant fracture mechanism in polymeric materials is called crazing. Crazes are planar defects, where two faces of the craze are bridged by thin fibrils. By increasing stress, the bridged crazes open up, and macroscopic fracture occurs because of the failure of these fibrils [165].

The intrinsic deformation behaviour can be determined in tests where localisation phenomena like necking and crazing are absent. To this end, true stress-strain curves are recorded in uniaxial compression [166] or in uniaxial tension using a video-controlled tensile test [167]. In this work, uniaxial compression tests were performed to learn more about the post-yield behaviour of the doped polystyrene samples.

The main differences in the stress-strain curves for glassy polymers in tensile tests and compression tests, respectively, are shown in Figure 88 for polystyrene as the example. Under tension, the crazing mechanism causes brittle failure, whereas in compression the specimen undergoes considerable plastic deformation. Three main types of compressive stress-strain diagrams are observed in glassy polymers usually [168]. Polystyrene belongs to type 1, which is characterized by a distinct peak on the stress-strain curve. Immediately after the yield point, the stress decreases with increasing deformation. This effect is referred to intrinsic strain softening [169], which induces a localisation of strain. At large deformations, the softening effect is saturated, and the true stress starts to rise again with increasing deformation. This strain

hardening effect is generally interpreted as a rubber elastic contribution by the molecularly entangled network [170]. Compressive deformation manifests itself by the development of shear bands at the yield point. As a consequence, the local deformation in polystyrene is quite high, ranging from 65 % to 130 % [171].

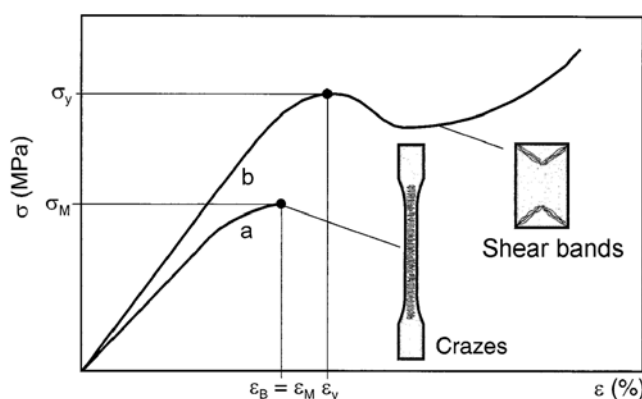


**Figure 88:** Deformation behaviour of polystyrene in tensile test (a) and compression test (b) [130]

Compression tests of undoped and doped PS samples were performed at room temperature on cylindrical specimens at a strain rate of  $0.013 \text{ s}^{-1}$ . The friction between the samples and the steel plates of the testing machine was reduced by placing a PTFE tape between sample and steel plate and by the use of a dish-washing detergent. Buckling and bulging during the tests was thus avoided. Figure 89 shows representative true stress – true strain diagrams for undoped polystyrene and polystyrene doped with 0.70 mol% of **Zr6** cluster as examples.

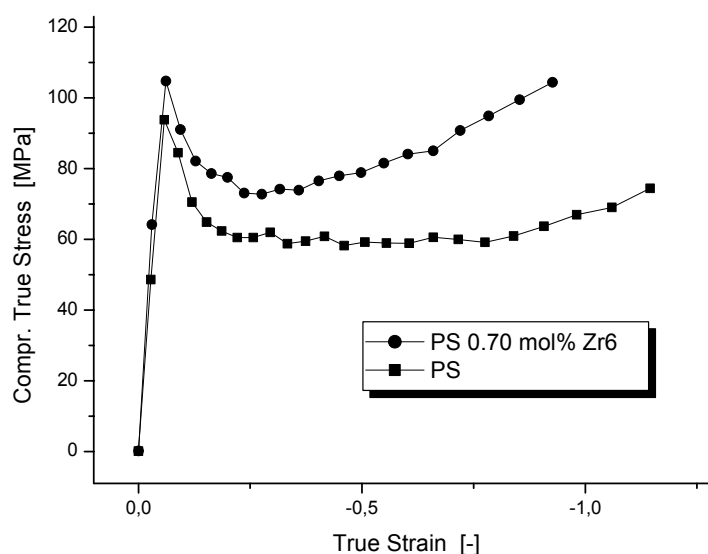


**Figure 89:** Compressive behaviour of an undoped and a doped polystyrene sample at room temperature at a strain rate of  $0.013 \text{ s}^{-1}$

The yield points were determined from the maxima of the true stress – true strain curves. Since there was no crazing mechanism in these tests, the yield strengths were found to be much higher when compared to tensile tests. Values obtained from compression tests and tensile strengths determined by tensile tests are compared in Table 68.

**Table 68:** Comparison of material strengths obtained from tensile tests and compression tests

| Zr6 Conc. [mol%] | Tensile Strength [MPa] | Yield Point [MPa] |
|------------------|------------------------|-------------------|
| 0                | 35                     | 93                |
| 0.24             | 46                     | 99                |
| 0.43             | 50                     | 100               |
| 0.70             | 51                     | 101               |
| 0.87             | 55                     | 99                |

The values of the compression yield points increased slightly upon doping the PS with **Zr6**. However, small influences of the cluster proportion and thus of crosslinking were observed. As a matter of fact, there have been many attempts to link the yield strengths of polymers with other properties such as free volume, tensile modulus, radius of the polymer unit, and the degree of crosslinking in thermosets [172-175]. By linking the yield strengths of the cluster doped polymers with properties such as density and glass transition temperature, inconsistent correlations were observed, not following a clear trend.

## Strain Hardening

An extension of Hooke's law for the case of large deformations is the neo-Hookean description. When this description can be applied to a system, from the strain energy function, which was proposed by Mooney for rubber-elastic materials [176], it can be derived that the true stress is proportional to  $\lambda^2 - \lambda^{-1}$ , where  $\lambda = 1 + \varepsilon$ .

The strain hardening moduli were determined from the compression tests at large strains. It is shown in Figure 90 that the assumption of a neo-Hookean solid was confirmed and true stress was indeed linear with  $\lambda^2 - \lambda^{-1}$  at large deformations. The validity of a neo-Hookean behaviour in crosslinked polystyrene-type systems was also verified with numerical simulations [147].

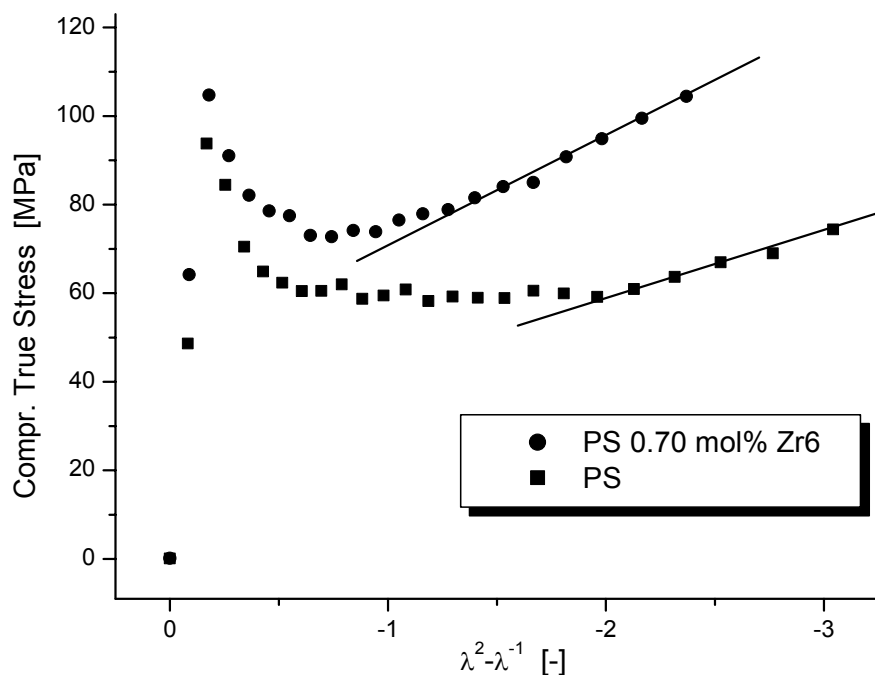


**Figure 90:** Validity of a neo-Hookean behaviour in an undoped and a doped PS sample

Another proof for the validity of a neo-Hookean behaviour was given from the fact that, if during a deformation the volume of the sample was conserved, i.e. if the product of cross-sectional area and length of a specimen remains constant, one may relate true stress and engineering stress by

$$\sigma_T = \sigma(1 + \varepsilon)$$

In Figure 91, the excellent agreement with theory is shown for neat polystyrene and a sample doped with 0.70 mol% of **Zr6** cluster.

Since crazing and necking were absent in compression tests, the post-yield behaviours of the undoped and the doped polystyrene samples (Figure 89) were strongly influenced by a change in the network density. For increasing network densities, i.e. increasing cluster proportions, the strain hardening moduli rose, whereas the yield strengths remained almost unaffected. In Figure 92 the linear relationship between the cluster proportion and the strain hardening moduli ( $G_R$ ) is shown.

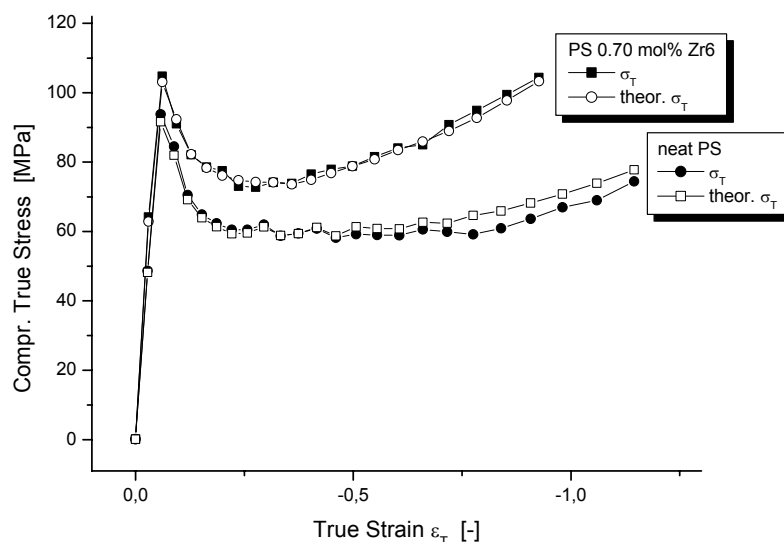


**Figure 91:** A neo-Hookean behaviour shows good agreement of measured and calculated true stress

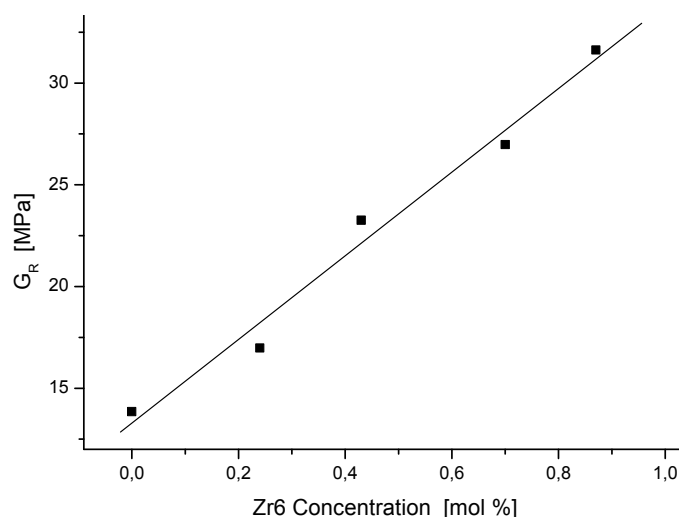


**Figure 92:** Strain hardening modulus,  $G_R$ , versus cluster concentration

Combining the results from DMA measurements, viz the calculation of the network densities from the rubber plateau moduli, with the results from compression tests, revealed a non-linear relationship between the strain hardening moduli and network densities,  $v_e$  (Figure 93; the curve is drawn to guide the eye). It was shown in section 5.2.8 that there was no linear relation between network densities and the **Zr6** concentration in the doped polystyrene samples. However, the strain hardening moduli and the cluster proportions revealed a linear relation. Therefore, the curve strain hardening modulus versus network density exhibited non-linearity.

It is necessary to point out here that the rubber plateau modulus was determined in the melt, i.e. above the glass transition temperature. In this region the polymer chains have full main-chain

segmental mobility, which was thermally induced. Thus, the dynamic response was fully dependent on the molecular network. The strain hardening moduli, on the other hand, were determined below the glass transition temperature, i.e. in the glassy state. Nevertheless, a correlation between these two values was given because the polymer chains also obtained a certain degree of mobility during plastic deformation, in this case stress-induced instead of temperature-induced. This mobility certainly activated a contribution of the molecular network [177]. Data for the network densities and the strain hardening moduli of undoped and doped polystyrene samples are given in Table 69.

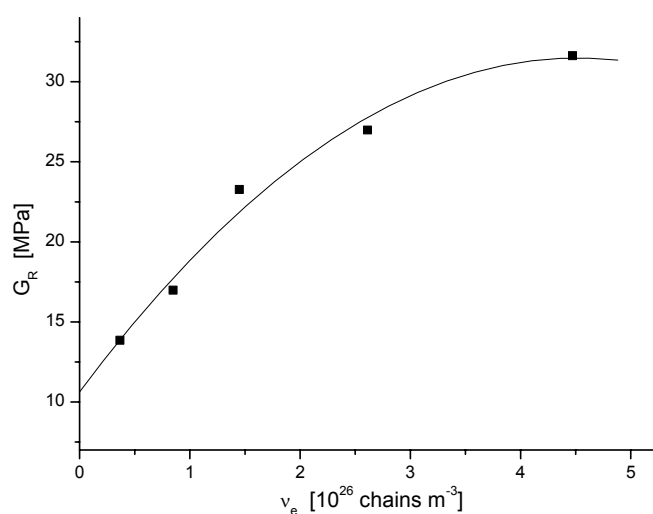


**Figure 93:** Strain hardening modulus ( $G_R$ ) versus the network density ( $v_e$ ) for undoped and doped PS

**Table 69:** Values of network densities and strain hardening moduli for cross-linked polystyrene samples

| Zr6-Conc. [mol%] | $v_e$ [ $10^{26}$ chains $m^{-3}$ ] | $G_R$ [MPa] |
|------------------|-------------------------------------|-------------|
| 0                | 0.37                                | 13.9        |
| 0.24             | 0.85                                | 17.0        |
| 0.43             | 1.45                                | 23.3        |
| 0.70             | 2.61                                | 27.0        |
| 0.87             | 4.47                                | 31.6        |

In conclusion, a neo-Hookean relation could be used to describe the strain hardening behaviour of the cluster cross-linked polystyrene samples. The strain hardening modulus was dependent on the network density. Whereas in rubber-elastic polymers this relation is linear, irrespective of the nature of the polymer network, i.e. physical entanglements or chemical cross-links [147], minor discrepancies were observed in the cluster doped systems.



### 5.2.10 Microhardness

Tensile tests were traditionally used to determine the properties of materials. If a tensile test is stopped before break of the specimen, it might, in principle, produce a curve that is similar to that in Figure 94. The initial linear portion of the curve indicates elastic deformation and the increase in curvature indicates plastic deformation. Once a preset maximum load was achieved, the tensile test machine can be programmed to unload and the material will retract. This is why one has a second linear portion. The curve will not retract back to the origin and what remains is the residual plastic strain.

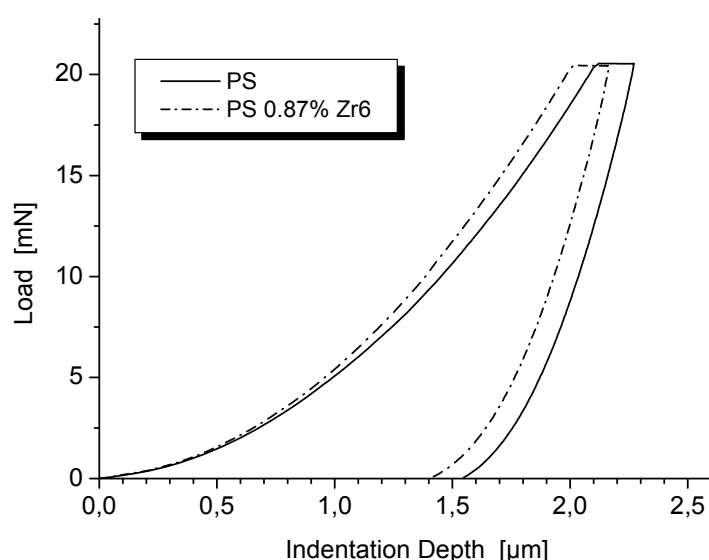


**Figure 94:** Typical loading-unloading curves for undoped and doped polystyrene recorded during microindentation

Nanoindentation is a method that can be used to determine properties of specimens at a length scale appropriate for nanomaterials. Instead of pulling the specimen, a diamond tip (e.g. Berkovich-type) is used for the indentations. The test consists of loading to a maximum value,  $F_{max}$ , and unloading to zero. Furthermore, a hold period is most commonly programmed. Depths of the indentation are recorded and through these data, indentation hardness,  $H$ , and indentation Young's modulus,  $E$ , can be determined.

Microhardness measurements of undoped and doped polystyrene samples were conducted at room temperature on lapped samples. The maximum load was 20 mN, and after 30 s hold time at maximum load the force was released with 100 nm/s. Typical loading-unloading curves are

shown in Figure 94. Young's moduli from indentation test ( $E_{IT}$ ) and hardnesses ( $H_{IT}$ ) were determined. The results are shown in Figure 95 and are summarized in Table 70.

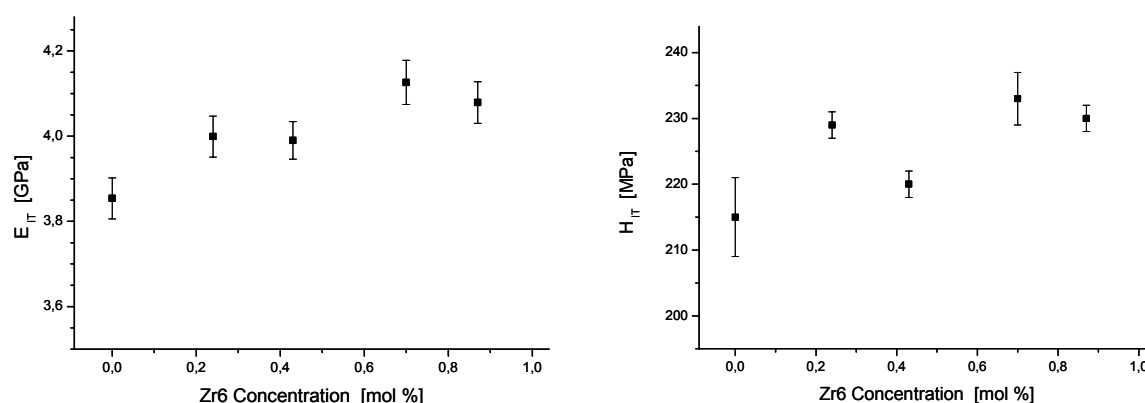


**Figure 95:** Indentation Young's modulus (left) and hardness (right) for PS and cluster doped samples

**Table 70:** Young's moduli and hardnesses for undoped and doped polystyrene samples

| Zr6 Conc. [mol%] | $E_{IT}$ [GPa]    | $H_{IT}$ [MPa] | Rel. $E_{IT}$ [-] | Rel. $H_{IT}$ [-] |
|------------------|-------------------|----------------|-------------------|-------------------|
| 0                | $3.854 \pm 0.048$ | $215 \pm 6$    | 1                 | 1                 |
| 0.24             | $3.999 \pm 0.048$ | $229 \pm 2$    | 1.038             | 1.065             |
| 0.43             | $3.990 \pm 0.044$ | $220 \pm 2$    | 1.035             | 1.023             |
| 0.70             | $4.126 \pm 0.052$ | $233 \pm 4$    | 1.071             | 1.084             |
| 0.87             | $4.079 \pm 0.049$ | $230 \pm 2$    | 1.058             | 1.070             |

By doping with different amounts of the **Zr6** cluster, the elastic modulus increased when compared to pure polystyrene. However, absolute values for the moduli were found to be much higher when compared to values determined by other methods, such as tensile tests or dynamic mechanical analyses. Lucas et al. made similar observations for polytetrafluoroethylene [178]. Whereas values of 0.4 GPa and 0.5 GPa were observed by tensile tests and by DMA, respectively, the modulus of elasticity was determined to 1.2 GPa with nanoindentation. A similar, but less dramatic trend for the cluster doped polystyrene samples can be seen from Figure 96. Compared to dynamic mechanical analysis, which showed the lowest values obtained, the moduli from microindentation were increased by about 20 %. In contrast, values obtained from tensile tests are higher by about 5 % only when compared to dynamic moduli.

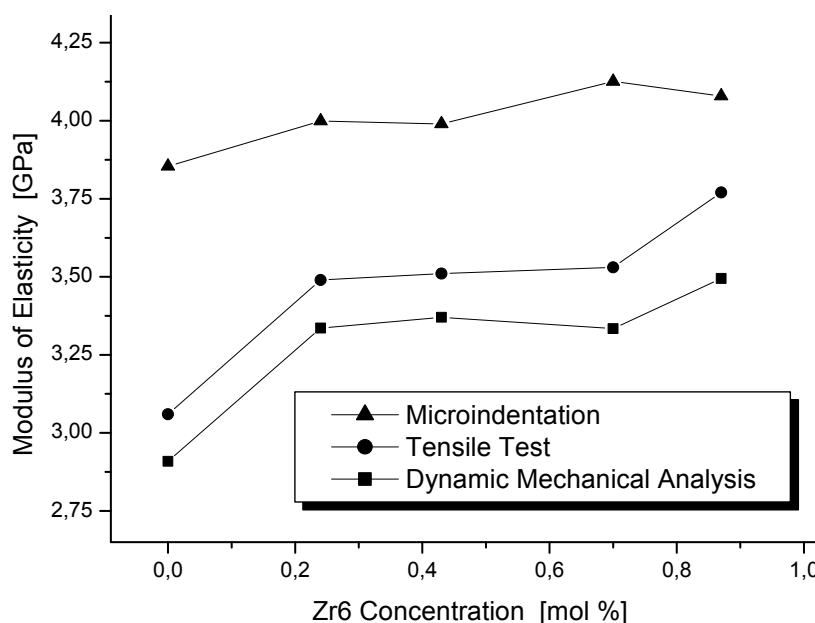


**Figure 96:** Comparison of the moduli of elasticity of cluster cross-linked PS samples determined by different methods

In addition to  $E_{IT}$ , the hardnesses of the samples were determined. These improved from 215 MPa for pure polystyrene to 230 MPa for they doped samples. Solely the sample containing 0.43 mol% of **Zr6** had only a hardness of 220 MPa and appeared to be an outlier. Measurements of  $E_{IT}$  and  $H_{IT}$  of pure polystyrene were in fairly good agreement with literature values. For instance, Maner et al. determined values for moduli of elasticity of pure polystyrene at an indentation depth of 1  $\mu\text{m}$  to 4 GPa and 218 MPa, respectively [179].

The changes in the properties derived from microindentation were not very large when PS was doped with the **Zr6** cluster. Figure 97 shows relative moduli and hardnesses, respectively. Improvements were little and seemed to be independent from the cluster proportion. It was assumed that either a saturation level in the cluster proportion was already reached or that more cluster was required to improve hardness values more significantly.

For comparison, Huang et al. observed a reduced hardness of epoxy thermosets when POSS were incorporated into the polymer matrix [107]. The authors cross-linked polyimide epoxides with two different types of octafunctional POSS. By increasing the amount of inorganic cross-linking agent gradually up to 45 wt%, the hardness decreased from 470 MPa for the neat polyimide matrix to 340 MPa for the sample doped with 45 wt% POSS.

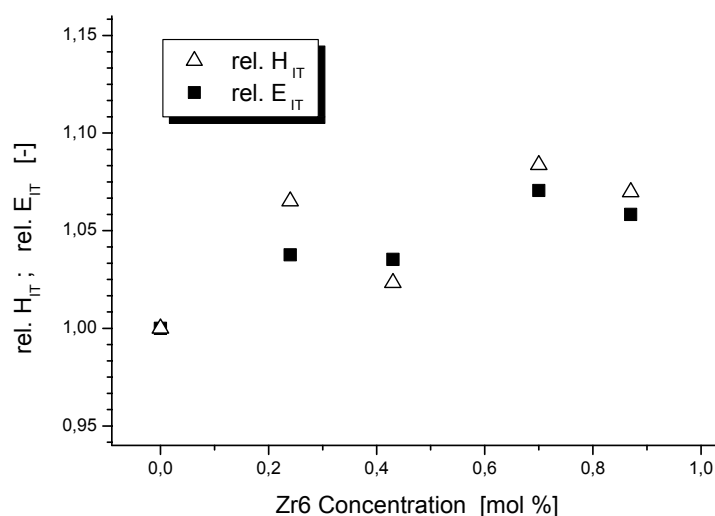


**Figure 97:** Relative hardnesses and moduli of elasticity determined from microindentation

In addition to determining moduli and hardnesses from nanoindentation, this technique was also a powerful tool for measuring the gradients of properties in a material. Gradients in properties in the polystyrene samples were possible because the preparation of the polymers was carried out in Schlenk tubes under stirring. After gelation, the stirring was hindered which probably resulted in a heterogeneous polymer caused by a gradient in temperature. Therefore, a plate was cut out of a cylindrical polymer sample containing 0.43 mol% of **Zr6** cluster. It was shown before that indentation properties did not change significantly by doping with **Zr6** cluster. However, residual monomer might be incorporated into the network due to uncomplete polymerization, acting as a softener to the material and thus changing both properties, elasticity and hardness. The measurements were performed in the z-dimension as well as in the x,y-dimension. For each point marked in Figure 98 the hardness as well as the modulus of elasticity was determined, the observations are summarized in Figure 99.

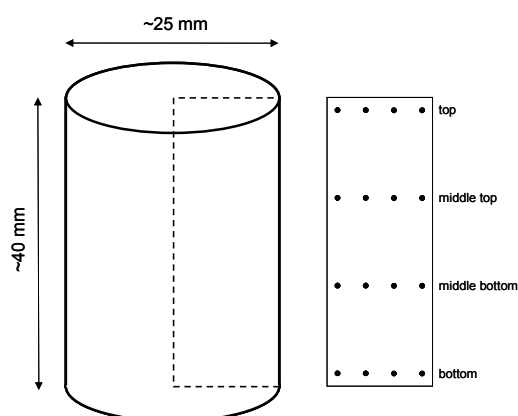


**Figure 98:** A plate cut out of a cylindrical sample for indentation mapping

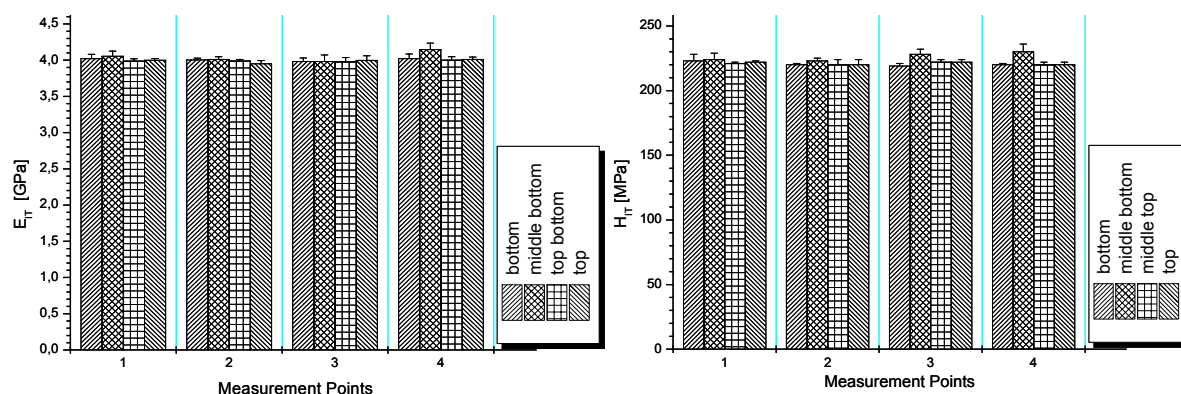


**Figure 99:** Mapping of a PS sample doped with 0.43 mol% **Zr6**; indentation modulus of elasticity (left) and hardness (right)

The results in modulus of elasticity as well as in hardness showed a uniform distribution of these properties in both the z- and the x,y-dimension. Thus, a gradient of properties in the polymers was ruled out. Furthermore, measurements were carried out for a neat polystyrene sample. No indication in the indentation measurements was observed for areas with incorporated monomer.

### 5.2.11 Small Angle X-Ray Scattering

Small angle X-ray scattering (SAXS) measurements of the **Zr6** doped polymer samples were performed to further characterize the distribution of the clusters in the final polymers. Since SAXS is sensitive to the differences in the electron density, the organic part of the hybrid material could be distinguished from the inorganic counterpart. After background correction from air and parasitic scattering, the scattering data were normalized at  $q = 7 \text{ nm}^{-1}$  (Figure 100).

The scattering intensity clearly depended on the cluster proportion and there was only one maximum in the scattering curves at about  $q = 3.7 \text{ nm}^{-1}$ , indicating one characteristic cluster - cluster distance. This was in agreement with other hybrid polymers, such as PMMA cross-linked with zirconium oxo clusters [119]. When using other transition metal oxo clusters, an additional distribution next to random was observed and ascribed to aggregation of clusters, i.e. a 'clustering of clusters' [87, 180].

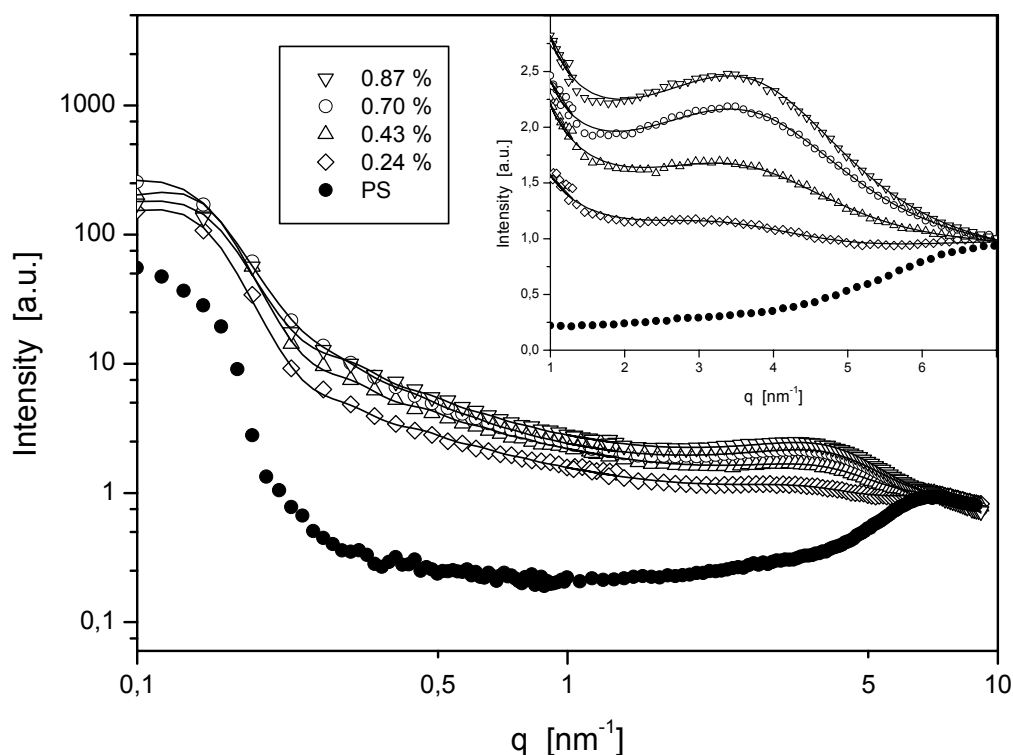


**Figure 100:** SAXS curves of PS doped with the **Zr6** cluster after background correction and normalization

Two ways were applied to interpret the scattering data:

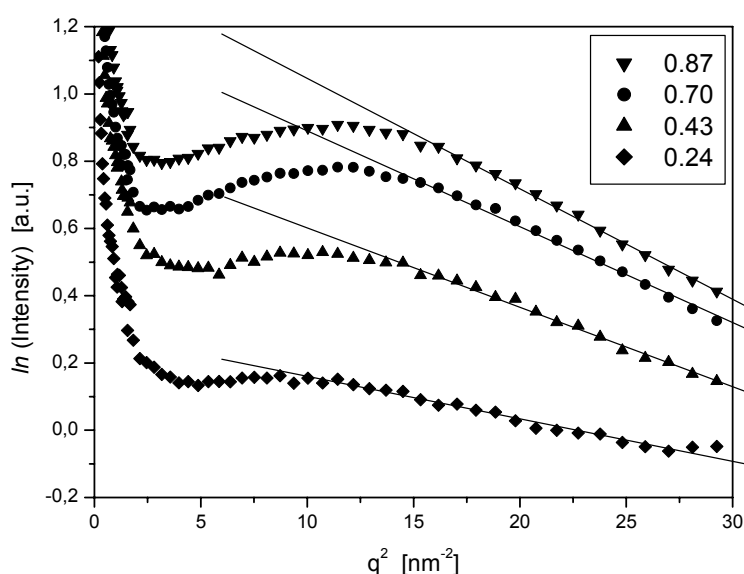
The first and simpler approach was to determine the characteristic cluster – cluster distance from the maxima of the scattering curves according to  $d = (2\pi/q)$ . Surprisingly, the distance was almost constant in all of the samples, solely the sample with the lowest cluster concentration showed a slightly larger distance (Table 71). However, this was in contradiction to the distances obtained from model calculations with the assumptions that the clusters were homogeneously and randomly distributed in the final hybrid materials and that the polymerization conversion was 100 %. The random distance was calculated as the edge length of a cube occupied by the cluster in a certain polymer volume, which was in turn corrected to the specific gravity of the material. The smaller values observed in the measurements when compared to theoretical calculations indicated that the clusters were not randomly distributed but showed an agglomeration, although a second maximum in the scattering curves is missing, i.e. ‘clusters of the clusters’ did not reveal a characteristic distance.

Whereas no significant shift in the scattering peak was observed with varying cluster proportions, the peak width decreased (full-width at half-maximum). This was attributed to either an increase in the size of the aggregates according to the Scherrer formula [181], or to a better pronounced short-range order. Though both cases were possible, the second interpretation seemed to be more probable (see the second approach below).

**Table 71:** Cluster - cluster distances calculated theoretically and determined from the maxima of the scattering curves

| Zr6 Concentration<br>[mol%] | Cluster distance calc.<br>[nm] | Cluster distance from Peak<br>[nm] |
|-----------------------------|--------------------------------|------------------------------------|
| 0                           | 0                              | -                                  |
| 0.24                        | 4.13                           | 1.835                              |
| 0.43                        | 3.41                           | 1.713                              |
| 0.70                        | 2.93                           | 1.710                              |
| 0.87                        | 2.73                           | 1.706                              |

Figure 101 shows Guinier plots of the scattering data. From the slope of the scattering curves towards low  $q$ -values (shown as solid lines), the radii of gyration,  $R_g$ , were found to be very similar in all of the samples.

**Figure 101:** Guinier plots of **Zr6** doped polystyrene

In the second, more detailed interpretation of the SAXS data, the scattering curves were fitted with the model developed by Beaucage [182], which describes scattering from complex systems containing multiple levels of structural features, such as polymers. The applicability of this model to describe two structural levels in cluster cross-linked polymers had already been reported in the literature for a related system [104]. The fit-curves obtained from this model are shown as solid lines in Figure 100 together with the scattering data. The parameters obtained from the fits are summarized in Table 72.

**Table 72:** Fitting parameters of SAXS profiles for the **Zr6** doped polystyrene samples

| Zr6<br>Concentration<br>[mol%] | $R_{g1}$<br>[nm] | $P_1$ | $k_1$ | $d_1$<br>[nm] | $R_{g2}$<br>[nm] | $P_2$ | $k_2$ | $d_2$<br>[nm] |
|--------------------------------|------------------|-------|-------|---------------|------------------|-------|-------|---------------|
| 0.24                           | 16.4             | 1.33  | 3.07  | 39.5          | 0.41             | 4.00  | 1.32  | 1.38          |
| 0.43                           | 16.1             | 1.45  | 3.65  | 38.7          | 0.40             | 4.00  | 1.56  | 1.32          |
| 0.70                           | 15.5             | 1.89  | 2.23  | 41.0          | 0.40             | 4.00  | 1.67  | 1.29          |
| 0.87                           | 16.1             | 1.70  | 2.85  | 38.1          | 0.40             | 4.00  | 1.73  | 1.29          |

The power law exponent  $P_1$  described the decrease of the scattering intensity due to large structures with a radius of gyration  $R_{g1}$ . The second power law exponent  $P_2$  and the gyration radius  $R_{g2}$  described the morphology of the small structures. As  $P_2$  was found to be 4 towards high  $q$ -values as described by Porod's law [183], which indicated a smooth surface with a sharp interface, this parameter was set to 4 and kept constant during the fit. This procedure was also chosen in the literature [104].

The value of the power law exponent  $P_1$  of 1.3 - 1.9 indicated that the large structures were mass fractals where the fractal dimensions increased with increasing cluster proportion. That distribution was mainly attributed to the polymer matrix because the slope of neat PS was found to be in a comparable range as it was for the cluster doped samples. The second power law exponent  $P_2 = 4$  indicated the presence of subunits within the first, larger distribution. The radii of gyration,  $R_{g2}$ , of the subunits remained constant at 0.4 nm and, assuming that the subunits were spherical, corresponded to diameters of 1.06 nm. This was in good agreement with the size of the **Zr6** core plus the oxygen shell as determined from single crystal X-ray measurements. The average correlation distances  $d_2$  were a measure for the cluster - cluster distances and were found to be larger than the radii of the subunits. As already stated, these distances were much smaller when compared to theoretical values assuming a random distribution.

A further parameter obtained from the fits was the packing factor  $k$  which is proportional to the number of coherently scattering objects in a certain volume. The packing factor  $k_2$  of the subunits increased from 2.0 to 2.7 with increasing cluster proportion, showing that the clusters showed better short range order with increasing concentration because of denser packing.

Summarizing the results from SAXS measurements, it was obvious that the **Zr6** clusters were not randomly distributed but showed an aggregation in the polymer matrix. When following interpretation 1, viz. cluster - cluster distances determined from the maxima of the peaks in the scattering curves, the distance was constant at about 1.7 nm and did not change with increasing cluster proportion. Taking the sample doped with 0.43 mol% cluster as an example, the distance



was only half the theoretical value, in the sample doped with 0.87 mol% this ratio was reduced, but the distance was still 1 nm smaller than expected. Nevertheless, it could be ruled out that the formation of a dimeric structure, a  $\text{Zr}_{12}$  cluster, was responsible for the low distances. Judging from single crystal measurements, this would have resulted in a distance smaller than 0.9 nm. Interpretation 2 from the Beaucage model gave a more detailed picture: The **Zr6** clusters had distances of about 1.3 nm. Again, this value did not change when cluster concentration was increased. The radii of gyration remained constant at 0.4 nm which corresponded to a size of the subunits of 1.06 nm. The packing factor increased with higher cluster proportions and indicated a better short-range order of the clusters because of denser packing. The first distribution in the fits was related to both the polymer and the size of the cluster aggregates.

### 5.2.12 Transmission Electron Microscopy

The observations in the SAXS investigations required further confirmation. Therefore, samples with the highest and the lowest **Zr6** concentrations, 0.24 and 0.87 mol%, respectively, were investigated with transmission electron microscopy (TEM). Samples were cut from polymer pieces and images were taken at the edges of the slices to allow best visibility of the small objects. Figure 102 shows an STEM image of the sample doped with 0.24 mol% of **Zr6** cluster. The light spots in the image indeed showed a clustering of the clusters as it was indicated by SAXS. The aggregates differed in their size and were randomly distributed. A quantitative determination of the sizes of aggregates was not possible because only a few images were recorded and the aggregates differed very much in size, showing a ramified structure rather than a spherical.

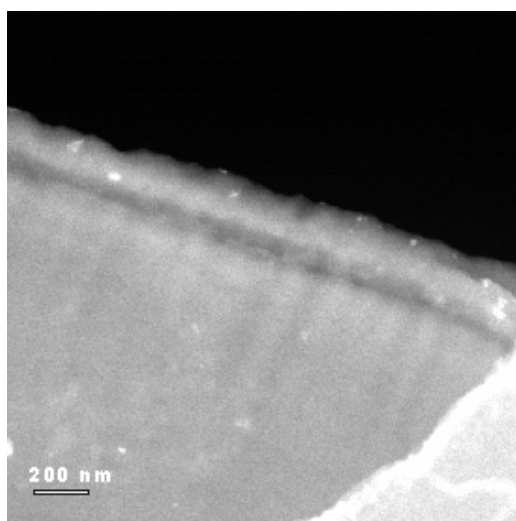


**Figure 102:** STEM image of PS doped with 0.24 mol% of **Zr6**

In Figure 103, TEM images of the 0.24 mol% sample are shown. The black spot in the left image shows a typical aggregate with about 20 nm in diameter. A smaller aggregate is shown in the right picture. Next to the big aggregates, black spots were apparent in the images, originating from non-aggregated clusters which were randomly distributed. A determination of the distances between the black spots was not possible because of multiple layers caused by the thickness of the slides.

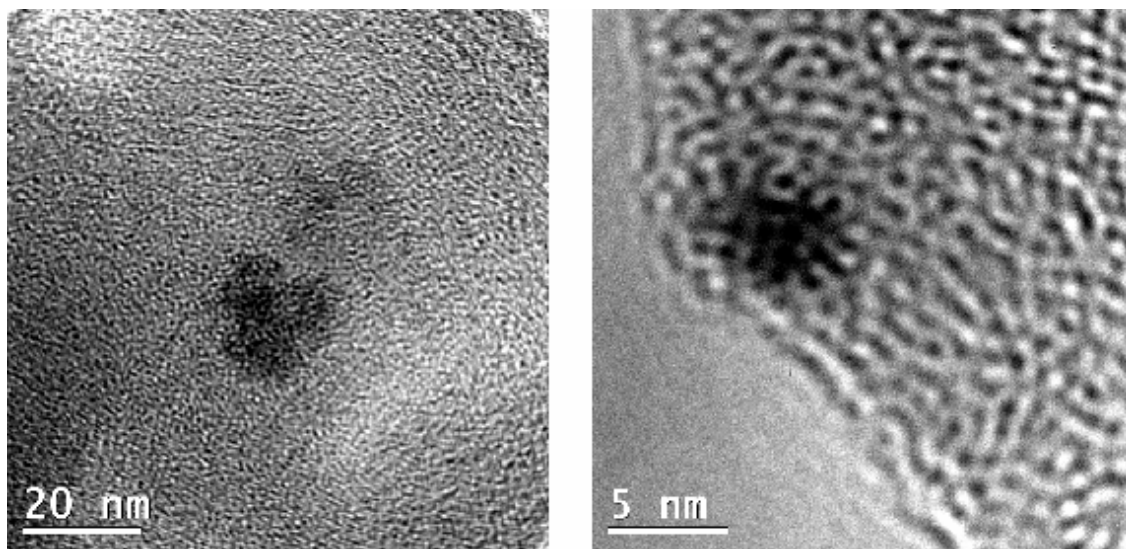


**Figure 103:** TEM images of PS doped with 0.24 mol% of **Zr6**

For the sample doped with 0.87 mol% of **Zr6**, the same situation was observed: The cluster formed aggregates and these aggregates were randomly distributed. Figure 104 shows STEM images in different magnifications. In the top left image the aggregates were identified as bright spots in the polymer matrix. The sizes of the aggregates were typically found in a range of 50 - 100 nm. A higher degree of aggregation was expected when compared to the sample doped with 0.24 mol% of **Zr6** because of the higher cluster concentration. However, general conclusions could not be drawn based on the few images recorded.

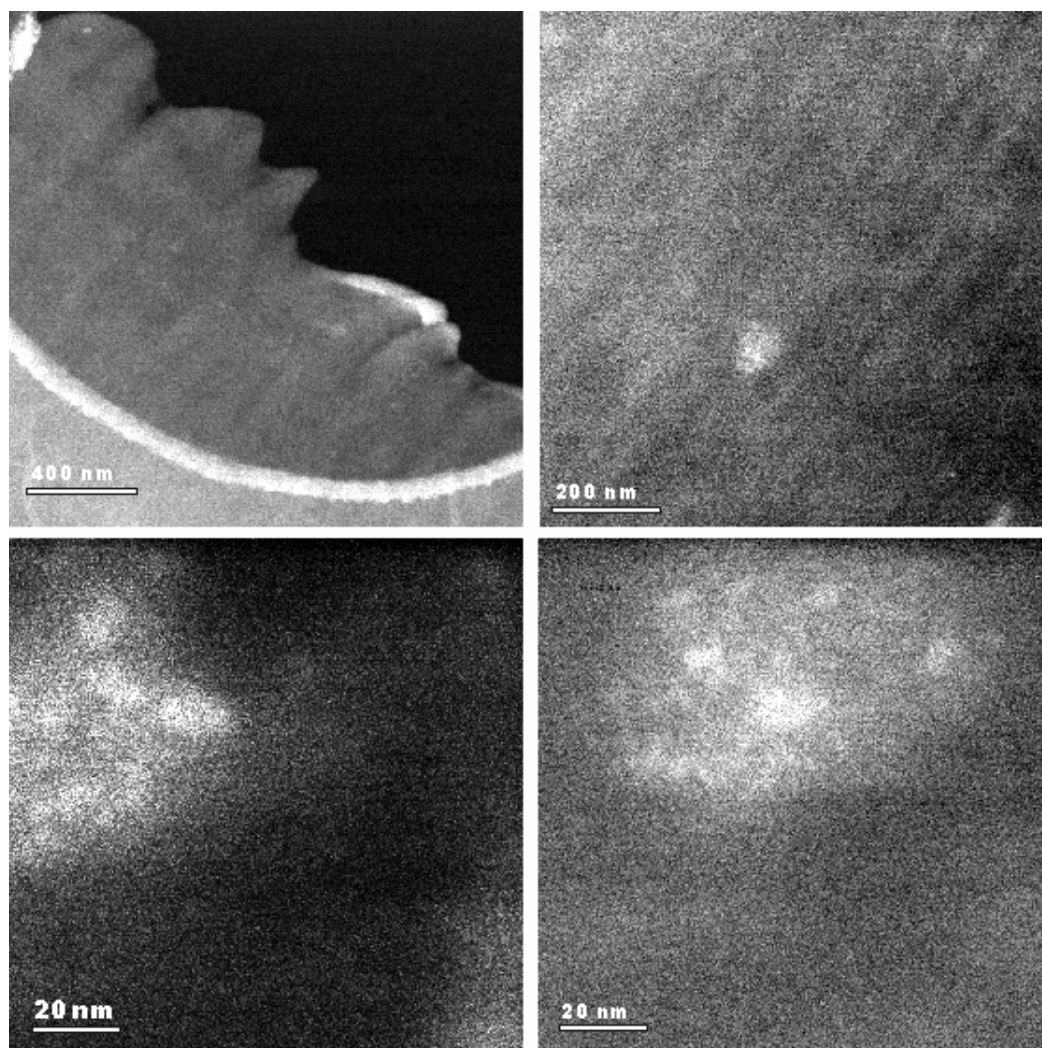


**Figure 104:** STEM images of polystyrene doped with 0.87 mol% of **Zr6** cluster

In conclusion, the TEM and STEM pictures confirmed the results from SAXS measurements. The **Zr6** clusters were aggregated to some extent to 'clusters of clusters', but also showed a random distribution. The aggregates were randomly distributed in the polymer matrix and had no defined shape, i.e. spherical aggregates were found as well as ramified structures. The sizes varied in the range of 5 nm up to about 100 nm. Bigger units than ~300 nm were not observed and also not expected because the samples were macroscopically transparent.

### 5.2.13 Conclusions

The  $\text{Zr}_6\text{O}_4(\text{OH})_4(\text{OMc})_{12}$  doped polystyrene samples were prepared by a step-wise polymerization with lauroyl peroxide as the initiator. In a first step, the optimum polymerization conditions for small amounts of monomers were investigated. Initiation of a solution of 0.5 mol% of **Zr6** with 0.05 wt% of LPO at 80 °C for 5 minutes, quenching to 0 °C and polymerization at 60 °C for one day and at 120 °C for another day were the optimum conditions with respect to the thermal properties of the final materials. The onset temperature of thermal decomposition was shifted from 340 °C for neat PS to 390 °C for the sample doped with 0.5 mol% of **Zr6**. At the same time, the glass transition temperature was increased from 104 °C to 121 °C. SEC measurements were not possible because the **Zr6** units in the hybrid polymers were not degraded by acetyl acetone.

For mechanical and thermomechanical testing, bulk samples on a ~30 grams scale were prepared with different concentrations of the **Zr6** cluster, ranging from 0.24 mol% to 0.87 mol%. To this end, the step-wise polymerization process was somewhat modified: The initiation time at 80 °C was reduced to 2.5 minutes and an additional step at 80 °C for 24 hours was introduced. As a reference, an undoped PS sample was polymerized under the same conditions.

The onset temperature of thermal decomposition shifted from 320 °C for neat PS to 350 °C for the sample cross-linked with 0.87 mol% of **Zr6**. In DSC and MDSC measurements, no signals apart from exothermic combustion were observed, and the glass transition temperatures increased when compared to neat PS.

Swelling experiments confirmed that the hybrid polymers were indeed cross-linked by the **Zr6** cluster. Cross-linking was expressed as the degree of swelling in ethyl acetate, i.e. the percentage solvent uptake, which decreased from 135 % for the sample doped with 0.24 mol% of **Zr6** to 73 % for the sample doped with 0.87 mol% of **Zr6**.

The thermal expansion coefficients were determined by thermal mechanical analysis. No differences among the samples with different cluster concentrations were observed below the glass transition temperatures, where  $\alpha$  was found at about 70 ppm/°C. Above the glass transition temperatures, the expansion coefficients decreased gradually with increasing cluster concentration from 213 ppm/°C for neat PS to 190 ppm/°C for the sample doped with 0.87 mol% of **Zr6**.

Dynamic moduli were determined by dynamic mechanical analysis. The moduli at room temperature were slightly increased from 2.9 GPa for PS to 3.3 - 3.5 GPa for the hybrid polymers. Above the glass transition temperatures, which were found to increase from 100 °C for PS to 110 °C for the hybrid polymers in this technique, the effect was much more pronounced: Whereas no plateau modulus for neat PS was observed, the plateau moduli increased gradually from 1.5 GPa to 7.8 GPa for the samples doped with 0.24 mol% and

0.87 mol% of **Zr6**, respectively. These values were used to calculate network parameters according to the theory of rubber elasticity. The network densities increased with increasing cluster concentration and, as a consequence, the entanglement molecular weights decreased.

The mechanical properties of the **Zr6** doped hybrid materials were investigated in tension tests. The Young's moduli at room temperature increased from 3 GPa for neat PS to 3.8 GPa for the sample doped with 0.87 mol% of **Zr6**; and the tensile strengths increased from 35 MPa to 55 MPa.

Compression tests were performed to characterize the post-yield behaviour of the hybrid polymers. The strain hardening moduli were determined at large deformations and increased linearly with increasing cluster concentration from 14 MPa for neat PS to 32 MPa for the sample doped with 0.87 mol% of **Zr6**. Furthermore, a clear correlation between the network densities, as calculated from dynamic moduli in the rubbery state, and the strain hardening moduli, as determined in the glassy state, was observed.

Microhardness measurements revealed no significant changes of indentation Young's moduli and of indentation hardnesses when PS was doped with **Zr6**. A mapping of an undoped and a doped polymer sample revealed homogeneous properties in all dimensions, proving that polymerization was complete through the bulk of the materials and no monomer was incorporated in the matrix.

Small angle X-ray scattering measurements were performed to characterize the distribution of the **Zr6** clusters in the polymer. The scattering intensities clearly depended on the cluster proportions. Cluster - cluster distances, determined from the maxima of the scattering curves, were at about 1.7 nm for different concentrations of **Zr6**. This was in contradiction to values calculated theoretically when assuming a random distribution of the clusters in the polymer matrix. Together with a more detailed interpretation of the SAXS data using the model developed by Beaucage, a strong indication for aggregation of the clusters, i.e. 'clusters of clusters' was given. This was confirmed with TEM and STEM images, where aggregation of clusters was apparent. The aggregates differed in their sizes and showed a random distribution. However, apart from agglomerated clusters also non-agglomerated clusters were observed.

## 5.3 Polystyrene Modified with Clusters Carrying Less- or Non-reactive Ligands

In previous sections it was shown that polymer properties were improved when they were doped with the **Zr4** and the **Zr6** clusters carrying 12 methacrylate ligands each and therefore acted as cross-linkers in polymerization reactions. Swelling in organic solvents such as ethyl acetate was a clear prove that network formation due to cross-linking took place. Furthermore, the higher moduli of elasticity in the rubbery state, the rubber plateau moduli, proved network formation. However, not only the cluster shell might influence materials properties but also the inorganic filler part had to be discussed because it affected properties such as glass transition temperatures and onset temperatures of thermal degradation. Therefore, zirconium oxo clusters without polymerizable groups, such as acetate or propionate, and also clusters with ligands bearing double bonds which are little or non-reactive, such as vinylacetate and 5-norbornene-2-carboxylate, were used in the co-polymerizations with styrene. Moreover, the mixed-carboxylate cluster **Zr12-AcMc**, was applied in polymerizations.

### 5.3.1 Polystyrene Modified with $\text{Zr}_{12}\text{O}_8(\text{OH})_8(\text{OAc})_{24}$ or $\text{Zr}_{12}\text{O}_8(\text{OH})_8(\text{OProp})_{24}$

The co-polymerizations of the clusters  $\text{Zr}_{12}\text{O}_8(\text{OH})_8(\text{OAc})_{24}$  (**Zr12-Ac**) and  $\text{Zr}_{12}\text{O}_8(\text{OH})_8(\text{OProp})_{24}$  (**Zr12**) with styrene were carried out in the same way as for the **Zr6** hybrid polymers: Lauroyl peroxide was used as the initiator and a step-wise polymerization was applied. 0.5 mol% of cluster was applied for polymerizations in a first attempt. However, whereas **Zr6** showed good solubility in styrene due to interactions of the cluster shell with the organic monomer, the acetate and propionate ligands revealed poor solubility and 0.44 mol% in the acetate case and 0.48 mol% in the propionate case were the solubility limits at room temperature. Therefore, this maximum concentration was applied in the preparation of the hybrid polymers.

The gelation times were in both cases at about 120 min and thus considerably longer when compared to the **Zr6** - PS system. Another difference was observed in the appearance of the final polymers. Whereas the **Zr6** doped polystyrene samples were clear solids, the propionate and acetate cluster doped PS samples appeared whitish, indicating that aggregates were formed within the polymer matrix with a size in the range of visible light.

The thermal properties were investigated by TGA and DSC. In Figure 105 the curves for the cluster doped samples are compared with neat PS.

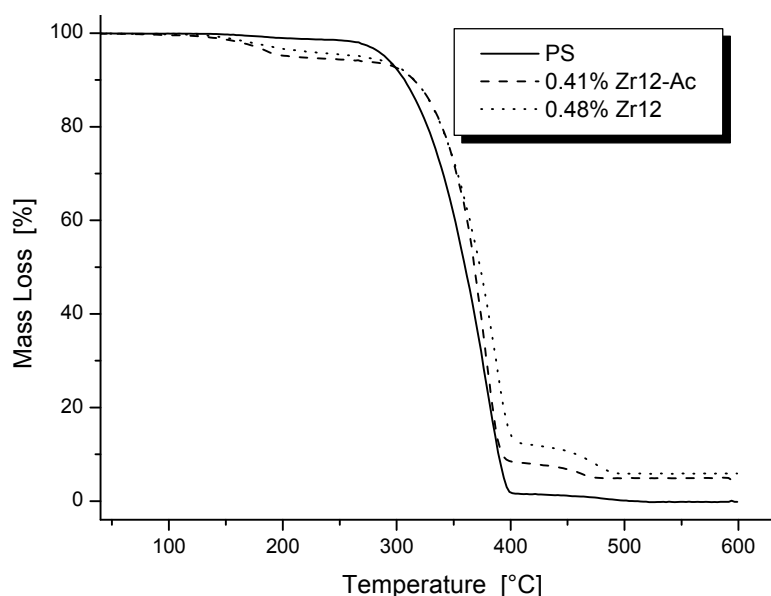


**Figure 105:** TGA curves of undoped and  $\text{Zr}_{12}$  cluster doped PS samples

The thermal degradation of the  $\text{Zr}_{12}$  doped hybrid polymers took place in three stages which are summarized in Table 73. For purposes of comparison, the values observed for a PS sample doped with the same molar amount of **Zr6** cluster are also given, irrespective of the molecular mass of the different clusters.

**Table 73:** Thermal data for neat and  $\text{Zr}_{12}$  doped polystyrene; for comparison the data of pure PS and a Zr6 doped sample are also shown

| Sample               | Onset 1 [°C] | Mass loss 1 [%] | Onset 2 [°C] | Mass loss 2 [%] | Onset 3 [°C] | Mass loss 3 [%] | Residual mass [%] | Residual mass calc. [%] |
|----------------------|--------------|-----------------|--------------|-----------------|--------------|-----------------|-------------------|-------------------------|
| <b>PS</b>            | 148          | 1.78            | 321          | 96.37           | 473          | 1.97            | -0.12             | 0.00                    |
| <b>0.41% Zr12-Ac</b> | 155          | 5.50            | 347          | 86.52           | 451          | 3.00            | 5.00              | 5.16                    |
| <b>0.48% Zr12</b>    | 141          | 4.45            | 349          | 83.70           | 455          | 5.89            | 5.95              | 6.01                    |
| <b>0.43% Zr6</b>     | 167          | 1.68            | 345          | 90.84           | 466          | 4.91            | 2.57              | 2.86                    |

The first loss originated in volatile compounds such as unreacted monomers and small oligomers, and step 2 from the loss due to the thermal degradation of the main polymer chains. As obvious, Onset 2 was the same for all of the hybrid materials, irrespective whether cross-

linking was chemically possible or not. Therefore, it was assumed that the inorganic filler perception was also responsible for the improvements in thermal properties and cross-linking was not the only decisive factor. The amount of char produced during step 2 was given as the Mass loss 3 and was also present in the non-crosslinked samples, again indicating that char formation not only depended on cross-linking but for a big part also on inorganic moieties. Nevertheless, there was a clear difference in the amount of the produced char. It was already shown in the **Zr6** hybrid polymers that char formation increased with increasing cluster proportion. The picture was different in this case: Whereas 0.48 mol% of **Zr12** cluster formed about 6 mass% of char during the combustion, a comparable amount of the **Zr12-Ac** cluster produced only 3 mass%. For comparison, 0.43 mol% of **Zr6** cluster in polystyrene produced 4.91 mass% of char; when the concentration was increased to 0.87 mol%, char formation was increased to 10 mass%. By comparing results from the non-crosslinked Zr<sub>12</sub>-cluster doped polymers with the **Zr6** cross-linked samples, it was assumed that the interplay of both inorganic filler and cross-linking was responsible for char formation.

DSC measurements revealed the same results as it was described for the **Zr6** doped polymers, i.e. no signals apart from the glass transition and the thermal combustion were observed at heating rates of 3 °C/min and 40 °C/min, respectively.

Swelling experiments were carried out to investigate whether solvent uptake was possible in the non-crosslinked samples. As expected, the polymers dissolved in ethyl acetate. A white, insoluble precipitate was obtained in both samples and was ascribed to zirconium dioxide. The polymers were isolated from the solution by filtration and precipitated in methanol. After re-dissolving in THF, SEC measurements were carried out. The results of DSC and SEC investigations are summarized in Table 74 together with data for neat PS for comparison.

**Table 74:** Glass transition temperatures, molecular weights and polydispersities for Zr<sub>12</sub> doped PS

| Sample           | Gelation Time<br>[min] | Onset 2<br>[°C] | T <sub>g</sub><br>[°C] | M <sub>n</sub><br>[kg mol <sup>-1</sup> ] | P <sub>d</sub> |
|------------------|------------------------|-----------------|------------------------|---|----------------|
| PS               | >240                   | 321             | 100                    | 181.1                                     | 6.56           |
| 0.41%<br>Zr12-Ac | 160                    | 347             | 105                    | 137.4                                     | 5.85           |
| 0.48%<br>Zr12    | 190                    | 349             | 107                    | 362.4                                     | 9.96           |

The gelation times in the co-polymerizations of **Zr12-Ac** and **Zr12** with styrene were significantly longer when compared to the **Zr6** cluster doped polymers. These longer gelation times were reflected in higher molecular weights, thus showing the same behaviour as the **Zr4** systems.

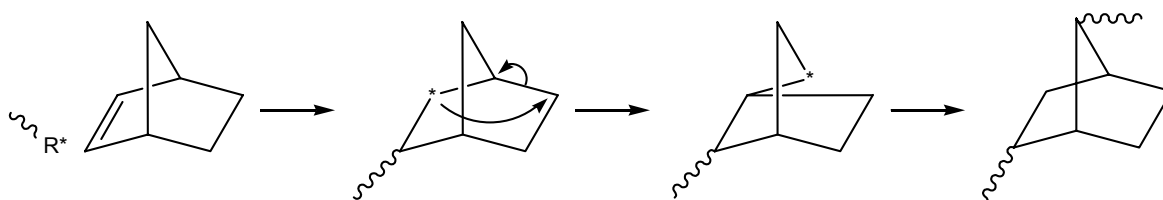


### 5.3.2 Polystyrene Modified with $\text{Zr}_{12}\text{O}_8(\text{OH})_8(\text{OVinac})_{24}$ or $\text{Zr}_6\text{O}_4(\text{OH})_4(\text{ONorb}_{\text{mix}})_{12}$

In contrast to methacrylic acid, which has the double bond at the  $\alpha$  position, vinylacetic acid carries the double bond at the  $\beta$  position. It is known that allyl compounds ( $\text{CH}_2=\text{CH}-\text{CH}_2-\text{X}$ ) usually polymerize with lower reaction rates and give oligomeric products because of degradative chain transfer to the monomer during radical polymerization [184]. Therefore, vinylacetic acid can be assumed as a polymerization inhibitor rather. However, it was shown that in the presence of Lewis acids the rates of polymerization and the molecular weights of the polymers were increased [185].

In the co-polymerizations with styrene, the cluster  $\text{Zr}_{12}\text{O}_8(\text{OH})_8(\text{OVinac})_{24}$  (**Zr12-Vinac**) was applied in a concentration of 0.44 mol% and a step-wise polymerization was applied as described above. Whereas polystyrene had a gelation time of about 5 hours, gelation did not occur at 60 °C in the sample polymerized with the **Zr12-Vinac** cluster. After 24 hours, the temperature was raised to 120 °C and the solution formed a gel. However, auto-acceleration took place in this step, thus the polymer was obtained as a porous solid with many bubbles incorporated.

Free radical polymerization of norbornene is possible in principle, but very low yields were reported especially for low reaction temperatures (60 °C) [186]. The mechanism of the polymerization was explained with a rearrangement of the bicyclic structure, followed by a double bond addition (Scheme 11). However, it was reported that polymerization of norbornene does not occur when the catalyst half-life is less than 2 hours at the reaction temperature. The higher the temperature the higher the yields, i.e. high temperatures are necessary to obtain a high propagation rate [187].



**Scheme 11:** Rearrangements of norbornene during radical polymerization

Co-polymerization of the cluster  $\text{Zr}_6\text{O}_4(\text{OH})_4(\text{ONorb}_{\text{mix}})_{12}$  (**Zr6-Norb<sub>mix</sub>**) in an amount of 0.50 mol% with styrene was carried out as described for **Zr12-Ac**. In contrast to the clusters

**Zr12-Ac** and **Zr12**, the solubility was quite high because of the large hydrophobic structures of the carboxylate ligands.

TGA measurements of the **Zr12-Vinac** and the **Zr6-Norb<sub>mix</sub>** cluster doped polystyrene samples are shown in Figure 106. The entire mass loss took place in three stages which are summarized in Table 75. Both polymers showed a pronounced mass loss below 300 °C, indicative of unreacted monomers. The onset temperatures of thermal decomposition were in the same range as they were observed for cross-linked samples, again indicating that the inorganic filler was responsible for improvements in thermal properties rather than cross-linking.

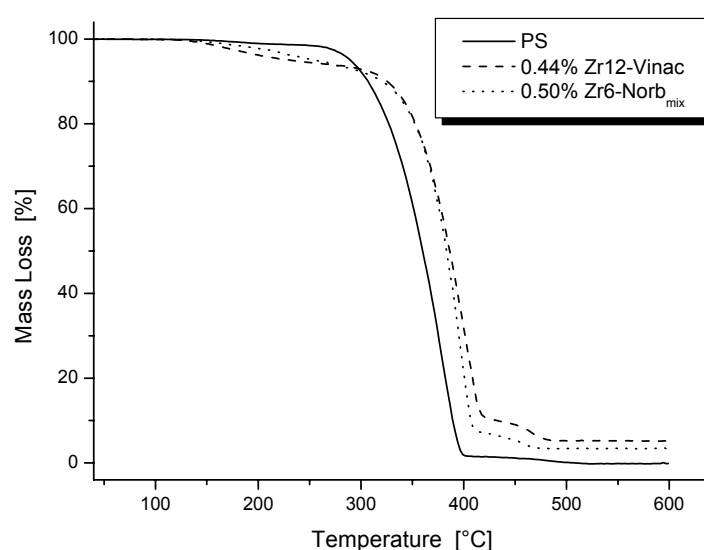


**Figure 106:** TGA curves of PS and **Zr12-Vinac** and **Zr6-Norb<sub>mix</sub>** doped PS samples

**Table 75:** Thermal data for neat and for **Zr12-Vinac** and **Zr6-Norb<sub>mix</sub>** doped PS

| Sample]                                 | Onset 1<br>[°C] | Mass<br>loss 1<br>[%] | Onset 2<br>[°C] | Mass<br>loss 2<br>[%] | Onset 3<br>[°C] | Mass<br>loss 3<br>[%] | Residual<br>mass<br>[%] | Residual<br>mass calc.<br>[%] |
|---|-----------------|-----------------------|-----------------|-----------------------|-----------------|-----------------------|-------------------------|-------------------------------|
| <b>PS</b>                               | 148             | 1.78                  | 321             | 96.37                 | 473             | 1.97                  | -0.12                   | 0.00                          |
| <b>0.44%<br/>Zr12-Vinac</b>             | 136             | 5.94                  | 358             | 84.33                 | 455             | 4.57                  | 5.10                    | 5.35                          |
| <b>0.50%<br/>Zr6-Norb<sub>mix</sub></b> | -               | 4.83                  | 359             | 93.37                 | 441             | 3.35                  | 3.42                    | 3.13                          |

DSC measurements showed no signals apart from exothermic combustion at high temperatures, the glass transition temperatures were determined at a ramp of 40 °C/min. The **Zr12-Vinac** and **Zr6-Norb<sub>mix</sub>** doped polymers were soluble in ethyl acetate, indicating that cross-linking did not take place to a sufficient amount. After separating the polymer solution from ZrO<sub>2</sub>, the polymers were precipitated in methanol and dissolved in THF for SEC measurements. Both samples showed high molecular weights, but also high polydispersities (Table 76).

**Table 76:** Glass transition temperatures, molecular weights and polydispersities for **Zr12-Vinac** and **Zr6-Norb<sub>mix</sub>** doped PS samples

| Sample              | Gelation Time [h] | Onset 2 [°C] | T <sub>g</sub> [°C] | M <sub>n</sub> [kg mol <sup>-1</sup> ] | P <sub>d</sub> |
|---------------------|-------------------|--------------|---------------------|--|----------------|
| PS                  | >4                | 321          | 100                 | 181.1                                  | 6.56           |
| 0.44%<br>Zr12-Vinac | >24               | 358          | 105                 | 385.7                                  | 6.55           |
| 0.48%<br>Zr6-Norb   | 2.5               | 359          | 107                 | 279.8                                  | 7.00           |

### 5.3.3 Polystyrene Modified with Zr<sub>12</sub>O<sub>8</sub>(OH)<sub>8</sub>(OAc)<sub>16</sub>(OMc)<sub>8</sub>

The cluster Zr<sub>12</sub>O<sub>8</sub>(OH)<sub>8</sub>(OAc)<sub>16</sub>(OMc)<sub>8</sub> (**Zr12-AcMc**) carried both non-reactive acetate and reactive methacrylate ligands. As a consequence, it was expected that cross-linking occurs. A step-wise polymerization was carried out and the hybrid polymers were characterized by TGA, DSC and swelling experiments. The gelation time of ~50 minutes was comparable to the gelation times observed in the preparation of the **Zr6** cross-linked polystyrene. The obtained hybrid polymers were transparent and crack- and bubble-free.

The TGA curve of **Zr12-AcMc** doped PS is shown in Figure 107 together with pure PS for purposes of comparison. The mass losses during thermal combustion were described by three steps, which are summarized in Table 77.

The onset temperature of thermal decomposition was very low when compared to other cluster doped samples. This was mainly attributed to the slope of the curve during thermal combustion. Char formation was very high when compared to other polymers doped with less- or non-reactive clusters, proving the assumption that cross-linking indeed is a main factor in char formation next to the inorganic filler.

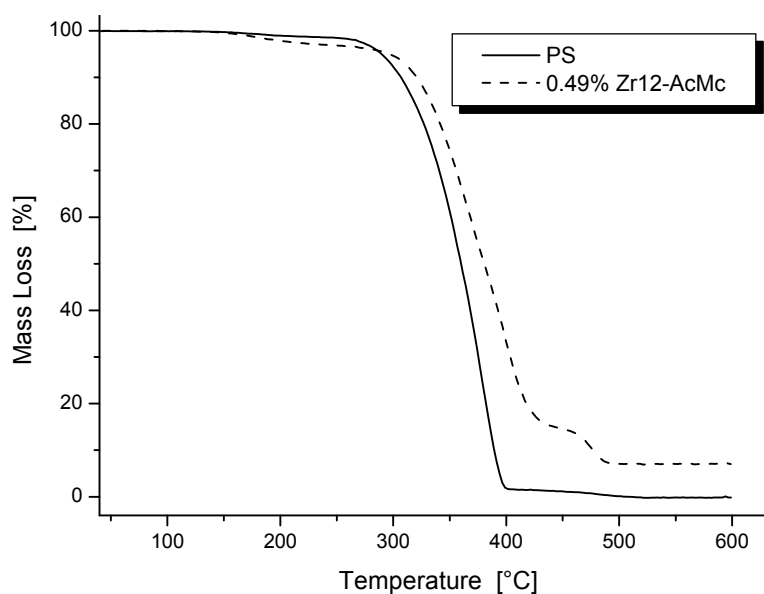


**Figure 107:** TGA curves of PS and **Zr12-AcMc** doped PS

**Table 77:** Thermal data for neat PS and Zr12-AcMc doped PS

| Sample]                         | Onset 1<br>[°C] | Mass<br>loss 1<br>[%] | Onset 2<br>[°C] | Mass<br>loss 2<br>[%] | Onset 3<br>[°C] | Mass<br>loss 3<br>[%] | Residual<br>mass<br>[%] | Residual<br>mass calc.<br>[%] |
|---------------------------------|-----------------|-----------------------|-----------------|-----------------------|-----------------|-----------------------|-------------------------|-------------------------------|
| <b>PS</b>                       | 148             | 1.78                  | 321             | 96.37                 | 473             | 1.97                  | -0.12                   | 0.00                          |
| <b>0.49%<br/>Zr12-<br/>AcMc</b> | 156             | 3.05                  | 328             | 82.13                 | 465             | 7.74                  | 7.01                    | 6.08                          |

The glass transition temperature was 115 °C, as determined by DSC and thus constituted the highest value observed by DSC measurements for the entire cluster doped polystyrene samples prepared in this work. The polymer showed solvent uptake in ethyl acetate and a degree of swelling of 114 % was determined. A comparable degree of swelling was observed for polystyrene cross-linked with 0.43 mol% of **Zr6**.

### 5.3.4 Conclusion

In summary, the use of clusters carrying less- or non-reactive ligands in the hybrid polymer preparation resulted materials which showed improved thermal properties. Therefore, it was concluded that the crosslinking ability of the **Zr6** cluster was only in parts responsible for the shifts in the onset temperatures of thermal decomposition and in the glass transition temperatures.

In contrast to clusters bearing unsaturated ligands, such as methacrylate, vinyl acetate and norborneate, derivatives with acetate and propionate ligands showed a low solubility in styrene. On account of this, an aggregation of the clusters in solution during polymerization probably took place. This was reasoned in the appearance of the final materials, which appeared whitish instead of clear, as it was observed for the **Zr6** doped polystyrene samples. The thermal properties were comparable to cross-linked samples.

The use of **Zr12-Vinac** as the co-monomer in the polymerization with styrene led to a significant lowering of the reaction rate during radical polymerization due to degradative chain transfer to the monomer during polymerization. This was reflected in the missing of gel formation at 60 °C within 24 hours. The solution gelled by raising the temperature. However, this led to auto-acceleration and a solid polymer with many bubbles incorporated was obtained. The hybrid material was soluble in ethyl acetate, indicating that the vinyl acetate cluster did not form a chemically cross-linked network.

A similar picture was obtained for the **Zr6-Norb<sub>mix</sub>** cluster: Norbornene groups are in principle accessible to free radical polymerization. However, propagation rates are very low and poor yields at a polymerization temperature of 60 °C and little initiator concentrations were reported. As a consequence, the resulting hybrid polymers were not cross-linked and were soluble in ethyl acetate, indicating that the norbornene groups did not take part in the polymerization process and that no network was formed.

When the cluster **Zr12-AcMc** was applied as a co-monomer in the polymerizations with styrene, the picture was very similar to the **Zr6** polymers: The gelation times were comparable to the **Zr6** systems and the obtained polymers were insoluble in ethyl acetate. Moreover, a remarkably high glass transition temperature was observed.

## 6 Experimental

### 6.1 General Techniques and Used Materials

All reactions that were sensitive to atmospheric conditions were carried out in an oxygen- and moisture free atmosphere by applying the Schlenk technique or by working in a glove box. Solvents were purified and desiccated by standard methods and stored under an argon atmosphere. All chemicals were purchased from ABCR, ACROS, Riedel-de H  en and Sigma-Aldrich.

Ti(OEt)<sub>4</sub> (95 %, ABCR), Ti(OPr)<sub>4</sub> (98 %, Aldrich), Ti(O<sup>i</sup>Pr)<sub>4</sub> (97 %, Aldrich), Zr(Obu)<sub>4</sub> (80 % in BuOH, Aldrich) were used as received and stored under argon atmosphere. Styrene (99 %, Aldrich) and methyl methacrylate (99 %, Aldrich) were distilled once, dried with CaH<sub>2</sub> and distilled again prior use. Benzoyl peroxide (98%, Aldrich) and lauroyl peroxide (99%, ACROS) were used as received and stored at -20 °C. Acetic acid (99 %, Aldrich) was dried with CaSO<sub>4</sub>, distilled and stored under argon atmosphere; acetyl acetone (99 %, Aldrich) was distilled and stored at -20 °C; cyclopentadiene was freshly cracked from dicyclopentadiene (95 %, Aldrich) prior use and distilled; 2,3-dimethyl-butadiene (98 %, Aldrich) was stored at -20 °C and freshly distilled prior use; formic acid (98-100 %, Riedel-de H  en) was dried with freshly prepared boric anhydride and stored in Ar atmosphere; isobutyric acid (99 % or 99+ %, Aldrich) was used as received; isoeugenol (98 %, Aldrich) was used as received; methacrylic acid (99 %, Aldrich) was distilled under reduced pressure and stored at -20 °C; methyl acrylate (99 %, Aldrich) was used as received and stored at -20 °C; 5-norbornene-2-carboxylic acid (98 %, Aldrich) was used as received; propionic acid (99.5 %, Aldrich) was distilled and stored under Ar; vinylacetic acid (97 %, Aldrich) was used as received and stored at 4 °C.

The following solvents were employed for the NMR experiments: CDCl<sub>3</sub> (99.8 %, euriso-top), CD<sub>2</sub>Cl<sub>2</sub> (99.6 %, euriso-top), d<sub>8</sub>-toluene (99.6 %, euriso-top), C<sub>6</sub>D<sub>6</sub> (99.6 % euriso-top).

## 6.2 Analytical Techniques

### 6.2.1 Single Crystal X-Ray Diffraction

Selected crystals were mounted on a Siemens SMART diffractometer with a CCD area detector. Graphite-monochromated Mo-K $\alpha$  radiation (0.71073 pm) was used for all measurements. The crystal-to-detector distance was 4.40 cm. A hemisphere of data was collected by a combination of three or four sets of exposures at 173 K. Each set had a different  $\phi$  angle for the crystal, and each exposure took 15 - 20 s and covered 0.3 ° in  $\omega$ . The data were corrected for polarization and Lorentz effects, and an empirical absorption correction (SADABS) was applied. The cell dimensions were refined with all unique reflections. The structures were solved by Patterson search or by direct methods (SHELXS86). Refinement was carried out with the full-matrix least-squares method based on  $F^2$  (SHELXL93) with anisotropic thermal parameters for all non-hydrogen atoms. Hydrogen atoms were inserted in calculated positions and refined riding with the corresponding atom.

### 6.2.2 Nuclear Magnetic Resonance Spectroscopy

NMR spectra were recorded on a Bruker Avance 300 ( $^1\text{H}$ : 300.13 MHz,  $^{13}\text{C}$ : 75.47 MHz) equipped with a 5 mm broadband probe head and a z-gradient unit.

2D spectra [78, 188] were measured with Bruker standard pulse sequences:

#### **COSY (COrelated SpectroscopY)**

The two-dimensional homonuclear (H, H)-correlated NMR experiment yields NMR spectra in which  $^1\text{H}$  chemical shifts along both frequency axes are correlated with each other. Magnetization is transferred by scalar coupling.

#### **TOCSY (TOtal Correlated SpectroscopY)**

In the TOCSY experiment, magnetization is dispersed over a complete spin system by successive scalar coupling. In contrast to COSY, the TOCSY experiment correlates all protons of a spin system. The mixing time was usually 160 ms.

### **EXSY (EXchange SpectroscopY)**

The 2D EXSY experiment offers qualitative information about inter- and intramolecular chemical exchange. The mixing time was usually 1 s.

### **HSQC (Heteronuclear Single Quantum Coherence)**

HSQC is the most important inverse 2D heteronuclear (H, C)-correlated experiment. The strategy is to transfer magnetization from a proton to a carbon nucleus. Magnetization vectors are allowed to develop for a time and  $^{13}\text{C}$  polarization is transferred back to the proton where the resonance is recorded.

### **$^1\text{H} / ^{13}\text{C}$ -HMBC (Heteronuclear Multiple Bond Correlation)**

In this experiment, cross-peaks are observed connecting carbon signals to signals for protons two or more bonds away. Thus, HMBC spectra can be used to assign, inter alia, quarternary carbons.

## **6.2.3 Thermogravimetric Analysis**

Thermogravimetric analysis (TGA) is a technique in which the mass change of a substance is measured as a function of temperature whilst the substance is subjected to a controlled temperature programme [189]. Mass loss is only seen if a process occurs where a volatile component is lost. Results are presented as a plot of mass against temperature or time [190].

Mass changes of polymer samples as functions of temperature were determined on a Netzsch TG 209C Iris thermal analyzer in dynamic synthetic air atmosphere at a flow rate of 30 ml/min. Samples were measured in an open platinum pan from 35 °C to a temperature, where complete thermo-oxidative decomposition of the polymers was assured, mostly 650 °C. Residual masses of transition metal oxo clusters were also determined in dynamic air atmosphere with a ramp of 20 °C/min applied from room temperature to 800 °C. Initial masses in measurements were kept in the range of 10 mg. A correction curve measured in the same conditions as the samples was subtracted from each thermogram to make allowance for buoyancy and gas viscosity.



## 6.2.4 Differential Scanning Calorimetry

In heat flux differential scanning calorimetry (DSC), a temperature difference between sample and reference is measured as the reference is heated at the required rate [191, 192]. This temperature difference is then converted into a heat flow by means of the appropriate conversion factor. The heat flow signal is composed of two parts: one is the heat flow required to raise the sample temperature at the programmed rate, and is directly related to the intrinsic heat capacity of the sample, and the other is the heat flow arising from kinetic processes that may occur during the heating scan, for example phase changes such as melting and crystallization, liquid crystalline transitions or second order transitions such as glass transition. Thus, the heat flow can be written in the form

$$\frac{dQ}{dt} = mc_P\beta + f(T,t)$$

where  $m$  is the sample mass,  $c_P$  is the specific heat capacity of the sample, which in general is temperature dependent,  $\beta$  is the heating rate, and  $f(T,t)$  represents the heat flow due to kinetic processes. The specific heat capacity ( $c$ ) is defined as the heat necessary to raise the temperature of unit mass of a substance by one degree, so that the temperature rise  $\Delta T$  for a heat input of  $Q$  is

$$\Delta T = \frac{Q}{mc}$$

In glass transition region at constant pressure the heat input is equal to the enthalpy change and the definition of the specific heat capacity becomes

$$c_P = \frac{1}{m} \frac{dH}{dT} = \frac{1}{m\beta} \frac{dH}{dt}$$

where  $H$  is the enthalpy of the sample. The quantity  $dH/dt$  is the heat flow in a quasi-equilibrium process at constant pressure. Therefore, for glass transition  $c_P$  defined by the latter equation is the sum of  $c_P$  and  $(1/m\beta)f(T,t)$  given in the first equation.

DSC measurements were performed on a Shimadzu DSC-50 instrument in static air atmosphere. Polymer samples were applied either as a powder or as a thin plate to assure good heat transfer. The sample mass was typically 2 - 4 mg. Samples were sealed in standardized

aluminum pans. For measurements above 200 °C, a hole was made into pans to assure constant pressure. Glass transition temperatures were determined by first removing thermal history of the samples and ensure good contact to the aluminum pan in a heating scan from room temperature to 200 °C with a ramp of 2 °C/min,  $T_g$  was then determined in a second heating scan with a ramp of 40 °C/min to 200 °C/min. Measurements from room temperature to 450 °C were conducted with a heating rate of 3 °C/min without prior heating cycle.

### 6.2.5 Elemental Analysis

Elemental analyses were carried out at the Microanalytical Laboratory at the Institute of Physical Chemistry, University of Vienna, on a 2400 CHN Elemental Analyzer by Perkin Elmer.

### 6.2.6 Fourier Transform Infrared Spectroscopy

FTIR spectra of cluster samples were recorded on a Bruker Tensor 27 with a 2.5 mm diameter sampling area of the ATR crystal in nitrogen atmosphere from 4000 to 550  $\text{cm}^{-1}$ . To obtain a better intensity at high frequencies 64 scans were applied by default and also the resolution was set to 2  $\text{cm}^{-1}$ . For this region KBr pellets are favoured for a better intensity, however, preparative limitations disallowed the preparation of pellets in inert gas atmosphere.

Polymer samples were measured using KBr pellets in transmission mode from 4000 to 450  $\text{cm}^{-1}$  at a resolution of 4  $\text{cm}^{-1}$ . The milled polymers were mixed with a defined amount of potassium ferricyanide as an internal standard before preparing the KBr pellets.

### 6.2.7 Size Exclusion Chromatography

Size exclusion chromatography (SEC), also known as Gel Permeation Chromatography (GPC), is a method used to separate solutions of mixtures according to the molecular size of the components. Solutions to be analyzed are percolated through columns filled with gel particles swollen in organic solvents. The gel particles are porous, and the pore diameters vary in size.

Different gels are characterized by different pore size distributions. When gels of appropriate pore size distributions have been properly matched with molecular weight ranges of materials to be separated, large molecules or extensive associations of molecules do not enter the gel pores, but pass through the gel columns between particles. Unlike most chromatographic methods, larger entities elute first. Somewhat smaller molecules, depending on their size, spend varying amounts of time within the gel particles during an SEC separation. The smallest molecules enter all pores in gel particles and are not separated [193].

SEC measurements were performed in THF using a Waters system including a 515 HPLC pump, a 717 autosampler, a 2410 differential refractive index detector and Styragel columns (HR 0.5, 3 and 4, linear and GPC phase SDV 50/100/10E5A) at 40 °C at a rate of 1 ml/min applying linear polystyrene standards. Molecular weight analysis was carried out using Waters Millennium software including the GPC/V option and related to an internal standard (diphenyl ether)

### 6.2.8 Modulated Differential Scanning Calorimetry

In contrast to common DSC, where a linear heating rate is used, an additional sinusoidal temperature modulation is applied in MDSC. The MDSC used was modulated in the block temperature  $T_b(t)$  with a sinusoidally changing amplitude that was governed, as in standard DSC, by the temperature measured at the sample position [194]

$$T_b(t) = T_0 + qt + A_{T_b} \sin \omega t$$

where  $q$  is the underlying, constant heating rate and  $T_0$  the initial isotherm at the beginning of the scanning experiment. The modulation frequency  $\omega$  is equal to  $2\pi/p$  in units of rad/s, with  $p$  representing the duration of one cycle in seconds. The sample and reference temperatures,  $T_s$  and  $T_r$ , respectively, are given at steady state by

$$T_s = T_0 + qt - \frac{qC_s}{K} + A_{T_s} \sin(\omega t - \varepsilon)$$

$$T_r = T_0 + qt - \frac{qC_r}{K} + A_{T_r} \sin(\omega t - \phi)$$

where  $K$  is the Newton's law constant in J/s·K and  $C_s$  and  $C_r$  represent the heat capacities of the sample and reference calorimeters. If a calorimeter consists of a pan with and without sample,

the heat capacities are given to  $C' + mc_p$  or  $C'$ , respectively (where  $C'$  = pan heat capacity,  $m$  = sample mass and  $c_p$  = specific heat capacity of the sample). The reversible heat capacity is extracted from the modulation amplitudes and is given, for the case of equal mass of the empty sample and the reference pan, by

$$mc_p = \frac{A_\Delta}{A_{T_s}} \sqrt{\left(\frac{K}{\omega}\right)^2 + C'^2}$$

with  $A_\Delta$  representing the modulation amplitude of the temperature difference  $T_r - T_s$  (proportional to the heat flow  $HF$  and phase difference  $\delta$ ). The total heat flow  $\langle HF(t) \rangle$  is evaluated in MDSC by taking sliding averages over full cycles of modulations. The common analysis is carried out by assuming that at steady state  $q$  can be equated to  $dT_r/dt$  (i.e.  $dt = dT_r/q$ )

$$mc_p = K\Delta T / q + [(K\Delta T / q) + C']d\Delta T / dT_s$$

The irreversible (non-reversing) part of the heat capacity is then taken as the difference between total and reversible heat capacity. It contains all the effects due to heat loss and different heating rates of sample and reference and is thus less precise [192, 195].

MDSC measurements were carried out on a TA Instruments DSC 2920 CE differential scanning calorimeter from room temperature to 150 °C in dynamic nitrogen atmosphere. The sample weight was kept around 4 mg, the pan weights were always around 24 mg. Non-isothermal experiments with a modulation amplitude of 0.5 °C and a period of 60 s were performed at a heating / cooling ramp of 3 °C/min. Samples were heated once with 3 °C/min to 150 °C and, after a 5 min isothermal hold temperature, cooled with the same ramp. From the second heating run the glass transitions were determined.

## 6.2.9 Inductively Coupled Plasma Optical Emission Spectroscopy

In plasma emission spectroscopy, a sample solution is introduced into the core of an inductively coupled argon plasma (ICP) at a temperature of approximately 8000 °C. All elements become thermally excited at this temperature and emit light at their characteristic wavelengths. This light is collected by the spectrometer and passes through a diffraction grating that serves to resolve the light into a spectrum of its constituent wavelengths. This diffracted light is then collected by wavelength within the spectrometer, and amplified to yield an intensity measurement that can be

converted to an elemental concentration by comparison with calibration standards. This measurement process is a form of optical emission spectroscopy (OES) [196].

A Spectro ICP-OES model Spectroflame P was used for the measurement of the Zr samples at 343.823 nm. The free running radiofrequency generator operating at 27.5 MHz was used at an output power of 5 kW at maximum (coolant argon flow rate 14 l/min, auxiliary argon 1 l/min, nebulizer argon gas flow 1 l/min).

### 6.2.10 Specific Gravity

Densities of pure and cluster doped polystyrene samples were determined with a Sartorius YDK01 LP Density Determination Kit using the Archimedean principle. A hydrostatic balance was used to weigh the polymers in air as well as in liquid, here water, and thus allowed for determining the specific gravity of the solid with the density of the liquid causing buoyancy known. The formula used makes allowance for air buoyancy and the measuring device setup [197]:

$$\rho = \frac{W_{(a)} \cdot [\rho_{(fl)} - \rho_{(a)}]}{C \cdot [W_{(a)} - W_{(fl)}]} + \rho_{(a)}$$

$\rho$  = specific gravity of the solid

$\rho_{(fl)}$  = density of the liquid (for water at 25.5 °C: 0.99694 g/cm<sup>3</sup>)

$\rho_{(a)}$  = density of air under standard conditions (0.0012 g/cm<sup>3</sup>)

$W_{(a)}$  = weight of the solid in air

$W_{(fl)}$  = weight of the solid in liquid

$C$  = correction factor determined by the geometry of the setup (0.99983)

### 6.2.11 Thermal Mechanical Analysis

In thermal mechanical analysis (TMA), stress is usually applied on cylindrical or cubic specimens in compression or tension and is defined as the mechanical force  $F$  divided by the area  $A$  over which it acts.

$$\sigma = \frac{F}{A}$$

If the applied stress is negligible, the technique becomes that of thermodilatometry. For plastics, the measurement of the linear thermal expansion coefficient with constant and low extra load has established. The differential thermal expansion coefficient is defined as

$$\alpha = \frac{1}{l_0} \cdot \frac{dl}{dT}$$

where  $l_0$  is the original length of the specimen and  $dl/dT$  is the rate of change of sample length with temperature. Units of  $\alpha$  are most commonly given in  $10^{-6}/^{\circ}\text{C}$ . For isotropic samples the cubic coefficient of thermal expansion is three times that of the linear one.

$$\beta = 3\alpha$$

Measurements were performed according to ISO 11359-2 on a TA Instruments TMA 2940 thermal mechanical analyzer at a constant heating rate of  $1^{\circ}\text{C}/\text{min}$  in flowing nitrogen atmosphere from room temperature to  $135^{\circ}\text{C}$ . The specimens had a cubic geometry with coplanar surfaces in the dimensions of  $13 \times 4 \times 4$  mm. They were measured in compression by applying a constant load of 5mN via a quartz macro stamp. In order to obtain good contact between sample surface and macro stamp and to remove thermal history, the samples were heated once or twice above glass transition temperature with a heating and cooling rate of  $1^{\circ}\text{C}/\text{min}$ . Thermal expansion coefficients were then determined from following cycles by determining the slope of the thermographs via a linear regression of the data between 30 and  $40^{\circ}\text{C}$  for  $\alpha$  below  $T_g$  and 110 and  $120^{\circ}\text{C}$  for  $\alpha$  above  $T_g$ .

## 6.2.12 Dynamic Mechanical Analysis

The oscillating stress  $\sigma$  usually follows a sinusoidal waveform

$$\sigma(t) = \sigma_{\max} \sin \omega t$$

where  $\sigma_{max}$  is the maximum stress and  $\omega$  is the angular frequency of oscillation ( $\omega=2\pi f$ ,  $f$  is the frequency in Hertz). The corresponding strain  $\varepsilon$  is defined by

$$\varepsilon = \frac{\Delta l}{l_0}$$

and dimensionless, but often expressed as a percent.

In a Hookean solid, i.e. in an elastic material, the strain of a sample is directly proportional to the applied stress.

$$E = \frac{d\sigma}{d\varepsilon}$$

where  $E$  is the elastic or Young's modulus.

If the material is viscous, Newton's law holds and the specimen possesses a resistance to deformation or viscosity  $\eta$  which is proportional to the rate of application of strain

$$\eta = \frac{d\sigma}{d\varepsilon/dt}$$

If a sinusoidal oscillating stress is applied to a specimen, a corresponding oscillating strain will lag behind the applied stress by a phase difference  $\delta$ . The ratio of peak stress to peak strain gives the complex modulus  $E^*$  which consists of an in-phase component, which is called storage modulus  $E'$ , and an out-of-phase component, which is called loss modulus  $E''$ . The storage modulus is in phase with the applied stress and represents the energy stored per cycle within the sample, i.e. the 'solid' response, whereas the loss modulus represents the energy dissipated within a cycle, i.e. the 'liquid' response. The ratio between the loss and the storage modulus is called the mechanical damping factor  $\tan \delta$ .

$$\tan \delta = \frac{E''}{E'}$$

Dynamic Mechanical Analysis was performed according to ISO 6721 using a TA Instruments DMA 2980. Dynamic moduli at room temperature were determined in single cantilever clamping

mode at a frequency of 1 Hz, temperature sweeps from room temperature to 220 °C were performed in tension mode, also at a frequency of 1 Hz and a heating rate of 2 °C/min. The sample size was 35x5x1.4 mm and a fixed amplitude deformation of 20 µm was applied. All the measurements were conducted in a dynamic nitrogen atmosphere.

### 6.2.13 Tension Tests

These tests are used to ascertain several mechanical properties of materials that are important to design, such as modulus of elasticity or tensile strength [130, 159]. A specimen is deformed, usually to fracture, with a gradually increasing tensile load that is applied uniaxially along the axis of the specimen. The output is recorded as load or force, the engineering stress  $\sigma$ , versus elongation, the engineering strain  $\varepsilon$ , where strain is unitless, but commonly expressed as a percentage.

$$\sigma = \frac{F}{A_0}$$

$$\varepsilon = \frac{l_i - l_0}{l_0} = \frac{\Delta l}{l_0} (\cdot 100\%)$$

The plot of stress versus strain results in a linear relationship when the strain is kept within the elastic region of a specimen. The slope on the curve in the linear viscoelastic region, for polymers between 0.05 and 0.25 % strain, yields the modulus of elasticity or Young's modulus  $E$  which is given by Hooke's law:

$$\sigma = E \cdot \varepsilon$$

Tensile tests were performed on a Zwick Z050 tensile testing machine fitted with a 1 kN load cell at room temperature. A Multisens extensometer was used to determine accurate displacement data with an initial gauge length of 10 mm. Dog-bone-shaped tensile bars were prepared from cylindrical polymer samples by cutting and stamping out with a punch, edges were manually grinded to avoid shivering during testing. The sample geometry was 35 x 2 x 0.5 mm, according



to EN ISO 527-2 5B, the clamping length was 20 mm, the gauge length 10 mm. All samples were left for 12 hours at test temperature to equilibrate thermally. Measurements were carried out with a constant traverse speed of 0.5 mm/min until break.

### 6.2.14 Compression Tests

In compression tests the material's behaviour under crushing loads is determined. The specimens, typically prisms or cylinders, are compressed and deformations at various uniaxial loads are recorded [130, 159].

In analogy to tensile tests, the stress  $\sigma$  is defined as the load  $F$  divided by the cross-sectional area  $A_0$

$$\sigma = \frac{F}{A_0}$$

and the strain  $\varepsilon$  is given by the traverse way  $\Delta l$  divided by the initial height of the sample  $l_0$ .

$$\varepsilon = \frac{\Delta l}{l_0}$$

Since specimen's diameters change during compression tests it is more meaningful to use a true stress - true strain scheme. True stress  $\sigma_T$  is defined as the load  $F$  divided by the instantaneous cross-sectional area  $A_i$  over which deformation is occurring.

$$\sigma_T = \frac{F}{A_i}$$

If the volume of a specimen during testing remains constant, i.e. cavities are absent, true stress may also be defined by

$$\sigma_T = \frac{F}{A_0}(1 + \varepsilon)$$

Furthermore, true strain  $\varepsilon_T$  is defined by

$$\varepsilon_T = \ln \frac{l_i}{l_0} = \ln(1 + \varepsilon) = \ln \lambda$$

Compression tests were performed on a Zwick Z050 tensile testing machine with a 50 kN load sensor at room temperature. Cylindrical specimens were compressed at a constant traverse speed of 0.015 mm/s between two parallel, flat steel plates. The friction between the samples and steel plates was reduced by placing a thin film of PTFE tape (3M 5480, PTFE skived film tape) between the sample and the steel plates. Additionally, the surface between steel and tape was lubricated with dish-washing detergent. In this way no buckling of the sample during the compression test was observed. The relative displacement of the steel plates was recorded with a Multisens extensometer, changes in the y/z-dimension were determined by analyzing calibrated photographs which were taken during the compression test. The tests were performed at 23 °C and the samples were tempered prior measurement to assure thermal equilibrium

### 6.2.15 Microhardness

Nanoindentation is a method that can be used to determine properties of specimens at a length scale appropriate for nanomaterials. Instead of pulling the specimen, a diamond tip (e.g. Berkovich-type) will be used to make indentations. The test consists of loading to a maximum value  $F_{max}$  and unloading to zero. Additionally, a hold period is most commonly programmed. Depths of the indentation are recorded and through these data, hardness  $H$  and Young's modulus  $E$  can be determined.

A general relationship between penetration depth  $h$  and load  $F$  in the unloading curve for various indenter geometries can be fitted by [11, 198]

$$F = \alpha(h - h_r)^m$$

where  $F$  is the load applied to the indenter,  $h$  its penetration and  $h_r$  the residual depth after complete unloading.  $\alpha$  contains geometric constants, the sample elastic modulus, the sample

Poisson's ratio, the indenter elastic modulus and the indenter Poisson's ratio.  $m$  is an exponent that is related to the geometry of the indenter and found to be between 1 and 2. Oliver and Pharr [199] realized that the slope of the unloading curve changes constantly due to changing contact area and that the derivative  $dF/dh$  at the maximum loading point  $(h_{max}, F_{max})$  yields information about the state of contact. This derivative, named 'contact stiffness', is given by

$$S = km(h_m - h_r)^{m-1}$$

where  $k$  is a constant and  $h_m$  is the maximum penetration of the indenter. The contact depth  $h_c$  is then given by

$$h_c = h_m - \frac{\varepsilon F_{max}}{S}$$

where  $\varepsilon$  is a function of the particular tip geometry. From contact depth knowledge the contact area  $A_c$  for a perfect Berkovich indenter is determined by

$$A_c = 24.5h_c^2$$

and hardness  $H$  is calculated as

$$H = \frac{F_{max}}{A_c}$$

Additionally, elastic properties can be determined. The reduced modulus  $E_r$  includes both, the modulus of the indenter and the sample, and can be extracted from the contact stiffness by

$$S = \frac{\partial F}{\partial h} = 2\beta E_r \sqrt{\frac{A_c}{\pi}} \rightarrow \frac{1}{E_r} = \frac{1-\nu^2}{E} + \frac{1-\nu_i^2}{E_i}$$

where  $\beta$  is a correction factor depending on the tip geometry,  $E$  and  $\nu$  the sample elastic modulus and Poisson's ratio, respectively, and  $E_i$  and  $\nu_i$  the elastic modulus and Poisson's ratio of the indenter material.

The hardness and elastic modulus were measured on a Nanoindenter XP (MTS Systems) apparatus with a Berkovich tip at 23 °C. The maximum penetration depth was 2 µm with a penetration velocity of 100 nm/s. The tip was held at the maximum load for 30 seconds and then unloaded again with 100 nm/s. Coplanar sample surfaces were grinded by reducing the grain size of the used abrasive paper gradually. Finally, surfaces were lapped with the aid of a 1 µm grinding paste. The analysis of indentation load - penetration curves was done following the method of Oliver and Pharr [199] and ISO 14577, respectively.

### 6.2.16 Small Angle X-Ray Scattering

Small-Angle X-ray Scattering (SAXS) is a tool for studying structures in the size range typically between 1 and 100 nm. This includes microstructures in materials, microporosity, micro emulsions and many other questions.

Small-angle scattering considers a range of sizes sufficiently larger than inter atomic distances, so that the scattering length density  $\rho(r)$  can be approximated as a continuous variable of the position  $r$  in the specimen [200, 201]. The general equation for the SAXS intensity  $I(q)$  can be written as

$$I(q) = I_0 \left| \int_V \rho(r) \cdot e^{i \cdot q \cdot r} d^3r \right|^2$$

where  $q$  is the scattering vector,  $V$  the specimen volume illuminated by the X-ray beam and  $I_0$  a constant defined by the conditions of the instrument.

The measurements were performed by Herwig Peterlik, University Vienna, using a pinhole camera with a rotating anode generator (Ni-monochromated Cu K $\alpha$  radiation) and an area detector (Bruker AXS, Karlsruhe). All SAXS patterns were first corrected for background scattering from the experimental setup and then radially averaged to obtain the function  $I(q)$ , where  $q = (4\pi/\lambda) \sin \theta$  is the scattering vector,  $2\theta$  being the angle between the incident and the diffracted beam, and  $\lambda = 0.154$  nm the X-ray wavelength. Scattering curves were obtained in the  $q$  range from 0.15 to 9 nm<sup>-1</sup> by combining data measured at two different sample-detector distances.

Cluster - cluster distances,  $d$ , were determined from the maximum of the peak in the scattering curves according to

$$d = \frac{2\pi}{q_{\max}}$$

The curves were fitted additionally using the model developed by Beaucage. The model was extended with an interference function for small  $q$  values with

$$inter(q, k, d) = \frac{1}{1 + k\theta(q, d)}$$

$$\theta(q, d) = 3 \frac{\sin(qd) - \cos(qd)}{(qd)^3}$$

$$I(q) = g_1 \exp(-q^2 r_{g1}^2 / 3) inter(q, k_1, d_1) + b_1 \exp(-q^2 r_{g2}^2 / 3) \left( \left( \text{Erf}(q r_{g1} / \sqrt{6}) \right)^3 / q \right)^{p1} inter(q, k_1, d_1) + \\ + g_2 \exp(-q^2 r_{g2}^2 / 3) inter(q, k_2, d_2) + b_2 \exp(-q^2 r_{g2}^2 / 3) \left( \left( \text{Erf}(q r_{g2} / \sqrt{6}) \right)^3 / q \right)^{p2} inter(q, k_2, d_2)$$

where  $g_1$ ,  $b_1$ ,  $g_2$ ,  $b_2$  are parameters originating from the intensity of the beam.

Fitting was carefully performed in an iterative way due to the high number of parameters: In a first step, the intensity values were fitted with only the set of parameters for the particles in the high and the low  $q$ -range, respectively, to find appropriate starting values. In a second step, the intensity within the complete  $q$ -range was fitted with both distributions using the fitted values from the first step as starting values.

## 6.2.17 Transmission Electron Microscopy

Transmission electron microscope (TEM) measurements were performed by Thomas Koch and Michael Stöger-Pollach on a FEI Tecnai F20 field emission gun transmission electron microscope (USTEM, Vienna University of Technology). Samples were cut from polymer pieces on a Reichert Ultracut-E ultramicrotome at room temperature using a diamond knife. Investigations were done in TEM and scanning TEM (STEM) mode [202].

TEM uses a wide beam of electrons passing through a thin sliced specimen to form an image. This microscope is analogous to a standard upright or inverted light microscope. Stained areas of the sample absorb or scatter the beam, producing dark spots, unstained areas appear light.

STEM uses a focused beam of electrons scanning through the specimen to form an image. Images are produced as in scanning electron microscopy one spot a time. Stained areas of the sample produce light spots in the image, unstained areas remain dark.

## 6.3 Synthesis of Zirconium Oxo Clusters

### 6.3.1 Synthesis of $\text{Zr}_6\text{O}_4(\text{OH})_4(\text{OIsob})_{12}(\text{H}_2\text{O}) \cdot 3\text{HOIsob}$

An amount of 1.717 g (19.5 mmol) of isobutyric acid was added dropwise to 1.364 g (2.84 mmol) of  $\text{Zr}(\text{O}i\text{Bu})_4$  (80 % solution in  $\text{BuOH}$ ) under stirring in a Schlenk tube. After 4 weeks at room temperature, colourless crystals were isolated by decanting the mother liquid and drying *in vacuo*.

**Yield:** 0.351 g (37 %),  $M = 2006.9$

**Elemental analysis** found (calc.): C, 35.65 (35.91); H, 5.45 (5.73);  $\text{ZrO}_2$ , 37.21 (36.84) %

For **NMR** measurements, the solvate molecules were removed as follows: The compound was dissolved in  $\text{CH}_2\text{Cl}_2$ , and all volatiles were removed *in vacuo*. This process was repeated with toluene and once more with  $\text{CH}_2\text{Cl}_2$  as the solvent. The obtained solid was dried at room temperature at  $\sim 10^{-7}$  bar. (Table 4, p.19)

**FTIR** (ATR):  $\nu = 3266$  (w, br, OH), 2970 (m, CH), 2931 (w, CH), 2908 (sh, CH), 2872 (w, CH), 1584 (s,  $\text{COO}^-_{\text{as}}$ ), 1553 (s,  $\text{COO}^-_{\text{as}}$ ), 1473 (s,  $\text{COO}^-_{\text{sy}}$ ), 1427 (s,  $\text{COO}^-_{\text{sy}}$ ), 1376 (m), 1360 (w), 1303 (sh), 1292 (m), 1260 (w), 1213 (w), 1169 (w), 1096 (m), 1074 (w), 965 (w), 930 (w), 911 (w), 865 (w), 839 (w), 797 (w), 765 (w), 725 (w), 705 (w), 671 (sh), 641 (s, OCO)  $\text{cm}^{-1}$ .

### 6.3.2 Synthesis of $\text{Zr}_6\text{O}_4(\text{OH})_4(\text{OMc})_8(\text{OIsob})_4(\text{BuOH}) \cdot 4\text{HOOCR}$

An amount of 0.598 g (6.95 mmol) of methacrylic acid and 0.571 g (6.48 mmol) of isobutyric acid was added dropwise to 0.931 g (1.94 mmol) of  $\text{Zr}(\text{O}i\text{Bu})_4$  (80 % in  $\text{BuOH}$ ) under stirring in a Schlenk tube. After 1 week at room temperature, colourless crystals were isolated by decanting the mother liquid and drying *in vacuo*.

**Yield:** 0.629 g (91 %).  $M = 2129.6$  (calculated by setting the solvate ratio, methacrylic / isobutyric acid 2 : 1).

**Elemental analysis** found (calc.): C, 36.33 (38.30); H, 5.59 (5.20);  $\text{ZrO}_2$ , 35.50 (34.70) %

For **NMR** measurements, the solvate molecules were removed as described for **Zr6-Isob**. The obtained solid was dried at room temperature at  $\sim 10^{-7}$  bar. (Table 7, p.23)

**FTIR** (ATR):  $\nu$  = 3244 (w, br, OH), 2975 (w, CH), 2959 (sh, CH), 2927 (w, CH), 2906 (sh, CH), 2873 (w, CH), 1698 (m, C=O), 1644 (w, C=C), 1579 (s,  $\text{COO}^-_{\text{as}}$ ), 1553 (m,  $\text{COO}^-_{\text{as}}$ ), 1456 (m,  $\text{COO}^-_{\text{sy}}$ ), 1419 (s,  $\text{COO}^-_{\text{sy}}$ ), 1372 (m), 1333 (w), 1298 (sh), 1286 (sh), 1244 (m, COOH), 1205 (m), 1186 (vw), 1170 (m), 1098 (m), 1069 (w), 1006 (m), 978 (w, br), 946 (sh), 936 (m,  $=\text{CH}_2$ ), 882 (w), 865 (w), 852 (w), 825 (s), 794 (w), 781 (w), 764 (w), 689 (sh), 653 (s, OCO), 615 (s)  $\text{cm}^{-1}$ .

### 6.3.3 Synthesis of $\text{Zr}_6\text{O}_4(\text{OH})_4(5\text{-norbornene-2-carboxylate})_{12}$

#### Synthesis of $\text{Zr}_6\text{O}_4(\text{OH})_4(\text{ONorb}_{\text{mix}}) \cdot 3\text{HONorb}_{\text{mix}}$

An endo/exo - isomeric mixture of 5-norbornene-2-carboxylic acid (81 % endo, 19 % exo) was liquefied by warming to 35 °C and vigorous stirring. 1.710 g (12.38 mmol) of this mixture was added to 0.849 g (1.77 mmol) of  $\text{Zr}(\text{OBu})_4$  (80 % in BuOH) under stirring. After three weeks at room temperature, colourless crystals were obtained. The crystals were separated from the mother liquid by decanting, washed three times with 3 ml of n-heptane each, and dried at  $\sim 10^{-7}$  bar.

**Yield:** 0.809 g (100 %),  $M = 2739.8$

**Elemental analysis** found (calc.): C, 52.88 (52.61); H, 5.25 (5.08);  $\text{ZrO}_2$ , 27.33<sub>TGA</sub> (26.98) %.

For **NMR** measurements, the solvate acids were removed as follows: Crystalline cluster was dissolved in  $\text{CH}_2\text{Cl}_2$  and twice the volume of n-heptane was added to the solution. About 3/4 of the solvents were removed *in vacuo* until the cluster precipitated from the cold solution. After sedimentation, the less volatile solvent (n-heptane) was decanted and the solid was washed with n-heptane. This procedure was repeated once; the solid was then dried at  $10^{-7}$  bar. (Table 10, p.27)

**FTIR** (ATR):  $\nu$  = 3237 (w, br, OH), 2972 (w, CH), 2942 (w, CH), 2911 (sh, CH), 2872 (w, CH), 1708 (m, C=O), 1576 (s,  $\text{COO}^-_{\text{as}}$ ), 1545 (m,  $\text{COO}^-_{\text{as}}$ ), 1502 (m,  $\text{COO}^-_{\text{sy}}$ ), 1427 (s,  $\text{COO}^-_{\text{sy}}$ ), 1334 (m), 1302 (m), 1291 (m), 1269 (w), 1252 (w, COOH), 1223 (w), 1200 (m), 1178 (w), 1155 (w), 1130 (w), 1111 (w), 1096 (w), 1061 (w), 1027 (w), 989 (w), 968 (w), 954 (w), 944 (w), 925 (w), 907 (w), 875 (w), 854 (w), 840 (w), 815 (w), 777 (w), 737 (w), 708 (s), 697 (m), 676 (s, OCO), 652 (s, OCO), 601 (sh)  $\text{cm}^{-1}$ .



## Separation of endo- and exo-5-norbornene-2-carboxylic acid

Freshly cracked cyclopentadiene (20.6 g, 0.311 mol) and methyl acrylate (29.7 g, 0.345 mol) was dissolved in 30 ml of  $\text{CH}_2\text{Cl}_2$  and the solution was refluxed for 24 hours. The solvent was removed under reduced pressure and the resulting solid was dissolved in a sodium methoxide solution (5.4 g Na in 80 ml dry methanol). This solution was maintained at refluxing temperature for 5 hours and was allowed to cool to room temperature. Methanol was removed by concentration under reduced pressure and the resulting residue was dissolved in 60 ml of  $\text{H}_2\text{O}$ . This solution was heated to reflux for 6 hours to transform the methyl ester into the acid. The basic solution was cooled and extracted with diethyl ether (2 x 30ml) to remove dicyclopentadiene. The aqueous solution was acidified with diluted sulphuric acid to pH 2 and extracted with ether (4 x 25 ml). The combined ether extracts were washed with cold water (2 x 25 ml), dried with  $\text{Na}_2\text{SO}_4$  and then concentrated by means of a rotavapor.

**Yield:** 38.01 g (88.5 %); 74 % endo, 26 % exo

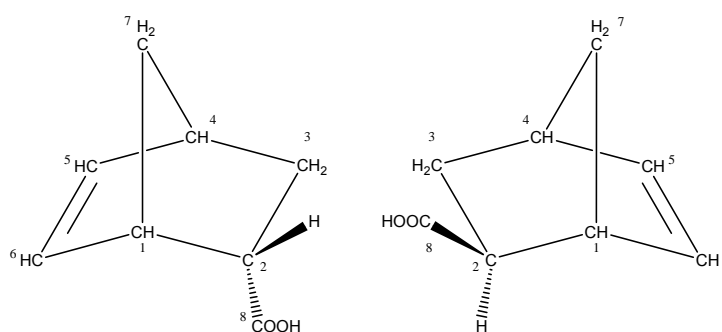


**Figure 108:** endo- (left) and exo- (right) 5-norbornene-2-carboxylic acid; the labelling is shown for NMR data

An iodolactonization reaction was carried out to separate the acid isomers. The acid mixture (32.1 g, 0.232 mol) was dissolved in a solution of sodium bicarbonate (30 g) in  $\text{H}_2\text{O}$  (500 ml). An addition funnel was attached, and a solution of iodine (33.6 g, 0.132 mol) and potassium iodide (70.9 g, 0.427 mol) in  $\text{H}_2\text{O}$  (200 ml) was added dropwise until a dark brown colour persisted. The solution was extracted with diethyl ether (5 x 250 ml) to remove the iodolactone.

The aqueous solution, containing the exo isomer, was decolourized with a 10 %  $\text{Na}_2\text{S}_2\text{O}_3$  solution (~70 ml) and adjusted to pH 2 with 1 N  $\text{H}_2\text{SO}_4$ . The resulting mixture was extracted with diethyl ether (5 x 150 ml), and the aqueous solution was readjusted to pH 2 after each extraction. The diethyl ether extracts were combined, dried with  $\text{Na}_2\text{SO}_4$  and then filtered over Cellite. The resulting filtrate was concentrated to afford a yellow crystalline solid. The yellow by-products were removed by recrystallization from cold n-pentane (~ -80 °C) twice.

**Yield:** 5.848 g (70 %)

**$^1\text{H-NMR}$**  ( $\text{CDCl}_3$ , 20 °C):  $\delta$  = 6.16 (dd,  $J_{\text{HH}} = 5.7$  Hz,  $J_{\text{HH}} = 2.9$  Hz, 1 H,  $H^6$ ), 6.12 (dd,  $^3J_{\text{HH}} = 5.7$  Hz,  $^3J_{\text{HH}} = 3.0$  Hz, 1H,  $H^5$ ), 3.10 (bs, 1H,  $H^4$ ), 3.02 (dt,  $^3J_{\text{HH}} = 9.3$  Hz,  $^3J_{\text{HH}} = 2.8$  Hz, 1H,  $H^2$ ), 2.93 (b, 1H,  $H^1$ ), 1.95 (m, 1H,  $H^3$ ), 1.53 (d,  $J_{\text{HH}} = 8.4$  Hz, 1H,  $H^7$ ), 1.45-1.35 (m, 2H,  $H^3$ ,  $H^7$ ) ppm.

**$^{13}\text{C}\{^1\text{H}\}\text{-NMR}$**  ( $\text{CDCl}_3$ , 20 °C):  $\delta$  = 182.6 ( $\text{C}^8$ ), 138.0 ( $\text{C}^6$ ), 135.6 ( $\text{C}^5$ ), 46.5 ( $\text{C}^4$ ), 46.2 ( $\text{C}^7$ ), 43.0 ( $\text{C}^2$ ), 41.6 ( $\text{C}^1$ ), 30.2 ( $\text{C}^3$ ) ppm.

**FTIR** (ATR):  $\nu$  = 3061 (m, CH), 2977 (m, CH), 2954 (m, CH), 2878 (m, CH), 2834 (sh, CH), 2739 (w), 2662 (w), 2618 (w), 2570 (w), 2541 (w), 1695 (vs, C=O), 1573 (w), 1463 (w), 1447 (w), 1416 (m), 1336 (m), 1289 (m), 1280 (m), 1266 (w), 1242 (s, COOH), 1216 (s), 1181 (w), 1148 (w), 1116 (w), 1101 (w), 1074 (w), 1033 (w), 1022 (w), 1003 (w.), 930 (m), 902 (m), 861 (m), 845 (w), 813 (w), 786 (w), 714 (s, OCO), 677 (m)  $\text{cm}^{-1}$ .

To regenerate the endo isomer, the ether was removed under reduced pressure and the lactone was dissolved in 70 ml of EtOH followed by a slow addition of 10.5 g (0.161 mol) of Zn-dust. The mixture was stirred and heated slowly to 65 °C for 3 hours. Afterwards it was hot filtered and the Zn cake was washed with ethanol. The filtrate was then concentrated to about 20 ml, and 25 ml of diethyl ether was added followed by 50 ml of water containing 2.5 ml of concentrated hydrochloric acid. The ether layer was separated, washed with water and dried over  $\text{MgSO}_4$ . The ether extract was concentrated under reduced pressure and then cooled to 4 °C. A crystalline, slightly yellowish product was obtained which was recrystallized from cold n-pentane ( $\sim -80$  °C) twice.

**Yield:** 8.131 g (34.2 %)

**$^1\text{H-NMR}$**  ( $\text{CDCl}_3$ , 20 °C):  $\delta$  = 6.23 (dd,  $J_{\text{HH}} = 5.7$  Hz,  $J_{\text{HH}} = 5.7$  Hz, 1 H,  $H^6$ ), 6.02 (dd,  $^3J_{\text{HH}} = 5.7$  Hz,  $^3J_{\text{HH}} = 2.8$  Hz, 1H,  $H^5$ ), 3.26 (bs, 1H,  $H^4$ ), 3.02 (dt,  $^3J_{\text{HH}} = 9.3$  Hz,  $^3J_{\text{HH}} = 2.8$  Hz, 1H,  $H^2$ ), 2.94 (b, 1H,  $H^1$ ), 1.94 (ddd, 1H,  $^3J_{\text{HH}} = 11.7$  Hz,  $^3J_{\text{HH}} = 9.3$  Hz,  $^3J_{\text{HH}} = 3.7$  Hz, 1H,  $H^7$ ), 1.43-1.51 (m, 1H,  $H^3$ ), 1.38-1.47 (m, 1H,  $H^7$ ), 1.27-1.35 (m, 1H,  $H^3$ ) ppm.

**$^{13}\text{C}\{^1\text{H}\}\text{-NMR}$**  ( $\text{CDCl}_3$ , 20 °C):  $\delta$  = 180.9 ( $\text{C}^8$ ), 137.8 ( $\text{C}^6$ ), 132.2 ( $\text{C}^5$ ), 49.8 ( $\text{C}^3$ ), 45.7 ( $\text{C}^4$ ), 43.2 ( $\text{C}^2$ ), 42.5 ( $\text{C}^1$ ), 29.1 ( $\text{C}^7$ ) ppm.

**FTIR** (ATR):  $\nu$  = 3063 (m, CH), 2976 (w, CH), 2963 (m, CH), 2947 (sh, CH), 2911 (m, CH), 2882 (w, CH), 2869 (w, CH), 2828 (sh, CH), 2736 (w), 2627 (w), 2544 (w), 1695 (s, C=O), 1625 (w, C=C), 1571 (w), 1524 (m), 1445 (sh), 1420 (m), 1335 (m), 1299 (w), 1277 (m), 1255 (w, COOH), 1233 (m), 1223 (m), 1183 (sh), 1156 (w), 1132 (m), 1112 (w), 1090 (w), 1061 (w), 1021 (w), 989 (w.), 936 (sh), 912 (m), 839 (m), 827 (w), 814 (w), 778 (m), 745 (m), 707 (vs, CH), 674 (m, OCO)  $\text{cm}^{-1}$ .

### Synthesis of $\text{Zr}_6\text{O}_4(\text{OH})_4(\text{ONorb}_{\text{endo}}) \cdot 3\text{HONorb}_{\text{endo}}$

An amount of 0.636 g (4.60 mmol) of endo-5-norbornene-2-carboxylic acid was dissolved in 5 ml of n-heptane. To this solution an amount of 0.32 ml (667  $\mu\text{mol}$ ) of  $\text{Zr}(\text{O}i\text{Bu})_4$  (80 % in BuOH) was added dropwise. After one week at room temperature, colourless crystals were formed. These were separated from the mother liquid by decanting, washed three times with 3 ml of n-heptane each and dried *in vacuo* ( $10^{-7}$  bar).

**Yield:** 0.304 g (99.8 %),  $M = 2739.8$

**Elemental analysis** found (calc.): C, 52.69 (52.61); H, 5.13 (5.08);  $\text{ZrO}_2$ , 26.71<sub>TGA</sub> (26.98) %.

For **NMR** measurements, the solvate acids were removed by a precipitation procedure as described above for **Zr6-Norb<sub>mix</sub>**. (Table 13, p.31)

**FTIR** (ATR):  $\nu = 3244$  (w, br, OH), 3058 (w, CH), 2972 (m, CH), 2936 (w, CH), 2915 (sh, CH), 2873 (w, CH), 1710 (m, C=O), 1597 (w), 1576 (s,  $\text{COO}^-_{\text{as}}$ ), 1544 (m,  $\text{COO}^-_{\text{as}}$ ), 1502 (w,  $\text{COO}^-_{\text{sy}}$ ), 1494 (w), 1475 (m), 1461 (sh), 1434 (vs,  $\text{COO}^-_{\text{sy}}$ ), 1378 (w), 1361 (w), 1335 (m), 1303 (m), 1290 (m), 1268 (w), 1252 (w, COOH), 1223 (w), 1200 (m), 1176 (w), 1165 (w), 1152 (w), 1130 (m), 1114 (sh), 1097 (w), 1061 (w), 1011 (m), 967 (vw), 954 (w), 944 (w), 926 (w), 907 (w), 856 (w), 840 (m), 815 (w), 777 (m), 733 (sh), 712 (s), 698 (m), 676 (m, OCO), 671 (sh), 652 (s, OCO)  $\text{cm}^{-1}$ .

### Synthesis of $\text{Zr}_6\text{O}_4(\text{OH})_4(\text{ONorb}_{\text{exo}})_{12}(\text{BuOH}) \cdot 3\text{HONorb}_{\text{exo}}$

An amount of 0.626 g (4.53 mmol) of exo-5-norbornene-2-carboxylic acid was dissolved in 4 ml of n-heptane. To this solution an amount of 0.31 ml (646  $\mu\text{mol}$ ) of  $\text{Zr}(\text{O}i\text{Bu})_4$  (80 % in BuOH) was added dropwise. After 10 days at room temperature, colourless crystals were formed. These were separated from the mother liquid by decanting, washed three times with 3 ml of n-heptane each and dried *in vacuo* ( $10^{-7}$  bar).

**Yield:** 0.215 g (71.0 %),  $M = 2813.9$

**Elemental analysis** found (calc.): C, 53.15 (52.93); H, 5.25 (5.30);  $\text{ZrO}_2$ , 25.25 (26.27) %.

For **NMR** measurements, the solvate acids were removed by an precipitation procedure as described above for **Zr6-Norb<sub>mix</sub>**. (Table 16, p.34)

**FTIR** (ATR):  $\nu = 3238$  (w, br, OH), 3058 (w, CH), 2973 (m, CH), 2950 (w, CH), 2874 (w, CH), 1703 (m, C=O), 1577 (s,  $\text{COO}^-_{\text{as}}$ ), 1547 (m,  $\text{COO}^-_{\text{as}}$ ), 1504 (sh,  $\text{COO}^-_{\text{sy}}$ ), 1455 (sh), 1419 (vs,  $\text{COO}^-_{\text{sy}}$ ), 1333 (m), 1306 (m), 1283 (m), 1268 (w), 1252 (w, COOH), 1233 (sh), 1222 (w), 1199 (w), 1180 (sh), 1156 (w), 1139 (sh), 1114 (sh), 1098 (w), 1064 (vw), 1036 (m),

1020 (w), 1001 (w), 975 (w), 945 (w), 930 (w), 904 (m), 874 (w), 861 (m), 842 (w), 818 (vw), 796 (sh), 782 (m), 758 (m), 713 (s), 701 (w), 691 (w), 679 (m, OCO), 672 (w), 667 (vw), 644 (vs, OCO)  $\text{cm}^{-1}$ .

### Reaction of $\text{Zr}_6\text{O}_4(\text{OH})_4(\text{OMc})_{12}$ with Cyclopentadiene

An amount of 0.218 g (128  $\mu\text{mol}$ ) of **Zr6** was dissolved in 6 ml of  $\text{CH}_2\text{Cl}_2$ , and 50  $\mu\text{l}$  (0.61 mmol) of freshly cracked cyclopentadiene was added. The solution was heated to reflux for 24 hours and the solvent was removed under reduced pressure. Formed dicyclopentadiene was removed by a precipitation procedure: The product was dissolved in 2 ml of  $\text{CH}_2\text{Cl}_2$  and 3 ml of n-heptane was added. The mixture was concentrated under reduced pressure until a white solid precipitated from the solution. This procedure was repeated once, and the solid was washed with n-heptane. The product was then dried at  $10^{-7}$  bar.

### Reaction of $\text{Zr}_6\text{O}_4(\text{OH})_4(\text{OMc})_{12}$ with 2,3-Dimethyl Butadiene

An amount of 0.239 g (0.14 mmol) of **Zr6** was dissolved in 5 ml of benzene. After addition of 190  $\mu\text{l}$  (1.68 mmol) of 2,3-dimethyl butadiene, the solution was refluxed for 40 hours. After 1 hour, a precipitate was formed which was not soluble in n-heptane after the reaction time.

### 6.3.4 Synthesis of $\text{Zr}_{12}\text{O}_8(\text{OH})_8(\text{OVinac}) \cdot 6\text{HOVinac}$

An amount of 0.996 g (11.22 mmol) of vinylacetic acid was added dropwise to an amount of 0.776 g (1.62 mmol) of  $\text{Zr}(\text{OBu})_4$  (80 % in BuOH). After 5 minutes reaction time, a micro-crystalline precipitate was obtained which formed colourless crystals within two days. After decantation of the mother liquid, the crystals were washed twice with 2 ml of n-heptane each and dried at  $10^{-7}$  bar.

**Yield:** 0.332 g (63 %),  $M = 3917.2$

**Elemental analysis** found (calc.): C, 36.54 (36.79); H, 4.06 (4.22);  $\text{ZrO}_2$ , 38.39<sub>TGA</sub> (37.75) %.

For **NMR** measurements, the solvate molecules were removed as follows: The compound was dissolved in  $\text{CH}_2\text{Cl}_2$  and all volatiles were removed *in vacuo*. This process was repeated with

toluene and once more with  $\text{CH}_2\text{Cl}_2$  as the solvent. The obtained solid was then dried at room temperature at  $\sim 10^{-7}$  bar. (Table 19, p.39)

**FTIR** (ATR):  $\nu = 3396$  (w, -OH), 3080 (w, CH), 3020 (w, CH), 2982 (w, CH), 1711 (m, C=O), 1641 (w, C=C), 1603 (m,  $\text{COO}^-_{\text{as}}$ ), 1547 (sh,  $\text{COO}^-_{\text{as}}$ ), 1537 (s,  $\text{COO}^-_{\text{as}}$ ), 1436 (s,  $\text{COO}^-_{\text{s}}$ ), 1417 (s,  $\text{COO}^-_{\text{s}}$ ), 1392 (s,  $\text{COO}^-_{\text{s}}$ ), 1314 (w), 1295 (w), 1268 (m), 1199 (m), 1121 (w), 994 (m), 914 (m, C=C), 893 (sh), 811 (m), 782 (sh), 762 (w), 724 (m, CH), 676 (sh), 627 (s, OCO)  $\text{cm}^{-1}$ .

### 6.3.5 Synthesis of $\text{Zr}_{12}\text{O}_8(\text{OH})_8(\text{OMc})_8(\text{OAc})_{16} \cdot 6\text{HOAc}$

An amount of 0.239 g (2.78 mmol) of methacrylic acid and 0.423 g (7.04 mmol) of acetic acid was added successively to 0.945g (1.97 mmol) of  $\text{Zr}(\text{O}i\text{Bu})_4$  (80 % solution in BuOH) under stirring. After 12 hours at room temperature, colourless needles were formed. The crystals were washed two times with 1 ml of n-heptane each and dried at  $10^{-7}$  bar.

**Yield:** 0.540 g (98 %),  $M = 3344.3$

**Elemental analysis** found (calc.): C, 30.84 (27.30); H, 3.76 (3.62);  $\text{ZrO}_2$ , 41.07 (44.21) %.

For **NMR** measurements, the solvate molecules were removed as described above for the **Zr12-Vinac** cluster. (Table 22, p.43)

**FTIR** (ATR):  $\nu = 3221$  (w, -OH), 2980 (vw, CH), 2956 (vw, CH), 2927 (vw, CH), 2875 (vw, CH), 1711 (m, C=O), 1643 (w, C=C), 1595 (sh), 1547 (s,  $\text{COO}^-_{\text{as}}$ ), 1448 (sh), 1422 (s,  $\text{COO}^-_{\text{s}}$ ), 1373 (m,  $\text{COO}^-_{\text{s}}$ ), 1344 (w), 1298 (w), 1245 (s), 1207 (sh), 1179 (w), 1047 (w), 1029 (w), 1007 (w), 937 (w), 902 (w), 883 (w), 852 (w), 827 (m), 798 (m), 674 (sh), 644 (vs, OCO), 631 (sh), 612 (vs, OCO)  $\text{cm}^{-1}$ .

## 6.4 Zirconium Oxo Clusters in Solution

### 6.4.1 $\text{Zr}_4\text{O}_2(\text{OMc})_{12}$

#### Preparation of $\text{Zr}_4\text{O}_2(\text{OMc})_{12}$

$\text{Zr}_4\text{O}_2(\text{OMc})_{12}$  was prepared as reported by reacting 7 equivalents of methacrylic acid with 1 equivalent of  $\text{Zr}(\text{OBu})_4$  (80 % solution in BuOH). The occurrence of gelation instead of crystallization could be reduced by cooling the flask to 0 °C while adding the methacrylic acid dropwise. Another possibility to avoid gelation was the addition of n-heptane to the starting solution:

To a solution of 5.322 g (11.10 mmol) of  $\text{Zr}(\text{OBu})_4$  (80 % solution in BuOH) in 5 ml of n-heptane an amount of 7.031 g (81.67 mmol) of methacrylic acid was added. After three days at room temperature, the crystals were separated from the mother liquid by decanting. The crystals were washed two times with 3 ml of n-heptane each and then dried at  $10^{-7}$  bar.

**Yield:** 3.89 g (99.0 %)

#### Recrystallization of $\text{Zr}_4\text{O}_2(\text{OMc})_{12}$

0.227 g (160  $\mu\text{mol}$ ) of **Zr4** was dissolved in 4 ml of benzene at refluxing temperature. After addition of 0.5 ml of triethylamine, the solution was allowed to cool to room temperature slowly, afterwards the flask was stored at 5 °C. Colourless crystals of the type  $\text{Zr}_4\text{O}_2(\text{OMc})_{12} \cdot \text{C}_6\text{H}_6$  were obtained after 24 hours. They were separated from the mother liquid by decanting, washed twice with 1 ml of n-heptane each and dried at  $10^{-7}$  bar. By concentrating the mother liquid *in vacuo* and once again storing at 5 °C, additional crystals were obtained. However, NMR measurements revealed impurities. Thus, they were not considered in the overall yield.

**Yield:** 0.099 g (43.7 %)

**Elemental analysis** found (calc.): C, 42.95 (43.36); H, 4.42 (4.41);  $\text{ZrO}_2$ , 33.65 (32.95) %.

For **NMR** measurements, the solvate molecules were removed by dissolving the cluster in  $\text{CH}_2\text{Cl}_2$  and drying *in vacuo*.

**FTIR** (ATR):  $\nu$  = 2992 (w, CH), 2980 (w, CH), 2957 (w, CH), 2926 (w, CH), 1702 (w, C=O), 1644 (m, C=C), 1593 (sh), 1574 (m, COO<sup>-</sup><sub>as.</sub>), 1512 (w), 1501 (w), 1481 (w), 1458 (w), 1417 (vs, COO<sup>-</sup><sub>s</sub>), 1372 (m, COO<sup>-</sup><sub>s</sub>), 1245 (s), 1210 (sh), 1171 (sh), 1099 (w), 1040 (w), 1008 (m), 944 (s), 879 (m), 854 (w), 825 (s), 807 (sh), 697 (m), 654 (m), 613 (sh), 599 (s, CH) cm<sup>-1</sup>.

### Titration of Zr<sub>4</sub>O<sub>2</sub>(OMc)<sub>12</sub> with Water

An amount of 4.3 mg (3  $\mu$ mol) of **Zr4** cluster was dissolved in 0.5 ml of CD<sub>2</sub>Cl<sub>2</sub> in an NMR tube in the glove box. For titrations, CD<sub>2</sub>Cl<sub>2</sub> was saturated with water at room temperature (solubility: 1.32 %,  $\rho$  = 1.3168 g/ml) and 2.7  $\mu$ l (approximating 1.5  $\mu$ mol of H<sub>2</sub>O) was added to the **Zr4** solution. A <sup>1</sup>H spectrum was recorded immediately. This procedure was repeated five times until the solution contained three equivalents of water and a white precipitate was observed (ZrO<sub>2</sub>).

### 6.4.2 Zr<sub>6</sub>O<sub>4</sub>(OH)<sub>4</sub>(OMc)<sub>12</sub>

#### Preparation of Zr<sub>6</sub>O<sub>4</sub>(OH)<sub>4</sub>(OMc)<sub>12</sub>

Zr<sub>6</sub>O<sub>4</sub>(OH)<sub>4</sub>(OMc)<sub>12</sub> was prepared as reported by reacting 3.5 equivalents of methacrylic acid with 1 equivalent of Zr(OBu)<sub>4</sub> (80 % solution in butanol). The occurrence of gelation instead of crystallization could be reduced by cooling the flask to 0 °C while adding the methacrylic acid dropwise.

For **NMR** measurements, the solvate molecules were removed as follows: The compound was dissolved in CH<sub>2</sub>Cl<sub>2</sub> and all volatiles were removed *in vacuo*. This process was repeated with toluene and once more with CH<sub>2</sub>Cl<sub>2</sub> as the solvents. The obtained solid was dried at room temperature at  $\sim 10^{-7}$  bar.

**FTIR** (ATR):  $\nu$  = 3210 (br, w, OH), 2975 (w, CH), 2959 (w, CH), 2927 (w, CH), 2876 (w, CH), 1698 (w, C=O), 1643 (m, C=C), 1575 (m, COO<sup>-</sup><sub>as.</sub>), 1549 (m), 1521 (w), 1497 (w), 1458 (m), 1418 (s, COO<sup>-</sup><sub>s</sub>), 1398 (sh), 1372 (m, COO<sup>-</sup><sub>s</sub>), 1291 (w), 1244 (m), 1205 (w), 1190 (w), 1112 (w), 1072 (w), 1037 (w), 1006 (m), 987 (w), 933 (m), 883 (w), 851 (w), 825 (m), 796 (w), 777 (w), 685 (m), 662 (m), 636 (m), 615 (s, CH) cm<sup>-1</sup>.

## Reaction of $\text{Zr}_6\text{O}_4(\text{OH})_4(\text{OMc})_{12}$ with Ethyl Acetate

An amount of 0.473 g (278  $\mu\text{mol}$ ) of **Zr6** was dissolved in 3 ml of  $\text{CHCl}_3$ . 3 ml of ethyl acetate (30.5 mmol) was added to the solution which was then heated to reflux for 1 hour. After cooling to room temperature, the volatiles were removed under reduced pressure, and the solid was dried at  $10^{-7}$  bar.

### 6.4.3 $\text{Zr}_{12}\text{O}_8(\text{OH})_8(\text{OProp})_{24}$

$\text{Zr}_{12}\text{O}_8(\text{OH})_8(\text{OProp})_{24}$  was prepared as reported by reacting 10 equivalents of propionic acid with 1 equivalent of  $\text{Zr}(\text{OBu})_4$  (80 % solution in butanol).

For **NMR** measurements, the solvate molecules were removed as follows: The compound was dissolved in  $\text{CH}_2\text{Cl}_2$  and all volatiles were removed *in vacuo*. This process was repeated with toluene and once more with  $\text{CH}_2\text{Cl}_2$  as the solvents. The obtained solid was dried at room temperature at  $\sim 10^{-7}$  bar.

## 6.5 Considerations about Cluster Formation

### 6.5.1 Deuteration of Methacrylic Acid

To an amount of 10 ml of methacrylic acid 3 ml of  $\text{D}_2\text{O}$  were added in a separation funnel. After intimate mixing, phase separation was forced by the addition of a spatula tip of NaCl. This procedure was repeated with 2 ml of  $\text{D}_2\text{O}$ . After that, the organic phase was dried with  $\text{CaCl}_2$  at 5 °C over night, filtrated with Cellite and distilled under reduced pressure. Judging from NMR spectra, the deuteration degree was  $\sim 80\%$ .

### 6.5.2 Synthesis of $\text{Zr}(\text{isoeugenolate})_4$

To an amount of 1.272 g (2.65 mmol) of  $\text{Zr}(\text{OBu})_4$  (80 % in BuOH) 3.05 g (20.15 mmol) of isoeugenol (mixture of 9 % syn, 91 % anti isomer) was added dropwise. After 1 week at room temperature colourless crystals were formed.



## 6.6 Synthesis of Titanium Oxo Clusters

### 6.6.1 Synthesis of $\text{Ti}_6\text{O}_4(\text{OPr})_8(\text{ONorb}_{\text{mix}})_8$

An endo/exo - isomeric mixture of 5-norbornene-2-carboxylic acid was liquefied by warming to 35 °C and stirring. An amount of 1.021 g (7.39 mmol) of this mixture was added dropwise to a solution of 0.494 g (1.74 mmol) of  $\text{Ti}(\text{OPr})_4$  in 0.5 ml of propanol. After 2 weeks at room temperature, slightly yellowish crystals were obtained. The crystals were washed twice with 2 ml of cold n-heptane (-80 °C) each and then dried at  $10^{-7}$  bar.

**Yield:** 0.411 g (73.8 %),  $M = 1921.2$

**Elemental analysis** found (calc.): C, 55.06 (55.02); H, 6.58 (6.72);  $\text{ZrO}_2$ , 27.06<sub>TGA</sub> (24.94) %.

**FTIR** (ATR):  $\nu = 3059$  (w, CH), 2964 (m, CH), 2937 (w, CH), 2873 (m, CH), 2847 (w, CH), 1558 (vs,  $\text{COO}^-_{\text{as}}$ ), 1541 (s,  $\text{COO}^-_{\text{as}}$ ), 1434 (s,  $\text{COO}^-_{\text{sy}}$ ), 1407 (s,  $\text{COO}^-_{\text{sy}}$ ), 1379 (sh), 1359 (sh), 1335 (m), 1299 (m), 1289 (m), 1265 (w), 1256 (w, COOH), 1224 (w), 1122 (s), 1076 (s), 1025 (w), 995 (s), 953 (w), 945 (w), 923 (w), 905 (w), 889 (w), 861 (w), 840 (m), 783 (s, Ti-O-Ti), 710 (s), 692 (s, Ti-O-Ti), 680 (sh, OCO), 664 (vs)  $\text{cm}^{-1}$ .

### 6.6.2 Synthesis of $\text{Ti}_6\text{O}_4(\text{OEt})_8(\text{OIsob})_8$

An amount of 0.525 g (2.30 mmol) of  $\text{Ti}(\text{OEt})_4$  was added to a solution of 0.474 g (5.39 mmol) of isobutyric acid in 0.5 ml of ethanol under stirring. After two weeks at room temperature, colourless crystals were obtained which were separated from the mother liquid by decanting, washed twice with 2 ml of cold n-heptane (~ 80 °C) each and then dried at  $10^{-7}$  bar.

**Yield:** 0.255 g (47.2 %),  $M = 1408.6$

**Elemental analysis** found (calc.): C, 41.06 (40.93); H, 6.64 (6.87);  $\text{TiO}_2$ , 37.78<sub>TGA</sub> (34.03) %.

**FTIR** (ATR):  $\nu = 2970$  (m, CH), 2928 (w, CH), 2872 (w, CH), 2859 (w, CH), 1592 (sh,  $\text{COO}^-_{\text{as}}$ ), 1568 (m,  $\text{COO}^-_{\text{as}}$ ), 1547 (m,  $\text{COO}^-_{\text{s}}$ ), 1504 (w), 1495 (w), 1472 (m,  $\text{COO}^-_{\text{s}}$ ), 1455 (w), 1430 (m,  $\text{COO}^-_{\text{s}}$ ), 1414 (m,  $\text{COO}^-_{\text{s}}$ ), 1374 (m), 1362 (m), 1352 (sh), 1297 (m), 1280 (m), 1169 (sh), 1146 (sh), 1117 (sh), 1097 (s), 1065 (s), 1054 (w), 1002 (w), 961 (w), 925 (sh), 918 (w), 902 (w), 840 (w), 786 (s, Ti-O-Ti), 686 (m), 653 (m), 578 (vs)  $\text{cm}^{-1}$ .

### 6.6.3 Synthesis of $\text{Ti}_6\text{O}_4(\text{OPr})_8(\text{Olsob})_8$

An amount of 0.421 g (1.48 mmol) of  $\text{Ti}(\text{OPr})_4$  was added to a solution of 0.316 g (3.59 mmol) of isobutyric acid in 0.5 ml of propanol under stirring. After 10 days at room temperature, colourless crystals were obtained which were separated from the mother liquid by decanting, washed twice with 2 ml of cold n-heptane ( $\sim 80^\circ\text{C}$ ) each and then dried at  $10^{-7}$  bar.

**Yield:** 0.338 g (90.0 %),  $M = 1520.8$

**Elemental analysis** found (calc.): C, 43.57 (44.23); H, 6.95 (7.42);  $\text{TiO}_2$ , 34.87<sub>TGA</sub> (31.51) %.

**FTIR** (ATR):  $\nu = 2965$  (m, CH), 2928 (m, CH), 2874 (w, CH), 2850 (w, CH), 1596 (sh,  $\text{COO}^-_{\text{as}}$ ), 1565 (m,  $\text{COO}^-_{\text{as}}$ ), 1548 (m,  $\text{COO}^-_{\text{s}}$ ), 1472 (m,  $\text{COO}^-_{\text{s}}$ ), 1429 (m), 1417 (m,  $\text{COO}^-_{\text{s}}$ ), 1376 (m), 1361 (w), 1304 (w), 1285 (m), 1247 (w), 1172 (w), 1142 (sh), 1112 (sh), 1098 (m), 1077 (m), 1060 (m), 1019 (sh), 1001 (m), 966 (w), 933 (w), 889 (w), 863 (w), 841 (w), 778 (s, Ti-O-Ti), 688 (m), 650 (m), 613 (w), 579 (vs)  $\text{cm}^{-1}$ .

### 6.6.4 Synthesis of $\text{Ti}_6\text{O}_6(\text{O}^i\text{Pr})_6(\text{Olsob})_6$

An amount of 0.507 g (1.78 mmol) of  $\text{Ti}(\text{O}^i\text{Pr})_4$  was added to a solution of 0.355 g (4.03 mmol) of isobutyric acid in 0.5 ml of isopropanol under stirring. After three weeks at room temperature, colourless crystals were obtained which were separated from the mother liquid by decanting, washed twice with 2 ml of cold n-heptane ( $\sim -80^\circ\text{C}$ ) each and then dried at  $10^{-7}$  bar.

**Yield:** 0.195 g (52.0 %),  $M = 1260.4$

**Elemental analysis** found (calc.): C, 39.83 (40.02); H, 6.42 (6.71);  $\text{TiO}_2$ , 36.77<sub>TGA</sub> (38.03) %.

**FTIR** (ATR):  $\nu = 2970$  (m, CH), 2931 (m, CH), 2916 (sh, CH), 2872 (w, CH), 1593 (m,  $\text{COO}^-_{\text{as}}$ ), 1539 (m,  $\text{COO}^-_{\text{as}}$ ), 1474 (m,  $\text{COO}^-_{\text{s}}$ ), 1436 (m,  $\text{COO}^-_{\text{s}}$ ), 1376 (m), 1362 (m), 1328 (w), 1303 (m), 1290 (w), 1247 (w), 1127 (s), 1098 (m), 1005 (br, s), 933 (sh), 854 (m), 721 (s, Ti-O-Ti), 650 (sh), 619 (s), 597 (s), 573 (s)  $\text{cm}^{-1}$ .

### 6.6.5 Synthesis of $\text{Ti}_2(\text{OPr})_6(\text{isoeugenolate})_2$

An amount of 376 mg (2.29 mmol) of isoeugenol (2-methoxy-4-propenylphenol, mixture of 9.4 % *syn* and 90.6 % *anti* isomers) was added dropwise to 788 mg (2.01 mmol) of  $\text{Ti}(\text{OPr})_4$  under

stirring. Orange-red crystals were obtained from the red solution after 10 days at room temperature. The crystals were isolated by decantation, washing with several portions of propanol at  $-70\text{ }^{\circ}\text{C}$  and drying at  $10^{-7}$  bar for 10 hours.

**Yield:** 0.295 g (38%),  $M = 776.7$

The labelling for NMR measurements is shown in Figure 109.

**$^1\text{H}$  NMR** ( $\text{CD}_2\text{Cl}_2$ ,  $20\text{ }^{\circ}\text{C}$ ):  $\delta = 6.93\text{--}6.78$  (m, 4 H,  $\text{Ar}^{3,5}$ ), 6.62 (d,  $J_{\text{HH}} = 8.1\text{ Hz}$ , 2 H,  $\text{Ar}^6$ ), 6.32 (dd,  $J_{\text{HH}} = 15.7\text{ Hz}$ ,  $J_{\text{HH}} = 1.6\text{ Hz}$ , 2 H,  $\text{H}^7$ ), 6.05 (dq,  $J_{\text{HH}} = 15.7\text{ Hz}$ ,  $J_{\text{HH}} = 6.5\text{ Hz}$ , 2 H,  $\text{H}^8$ ), 4.45 (t,  $J_{\text{HH}} = 6.6\text{ Hz}$ , 12 H,  $\text{OCH}_2$ ), 3.88 (s, 6 H,  $\text{CH}_3^{10}$ ), 1.86 (dd,  $J_{\text{HH}} = 6.5\text{ Hz}$ ,  $J_{\text{HH}} = 1.6\text{ Hz}$ , 6H,  $\text{CH}_3^9$ ), 1.70–1.51 (m, 12 H,  $\text{CH}_3\text{CH}_2$ ), 0.97–0.88 (m, 18H,  $\text{CH}_2\text{CH}_3$ ) ppm.

**$^{13}\text{C}\{^1\text{H}\}$  NMR** ( $\text{CD}_2\text{Cl}_2$ ,  $20\text{ }^{\circ}\text{C}$ ):  $\delta = 153.5$  ( $\text{C}^1$ ), 149.4 ( $\text{C}^2$ ), 130.8 ( $\text{C}^7$ ), 129.0 ( $\text{C}^4$ ), 122.7 ( $\text{C}^8$ ), 120.8 ( $\text{C}^3$ ), 114.1 ( $\text{C}^5$ ), 106.8 ( $\text{C}^6$ ), 80.0 ( $\text{OCH}_2$ ), 56.8 ( $\text{C}^{10}$ ), 26.4 ( $\text{CH}_3\text{CH}_2$ ), 18.1 ( $\text{C}^9$ ), 10.0 ( $\text{CH}_2\text{CH}_3$ ) ppm.

The signal at  $^1\text{H} / ^{13}\text{C} = 3.59$  (t,  $J_{\text{HH}} = 6.6\text{ Hz}$ ,  $\text{HOCH}_2$ ) / 64.4 ( $\text{HOCH}_2$ ) was assigned as non-coordinated propanol.

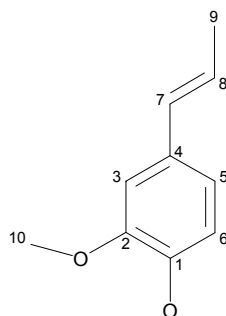


**Figure 109:** Labelling of the isoeugenolate ligand

## 6.7 Crystallographic Data

**Table 78:** Crystallographic and structural parameters of  $\text{Zr}_6\text{O}_4(\text{OH})_4(\text{OIsob})_{12}(\text{H}_2\text{O})\cdot 3\text{HOIsob}$  (**Zr6-Isob**) and  $\text{Zr}_6\text{O}_4(\text{OH})_4(\text{OMc})_8(\text{OIsob})_4(\text{BuOH})\cdot 4\text{RCOOH}$  (**Zr6-McIsob**)

|  | <b>Zr6-Isob</b>                                       | <b>Zr6-McIsob</b>                                     |
|--|---|---|
| Empirical formula  | $\text{C}_{60}\text{H}_{114}\text{O}_{39}\text{Zr}_6$ | $\text{C}_{68}\text{H}_{110}\text{O}_{41}\text{Zr}_6$ |
| Formula weight [ $\text{g}\cdot\text{mol}^{-1}$ ]              | 2006.9  | 2131.0 *  |
| Space group  | $P\bar{1}$  | Cc  |
| a [pm]   | 1377.31(8)  | 1191.26(10)   |
| b [pm]   | 1507.64(9)  | 1203.95(10)   |
| c [pm]   | 2277.28(14)   | 2481.90(10)   |
| $\alpha$ [deg]   | 91.089(2)   | 90  |
| $\beta$ [deg]  | 97.601(2)   | 93.9370(10)   |
| $\gamma$ [deg]   | 104.5500(10)  | 90  |
| V [ $\text{pm}^3$ ]  | $4530.1(5)\cdot 10^6$                                 | $9093.5(3)\cdot 10^6$                                 |
| Z / Calc.density [ $\text{g}\cdot\text{cm}^{-3}$ ]             | 2 / 1.468   | 4 / 1.544   |
| $\mu$ [ $\text{mm}^{-1}$ ]                                     | 0.744   | 1.393   |
| Crystal size [mm]  | 0.24×0.15×0.06  | 0.21×0.13×0.11  |
| $\theta$ range [deg]   | 2.2 - 20.82   | 2.22 - 28.28  |
| Reflections coll. / unique                                     | 16542 / 9412  | 31850 / 15633   |
| Data / parameters  | 9412 / 951  | 15633 / 1040  |
| GoF  | 1.080   | 1.076   |
| $R_1$ [ $I > 2\sigma(I)$ ]                                     | 0.0873  | 0.0610  |
| w $R_2$  | 0.1916  | 0.1107  |
| Largest diff. peak and hole [ $\text{e}\cdot\text{\AA}^{-3}$ ] | 0.823 / -0.783  | 0.716 / -0.796  |

\* For the calculation of the formula weight, the solvate acids were assumed to be two methacrylic and isobutyric acid molecules each.

**Table 79:** Crystallographic and structural parameters of  $\text{Zr}_6\text{O}_4(\text{OH})_4(\text{ONorb}_{\text{mix}})_{12} \cdot 3\text{HONorb}_{\text{mix}}$  (**Zr6-Norb<sub>mix</sub>**),  $\text{Zr}_6\text{O}_4(\text{OH})_4(\text{ONorb}_{\text{endo}})_{12} \cdot 3\text{HONorb}_{\text{endo}}$  (**Zr6-Norb<sub>endo</sub>**) and  $\text{Zr}_6\text{O}_4(\text{OH})_4(\text{ONorb}_{\text{exo}})_{12}(\text{BuOH}) \cdot 3\text{HONorb}_{\text{exo}}$  (**Zr6-Norb<sub>exo</sub>**)

|  | <b>Zr6-Norb<sub>mix</sub></b>                          | <b>Zr6-Norb<sub>endo</sub></b>                         | <b>Zr6-Norb<sub>exo</sub></b>                          |
|--|--|--|--|
| Empirical formula  | $\text{C}_{120}\text{H}_{142}\text{O}_{38}\text{Zr}_6$ | $\text{C}_{120}\text{H}_{142}\text{O}_{38}\text{Zr}_6$ | $\text{C}_{124}\text{H}_{152}\text{O}_{39}\text{Zr}_6$ |
| Formula weight [ $\text{g}\cdot\text{mol}^{-1}$ ]              | 2739.8   | 2739.8   | 2813.9   |
| Space group  | $P2_1/n$   | $P2_1/n$   | $P\bar{1}$   |
| a [pm]   | 1494.29(5)   | 1513.89(6)   | 1562.1(4)  |
| b [pm]   | 2762.32(10)  | 2791.90(11)  | 1564.1(4)  |
| c [pm]   | 2867.73(10)  | 2822.35(11)  | 3080.0(8)  |
| $\alpha$ [deg]   | 90   | 90   | 99.360(6)  |
| $\beta$ [deg]  | 94.9090(10)  | 93.8220(10)  | 95.793(5)  |
| $\gamma$ [deg]   | 90   | 90   | 113.343(5)   |
| V [ $\text{pm}^3$ ]  | $11793.7(7) \cdot 10^6$                                | $11902.5(8) \cdot 10^6$                                | $6703(3) \cdot 10^6$                                   |
| Z/Calc. density [ $\text{g}\cdot\text{cm}^{-3}$ ]              | 4 / 1.539  | 4 / 1.527  | 2 / 1.392  |
| $\mu$ [ $\text{mm}^{-1}$ ]                                     | 0.594  | 0.589  | 0.525  |
| Crystal size [mm]  | 0.32x0.14x0.09   | 0.23x0.17x0.09   | 0.51x0.17x0.04   |
| $\theta$ range [deg]   | 2.03 - 25.00   | 1.99 - 25.00   | 2.20 - 25.00   |
| Reflections coll./unique                                       | 64622 / 20711  | 76723 / 20829  | 36317 / 23356  |
| Data/parameters  | 20711 / 1477   | 20829 / 1477   | 23356 / 1523   |
| GoF  | 0.905  | 0.950  | 0.910  |
| $R_1$ [ $ I  > 2\sigma(I)$ ]                                   | 0.0708   | 0.0708   | 0.0923   |
| wR <sub>2</sub>  | 0.1695   | 0.1671   | 0.2069   |
| Largest diff. peak and hole [ $\text{e}\cdot\text{\AA}^{-3}$ ] | 0.977 / -0.387   | 1.313 / -0.584   | 1.199 / -1.032   |

**Table 80:** Crystallographic and structural parameters of  $\text{Zr}_{12}\text{O}_8(\text{OH})_8(\text{OVinac})_{24} \cdot 6\text{HOVinac}$  (**Zr12-Vinac**) and  $\text{Zr}_{12}\text{O}_8(\text{OH})_8(\text{OAc})_{16}(\text{OMc})_8 \cdot 6\text{HOAc}$  (**Zr12-AcMc**)

|   | <b>Zr12-Vinac</b>   | <b>Zr12-AcMc</b>   |
|---|---|--|
| Empirical formula                                   | $\text{C}_{120}\text{H}_{164}\text{O}_{76}\text{Zr}_{12}$ | $\text{C}_{76}\text{H}_{114}\text{O}_{76}\text{Zr}_{12}$ |
| Formula weight [ $\text{g mol}^{-1}$ ]              | 3917.2  | 3344.3   |
| Space group   | $C2/c$  | $C2/m$   |
| a [pm]  | 3427.56(18)   | 3626.9(3)  |
| b [pm]  | 2716.71(14)   | 1574.10(15)  |
| c [pm]  | 2075.45(10)   | 1369.76(12)  |
| $\alpha$ [deg]                                      | 90  | 90   |
| $\beta$ [deg]                                       | 125.9680(10)  | 109.385(2)   |
| $\gamma$ [deg]                                      | 90  | 90   |
| V [ $\text{pm}^3$ ]                                 | $15641.3(14) \cdot 10^6$                                  | $7376.8(12) \cdot 10^6$                                  |
| Z / Calc.density [ $\text{g cm}^{-3}$ ]             | 4 / 1.660   | 2 / 1.497  |
| $\mu$ [ $\text{mm}^{-1}$ ]                          | 0.859   | 0.896  |
| Crystal size [mm]                                   | 0.37x0.26x0.25  | 0.18x0.16x0.12   |
| $\theta$ range [deg]                                | 2.10 - 28.32  | 2.38 - 25.00   |
| Reflections coll. / unique                          | 54899 / 19363   | 20132 / 12844  |
| Data / parameters                                   | 19363 / 940   | 12844 / 772  |
| GoF   | 1.016   | 0.970  |
| $R_1$ [ $>2\sigma(I)$ ]                             | 0.0409  | 0.0724   |
| wR <sub>2</sub>                                     | 0.1010  | 0.1798   |
| Largest diff. peak and hole [ $\text{e \AA}^{-3}$ ] | 1.248 / -0.869  | 1.115 / -0.688   |

**Table 81:** Crystallographic and structural parameters of  $\text{Zr}_4\text{O}_2(\text{OMc})_{12} \cdot \text{C}_6\text{H}_6$ 

|  |  |
|--|--|
| Empirical formula  | $\text{C}_{24}\text{H}_{66}\text{O}_{14}\text{Zr}_4$ |
| Formula weight [ $\text{g mol}^{-1}$ ]                           | 1496.0   |
| Space group  | $P\bar{1}$   |
| a [pm]   | 1115.45(10)  |
| b [pm]   | 1184.50(11)  |
| c [pm]   | 1204.87(11)  |
| $\alpha$ [deg]   | 76.062(2)  |
| $\beta$ [deg]  | 85.173(2)  |
| $\gamma$ [deg]   | 85.040(2)  |
| V [ $\text{pm}^3$ ]  | $1536.0(2) \cdot 10^6$                               |
| Z / Calc.density [ $\text{g cm}^{-3}$ ]                          | 2 / 1.617  |
| $\mu$ [ $\text{mm}^{-1}$ ]                                       | 0.741  |
| Crystal size [mm]  | 0.40x0.32x0.24                                       |
| $\theta$ range [deg]   | 2.47 - 26.37   |
| Reflections coll. / unique                                       | 9283 / 6195  |
| Data / parameters  | 6195 / 397   |
| GoF  | 1.059  |
| $R_1$ [ $ I  > 2\sigma(I)$ ]                                     | 0.0292   |
| $wR_2$   | 0.0349   |
| Largest diff. peak and hole [ $\text{e} \cdot \text{\AA}^{-3}$ ] | 0.618 / -0.389                                       |

**Table 82:** Crystallographic and structural parameters of Zr(isoeugenolate)<sub>4</sub> and Ti<sub>2</sub>(OPr)<sub>6</sub>(isoeugenolate)<sub>2</sub>

|  | <b>Zr(isoeugenolate)<sub>4</sub></b>              | <b>Ti<sub>2</sub>(OPr)<sub>6</sub>(isoeugenolate)<sub>2</sub></b> |
|--|---|---|
| Empirical formula                                | C <sub>40</sub> H <sub>44</sub> O <sub>8</sub> Zr | C <sub>38</sub> H <sub>64</sub> O <sub>10</sub> Ti <sub>2</sub>   |
| Formula weight [g·mol <sup>-1</sup> ]            | 744.0   | 776.7   |
| Space group                                      | <i>C2/c</i>                                       | <i>P</i> $\bar{1}$  |
| a [pm]   | 1894.4(3)   | 999.27(7)   |
| b [pm]   | 1467.6(2)   | 1305.72(9)  |
| c [pm]   | 1610.2(2)   | 1729.7(1)   |
| $\alpha$ [deg]                                   | 90  | 72.008(2)   |
| $\beta$ [deg]                                    | 125.188(4)  | 89.339(2)   |
| $\gamma$ [deg]                                   | 90  | 81.167(2)   |
| V [pm <sup>3</sup> ]                             | 3658.7(9)·10 <sup>6</sup>                         | 2119.5(3)·10 <sup>6</sup>   |
| Z / Calc.density [g·cm <sup>-3</sup> ]           | 4 / 1.351   | 2 / 1.217   |
| $\mu$ [mm <sup>-1</sup> ]                        | 0.352   | 0.427   |
| Crystal size [mm]                                | 0.30x0.09x0.07                                    | 0.28x0.17x0.10  |
| $\theta$ range [deg]                             | 2.63 - 23.26                                      | 2.36 - 25.00  |
| Reflections coll. / unique                       | 8470 / 2632                                       | 11705 / 7416  |
| Data / parameters                                | 2632 / 223  | 7416 / 452  |
| GoF  | 1.146   | 1.021   |
| R <sub>1</sub> [ $I > 2\sigma(I)$ ]              | 0.0564  | 0.0778  |
| wR <sub>2</sub>                                  | 0.1212  | 0.1674  |
| Largest diff. peak and hole [e·Å <sup>-3</sup> ] | 0.371 / -0.494                                    | 0.478 / -0.478  |



**Table 83:** Crystallographic and structural parameters of  $\text{Ti}_6\text{O}_4(\text{OEt})_8(\text{OIsob})_8$  and  $\text{Ti}_6\text{O}_4(\text{OPr})_8(\text{OIsob})_8$ 

|   | $\text{Ti}_6\text{O}_4(\text{OEt})_8(\text{OIsob})_8$ | $\text{Ti}_6\text{O}_4(\text{OPr})_8(\text{OIsob})_8$ |
|---|---|---|
| Empirical formula                                   | $\text{C}_{48}\text{H}_{96}\text{O}_{28}\text{Ti}_6$  | $\text{C}_{56}\text{H}_{112}\text{O}_{28}\text{Ti}_6$ |
| Formula weight [ $\text{g mol}^{-1}$ ]              | 1408.6  | 1520.8  |
| Space group   | $P\bar{1}$  | $P\bar{1}$  |
| a [pm]  | 1191.26(10)   | 1225.32(17)   |
| b [pm]  | 1203.95(10)   | 1266.04(18)   |
| c [pm]  | 1335.69(11)   | 1407.11(19)   |
| $\alpha$ [deg]                                      | 96.050(2)   | 76.112(3)   |
| $\beta$ [deg]                                       | 113.850(2)  | 64.627(3)   |
| $\gamma$ [deg]                                      | 94.324(2)   | 78.502(3)   |
| V [ $\text{pm}^3$ ]                                 | $1727.6(2) \cdot 10^6$                                | $1903.0(5) \cdot 10^6$                                |
| Z / Calc. density [ $\text{g cm}^{-3}$ ]            | 2 / 1.354   | 2 / 1.327   |
| $\mu$ [ $\text{mm}^{-1}$ ]                          | 0.734   | 0.672   |
| Crystal size [mm]                                   | 0.27x0.16x0.15  | 0.32x0.27x0.20  |
| $\theta$ range [deg]                                | 2.22 - 28.34  | 2.12 - 25.00  |
| Reflections coll. / unique                          | 14546 / 8478  | 10127 / 6620  |
| Data / parameters                                   | 8478 / 381  | 6620 / 418  |
| GoF   | 1.186   | 1.066   |
| $R_1$ [ $I > 2\sigma(I)$ ]                          | 0.0860  | 0.0582  |
| $wR_2$  | 0.1926  | 0.1571  |
| Largest diff. peak and hole [ $\text{e \AA}^{-3}$ ] | 0.954 / -0.522  | 1.018 / -0.494  |

**Table 84:** Crystallographic and structural parameters of  $\text{Ti}_6\text{O}_4(\text{OPr})_8(\text{ONorb}_{\text{mix}})_8$  and  $\text{Ti}_6\text{O}_6(\text{OPr})_6(\text{Olsob})_6$ 

|  | $\text{Ti}_6\text{O}_4(\text{OPr})_8(\text{ONorb}_{\text{mix}})_8$ | $\text{Ti}_6\text{O}_6(\text{OPr})_6(\text{Olsob})_6$ |
|--|--|---|
| Empirical formula  | $\text{C}_{88}\text{H}_{128}\text{O}_{28}\text{Ti}_6$              | $\text{C}_{42}\text{H}_{84}\text{O}_{24}\text{Ti}_6$  |
| Formula weight [ $\text{g mol}^{-1}$ ]                           | 1921.2   | 1260.4  |
| Space group  | $P2_1/c$   | $P\bar{1}$  |
| a [pm]   | 2319.26(16)  | 1086.46(10)   |
| b [pm]   | 1494.81(11)  | 1302.73(12)   |
| c [pm]   | 2801.5(2)  | 1314.18(12)   |
| $\alpha$ [deg]   | 90   | 61.002(2)   |
| $\beta$ [deg]  | 103.5360(10)   | 67.311(2)   |
| $\gamma$ [deg]   | 90   | 80.019(2)   |
| V [ $\text{pm}^3$ ]  | $9442.5(12) \cdot 10^6$  | $1500.7(2) \cdot 10^6$                                |
| Z / Calc. density [ $\text{g cm}^{-3}$ ]                         | 4 / 1.352  | 1 / 1.395   |
| $\mu$ [ $\text{mm}^{-1}$ ]                                       | 0.558  | 0.831   |
| Crystal size [mm]  | 0.27x0.15x0.10   | 0.26x0.15x0.09  |
| $\theta$ range [deg]   | 2.02 - 25.00   | 2.68 - 28.34  |
| Reflections coll. / unique                                       | 96580 / 16570  | 10594 / 7324  |
| Data / parameters  | 16570 / 1100   | 7324 / 337  |
| GoF  | 0.702  | 1.029   |
| $R_1$ [ $I > 2\sigma(I)$ ]                                       | 0.0630   | 0.0598  |
| $wR_2$   | 0.1370   | 0.1535  |
| Largest diff. peak and hole [ $\text{e} \cdot \text{\AA}^{-3}$ ] | 0.531 / -0.227   | 1.402 / -0.707  |

## 6.8 Synthesis of Hybrid Polymers

### 6.8.1 Preparation of $\text{Zr}_4\text{O}_2(\text{OMc})_{12}$ Modified Poly(methyl methacrylate)

The condition for the preparation of pristine PMMA was as follows: An amount of 22.3 mg of benzoyl peroxide was added to 2.130 g (21.28 mmol) of methyl methacrylate, and polymerization was carried out at 70 °C for 24 hours. The sample was then dried *in vacuo*.

#### Polymerizations with Initiator Variation

An amount of 0.558 g (0.39 mmol) of **Zr4** cluster was dissolved in 9.8 g of benzene. After addition of 4.067 g (40.63 mmol) of methyl methacrylate, 0.01 wt%, 0.1 wt% or 1.0 wt% of BPO were added to aliquots of this solution (Table 85). The samples were polymerized at 70 °C for 24 hours. After removal of the solvent *in vacuo*, the polymers were twice swollen in ethyl acetate for 3 days each and then dried *in vacuo*.

**Table 85:** Amounts used in the preparation of **Zr4** doped PMMA; initiator variation

| Sample                     | Stock solution<br>[g] | MMA<br>[mmol] | BPO<br>[mg] | Gelation time<br>[min] |
|----------------------------|-----------------------|---------------|-------------|------------------------|
| p(MMA+ <b>Zr4</b> ) 0.01 % | 4.119                 | 11.602        | 0.1         | 40                     |
| p(MMA+ <b>Zr4</b> ) 0.1 %  | 3.699                 | 10.419        | 1.1         | 30                     |
| p(MMA+ <b>Zr4</b> ) 1 %    | 2.977                 | 8.385         | 8.6         | 7                      |

#### Polymerizations with Solvent Variation

An amount of 0.105 g (74  $\mu\text{mol}$ ) of **Zr4** cluster was dissolved in 7.458 g of benzene. After addition of 0.724 g (7.23 mmol) of methyl methacrylate, the solution was heated to 70 °C, and polymerization was started by the addition of 0.7 mg of BPO. The sample was heated to 70 °C for 1 day, benzene was then removed *in vacuo*. The sample was freed from the Schlenk tube and milled to a fine powder which was then extracted two times with ethyl acetate for 3 days

each and then dried *in vacuo* again. The amounts used for the preparation of the samples with different monomer / solvent ratios are given in Table 86.

**Table 86:** Amounts used in the preparation of **Zr4** doped PMMA; solvent variation

| Sample                       | Zr4 cluster<br>[g] | MMA<br>[g] | Benzene<br>[g] | BPO<br>[mg] | Gelation<br>time [min] |
|------------------------------|--------------------|------------|----------------|-------------|------------------------|
| P(MMA+ <b>Zr4</b> ) 1 : 2.4  | 0.160              | 1.161      | 2.789          | 1.3         | 30                     |
| P(MMA+ <b>Zr4</b> ) 1 : 5.2  | 0.085              | 0.605      | 3.138          | 0.6         | 40                     |
| P(MMA+ <b>Zr4</b> ) 1 : 10.1 | 0.105              | 0.724      | 7.458          | 0.7         | 120                    |

### Polymerizations without Solvent

To an amount of 0.517 g of **Zr4** cluster an amount of 5.029 g of methyl methacrylate was added. The solution was stirred at room temperature for 15 minutes, the stirring was then turned off, and non-dissolved **Zr4** cluster was allowed to sediment. An amount of 2 ml of the clear solution was polymerized at 70 °C by initiating with 2.1 mg of BPO. After 24 hours, the sample was dried *in vacuo* and freed from the Schlenk tube.

The residual MMA in the non-polymerized solution/dispersion was dried *in vacuo*, and the **Zr4** amount was then weighed to 0.4688 g. This procedure was repeated twice, the solubility of **Zr4** cluster in MMA at room temperature was determined to 0.17 mol%. This result was confirmed by elemental analysis. The residual mass after thermal combustion in oxygen corresponded to a **Zr4** cluster concentration of 0.16 mol% in the polymer.

### 6.8.2 Preparation of $\text{Zr}_4\text{O}_2(\text{OMc})_{12}$ Modified Polystyrene

The condition for the preparation of pristine PS was as follows: An amount of 36.7 mg of benzoyl peroxide was added to 3.879 g (37.24 mmol) of styrene, and polymerization was carried out at 70 °C for 24 hours. The sample was then dried *in vacuo*.

## Polymerizations with Initiator Variation

An amount of 0.132 g (93  $\mu\text{mol}$ ) of **Zr4** was dissolved in 2.027 g of benzene. An amount of 0.977 g (9.38 mmol) of styrene was added to this solution, followed by heating to 70 °C. Polymerization was initiated by adding 1.1 mg of BPO. The sample was polymerized at 70 °C for 24 hours. After removal of the solvent *in vacuo*, the polymer was swollen twice in ethyl acetate for 3 days each and then dried *in vacuo*. The amounts used in the preparation of the samples with 1 % and 0.01 % of BPO, respectively, are given in Table 87.

**Table 87:** Amounts used in the preparation of **Zr4** doped PS; initiator variation

| Sample                     | Zr4 cluster<br>[g] | Styrene<br>[g] | Benzene<br>[g] | BPO<br>[mg] | Gelation time<br>[min] |
|----------------------------|--------------------|----------------|----------------|-------------|------------------------|
| p(Sty+ <b>Zr4</b> ) 0.01 % | 0.153              | 1.074          | 1.679          | 0.1         | 20                     |
| p(Sty+ <b>Zr4</b> ) 0.1 %  | 0.132              | 0.977          | 2.027          | 1.1         | 50                     |
| p(Sty+ <b>Zr4</b> ) 1 %    | 0.139              | 1.000          | 1.753          | 11.2        | 100                    |

## Polymerizations with Solvent Variation

An amount of 0.152 g (107  $\mu\text{mol}$ ) of **Zr4** cluster was dissolved in 5.536 g of benzene. An amount of 1.162 g (11.16 mmol) of styrene was added to the solution, followed by heating to 70 °C. Polymerization was initiated by adding 1.2 mg of BPO, the sample was then polymerized at 70 °C for 24 hours. After removal of the solvent *in vacuo*, the polymer was swollen twice in ethyl acetate for 3 days each and then dried *in vacuo*. Amounts used in the preparation of the samples with a solvent : monomer ratio of 1 : 2.1 and 1 : 8.3, respectively, are given in Table 88.

**Table 88:** Amounts used in the preparation of **Zr4** doped PS; solvent variation

| Sample                      | Zr4 cluster<br>[g] | Styrene<br>[g] | Benzene<br>[g] | BPO<br>[mg] | Gelation time<br>[min] |
|-----------------------------|--------------------|----------------|----------------|-------------|------------------------|
| p(Sty+ <b>Zr4</b> ) 1 : 2.1 | 0.132              | 0.977          | 2.027          | 1.1         | 50                     |
| p(Sty+ <b>Zr4</b> ) 1 : 4.8 | 0.152              | 1.162          | 5.536          | 1.2         | 145                    |
| p(Sty+ <b>Zr4</b> ) 1 : 8.3 | 0.116              | 1.031          | 8.519          | 0.9         | 260                    |

## Polymerizations without Solvent

To an amount of 0.322 g (227  $\mu\text{mol}$ ) of **Zr4** cluster an amount of 4.311 g (41.39 mmol) of styrene was added. The solution was stirred at room temperature for 15 minutes, the stirring was then turned off and non-dissolved **Zr4** cluster was allowed to sediment. An amount of 2 ml of the clear solution was polymerized at 70 °C by initiating with 1.9 mg of BPO. After 24 hours, the sample was dried *in vacuo* and freed from the Schlenk tube.

The residual styrene in the non-polymerized solution/dispersion was dried *in vacuo* and the **Zr4** amount was weighed to 0.2751 g. By repeating this procedure three times, the solubility of the **Zr4** cluster in styrene at room temperature was determined to 0.08 mol%. This result was confirmed by elemental analyses. The residual mass after thermal combustion in oxygen corresponded to a **Zr4** cluster concentration of 0.08 mol% in the polymer.

### 6.8.3 Destroying the Cross-Links with Acetyl Acetone

An amount of 100 mg of milled **Zr4** doped PMMA or PS sample was put into a solution consisting of 5 ml of acetyl acetone and 5 ml of ethyl acetate in a vial equipped with a magnetic stirrer. Depending on the grain size of the polymer, the solution was stirred up to two months. The viscous solution was then precipitated in a 30fold excess of methanol. The polymer was separated by decanting the solution or by centrifugation. The solid was re-dissolved in ethyl acetate by stirring for a few hours, and non-soluble precipitate was centrifuged. The precipitation / re-dissolving step was repeated twice; the sample was then dried *in vacuo* and dissolved in THF for SEC measurements.

### 6.8.4 Determination of Residual Zr in Cleaved Polymers

For the digestion of the  $\text{ZrO}_2$  powders, a Multiwave 3000 PMD (pressurized microwave digestion) system (Paar, Graz, Austria) was used with PTFE vessels at a maximum temperature of 180 °C and a maximum pressure of 20 bar.

Polymer samples were weighed into hand-made Duran-glass annealing liners and heated to 550 °C in air with a heating rate of 5 °C/min. The maximum temperature was maintained for one hour. The residue, consisting of  $\text{ZrO}_2$ , was then washed out of the liners successively with 2.5 ml of  $\text{HCl}_{\text{conc}}$ , 2 ml  $\text{HNO}_3_{\text{conc}}$  and 0.5 ml  $\text{HF}_{\text{conc}}$ . The acid fractions were combined in PTFE vessels for microwave digestion and a ramp was applied from 0 - 1400 Watt in 7 minutes. The mixture was then held for 23 minutes ( $P_{\text{max}}$  20 bar,  $T_{\text{max}}$  180 °C). After cooling to room temperature, the solutions were transferred into smaller PTFE vessels. The pressure vessels were cleaned by washing with bidistilled water several times. The washing and the sample solutions were combined, and 100  $\mu\text{l}$  of perchloric acid was added. After evaporating the volatiles overnight in an aluminum heating block, 1.5 ml of aqua regia was added, and the solution was heated to 105 °C. By increasing the temperature to 150 °C, the volatiles were removed until a perchloric acid bead remained. The bead was dissolved in 4 ml of 5 % HCl and filled up to 10 g with bidistilled water.

## 6.8.5 Optimization of Polymerization Conditions

### Preparation of $\text{Zr}_4\text{O}_2(\text{OMc})_{12}$ Modified Poly(methyl methacrylate)

The preparation of sample **MMA1** is given as an example: An amount of 0.252 g (178  $\mu\text{mol}$ ) of **Zr4** cluster was dissolved in 5.008 g of benzene. After addition of 3.55 g (35.46 mmol) of methyl methacrylate, the solution was heated to 80 °C and polymerization was initiated by the addition of 3.5 mg of LPO. The sample was kept at 80 °C for 3 minutes. The flask was then quenched in an ice-water bath to 0 °C. Polymerization was then carried out at 40 °C for 48 hours. After removal of the solvent *in vacuo*, the temperature was raised to 100 °C for another two hours. The sample was freed from the Schlenk tube and dried *in vacuo*. After milling, the polymer was swollen in ethyl acetate two times for 3 days each and afterwards dried again *in vacuo* at elevated temperatures. Samples **MMA2** - **MMA4** were prepared accordingly by changing the pre-polymerization periods and initiator concentrations, respectively (Table 46, Table 89).

The sample PMMA represented a reference sample polymerized without cluster and solvent. The sample was not treated with ethyl acetate.

**Table 89:** Amounts used for optimization of the system **Zr4** - MMA

| Sample      | Cluster [g] | MMA [g] | Benzene [g] | LPO [mg] | LPO [wt%] | Time at 80 °C [min] |
|-------------|-------------|---------|-------------|----------|-----------|---------------------|
| <b>PMMA</b> | -           | 9.36    | -           | 9.3      | 0.1       | 3                   |
| <b>MMA1</b> | 0.252       | 3.55    | 5.008       | 3.5      | 0.1       | 5                   |
| <b>MMA2</b> | 0.252       | 3.55    | 5.008       | 3.5      | 0.1       | 3                   |
| <b>MMA3</b> | 0.332       | 4.675   | 6.589       | 2.3      | 0.05      | 5                   |
| <b>MMA4</b> | 0.345       | 4.862   | 6.853       | 2.4      | 0.05      | 3                   |

**FTIR** bands of the sample **MMA3** are given as an example:

**IR** (KBr): 3000 (m, CH), 2953 (m, CH), 2844 (w, CH), 1732 (s, br, C-O ester), 1637 (w, C=C), 1485 (m, C-H), 1451 (m, C-H), 1437 (sh, C-H), 1389 (w, C-H), 1368 (w, C-H), 1272 (m, C-O-C), 1245 (m, C-O-C), 1194 (s), 1150 (s, C-O), 1063 (w, C-O), 988 (m, C-O), 965 (m), 914 (w), 842 (m), 828 (sh), 809 (w), 750 (m), 685 (w), 514 (w), 483 (w)  $\text{cm}^{-1}$ .

### Preparation of $\text{Zr}_4\text{O}_2(\text{OMc})_{12}$ Modified Polystyrene

The preparation of sample **St1** is given as an example: An amount of 0.223 g (157  $\mu\text{mol}$ ) of **Zr4** cluster was dissolved in 4.746 g of benzene. After addition of 3.270 g (31.40 mmol) of styrene, the solution was heated to 80 °C, and polymerization was initiated by the addition of 3.2 mg of LPO. The sample was kept at 80 °C for 3 minutes. The flask was then quenched in an ice-water bath to 0 °C. Polymerization was carried out at 60 °C for 1 day. After removing the solvent *in vacuo*, the temperature was raised to 80 °C for one day and post-polymerization was carried out at 120 °C for another day. The sample was then freed from the Schlenk tube and dried *in vacuo*. After milling, the polymer was swollen in ethyl acetate two times for 3 days each and afterwards dried again *in vacuo* at elevated temperatures. Samples **St2** - **St8** were prepared accordingly by changing pre-polymerization periods and initiator concentrations, respectively (Table 49, Table 52 and Table 90).

The sample PS represented a reference sample polymerized without cluster and solvent. No swelling procedure in ethyl acetate was applied.



**Table 90:** Amounts used for optimization of the system **Zr4** - styrene

| Sample     | Zr4 Cluster<br>[g] | Styrene<br>[g] | Benzene<br>[g] | LPO<br>[mg] | LPO<br>[wt%] | Time at 80°C<br>[min] |
|------------|--------------------|----------------|----------------|-------------|--------------|-----------------------|
| <b>PS</b>  | -                  | 9.09           | -              | 4.5         | 0.05         | 5                     |
| <b>St1</b> | 0.223              | 3.270          | 4.746          | 3.2         | 0.1          | 2.5                   |
| <b>St2</b> | 0.236              | 3.452          | 5.009          | 3.4         | 0.1          | 5                     |
| <b>St3</b> | 0.273              | 3.997          | 5.801          | 3.9         | 0.1          | 10                    |
| <b>St4</b> | 0.248              | 3.635          | 5.271          | 3.6         | 0.1          | 15                    |
| <b>St5</b> | 0.298              | 4.360          | 6.328          | 4.3         | 0.1          | -                     |
| <b>St6</b> | 0.396              | 5.814          | 8.437          | 2.9         | 0.05         | 5                     |
| <b>St7</b> | 0.198              | 2.907          | 4.218          | 7.2         | 0.25         | 5                     |
| <b>St8</b> | 0.211              | 3.088          | 4.482          | 15.4        | 0.5          | 5                     |

**FTIR** data of sample **St6** are given as an example:

**IR** (KBr): 3082 (s, C-H arom.), 3059 (s, C-H arom.), 3025 (s, C-H arom.), 3001 (m, C-H arom.), 2978 (m, C-H arom.), 2916 (s, C-H), 2849 (s, C-H), 1943 (w, comb. arom.), 1874 (w, comb. arom.), 1804 (w, comb. arom.), 1743 (w, comb. arom.), 1724 (sh), 1702 (w), 1642 (vw, C=C), 1602 (s, C=C arom.), 1582 (m), 1561 (w), 1549 (w, COO<sup>-</sup><sub>as</sub>), 1536 (vw), 1494 (s, C=C arom.), 1468 (w), 1453 (s), 1419 (sh), 1370 (m), 1329 (w), 1312 (w), 1247 (m, C-O-C), 1196 (sh), 1183 (m), 1154 (m), 1111 (sh), 1096 (sh), 1071 (m), 1029 (m), 1006 (sh), 981 (w), 964 (w), 944 (w), 907 (w, C-H arom.), 879 (sh), 842 (w), 757 (s, C-H arom.), 697 (s, C-H arom.), 624 (sh), 537 (m) cm<sup>-1</sup>.

### 6.8.6 Optimization of the **Zr<sub>6</sub>O<sub>4</sub>(OH)<sub>4</sub>(OMc)<sub>12</sub>** - Styrene Polymerization Conditions

In the polymerization reactions with styrene, the concentration of **Zr6** in the styrene was 0.5 mol%, while the initiator concentration was varied (Table 55, p. 104). Preparation of sample **St3** is given as an example: An amount of 1.25 mg of lauroyl peroxide was added to a solution of 0.210 g (0.12 mmol) of **Zr6** in 2.58 g (24.8 mmol) of styrene. The solution was kept at 80 °C for 5 min and was then quenched to 0 °C by putting the flask into an ice-water bath. Polymerization

was carried out at 60 °C for 24h, post-polymerization at 120 °C for another 24 hours. The sample was dried *in vacuo*.

The condition for the preparation of pristine PS was similar to that of the cluster-crosslinked polymers: An amount of 1.25 mg of lauroyl peroxide (LPO) was added to 2.58 g (24.0 mmol) of styrene. After stirring for several minutes, the solution was kept at 80 °C for 5 min and then quenched by putting the flask into an ice-water bath. Polymerization was carried out at 60 °C for 1 d, post-polymerization at 120 °C for another 24 hours. The sample was dried *in vacuo*.

### 6.8.7 Preparation of $\text{Zr}_6\text{O}_4(\text{OH})_4(\text{OMc})_{12}$ - Styrene Bulk Polymers

Bulk polymers were prepared in a way similar to that described in section 5.2.1. A difference was made in the step-wise polymerization and in the use of the **Zr6** cluster. Whereas a solvate-free species was employed previously, this step was omitted. The molecular weight of the cluster, now carrying three additional methacrylic acids as a crystal solvate cluster unit, was corrected accordingly. The preparation of the sample containing 0.87 mol% of **Zr6** cluster is given as an example: An amount of 4.153 g (2.12 mmol) of **Zr6** cluster was added to 25.2 g (242 mmol) of styrene. The cluster was allowed to dissolve at room temperature. The flask was then heated to 80 °C until thermal equilibrium was reached. An amount of 12.7 mg of lauroyl peroxide was added and the solution was kept at 80 °C for 2.5 min. The flask was then quenched in an ice-water bath to 0 °C. Polymerization was carried out at 60 °C. After 24 hours the temperature was raised to 80 °C and after another 24 hours to 120 °C. The sample was freed from the Schlenk tube and dried *in vacuo* at elevated temperatures.

Amounts used for pure polystyrene and for the hybrid materials doped with lower amounts of **Zr6** are given in Table 91.

**Table 91:** Amounts used in the preparation of **Zr6** doped PS

| Sample | Zr6 Cluster<br>[g] | Styrene<br>[g] | LPO<br>[mg] | LPO<br>[wt%] |
|--------|--------------------|----------------|-------------|--------------|
| PS     | -                  | 28.544         | 5.4         | 0.05         |
| 0.24   | 1.314              | 29.043         | 5.9         | 0.05         |
| 0.43   | 2.109              | 25.977         | 5.2         | 0.05         |
| 0.70   | 3.106              | 23.433         | 4.9         | 0.05         |
| 0.87   | 4.153              | 25.200         | 5.1         | 0.05         |

Infrared spectra of the **Zr6** hybrid materials were recorded in transmission mode. Finely milled polymers were mixed with a defined amount of potassium ferricyanide and KBr pellets were prepared. Data are given for the PS sample doped with 0.87 mol% of **Zr6** cluster as an example.

**IR** (KBr): 3083 (m, C-H arom.), 3060 (m, C-H arom.), 3028 (m, C-H arom.), 3003 (m, C-H arom.), 2923 (m, C-H), 2850 (m, C-H), 1945 (w, comb. arom.), 1872 (w, comb. arom.), 1806 (w, comb. arom.), 1740 (w, comb. arom.), 1724 (w, sh), 1700 (w, COOH), 1644 (w, C=C), 1602 (m, C=C arom.), 1570 (m, COO<sup>-</sup><sub>as</sub>), 1547 (m, COO<sup>-</sup><sub>as</sub>), 1493 (s, C=C arom.), 1467 (sh), 1453 (s), 1373 (m), 1345 (sh), 1329 (sh), 1314 (sh), 1244 (m, COOH), 1200 (sh), 1183 (w), 1156 (w), 1112 (w), 1071 (w), 1029 (m), 1005 (sh), 983 (vw), 965 (vw), 944 (vw), 907 (m, C-H arom.), 841 (w), 757 (s, C-H arom.), 699 (s, C-H arom.)

## Swelling Behaviour

Dry and crack-free polymer pieces were weighed and then put into a beaker containing ethyl acetate. The samples were periodically taken out to notice weight constancy. The weighing procedure was as following: After taking out the sample, the surface was dried gently by moving in air. The sample was then sealed in a pre-weighed beaker in saturated ethyl acetate atmosphere to avoid evaporation of solvent during the weighing procedure.

### 6.8.8 Preparation of Polystyrene Doped with Clusters Carrying Less- or Non-Reactive Ligands

The polymerizations followed the procedures described in the optimization of the **Zr6** - methacrylate doped polystyrene samples (section 6.8.6). The preparation of the sample doped with **Zr12-Ac** is given as an example; the amounts used in the preparations of polystyrene doped with other clusters are given in Table 92.

An amount of 2.3 mg of lauroyl peroxide was added to a solution of 0.559 g (178  $\mu$ mol) of **Zr12-Ac** in 4.545 g (43.64 mmol) of styrene. The solution was kept at 80 °C for 3 minutes and was then quenched to 0 °C in an ice-water bath. Polymerization was carried out at 60 °C for 24 hours, post-polymerization at 120 °C for another 24 hours. The sample was dried *in vacuo* at elevated temperatures.

In the case of the **Zr12-Ac** and the **Zr12** cluster, the amounts given in the table represent almost maximum solubility in styrene at room temperature. The cluster **Zr12-Vinac** and **Zr6-Norb<sub>mix</sub>** showed higher solubility.

**Table 92:** Amounts used in the preparation of hybrid polymers with less- or non-reactive clusters

| Sample                               | Cluster<br>[g / $\mu$ mol] | Styrene<br>[g / mmol] | Cluster<br>concentration<br>[mol %] | LPO<br>[mg] | Comment                            |
|--------------------------------------|----------------------------|-----------------------|-------------------------------------|-------------|------------------------------------|
| <b>Zr12-Ac<br/>PS</b>                | 0.559 / 178                | 4.545 / 43.64         | 0.41                                | 2.3         | Cloudy, whitish<br>polymer         |
| <b>Zr12<br/>PS</b>                   | 0.664 / 212                | 4.545 / 43.64         | 0.48                                | 2.2         | Cloudy polymer                     |
| <b>Zr12-Vinac<br/>PS</b>             | 0.751 / 192                | 4.545 / 43.64         | 0.44                                | 2.8         | Holey, clear polymer               |
| <b>Zr6-Norb<sub>mix</sub><br/>PS</b> | 0.597 / 218                | 4.545 / 43.64         | 0.50                                | 2.3         | Cloudy polymer with<br>few bubbles |
| <b>Zr12-AcMc<br/>PS</b>              | 0.719 / 215                | 4.545 / 43.64         | 0.49                                | 2.1         | Clear polymer<br>without bubbles   |

## 7 Summary

The combination of different materials is a well-known concept in materials science and chemistry with the goal to fabricate materials with improved or even new properties. Inorganic-organic hybrid materials are not simply physical mixtures between two components, but they can be broadly defined as either co-polymers between organic and inorganic building blocks or as nanocomposites with intimately mixed inorganic and organic components, where at least one of the components has a length scale ranging from a few Ångstroms to a few tens of nanometers. Depending on the nature of the interactions between the building blocks and the polymer matrix, two main types of hybrid polymers have been classified: Class I hybrid materials correspond to systems in which the components show weak interactions such as van der Waals contacts, hydrogen bonding,  $\pi$  -  $\pi$  interactions or electrostatic forces. In class II hybrid materials, the inorganic and organic components are fully or partially linked through strong chemical bonds such as covalent or ionic bonds or Lewis acid-base interactions.

In this work, the so-called nanosized building blocks approach was used for the preparation of hybrid polymers. In a first step, structurally well-defined transition metal oxo clusters, the nanosized building blocks, were prepared and then used as co-monomers in polymerization reactions. Depending on the nature of the cluster-bonded ligands both class I and class II hybrid polymers were prepared. In the latter case highly cross-linked materials were obtained because of the high number of polymerizable surface ligands bonded to the clusters.

In a first research direction, zirconium oxo clusters both with polymerizable and non-polymerizable groups were prepared by the carboxylic acid sol-gel process. In controlled hydrolysis and condensation reactions of zirconium butoxide with carboxylic acids, crystalline clusters of the general composition  $\text{Zr}_6\text{O}_4(\text{OH})_4(\text{carboxylate})_{12}$  ( $\text{Zr}_6$ ) or  $\text{Zr}_{12}\text{O}_8(\text{OH})_8(\text{carboxylate})_{24}$  ( $\text{Zr}_{12}$ ) were obtained (Figure 110).

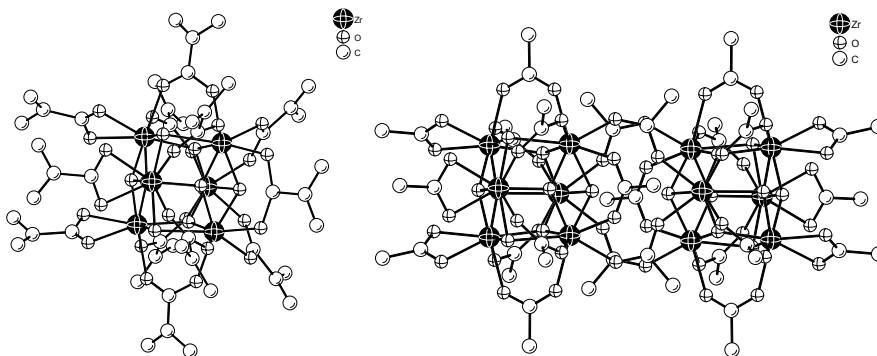


**Figure 110:** Molecular structures of  $\text{Zr}_6\text{O}_4(\text{OH})_4(\text{methacrylate})_{12}$  (left) and  $\text{Zr}_{12}\text{O}_8(\text{OH})_8(\text{acetate})_{24}$  (right); hydrogen atoms are not shown

The reaction of zirconium butoxide with either isobutyric acid, with a mixture of isobutyric acid and methacrylic acid or with 5-norbornene-2-carboxylic acid, resulted in the formation of  $Zr_6$  clusters. The use of isobutyric acid allowed the introduction of non-reactive groups bonded to the cluster surface. When a mixture of isobutyric acid and methacrylic acid was applied in the synthesis, a mixed-carboxylate substituted cluster was obtained, proving the general possibility of tuning the reactivities of the cluster surface by a simple variation of the carboxylic acids. The use of commercially available 5-norbornene-2-carboxylic acid (mixture of endo and exo isomers) resulted in a  $Zr_6$  cluster with ligands that are accessible to ring opening metathesis polymerizations. After separation of the endo and exo acid isomers by a iodolactonization reaction, a  $Zr_6$  cluster was obtained for each isomer, endo and exo. A post-synthesis modification by a Diels-Alder reaction of  $Zr_6O_4(OH)_4(\text{methacrylate})_{12}$  (**Zr6**) with cyclopentadiene or 2,3-dimethyl-1,3-butadiene was not possible.

Crystalline  $Zr_{12}$  clusters were obtained when zirconium butoxide was reacted with vinylacetic acid or a mixture of acetic acid and methacrylic acid. The latter example again showed the possibility of introducing both functional and non-functional groups bonded to the same cluster.

In all of the prepared zirconium clusters, an extensive hydrogen bonding was observed in the crystal structures. Three of the twelve carboxylate groups of a  $Zr_6$  (sub-)unit were always bonded in a chelating mode which was stabilized by three carboxylic acids both hydrogen-bonded to a  $\mu_3$ -OH group on the one hand and one oxygen atom of a chelating ligand on the other hand.

Nuclear magnetic resonance (NMR) spectroscopy was used to analyze the clusters in solution. Broad signals were observed at room temperature for the  $Zr_6$  structures because the cluster-bonded carboxylates showed fast ligand exchange. In low temperature measurements, the molecular symmetry ( $C_{3v}$ ) was confirmed for the  $Zr_6O_4(OH)_4(\text{isobutyrate})_{12}$  cluster. The  $Zr_{12}$  clusters showed signal splitting at room temperature which indicated that exchange processes were slower compared with the  $Zr_6$  molecules. The molecular symmetry of the cluster  $Zr_{12}O_8(OH)_8(\text{vinylacetate})_{24}$  was  $\sim C_{2h}$  at room temperature, a cooling to  $-80^\circ\text{C}$  was required for the cluster  $Zr_{12}O_8(OH)_8(\text{acetate})_{16}(\text{methacrylate})_8$  to observe the corresponding number of inequivalent ligand signals.

In a more detailed NMR spectroscopic investigation, the clusters  $Zr_4O_2(\text{methacrylate})_{12}$  (**Zr4**),  $Zr_6O_4(OH)_4(\text{methacrylate})_{12}$  (**Zr6**) and  $Zr_{12}O_8(OH)_8(\text{propionate})_{24}$  (**Zr12**) were characterized to learn more about the behaviour and stability of zirconium oxo clusters in solution.

The  $^1\text{H}$  NMR signals of the **Zr4** cluster coalesced at room temperature because of fast ligand exchange. Cooling the solution to  $-80^\circ\text{C}$  resulted in four resolved sets of ligand signals, which was in accordance with the molecular symmetry in the crystalline state ( $C_{2h}$ ). Judging from exchange spectroscopy experiments at this temperature, no exchange processes took place on

the NMR time scale. At  $-70\text{ }^{\circ}\text{C}$  a chelating ligand exchanged with a bridging ligand and at  $-60\text{ }^{\circ}\text{C}$  three inequivalent ligands exchanged with each other.

In the crystalline state, the **Zr6** molecule possesses  $C_{3v}$  symmetry. The  $^1\text{H}$  NMR spectrum showed signal splitting at room temperature, indicating that the coalescence temperature was somewhat higher than that of **Zr4**. Cooling the solution to  $-80\text{ }^{\circ}\text{C}$  resulted in three resolved sets of ligand signals, which was in accordance with molecular symmetry.

The  $^1\text{H}$  NMR spectra of **Zr12** showed sharp signals and six sets of ligand signals were observed in 2D NMR experiments which was in good agreement with molecular symmetry ( $C_{2h}$ ). In temperature dependent measurements it was confirmed that this symmetry was retained from room temperature to  $-20\text{ }^{\circ}\text{C}$ . Further cooling resulted in broad and unstructured  $^1\text{H}$  NMR signals, indicative of a lowering of the symmetry to  $C_i$  or even  $C_1$ . When the solution was heated above room temperature, the signals broadened successively. At  $100\text{ }^{\circ}\text{C}$  all signals except one coalesced, indicating fast ligand exchange, as it was observed for the **Zr4** cluster at room temperature.

The kind of carboxylic acid employed in the reactions with zirconium butoxide played a major role in the formation of crystalline zirconium oxo clusters. Next to steric parameters and additional functionalities at the carboxylic acids, a strong influence of the pK value was observed. As a rule of thumb, carboxylic acids with a pK value in the range of  $\sim 4 - 5$  formed crystalline clusters when they were reacted with zirconium butoxide.

In an attempt to extend the use of isobutyric acid and 5-norbornene-2-carboxylic acid to the preparation of titanium compounds, two different kinds of clusters were obtained (Figure 111).

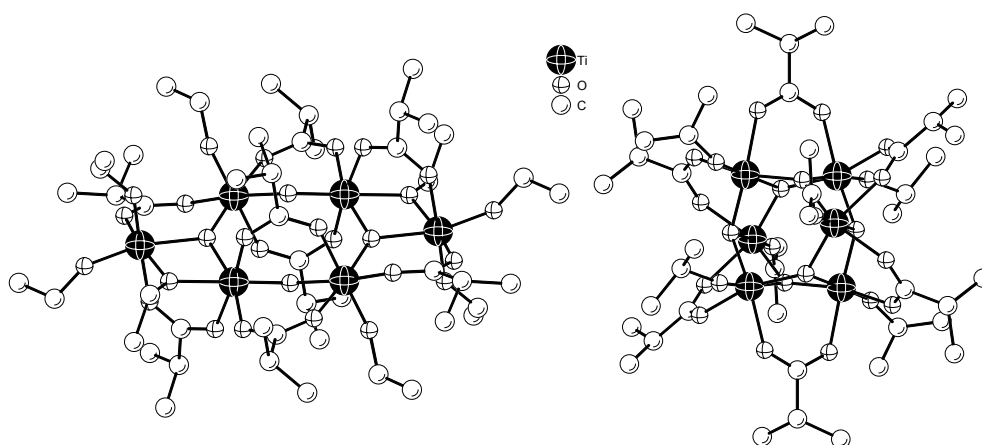


**Figure 111:** Molecular structures of  $\text{Ti}_6\text{O}_4(\text{ethoxide})_8(\text{isobutyrate})_8$  (left) and  $\text{Ti}_6\text{O}_6(\text{isopropoxide})_6(\text{isobutyrate})_6$  (right); hydrogen atoms are omitted for purposes of clarity

The reaction of titanium ethoxide with isobutyric acid in the presence of ethanol resulted in the crystalline cluster  $\text{Ti}_6\text{O}_4(\text{ethoxide})_8(\text{isobutyrate})_8$ . Clusters showing the same general composition were obtained when titanium propoxide was reacted with isobutyric acid or with 5-norbornene-2-carboxylic acid. All of the Ti atoms were located in a planar arrangement and revealed an octahedral coordination by oxygen atoms. The oxygen atoms originated from five different types of ligands:  $\mu_2$ - and  $\mu_3$ - oxo bridges, bridging and terminal alcoholates, and bridging carboxylates.

A different titanium cluster was obtained when isobutyric acid was reacted with titanium isopropoxide in the presence of isopropanol. The core of  $\text{Ti}_6\text{O}_6(\text{isopropoxide})_6(\text{isobutyrate})_6$  consisted of two six-membered rings of alternating Ti and O atoms that were stacked offset to each other. The observation of a  $\text{Ti}_6\text{O}_6$  core instead of a  $\text{Ti}_6\text{O}_4$  structure was attributed to a kinetic effect caused by the different size of the alkoxo ligands or the degree of aggregation of the parent alkoxides (titanium ethoxide and propoxide are trimeric in solution, while titanium isopropoxide is monomeric), or by different substitution and ester formation rates.

In a second research direction, zirconium oxo clusters were applied as co-monomers in free radical polymerization reactions with methyl methacrylate and styrene. The use of clusters carrying methacrylate ligands resulted in highly cross-linked polymers which were insoluble in organic solvents such as ethyl acetate and benzene.

Generally, when methyl methacrylate or styrene was co-polymerized with the **Zr4** cluster, the use of additional solvent was mandatory because of the low solubility of **Zr4** in the monomers. The polymerizations were difficult to control because of short gelation times and auto-acceleration. Therefore, appropriate reaction conditions were investigated. To this end, the amounts of benzoyl peroxide (BPO), which was used to initiate the polymerizations, were varied as well as the amount of additional solvent used in polymerizations. Furthermore, a step-wise polymerizations were carried out with lauroyl peroxide (LPO) as the initiator.

Co-polymerizations of 1 mol% of **Zr4** with methyl methacrylate and different amounts of BPO resulted in hybrid polymers with improved thermal properties. The onset temperatures of thermal decomposition were shifted from  $\sim 250^\circ\text{C}$  for neat poly(methyl methacrylate) (PMMA) to  $\sim 340^\circ\text{C}$  for the doped samples and no differences were observed in the thermal properties by variation of the initiator concentrations. However, gelation times were increased and auto-acceleration was avoided by using smaller amounts of initiator. The same features were observed when the initiator concentration was kept at a constant level and a different amount of benzene was used in the polymerizations: The gelation times increased with increasing solvent / monomer ratios, but no differences in the onset temperatures of thermal decomposition were observed. For very high solvent / monomer ratios, the hybrid polymers were obtained as powders instead of bulk



materials because of precipitation from the polymerization solution. Destroying of the **Zr4** units of the prepared hybrid polymers with acetyl acetone allowed the cleaved polymer chains to be investigated with size exclusion chromatography (SEC). A correlation between the gelation times and the molecular weights was observed, i.e. longer gelation times caused higher molecular weights.

In an extended investigation, a step-wise polymerization of methyl methacrylate was applied with different amounts of lauroyl peroxide (LPO) as the initiator and 0.5 mol% of **Zr4** as the co-monomer. The solutions were heated to 80 °C for a short time, and then quenched to 0 °C. Polymerizations were carried out at 40 °C and post-polymerization at 100 °C. By variations of the pre-polymerization periods and the initiator concentrations, different gelation times were observed and auto-acceleration was avoided. However, the onset temperatures of thermal decomposition were ~340 °C and no differences were observed when the reaction conditions were varied. In contrast to the samples prepared with BPO as the initiator and 1 mol% of **Zr4**, glass transition temperatures were detected in DSC measurements. These shifted from 115 °C for neat PMMA to 129 °C for the cluster doped samples. After destroying the **Zr4** units with acetyl acetone, the molecular weights were determined by SEC. Again, a correlation between the gelation times and the molecular weights was observed.

Co-polymerizations of 1 mol% of **Zr4** with styrene and BPO as the initiator were carried out in a similar way as described for the MMA systems. First, the amount of initiator was varied. By doing so, the gelation times were prolonged and auto-acceleration was avoided for low initiator concentrations. The onset temperatures of thermal decomposition were slightly shifted from 340 °C for neat polystyrene (PS) to ~360 °C for the cluster doped samples. When the initiator concentration was kept at a constant level and the amount of additional solvent was increased, the onset temperatures decreased from 340 °C for PS to 331 °C for a solvent / monomer ratio of 10 / 1. A correlation between the gelation times and the molecular weights was observed.

In step-wise polymerizations, 0.5 mol% of **Zr4** cluster was dissolved in benzene and polymerizations were initiated at 80 °C with different amounts of lauroyl peroxide. After a certain time, the solutions were cooled to 0 °C and polymerizations were carried out in different steps. By doing so, the onset temperatures of thermal decomposition were decreased when compared to undoped PS. Glass transition temperatures were increased from 100 °C for neat PS to 109 °C for the hybrid polymers. SEC measurements of the cleaved polymer chains revealed a correlation between the gelation times and the molecular weights.

Mechanical and thermomechanical testing of any **Zr4** doped polymer sample was not possible because great amounts of solvent were entrapped in the bulk polymer matrix which could not be removed.

By using the **Zr6** cluster in co-polymerizations with styrene as the monomer, the use of additional solvent was not required. In a first step, the polymerization conditions were optimized with regard to thermal properties. An amount of 0.5 mol% of **Zr6** cluster was dissolved in styrene and a step-wise polymerization was applied with LPO as the initiator. Initiation of the solution with 0.05 wt% of LPO at 80 °C for 5 minutes, quenching to 0 °C and polymerization at 60 °C for one day and at 120 °C for another day were the optimum conditions. The onset temperature of thermal decomposition was shifted from 340 °C for neat PS to 390 °C for the sample doped with 0.5 mol% of **Zr6**. The same time, the glass transition temperature was increased from 104 °C to 121 °C. SEC measurements were not possible because the **Zr6** units in the hybrid polymers were not degraded by acetyl acetone.

For mechanical and thermomechanical testing, bulk samples on a ~30 grams scale were prepared with different proportions of the **Zr6** cluster, ranging from 0.24 mol% to 0.87 mol%. The step-wise polymerization process was somewhat modified: Initiation time at 80 °C was reduced to 2.5 minutes and an additional step at 80 °C for 24 hours was applied. By doing so, the onset temperature of thermal decomposition shifted from 320 °C for neat PS to 350 °C for the sample doped with 0.87 mol% of **Zr6**. In differential scanning calorimetry and modulated differential scanning calorimetry measurements, no signals apart from exothermic combustion were observed, and the glass transition temperatures were increased when compared to neat PS.

Thermal expansion coefficients ( $\alpha$ ) were determined by thermal mechanical analysis and no differences among the samples with different cluster proportions were observed below the glass transition temperatures where  $\alpha$  was about 70 ppm/°C. Above the glass transition temperatures, the expansion coefficients decreased gradually with increasing cluster proportion from 213 ppm/°C for PS to 190 ppm/°C for the sample doped with 0.87 mol% of **Zr6**.

Dynamic moduli were determined by dynamic mechanical analysis. The moduli at room temperature were slightly increased from 2.9 GPa for PS to 3.3 - 3.5 GPa for the hybrid polymers. Above the glass transition temperatures, which were found to increase gradually from 100 °C for PS to 110 °C for the hybrid polymers with this technique, the effect was much more pronounced: Whereas no plateau modulus for neat PS was observed, the plateau moduli increased gradually from 1.5 GPa to 7.8 GPa for the samples doped with 0.24 mol% and 0.87 mol%, of **Zr6**, respectively. These values were used to calculate network parameters according to the theory of rubber elasticity. The network densities increased with increasing cluster concentration and, as a consequence, the entanglement molecular weight decreased.

The mechanical properties of the **Zr6** doped hybrid materials were investigated in tension tests. The Young's moduli at room temperature increased from 3 GPa for neat PS to 3.8 GPa for the sample doped with 0.87 mol% of **Zr6**; tensile strengths increased from 35 MPa to 55 MPa.

Compression tests were performed to learn more about the post-yield behaviour of the hybrid polymers. The strain hardening moduli were determined at large deformations and were increased linearly with increasing cluster proportion from 14 MPa for neat PS to 32 MPa for the

sample doped with 0.87 mol% of **Zr6**. Furthermore, a clear correlation between the network densities, as calculated from dynamic moduli in the rubbery state, and the strain hardening moduli, as determined in the glassy state, was observed.

Microhardness measurements revealed no significant changes of indentation Young's moduli and of indentation hardnesses when PS was doped with **Zr6**. A mapping of an undoped and a doped polymer sample revealed homogeneous properties in all dimensions, proving that polymerization was complete through the bulk of the material and no monomer was incorporated which would soften the material.

Small angle X-ray scattering (SAXS) measurements were performed to characterize the distribution of the **Zr6** clusters in the polystyrene matrix. The scattering intensities clearly depended on the cluster proportions. Cluster-cluster distances, determined from the maxima of the scattering curves, were found at about 1.7 nm for different proportions of **Zr6**. This was in contradiction to values calculated theoretically when assuming a random distribution of the clusters in the polymer matrix. Together with a more detailed interpretation of the SAXS data using the model developed by Beaucage, which describes scattering from complex systems containing multiple levels of structural features, a strong indication for aggregation of the clusters, i.e. 'clusters of clusters', was found. This notion was confirmed by transmission electron microscopy images, where aggregation of clusters was apparent. The aggregates differed in size and showed a random distribution. However, non-agglomerated clusters were also observed.

Swelling experiments confirmed that the hybrid polymers were indeed cross-linked by the **Zr6** cluster. Cross-linking was expressed as the degree of swelling in ethyl acetate, i.e. percentage solvent uptake, which decreased from 135 % for the sample doped with 0.24 mol% of **Zr6** to 73 % for the sample doped with 0.87 mol%.

When the clusters  $\text{Zr}_{12}\text{O}_8(\text{OH})_8(\text{acetate})_{24}$ ,  $\text{Zr}_{12}\text{O}_8(\text{OH})_8(\text{propionate})_{24}$ ,  $\text{Zr}_{12}\text{O}_8(\text{OH})_8(\text{vinylacetate})_{24}$  and  $\text{Zr}_6\text{O}_4(\text{OH})_4(5\text{-norbornene-2-carboxylate})_{12}$  were co-polymerized with styrene, class I hybrid materials were in fact obtained. Although the latter two examples carried polymerizable ligands, the reaction conditions were not sufficient to actually cause a cross-linking of the polymer matrix. This was confirmed in swelling experiments, where the hybrid materials dissolved in ethyl acetate. Thermal properties of the hybrid polymers were investigated. The onset temperatures of thermal decomposition were shifted to values comparable to the **Zr6** doped samples. However, the mass loss step at about 450 °C, which was ascribed to combustion of organic char which was formed during the degradation of the main polymer chains, was lower when compared to **Zr6** doped samples. Since char formation depended on both inorganic filler and cross-linking, this was explained with the lack of cross-linking in these samples.

## 8 Literature

1. Ruiz-Hitzky E., *Organic-inorganic materials. From intercalation chemistry to devices*, in *Functional Hybrid Materials*, Gómez-Romero P. and Sanchez C., Editors. **2004**, Wiley VCH: Weinheim, 15-49.
2. Schmidt H., Kaiser A., Patzelt H. and Scholze H., *Mechanical and physical properties of amorphous solids based on  $(CH_3)_2SiO$ -silica gels*. J. Phys. Colloque, **1982**, 275-278.
3. Livage J., Henry M. and Sanchez C., *Sol-gel chemistry of transition metal oxides*. Prog. Solid State Chem., **1988**, 18, 259-341.
4. Avnir D., Levy D. and Reisfeld R., *The nature of the silica cage as reflected by spectral changes and enhanced photostability of trapped Rhodamine 6G*. J. Phys. Chem., **1984**, 88, 5956-5959.
5. Brinker C.J. and Scherer G.W., *Sol-gel science* **1990**, Boston, Mass.: Academic Press, 908 pp.
6. Sanchez C. and Ribot F., *Design of hybrid organic-inorganic materials synthesized via sol-gel chemistry*. New J. Chem., **1994**, 18, 1007-1047.
7. Judeinstein P. and Sanchez C., *Hybrid organic-inorganic materials: a land of multidisciplinary*. J. Mater. Chem., **1996**, 6, 511-525.
8. Gómez-Romero P. and Sanchez C., *Hybrid Materials, Functional Applications. An Introduction*, in *Functional Hybrid Materials*, Gómez-Romero P. and Sanchez C., Editors. **2004**, Wiley VCH: Weinheim, 1-14.
9. Sanchez C., de Soler-Illia G.J., Ribot F., Lalot T., Mayer C.R. and Cabuil V., *Designed Hybrid Organic-Inorganic Nanocomposites from Functional Nanobuilding Blocks*. Chem. Mater., **2001**, 13, 3061-3083.
10. Sanchez C., Lebeau B., Chaput F. and Boilot J.-P., *Optical Properties of Functional Hybrid Organic-Inorganic Nanocomposites*, in *Functional Hybrid Materials*, Sanchez C. and Gómez-Romero P., Editors. **2004**, Wiley VCH: Weinheim, 122-168.
11. Mammeri F., Le Bourhis E., Rozes L. and Sanchez C., *Mechanical properties of hybrid organic-inorganic materials*. J. Mater. Chem., **2005**, 15, 3787-3811.
12. Sanchez C., Julian B., Belleville P. and Popall M., *Applications of hybrid organic-inorganic nanocomposites*. J. Mater. Chem., **2005**, 15, 3559-3592.
13. Schubert U., Huesing N. and Lorenz A., *Hybrid Inorganic-Organic Materials by Sol-Gel Processing of Organofunctional Metal Alkoxides*. Chem. Mater., **1995**, 7, 2010-2027.
14. Sanchez C., Lebeau B., Ribot F. and In M., *Molecular design of sol-gel derived hybrid organic-inorganic nanocomposites*. J. Sol-Gel Sci. Technol., **2000**, 19, 31-38.
15. Gómez-Romero P. and Sanchez C., *Functional Hybrid Materials* **2004**, Weinheim: Wiley VCH, 417 pp.
16. Schottner G., *Hybrid Sol-Gel-Derived Polymers: Applications of Multifunctional Materials*. Chem. Mater., **2001**, 13, 3422-3435.
17. Cotton F.A., *Strong homonuclear metal-metal bonds*. Acc. Chem. Res., **1969**, 2, 240-7.
18. Gautier-Luneau I., Mosset A. and Galy J., *Structural characterization of a hexanuclear titanium acetate complex,  $Ti_6(\mu_3-O)_2(\mu_2-O)_2(\mu_2-OC_2H_5)_2(\mu-CH_3COO)_8(OC_2H_5)_6$ , built up of two trinuclear, oxo-centered, units*. Z. Kristallogr., **1987**, 180, 83-95.
19. Kickelbick G. and Schubert U., *Oxozirconium methacrylate clusters.  $Zr_6(OH)_4O_4(OMc)_{12}$  and  $Zr_4O_2(OMc)_{12}$  ( $OMc$  = methacrylate)*. Chemische Berichte/Recueil, **1997**, 130, 473-477.
20. Turova N.Y., Turevskaya E.P., Kessler V.G. and Yanovskaya M.I., *The Chemistry of Metal Alkoxides* **2002**, Boston [et al.]: Kluwer Academic, 568 pp.

21. Yoldas B.E., *Hydrolysis of titanium alkoxide and effects of hydrolytic polycondensation parameters*. J. Mater. Sci., **1986**, 21, 1087-1092.
22. Sanchez C., Livage J., Henry M. and Babonneau F., *Chemical modification of alkoxide precursors*. J. Non-Cryst. Solids, **1988**, 100, 65-76.
23. Bourget L., Corriu R.J.P., Leclercq D., Mutin P.H. and Vioux A., *Non-hydrolytic sol-gel routes to silica*. J. Non-Cryst. Solids, **1998**, 242, 81-91.
24. Vioux P.A., *Nonhydrolytic Sol-Gel Routes to Oxides*. Chem. Mater., **1997**, 9, 2292-2299.
25. Hay J.N. and Raval H.M., *Synthesis of organic-inorganic hybrids via the nonhydrolytic sol-gel process*. Chem. Mater., **2001**, 13, 3396-3403.
26. Sharp K.G., *A two-component, non-aqueous route to silica gel*. J. Sol-Gel Sci. Technol., **1994**, 2, 35-41.
27. Sharp K.G., *Inorganic/organic hybrid materials*. Advanced Materials (Weinheim, Germany), **1998**, 10, 1243-1248.
28. Sumrell G. and Ham G.E., *Preparation of esters from the reaction of alkyl orthosilicates with organic acids*. J. Am. Chem. Soc., **1956**, 78, 5573-5575.
29. Emblem H.G., Hargreaves K. and Oxley C.E., *Preparation and properties of some acyloxysilanes*. J. Appl. Chem., **1968**, 18, 97-99.
30. Pope E.J.A. and Mackenzie J.D., *Sol-gel processing of silica. II. The role of the catalyst*. J. Non-Cryst. Solids, **1986**, 87, 185-198.
31. Karmakar B., De G., Kundu D. and Ganguli D., *Silica microspheres from the system tetraethyl orthosilicate-acetic acid-water*. J. Non-Cryst. Solids, **1991**, 135, 29-36.
32. Coltrain B.K., Kelts L.W., Armstrong N.J. and Salva J.M., *Silicon tetraacetate as a sol-gel precursor*. J. Sol-Gel Sci. Technol., **1994**, 3, 83-90.
33. Schubert U., *Chemical modification of titanium alkoxides for sol-gel processing*. J. Mater. Chem., **2005**, 15, 3701-3715.
34. Schwab J.J. and Lichtenhan J.D., *Polyhedral oligomeric silsesquioxane (POSS)-based polymers*. Appl. Organomet. Chem., **1998**, 12, 707-713.
35. Li G., Wang L., Ni H. and Pittman C.U., Jr., *Polyhedral oligomeric silsesquioxane (POSS) polymers and copolymers: A review*. J. Inorg. Organomet. Polym., **2002**, 11, 123-154.
36. Phillips S.H., Haddad T.S. and Tomczak S.J., *Developments in nanoscience: polyhedral oligomeric silsesquioxane (POSS)-polymers*. Curr. Opin. Solid State Mater. Sci., **2004**, 8, 21-29.
37. Joshi M. and Butola B.S., *Polymeric Nanocomposites-Polyhedral Oligomeric Silsesquioxanes (POSS) as Hybrid Nanofiller*. J. Macromol. Sci., Polym. Rev., **2004**, C44, 389-410.
38. Kickelbick G., Holzinger D., Brick C., Trimmel G. and Moons E., *Hybrid Inorganic-Organic Core-Shell Nanoparticles from Surface-Functionalized Titanium, Zirconium, and Vanadium Oxo Clusters*. Chem. Mater., **2002**, 14, 4382-4389.
39. Holmes R.R., Day R.O., Swamy K.C.K., Schmid C.G., Burton S.D. and Holmes J.M., *Cluster chemistry of a new class of organo oxotin compounds*. Main Group Met. Chem., **1989**, 12, 291-303.
40. Palacio F., Oliete P., Schubert U., Mijatovic I., Huesing N. and Peterlik H., *Magnetic behaviour of a hybrid polymer obtained from ethyl acrylate and the magnetic cluster  $Mn_{12}O_{12}(acrylate)_{16}$* . J. Mater. Chem., **2004**, 14, 1873-1878.
41. Price D.J., Batten S.R., Moubaraki B. and Murray K.S., *Synthesis, structure and magnetism of a new manganese carboxylate cluster:  $[Mn_{16}O_{16}(OMe)_6(OAc)_{16}(MeOH)_3(H_2O)_3] \cdot 6H_2O$* . Chem. Commun., **2002**, 762-763.
42. Coradin T., Larionova J., Smith A.A., Rogez G., Clerac R., Guerin C., Blondin G., Winpenny R.E.P., Sanchez C. and Mallah T., *Magnetic nanocomposites built by controlled incorporation of magnetic clusters into mesoporous silicates*. Advanced Materials (Weinheim, Germany), **2002**, 14, 896-898.

43. Brown D.A., Errington W. and Wallbridge M.G.H., *Niobium and tantalum oxo compounds: synthesis and crystal structure of the tetranuclear tantalum(V) oxo cluster*  $[ \{ \text{TaOCl}_2(\text{O}_2\text{CC}_6\text{H}_4\text{Me-p}) \}_4 ]$ . Journal of the Chemical Society, Dalton Transactions: Inorganic Chemistry (1972-1999), **1993**, 1163-1164.
44. Gross S., Di Noto V., Kickelbick G. and Schubert U., *Cluster-crosslinked inorganic-organic hybrid polymers: influence of the cluster type on the materials properties*. Mater. Res. Soc. Symp. Proc., **2002**, 726, 47-55.
45. Gross S., Kickelbick G., Puchberger M. and Schubert U., *Mono-, di-, and trimetallic methacrylate-substituted metal oxide clusters derived from hafnium butoxide*. [Erratum to document cited in CA140:156046]. Monatsh. Chem., **2004**, 135, 117.
46. Hubert-Pfalzgraf L.G., Abada V., Halut S. and Roziere J., *Metal alkoxides with polymerizable ligands: synthesis and molecular structure of*  $[\text{Nb}_4(\mu\text{-O})_4(\mu, \eta^2\text{-O}_2\text{CC}(\text{Me})=\text{CH}_2)_4(\text{OPr}^i)_8]$ . Polyhedron, **1996**, 16, 581-585.
47. Moraru B., Gross S., Kickelbick G., Trimmel G. and Schubert U., *A new type of methacrylate-substituted oxozirconium clusters:  $[\text{Zr}_3\text{O}(\text{OR})_5(\text{OMc})_5]_2$  and  $[\text{Zr}_3\text{O}(\text{OR})_3(\text{OMc})_7]_2$* . Monatsh. Chem., **2001**, 132, 993-999.
48. Ma L. and Payne D.A., *Studies on the Nature of a Lead Zirconate Titanate (PZT) Precursor Solution. Isolation and Structural Characterization of*  $[\text{PbZr}_2\text{O}(\text{OOCCH}_3)_2(\text{OCH}_2\text{CH}_3)_6]_2$ . Chem. Mater., **1994**, 6, 875-877.
49. Boyle T.J., Ottley L.A.M. and Rodriguez M.A., *Structurally characterized carboxylic acid modified zirconium alkoxides for the production of zirconium oxide thin films*. Polyhedron, **2005**, 24, 1727-1738.
50. Kickelbick G. and Schubert U., *Hydroxy carboxylate substituted oxozirconium clusters*. J. Chem. Soc., Dalton Trans., **1999**, 1301-1306.
51. Kickelbick G., Wiede P. and Schubert U., *Variations in capping the  $\text{Zr}_6\text{O}_4(\text{OH})_4$  cluster core: x-ray structure analyses of  $[\text{Zr}_6(\text{OH})_4\text{O}_4(\text{OOC-CH:CH}_2)_{10}]_2(\mu\text{-OOC-CH:CH}_2)_4$  and  $\text{Zr}_6(\text{OH})_4\text{O}_4(\text{OOCR})_{12}(\text{PrOH})$  ( $R = \text{Ph}$ ,  $\text{CMe:CH}_2$ )*. Inorg. Chim. Acta, **1999**, 284, 1-7.
52. Laaziz I., Larbot A., Guizard C., Julbe A. and Cot L., *Hydrolysis of zirconium propoxide by an esterification reaction*. Mater. Res. Soc. Symp. Proc., **1992**, 271, 71-76.
53. Jupa M., *Preparation and Modification of Carboxylate-Substituted Metal Oxo Clusters*. **2005**: Vienna University of Technology, Dissertation, 99 pp.
54. Reza M.Y., Matsushima H., Koikawa M., Nakashima M. and Tokii T., *Synthesis and Crystal Structure of a Novel Hexanuclear Zr(IV) Complex with Hydroxo and Carboxylato Bridging*. Bull. Chem. Soc. Jpn., **1998**, 71, 155-160.
55. Reza M.Y., Matsushima H., Koikawa M., Nakashima M. and Tokii T., *Synthesis and crystal structure of a novel hexanuclear Zr(IV) complex with 1,10-phenanthroline including carboxylato, hydroxo, and oxo bridging*. Polyhedron, **1999**, 18, 787-792.
56. Schubert U., *Polymers Reinforced by Covalently-Bonded Metal-Oxide Clusters*, in *Organic/Inorganic Hybrid Materials*, Blum F.D. and Laine R.M., Editors. **2003**, Electronic Publishing Services: Sonoma, California, 103-122.
57. Rardin R.L., Tolman W.B. and Lippard S.J., *Monodentate carboxylate complexes and the carboxylate shift: implications for polymetalloprotein structure and function*. New J. Chem., **1991**, 15, 417-430.
58. Williams R., Jencks W.P. and Westheimer F.H., *pKa Compilation*.
59. Trimmel G., *Anorganisch-organische Hybridmaterialien unter Verwendung modifizierter Metallalkoxide zur Herstellung nanostrukturierter Materialien*. **2000**: Vienna University of Technology, Dissertation, 226 pp.
60. Mijatovic I., Kickelbick G., Puchberger M. and Schubert U., *Preservation of the cluster core upon formation of  $\text{Ti}_3\text{O}(\text{OPr}^i)_8(\text{benzoate})_2$  from  $\text{Ti}_3\text{O}(\text{OR})_{10}$* . New J. Chem., **2003**, 27, 3-5.

61. Mijatovic I., Kickelbick G. and Schubert U., *Rearrangement of a titanium alkoxide cluster upon substitution of the alkoxide groups by carboxylate ligands - synthesis of  $[Ti_6O_4(OEt)_{14}(OOCPh)_2]$  from  $[Ti_7O_4(OEt)_{20}]$* . Eur. J. Inorg. Chem., **2001**, 1933-1935.
62. Moraru B., *Synthesis of Acrylate- and Methacrylate-Substituted Titanium and Zirconium Oxoclusters and Their Incorporation in Organic Polymers*. **2001**: Vienna University of Technology, Dissertation, 207 pp.
63. Ye B.-H., Li X.-Y., Williams Ian D. and Chen X.-M., *Synthesis and structural characterization of di- and tetranuclear zinc complexes with phenolate and carboxylate bridges. Correlations between  $^{13}C$  NMR chemical shifts and carboxylate binding modes*. Inorg. Chem., **2002**, 41, 6426-6431.
64. Grubbs R.H., *Handbook of Metathesis*. Vol. 3. Applications in polymer synthesis **2003**, Weinheim: Wiley VCH, 442 pp.
65. Alder K., Stein G., Liebmann M. and Rolland E., *Steric course of addition and substitution reactions. II. Stereo-chemistry of the diene synthesis(2)*. Ann., **1934**, 514, 197-211.
66. Beckmann S. and Geiger H., *Intramolecular rearrangements in the bicyclo[1.2.2]heptane series. IX. The lactones formed by hydration of bicyclo[1.2.2]heptenecarboxylic acids*. Chem. Ber., **1961**, 94, 48-58.
67. Alder K., Stein G., v. Buddenbrock F., Eckardt W., Frercks W. and Schneider S., *Steric course of addition and substitution reactions. I. Stereochemistry of the diene synthesis*. Ann., **1934**, 514, 1-33.
68. Alder K., Gunzl W. and Wolff K., *The steric course of the additions of  $\alpha$ - and  $\beta$ -methyl and phenyl-substituted acrylic acids to cyclopentadiene. A contribution to the stereochemistry of the diene synthesis*. Chem. Ber., **1960**, 93, 809-25.
69. Ver Nooy C.D. and Rondestvedt C.S., Jr., *Formation of nortricyclene derivatives by bromination of exo-2,5-methylene-1,2,5,6-tetrahydrobenzoic acids*. J. Am. Chem. Soc., **1955**, 77, 3583-3586.
70. Michelotti F.W. and Carter J.H., *Polymerization of norbornene and derivatives. II. Selectivity in the polymerization of exo-isomers by iridium catalysis*. Am. Chem. Soc., Div. Polymer Chem., Preprints, **1965**, 6, 224-233.
71. Manning D.D., Strong L.E., Hu X., Beck P.J. and Kiessling L.L., *Neoglycopolymer inhibitors of the selectins*. Tetrahedron, **1997**, 53, 11937-11952.
72. Diels O. and Alder K., *Syntheses in the hydroaromatic series. I. Addition of "diene" hydrocarbons*. Ann., **1928**, 460, 98-122.
73. Roberts J.D., Trumbull E.R., Jr., Bennett W. and Armstrong R., *Reaction of norbornylene with N-bromosuccinimide. Nortricyclene and its derivatives*. J. Am. Chem. Soc., **1950**, 72, 3116-3124.
74. Gao Y., Dragan D.S., Jupa M., Kogler F.R., Puchberger M. and Schubert U., *Surface-modified zirconium oxide clusters and their use as components for inorganic-organic hybrid materials*. Mater. Res. Soc. Symp. Proc., **2005**, 847, 539-544.
75. Gao Y., *New Inorganic Cluster-reinforced Polymers*. **2005**, Lise Meitner Scholarship, Report, 20 pp
76. Vollhardt K.P.C. and Schore N.E., *Organische Chemie*. 2<sup>nd</sup> ed **1995**, Weinheim: Wiley VCH, 1330 pp.
77. Trimmel G., Gross S., Kickelbick G. and Schubert U., *Swelling behavior and thermal stability of poly(methyl methacrylate) crosslinked by the oxo zirconium cluster  $Zr_4O_2(\text{methacrylate})_{12}$* . Appl. Organomet. Chem., **2001**, 15, 401-406.
78. Friebolin H., *Basic One- and Two-dimensional NMR spectroscopy*. 4<sup>th</sup> ed **2005**, Weinheim: Wiley-VCH, 406 pp.
79. Bradley D.C., Mehrotra R.C. and Gaur D.P., *Metal Alkoxides* **1978**, London: Academic Press, 412 pp.

80. Vaartstra B.A., Huffman J.C., Gradeff P.S., Hubert-Pfalzgraf L.G., Daran J.C., Parraud S., Yunlu K. and Caulton K.G., *Alcohol adducts of alkoxides: intramolecular hydrogen bonding as a general structural feature*. Inorg. Chem., **1990**, 29, 3126-3131.
81. Ahlfaenger R., Bertagnolli H., Ertel T., Friedrich B., Helmerich A., Kolb U., Nass R., Peter D. and Schmidt H., *Structural study of the formation of lead zirconate titanate via sol-gel process*. European Materials Research Society Monographs, **1992**, 5, 275-282.
82. Day V.W., Klemperer W.G. and Pafford M.M., *Isolation and Structural Characterization of Tetra-n-propyl Zirconate in Hydrocarbon Solution and the Solid State*. Inorg. Chem., **2001**, 40, 5738-5746.
83. Valdez-Castro L., Mendez-Vivar J. and Mendoza-Serna R., *Porous SiO<sub>2</sub>-TiO<sub>2</sub>-ZrO<sub>2</sub> obtained from polymeric systems prepared by the sol-gel process*. J. Porous Mater., **2001**, 8, 303-309.
84. Mendez-Vivar J., *Evolution of the Si-condensed species in a multicomponent polymeric system*. Silicon Chemistry, **2003**, 2, 167-173.
85. Delgado R., Frausto da Silva J.J.R., Amorim M.T.S., Cabral M.F., Chaves S. and Costa J., *Dissociation constants of Broensted acids in heavy water and water: studies of polyaza and polyoxa-polyaza macrocycles and a general correlation*. Anal. Chim. Acta, **1991**, 245, 271-282.
86. Gross S., *unpublished results*: Department of Chemical Sciences, University of Padova.
87. Moraru B., Huesing N., Kickelbick G., Schubert U., Fratzl P. and Peterlik H., *Inorganic-Organic Hybrid Polymers by Polymerization of Methacrylate- or Acrylate-Substituted Oxotitanium Clusters with Methyl Methacrylate or Methacrylic Acid*. Chem. Mater., **2002**, 14, 2732-2740.
88. Doeuff S., Dromzee Y., Taulelle F. and Sanchez C., *Synthesis and solid- and liquid-state characterization of a hexameric cluster of titanium(IV): Ti<sub>6</sub>(μ<sub>2</sub>-O)<sub>2</sub>(μ<sub>3</sub>-O)<sub>2</sub>(μ<sub>2</sub>-OC<sub>4</sub>H<sub>9</sub>)<sub>2</sub>(OC<sub>4</sub>H<sub>9</sub>)<sub>6</sub>(OCOCH<sub>3</sub>)<sub>8</sub>*. Inorg. Chem., **1989**, 28, 4439-4445.
89. Laaziz P.I., Larbot A., Guizard C., Durand J., Cot L. and Joffre J., *Structure of octakis(μ-acetato-O,O')bis(μ-isopropoxy)hexakis(isopropoxy)di-μ<sub>3</sub>-oxodi-μ-oxohexatitanium*. Acta Crystallogr., Sect. C: Cryst. Struct. Commun., **1990**, C46, 2332-2334.
90. Schubert U., Arpac E., Glaubitt W., Helmerich A. and Chau C., *Primary hydrolysis products of methacrylate-modified titanium and zirconium alkoxides*. Chem. Mater., **1992**, 4, 291-295.
91. Boyle T.J., Schwartz R.W., Doedens R.J. and Ziller J.W., *Synthesis and Structure of Novel Group IV Tridentate Alkoxide Complexes and Ceramic Thin Films Derived Therefrom. X-ray Structures of (H<sub>3</sub>CC(CH<sub>2</sub>-μ<sub>3</sub>-O)(CH<sub>2</sub>-μ-O)<sub>2</sub>)<sub>2</sub>Ti<sub>4</sub>(OCH(CH<sub>3</sub>)<sub>2</sub>)<sub>10</sub>, (H<sub>3</sub>CCH<sub>2</sub>C(CH<sub>2</sub>-μ<sub>3</sub>-O)(CH<sub>2</sub>-μ-O)<sub>2</sub>)<sub>2</sub>Ti<sub>4</sub>(OCH(CH<sub>3</sub>)<sub>2</sub>)<sub>10</sub>, and (H<sub>3</sub>CC(CH<sub>2</sub>-μ-O)<sub>3</sub>Zr<sub>4</sub>(μ-OCH(CH<sub>3</sub>)<sub>2</sub>)<sub>2</sub>(OCH(CH<sub>3</sub>)<sub>2</sub>)<sub>8</sub>*. Inorg. Chem., **1995**, 34, 1110-1120.
92. Ammala P.S., Batten S.R., Kepert C.M., Spiccia L., van den Bergen A.M. and West B.O., *The reaction of iron carboxylates with titanium alkoxides. Isolation and structural characterisation of [Ti<sub>6</sub>(μ<sub>3</sub>-O)<sub>6</sub>(O<sub>2</sub>CPh)<sub>6</sub>(OCH<sub>2</sub>C(CH<sub>3</sub>)<sub>3</sub>)<sub>6</sub>]*. Inorg. Chim. Acta, **2003**, 353, 75-81.
93. Papiernik R., Hubert-Pfalzgraf L.G., Vaissermann J. and Goncalves M.C.H.B., *Synthesis and characterization of new titanium hexanuclear oxo carboxylato alkoxides. Molecular structure of [Ti<sub>6</sub>(μ<sub>3</sub>-O)<sub>6</sub>(μ-O<sub>2</sub>CC<sub>6</sub>H<sub>4</sub>OPh)<sub>6</sub>(OEt)<sub>6</sub>]*. J. Chem. Soc., Dalton Trans., **1998**, 2285-2288.
94. Boyle T.J., Alam T.M., Tafoya C.J. and Scott B.L., *Formic Acid Modified Ti(OCHMe<sub>2</sub>)<sub>4</sub>. Syntheses, Characterization, and X-ray Structures of Ti<sub>4</sub>(μ<sub>4</sub>-O)(μ-O)(OFc)<sub>2</sub>(μ-OR)<sub>4</sub>(OR)<sub>6</sub> and Ti<sub>6</sub>(μ<sub>3</sub>-O)<sub>6</sub>(OFc)<sub>6</sub>(OR)<sub>6</sub> (OFc = O<sub>2</sub>CH; OR = OCHMe<sub>2</sub>)*. Inorg. Chem., **1998**, 37, 5588-5594.
95. Barglik-Chory C. and Schubert U., *Organically substituted titanium alkoxides with unsaturated organic groups*. J. Sol-Gel Sci. Technol., **1995**, 5, 135-142.



- 
96. Armareggo W.L.F. and Perrin D.D., *Purification of laboratory chemicals*. 4<sup>th</sup> ed **2000**, Oxford: Butterworth-Heinemann, 529 pp.
  97. Mikos A.G., Takoudis C.G. and Peppas N.A., *Kinetic modeling of copolymerization/crosslinking reactions*. *Macromolecules*, **1986**, 19, 2174-2182.
  98. Nyden M.R., Forney G.P. and Brown J.E., *Molecular modeling of polymer flammability: application to the design of flame-resistant polyethylene*. *Macromolecules*, **1992**, 25, 1658-1666.
  99. Zaikov G.E. and Aseeva R.M., *Some aspects of polymer pyrolysis*. *Makromol. Chem., Macromol. Symp.*, **1993**, 74, 21-33.
  100. Levchik G.F., Si K., Levchik S.V., Camino G. and Wilkie C.A., *The correlation between cross-linking and thermal stability: cross-linked polystyrenes and polymethacrylates*. *Polym. Degrad. Stab.*, **1999**, 65, 395-403.
  101. Gao Y., Choudhury N.R., Matison J., Schubert U. and Moraru B., *Organic-inorganic hybrid from surface-modified oxotitanate cluster*. *Polym. Mater. Sci. Eng.*, **2001**, 84, 986-987.
  102. Gao Y., Choudhury N.R., Matison J., Schubert U. and Moraru B., *Part 2: Inorganic-Organic Hybrid Polymers by Polymerization of Methacrylate-Substituted Oxotitanium Clusters with Methyl Methacrylate: Thermomechanical and Morphological Properties*. *Chem. Mater.*, **2002**, 14, 4522-4529.
  103. Schubert U., Trimmel G., Moraru B., Tesch W., Fratzl P., Gross S., Kickelbick G. and Husing N., *Inorganic-organic hybrid polymers from surface-modified oxometallate clusters*. *Mater. Res. Soc. Symp. Proc.*, **2001**, 628, CC2 3 1-CC2 3 11.
  104. Trabelsi S., Janke A., Haessler R., Zafeiropoulos N.E., Fornasieri G., Bocchini S., Rozes L., Stamm M., Gerard J.-F. and Sanchez C., *Novel Organo-Functional Titanium-oxo-cluster-Based Hybrid Materials with Enhanced Thermomechanical and Thermal Properties*. *Macromolecules*, **2005**, 38, 6068-6078.
  105. Strachota A., Kroutilova I., Kovarova J. and Matejka L., *Epoxy Networks Reinforced with Polyhedral Oligomeric Silsesquioxanes (POSS). Thermomechanical Properties*. *Macromolecules*, **2004**, 37, 9457-9464.
  106. Huang J., He C., Liu X., Xu J., Tay C.S.S. and Chow S.Y., *Organic-inorganic nanocomposites from cubic silsesquioxane epoxides: direct characterization of interphase, and thermomechanical properties*. *Polymer*, **2005**, 46, 7018-7027.
  107. Huang J., Xiao Y., Mya K.Y., Liu X., He C., Dai J. and Siow Y.P., *Thermomechanical properties of polyimide-epoxy nanocomposites from cubic silsesquioxane epoxides*. *J. Mater. Chem.*, **2004**, 14, 2858-2863.
  108. Peterson J.D., Vyazovkin S. and Wight C.A., *Stabilizing effect of oxygen on thermal degradation of poly(methyl methacrylate)*. *Macromol. Rapid Commun.*, **1999**, 20, 480-483.
  109. Troitskii B.B., Troitskaya L.S., Dmitriev A.A. and Yakhnov A.S., *Inhibition of thermo-oxidative degradation of poly(methyl methacrylate) and polystyrene by C<sub>60</sub>*. *Eur. Polym. J.*, **2000**, 36, 1073-1084.
  110. Li Y., Fan Y. and Ma J., *Thermal, physical, and chemical stability of porous polystyrene-type beads with different degrees of crosslinking*. *Polym. Degrad. Stab.*, **2001**, 73, 163-167.
  111. Moraru B., Kickelbick G., Battistella M. and Schubert U., *Degradation of a methacrylate-substituted oxozirconium cluster by acetylacetone*. *J. Organomet. Chem.*, **2001**, 636, 172-174.
  112. Wakeshima I., Kamogawa H. and Kijima I., *Preparation of tetrakis(b-diketonato)zirconium and its reactions with alcohols and phenols*. *Nippon Kagaku Kaishi*, **1991**, 1078-1082.
  113. Yamada B., Kageoka M. and Otsu T., *ESR study on radical polymerization of styrene. 2. Propagation rate constant of polystyrene radical with different molecular weights*. *Polym. Bull. (Berlin)*, **1992**, 28, 75-80.

114. Meyerhoff G., Sack R. and Kouloumbis M., *Rate processes for high conversion radical polymerization - experiments with methyl methacrylate*. Polym. Prepr. (Am. Chem. Soc., Div. Polym. Chem.), **1985**, 26, 293-294.
115. Lobinski R., Broekaert J.A.C., Tschoepel P. and Toelg G., *Inductively-coupled plasma atomic emission spectroscopic determination of trace impurities in zirconia powder*. Fresenius. J. Anal. Chem., **1992**, 342, 569-580.
116. Merten D., Broekaert J.A.C., Brandt R. and Jakubowski N., *Analysis of ZrO<sub>2</sub> powders by microwave assisted digestion at high pressure and ICP atomic spectrometry*. J. Anal. At. Spectrom., **1999**, 14, 1093-1098.
117. Gao Y., Kogler F.R. and Schubert U., *Improvement of the Thermal Stability of Cluster-Crosslinked Polystyrene and Poly(methyl methacrylate) by Optimization of the Polymerization Conditions*. J. Polym. Sci., Part A: Polym. Chem., **2005**, 43, 6586-6591.
118. Schubert U., Gao Y. and Kogler F.R., *Tuning the properties of nanostructured inorganic-organic hybrid polymers obtained from metal oxide clusters as building blocks*. Prog. Solid State Chem., **2005**, accepted.
119. Trimmel G., Fratzl P. and Schubert U., *Cross-Linking of Poly(methyl methacrylate) by the Methacrylate-Substituted Oxozirconium Cluster Zr<sub>6</sub>(OH)<sub>4</sub>O<sub>4</sub>(Methacrylate)<sub>12</sub>*. Chem. Mater., **2000**, 12, 602-604.
120. Schubert U., Voelkel T. and Moszner N., *Mechanical Properties of an Inorganic-Organic Hybrid Polymer Cross-linked by the Cluster Zr<sub>4</sub>O<sub>2</sub>(methacrylate)<sub>12</sub>*. Chem. Mater., **2001**, 13, 3811-3812.
121. Gross S., Di Noto V. and Schubert U., *Dielectric investigation of inorganic-organic hybrid film based on zirconium oxocluster-crosslinked PMMA*. J. Non-Cryst. Solids, **2003**, 322, 154-159.
122. Hild G., Okasha R. and Rempp P., *Free radical crosslinking copolymerization in the post-gel state, 3. Swelling and mechanical properties of polystyrene networks*. Makromol. Chem., **1985**, 186, 407-422.
123. Hild G. and Okasha R., *Kinetic investigations of the free radical crosslinking copolymerization in the pre-gel state, 2. Styrene/ethylene dimethacrylate and styrene/diisopropenylbenzene systems*. Makromol. Chem., **1985**, 186, 389-406.
124. Cioffi M., Hoffmann A.C. and Janssen L.P.B.M., *Reducing the gel effect in free radical polymerization*. Chem. Eng. Sci., **2001**, 56, 911-915.
125. Teodorescu M., *Free-radical copolymerization of methyl methacrylate with styrene in the presence of 2-mercaptoethanol II. Influence of methyl methacrylate/styrene ratio*. Eur. Polym. J., **2002**, 38, 841-846.
126. Graeme M. and Solomon D.H., *The chemistry of free radical polymerization*. First ed **1995**, Oxford: Pergamon, 408 pp.
127. Porter C.E. and Blum F.D., *Thermal Characterization of Adsorbed Polystyrene Using Modulated Differential Scanning Calorimetry*. Macromolecules, **2002**, 35, 7448-7452.
128. Reading M., Elliott D. and Hill V.L., *A new approach to the calorimetric investigation of physical and chemical transitions*. J. Therm. Anal., **1993**, 40, 949-955.
129. Danley R.L., *New modulated DSC measurement technique*. Thermochim. Acta, **2003**, 402, 91-98.
130. Grellmann W. and Seidler S., *Kunststoffprüfung 2005*, München, Wien: Carl Hanser Verlag, 706 pp.
131. Turi E.A., *Thermal characterization of polymeric materials*. 2<sup>nd</sup> ed. Vol. 1. **1997**, San Diego, Calif.: Academic Press, 1378 pp.
132. Kopesky E.T., Haddad T.S., McKinley G.H. and Cohen R.E., *Miscibility and viscoelastic properties of acrylic polyhedral oligomeric silsesquioxane-poly(methyl methacrylate) blends*. Polymer, **2005**, 46, 4743-4752.
133. Inoue T., *Reaction-induced phase decomposition in polymer blends*. Prog. Polym. Sci., **1995**, 20, 119-53.

134. Guo M., *Solid-state high-resolution NMR studies on the miscibility of polymer blends*. Trends Polym. Sci, **1996**, 4, 238-244.
135. Abad M.J., Barral L., Fasce D.P. and Williams R.J.J., *Epoxy Networks Containing Large Mass Fractions of a Monofunctional Polyhedral Oligomeric Silsesquioxane (POSS)*. Macromolecules, **2003**, 36, 3128-3135.
136. Boller A., Okazaki I. and Wunderlich B., *Modulated differential scanning calorimetry in the glass transition region. Part III. Evaluation of polystyrene and poly(ethylene terephthalate)*. Thermochim. Acta, **1996**, 284, 1-19.
137. Thomas L.C., Boller A., Okazaki I. and Wunderlich B., *Modulated differential scanning calorimetry in the glass transition region. IV. Pseudo-isothermal analysis of the polystyrene glass transition*. Thermochim. Acta, **1997**, 291, 85-94.
138. Schubert U., *Polymers Reinforced by Covalently Bonded Inorganic Clusters*. Chem. Mater., **2001**, 13, 3487-3494.
139. Sundell M.J., Pajunen E.O., Hormi O.O.E. and Nasman J.H., *Crosslinked polystyrene with improved mechanical properties*. J. Polym. Sci., Part A: Polym. Chem., **1993**, 31, 2305-2311.
140. Domininghaus H., *Die Kunststoffe und ihre Eigenschaften*. 6 ed. ed. Eyerer P., Elsner P. and Hirth T. **2005**, Berlin Heidelberg: Springer-Verlag, 1633 pp.
141. Price D.M., *Thermomechanical, Dynamic Mechanical and Dielectric Methods*, in *Principles of Thermal Analysis and Calorimetry*, Haines P.J., Editor. **2002**, The Royal Society of Chemistry Paperbacks: Cambridge, UK, 94-129.
142. Li F. and Larock R.C., *Synthesis, Structure and Properties of New Tung Oil-Styrene-Divinylbenzene Copolymers Prepared by Thermal Polymerization*. Biomacromol., **2003**, 4, 1018-1025.
143. Salgueiro W., Marzocca A., Somoza A., Consolati G., Cervený S., Quasso F. and Goyanes S., *Dependence of the network structure of cured styrene butadiene rubber on the sulphur content*. Polymer, **2004**, 45, 6037-6044.
144. Hagiwara K., Ougizawa T., Inoue T., Hirata K. and Kobayashi Y., *Studies on the free volume and the volume expansion behavior of amorphous polymers*. Radiat. Phys. Chem., **2000**, 58, 525-530.
145. Ehrenstein G.W., Riedel G. and Trawiel P., *Praxis der Thermischen Analyse von Kunststoffen* **1998**, München, Wien: Carl Hanser Verlag, 243 pp.
146. Menard K.P., *Dynamic Mechanical Analysis : A Practical Introduction* **1999**: CRC Press, 208 pp.
147. van Melick H.G.H., Govaert L.E. and Meijer H.E.H., *On the origin of strain hardening in glassy polymers*. Polymer, **2003**, 44, 2493-2502.
148. Bianchi U. and Rossi C., *A new transition in polystyrene. II. A transition of static polystyrene in bulk*. Polymer, **1963**, 4, 447-448.
149. Illers K.H. and Jenckel E., *Dynamic mechanical behavior of polystyrene, poly(p-chlorostyrene), and poly(p-bromostyrene) at low temperatures*. J. Polym. Sci., **1959**, 41, 528-531.
150. Li G.Z., Wang L., Toghiani H., Daulton T.L. and Pittman C.U., *Viscoelastic and mechanical properties of vinyl ester (VE)/multifunctional polyhedral oligomeric silsesquioxane (POSS) nanocomposites and multifunctional POSS-styrene copolymers*. Polymer, **2002**, 43, 4167-4176.
151. Basch A., Gross S., Choudhury N.R. and Matison J., *Inorganic-Organic Hybrid Polymers from the Polymerisation of Methacrylate-Substituted Oxotantalum Clusters with Methylmethacrylate: A Thermomechanical and Spectroscopic Study*. J. Sol-Gel Sci. Technol., **2005**, 33, 39-45.
152. Coltrain B.K., Landry C.J.T., O'Reilly J.M., Chamberlain A.M., Rakes G.A., Sedita J.S., Kelts L.W., Landry M.R. and Long V.K., *Role of trialkoxysilane functionalization in the preparation of organic-inorganic composites*. Chem. Mater., **1993**, 5, 1445-55.

153. Elias H.-G., *Makromoleküle*, in *Physikalische Strukturen und Eigenschaften*. **2001**, Wiley-VCH: Weinheim, 595-606.
154. Fetters L.J., Lohse D.J., Richter D., Witten T.A. and Zirkel A., *Connection between Polymer Molecular Weight, Density, Chain Dimensions, and Melt Viscoelastic Properties*. *Macromolecules*, **1994**, 27, 4639-4647.
155. Lomellini P. and Lavagnini L., *Molecular weight polydispersity effects on the melt viscoelasticity of styrene-acrylonitrile random copolymers*. *Rheol. Acta*, **1992**, 31, 175-182.
156. Mark J.E., Eisenberg A., Graessley W.W., Mandelkern L., Samulski E.T., Koenig J.L. and Wignall G.D., *Physical Properties of Polymers: Third Edition* **2004**, 519 pp.
157. Kopesky E.T., Haddad T.S., Cohen R.E. and McKinley G.H., *Thermomechanical Properties of Poly(methyl methacrylate)s Containing Tethered and Untethered Polyhedral Oligomeric Silsesquioxanes*. *Macromolecules*, **2004**, 37, 8992-9004.
158. Seidel C., Kulicke W.-M., Hess C., Hartmann B., Lechner M.D. and Lazik W., *Influence of the cross-linking agent on the gel structure of starch derivatives*. *Starch/Staerke*, **2001**, 53, 305-310.
159. Callister W.D.J., *Materials science and engineering* **2003**, New York: Wiley, 820 pp.
160. Mark H.F., Bikales N.M., Overberger C.G. and Menges G., *Encyclopedia of Polymer Science and Engineering*. 2<sup>nd</sup> ed. Vol. 4. ed. Kroschwitz J.I. **1986**: Wiley, 832 pp.
161. Oleinik E.F., *Epoxy-aromatic amine networks in the glassy state structure and properties*. *Adv. Polym. Sci.*, **1986**, 80, 49-99.
162. Schroeder J.A., Madsen P.A. and Foister R.T., *Structure-property relationships for a series of crosslinked aromatic-aliphatic epoxy mixtures*. *Polym. Prepr. (Am. Chem. Soc., Div. Polym. Chem.)*, **1986**, 27, 201-202.
163. Govaert L.E. and Tervoort T.A., *Strain hardening of polycarbonate in the glassy state: Influence of temperature and molecular weight*. *J. Polym. Sci., Part B: Polym. Phys.*, **2004**, 42, 2041-2049.
164. Tervoort T.A. and Govaert L.E., *Craze-initiation kinetics in polystyrene*. *J. Polym. Sci., Part B: Polym. Phys.*, **2004**, 42, 2066-2073.
165. Basu S., Mahajan D.K. and Van der Giessen E., *Micromechanics of the growth of a craze fibril in glassy polymers*. *Polymer*, **2005**, 46, 7504-7518.
166. Arruda E.M. and Boyce M.C., *Evolution of plastic anisotropy in amorphous polymers during finite straining*. *Int. J. Plast.*, **1993**, 9, 697-720.
167. G'Sell C., Hiver J.M., Dahoun A. and Souahi A., *Video-controlled tensile testing of polymers and metals beyond the necking point*. *J. Mater. Sci.*, **1992**, 27, 5031-5039.
168. Kozey V.V. and Kumar S., *Compression behavior of materials. Part I. Glassy polymers*. *J. Mater. Res.*, **1994**, 9, 2717-2726.
169. van Melick H.G.H., Govaert L.E. and Meijer H.E.H., *Localization phenomena in glassy polymers: influence of thermal and mechanical history*. *Polymer*, **2003**, 44, 3579-3591.
170. Haward R.N., *Strain hardening of thermoplastics*. *Macromolecules*, **1993**, 26, 5860-5869.
171. Lefebvre J.M., Escaig B., Coulon G. and Picot C., *Molecular scale deformation in the yielding behavior of glassy polymers*. *Polymer*, **1985**, 26, 1807-1813.
172. Brown N., *Relation between yield point and modulus for glassy polymers*. *Mater. Sci. Eng.*, **1971**, 8, 69-73.
173. Northolt M.G., *Compressive strength and glass transition temperature*. *J. Mater. Sci.*, **1981**, 16, 2025-2028.
174. Chang T.D., Carr S.H. and Brittain J.O., *Studies of epoxy resin systems. Part B. Effect of crosslinking on the physical properties of an epoxy resin*. *Polym. Eng. Sci.*, **1982**, 22, 1213-1220.
175. Fischer M., *Properties and failure of polymers with tailored distances between crosslinks*. *Adv. Polym. Sci.*, **1992**, 100, 313-355.
176. Mooney M., *A theory of large elastic deformation*. *J. Appl. Phys.*, **1940**, 11, 582-592.

- 
177. Evans K.E., *A scaling analysis of the fracture mechanisms in glassy polymers*. J. Polym. Sci., Part B: Polym. Phys., **1987**, 25, 353-368.
178. Lucas B.N., Rosenmayer C.T. and Oliver W.C., *Mechanical characterization of sub-micron polytetrafluoroethylene (PTFE) thin films*. Mater. Res. Soc. Symp. Proc., **1998**, 505, 97-102.
179. Maner K.C., Begley M.R. and Utz M., *Nanoindentation of amorphous and nano structured polymers*. Mater. Res. Soc. Symp. Proc., **2003**, 778, 145-149.
180. Torma V., Husing N., Peterlik H. and Schubert U., *Small-angle x-ray scattering investigation of the cluster distribution in inorganic-organic hybrid polymers prepared from organically substituted metal oxide clusters*. C. R. Chimie, **2004**, 7, 495-502.
181. Patterson A.L., *The Scherrer formula for x-ray particle-size determination*. Phys. Rev., **1939**, 56, 978-982.
182. Beaucage G., *Approximations leading to a unified exponential/power-law approach to small-angle scattering*. J. Appl. Crystallogr., **1995**, 28, 717-728.
183. Porod G., *The x-ray small-angle scattering of close-packed colloid systems. I*. Kolloid-Zeitschrift, **1951**, 124, 83-114.
184. Schildknecht C.E., *Allyl compounds and their polymers (including polyolefins)*. High Polymers, **1973**, 28, 720 pp.
185. Zubov V.P., Kumar M.V., Masterova M.N. and Kabanov V.A., *Reactivity of allyl monomers in radical polymerization*. J. Macromol. Sci., Chem., **1979**, A13, 111-131.
186. Gaylord N.G., Deshpande A.B., Mandal B.M. and Martan M., *2,3- and 2,7-Bicyclo[2.2.1]hept-2-enes. Preparation and structures of polynorbornenes*. J. Macromol. Sci., Chem., **1977**, A11, 1053-1070.
187. Gaylord N.G., *Temperature and dilution effects in the radical polymerization of maleic anhydride and norbornene derivatives*. Polym. Prepr. (Am. Chem. Soc., Div. Polym. Chem.), **1982**, 23, 327-328.
188. Bruch M.D., *NMR Spectroscopy Techniques*. 2<sup>nd</sup> ed **1996**, New York: Marcel Dekker, Inc., 616 pp.
189. Mackenzie R.C., *Nomenclature in Thermal Analysis*, in *Treatise on Analytical Chemistry*, Elving P.J. and Kolthoff I.M., Editors. **1983**, John Wiley & Sons: New York, 1-16.
190. Heal G.R., *Thermogravimetry and Derivative Thermogravimetry*, in *Principles of Thermal Analysis and Calorimetry*, Haines P.J., Editor. **2002**, Royal Society of Chemistry Paperbacks: Cambridge, UK, 10-53.
191. Laye P.G., *Differential Thermal Analysis and Differential Scanning Calorimetry*, in *Principles of Thermal Analysis and Calorimetry*, Haines P.J., Editor. **2002**, Royal Society of Chemistry: Cambridge, UK, 55-93.
192. Jiang Z., Imrie C.T. and Hutchinson J.M., *An introduction to temperature modulated differential scanning calorimetry (TMDSC): a relatively non-mathematical approach*. Thermochim. Acta, **2002**, 387, 75-93.
193. Mori S. and Barth H.G., *Size Exclusion Chromatography* **1999**, Berlin: Springer, 234 pp.
194. Wunderlich B., Boller A., Okazaki I. and Kreitmeier S., *Linearity, steady state, and complex heat capacity in modulated differential scanning calorimetry*. Thermochim. Acta, **1996**, 282/283, 143-155.
195. Boller A., Schick C. and Wunderlich B., *Modulated differential scanning calorimetry in the glass transition region*. Thermochim. Acta, **1995**, 266, 97-111.
196. Kellner R., Mermet J.-M., Otto M. and Widmer H.M., *Analytical Chemistry* **1998**, Weinheim: Wiley-VCH, 916 pp.
197. *Sartorius YDK 01 Density Determination Kit User's Manual*pp
198. VanLandingham M.R., Villarrubia J.S. and Meyers G.F., *Nanoindentation of polymers: overview*. Polym. Prepr. (Am. Chem. Soc., Div. Polym. Chem.), **2000**, 41, 1412-1413.

199. Oliver W.C. and Pharr G.M., *An improved technique for determining hardness and elastic modulus using load and displacement sensing indentation experiments*. J. Mater. Res., **1992**, 7, 1564-1583.
200. Glatter O. and Kratky O., *Small angle x-ray scattering* **1982**, London: Academic Press, 515 pp.
201. Guinier A. and Fournet G., *Small-angle scattering of x-rays* **1955**, New York: Wiley, 268 pp.
202. Williams D.B. and Carter C.B., *Transmission Electron Microscopy* **1996**, New York: Plenum Press, 729 pp.

## Curriculum Vitae

|                                |                                     |
|--------------------------------|-------------------------------------|
| <b>Name</b>                    | Franz René Kogler                   |
| <b>Address</b>                 | Zeileborgasse 14-16/12, 1120 Vienna |
| <b>Citizenship</b>             | Austria                             |
| <b>Date and Place of Birth</b> | 29.12.1977, Salzburg                |
| <b>Marital Status</b>          | Unmarried                           |

### Higher Education

|                   |  |
|-------------------|--|
| 10 / 02 – present | PhD Thesis at the Vienna University of Technology, Institute of Materials Chemistry; PhD Supervisor Prof. Ulrich Schubert; Topic: Synthesis and Characterization of Transition Metal Oxo Clusters and their Use as Co-Monomers in the Preparation of Hybrid Polymers |
| 04/04 – 05/04     | McKinsey&Company, Hands-On-Training for Managers-To-Be   |
| 06 / 02           | Master Degree  |
| 09 / 01 – 06 / 02 | Diploma Work in Analytical Chemistry, Supervisor Prof. Franz Dickert; Topic: Mass Sensitive Monitoring of Motor Oil Degradation with Quartz Crystal Microbalances  |
| 10 / 96 – 06 / 02 | University of Vienna, University Education in Chemistry  |

### School Education

|                       |                                  |
|-----------------------|----------------------------------|
| 06 / 1996             | High School Graduation, Matura   |
| 10 / 1988 – 06 / 1996 | Grammar School in Braunau am Inn |
| 09 / 1984 – 07 / 1988 | Primary School in Mattighofen    |

### Work Experience

|                      |  |
|----------------------|--|
| 07 / 99 – 08 / 99    | Wacker Siltronic GmbH, Burghausen; Processing of Silicon Wafers  |
| 08 – 09 / 95, 96, 97 | AMAG Austria Metall AG, Ranshofen, Austria; Processing of Aluminum Products, Division Rolling Products |